

# Dune erosion and overwash at wide beaches

Part B: measurement results of experiments in  
the Scheldt Flume





# **Dune erosion and overwash at wide beaches**

**Part B: measurement results of experiments in the Scheldt Flume**

Bas Hoonhout, Pieter van Geer, Robert McCall

1202124-007






**Title**  
Dune erosion and overwash at wide beaches

<b>Client</b>	<b>Project</b>	<b>Reference</b>	<b>Pages</b>
Rijkswaterstaat - Waterdienst	1202124-007	1202124-007-HYE-0005	173

**Keywords**  
Dunes, erosion, overwash, Scheldt Flume

**Summary**  
Dune erosion and overwash experiments are performed in the Scheldt Flume early 2010. For the experiments, a modified reference profile for the Holland coast was used containing a horizontal beach of 480m in prototype. The purpose of the experiments was twofold. First, the influence of the wide beach on the amount of dune erosion was determined. Second, the hydro- and morphodynamics in dune overwash situations was investigated. The latter experiments used the end profile of the former.

**References**  
This research is part of the program *Strength and Loads Water Defences – Dunes* (Sterkte en Belastingen Waterkeringen, SBW – Duinen) financed by the Dutch Directorate-General for Public Works and Water management (Rijkswaterstaat – Waterdienst).

Version	Date	Author	Initials	Review	Initials	Approval	Initials
	apr. 2011	Bas Hoonhout, Pieter van Geer, Robert McCall		Leo van Rijn		Marcel van Gent	

**State**  
final



## Contents

<b>1</b>	<b>Introduction</b>	<b>1</b>
1.1	Background	1
1.1.1	Dune erosion with shallow foreshores	1
1.1.2	Dune overwash	1
1.2	Objective	2
1.3	Demarcation	2
1.4	Reader's guide	2
1.5	Realisation	3
<b>2</b>	<b>Setup of the experiments</b>	<b>5</b>
2.1	Description of the Scheldt Flume	5
2.2	Dune profiles	5
2.3	Instrumentation	6
2.3.1	Wheel profiler	7
2.3.2	Wave height and flow velocity meters	8
2.3.3	Water level gauge	8
2.3.4	Layer thickness meters	8
2.3.5	Sieves	9
2.3.6	Thermometer	9
2.3.7	Cameras	9
2.3.8	Stereo photography	10
2.4	Measurement Programme	11
2.4.1	A-series	12
2.4.2	B-series	12
2.4.3	C-series	12
2.4.4	D-series	13
<b>3</b>	<b>Measurements</b>	<b>15</b>
3.1	Hydrodynamics	15
3.1.1	Hydrodynamics during erosion experiments	15
3.1.2	Hydrodynamics during overwash experiments	16
3.2	Bathymetry measurements	17
3.2.1	Morphology during erosion experiments	17
3.2.2	Morphology during overwash experiments	18
<b>4</b>	<b>Conclusions</b>	<b>21</b>





# 1 Introduction

## 1.1 Background

The motivation for the experiments described in this report was twofold. First, there was a demand for a dataset that describes dune erosion for coastal profiles with shallow foreshores. Such dataset can be used for validation of the currently used assessment methods for dune erosion of these coastal profiles. These profiles can be found on the Wadden Islands. Second, there was a demand for a dataset for validation of dune overwash computations by the morphological model XBeach.

### 1.1.1 Dune erosion with shallow foreshores

The current assessment of dune erosion in the Netherlands consists of three stages described in the VTV (2006): a simplified, detailed and advanced. The detailed method is based on a series of large-scale flume experiments in the Deltaflume (Vellinga, 1986; WL|Delft Hydraulics, 2006). A dune profile representative for the coast of Holland was used in these experiments.

Many areas on the Wadden Islands have foreshores that are less steep compared to the Holland coast. The steepness of the foreshore largely determines the amount and type of wave energy that reaches the dune during a storm event. Therefore, the dunes on the Wadden Islands will behave differently from the dunes along the Holland coast. It is expected that the dune erosion at locations with a shallow foreshore is described insufficiently accurate by the current detailed assessment method for dune erosion.

Short waves will break relatively early in case a shallow foreshore is present. It is expected that the early breaking of short waves will accommodate a transfer of energy from short waves to long waves. Long waves will then be able to reach the dune despite the presence of a shallow foreshore. Since the DUROS+ model (Vellinga, 1986; WL|Delft Hydraulics, 2007), used in the current detailed assessment method, does not consider long waves in particular, it is expected that dune erosion at locations with shallow foreshores is underestimated. This reasoning is confirmed in practice and by more advanced numerical models like XBeach (Roelvink *et al.*, 2009).

The small-scale dune erosion experiments described in this report were executed using a dune profile representative for areas at the Wadden coast. For example, Schiermonnikoog and Ameland. These experiments can be seen in reference to the experiments of Coeveld and De Vroeg (2004) and WL|Delft Hydraulics (2006).

### 1.1.2 Dune overwash

The US Army Corps of Engineers (USACE) commissioned the development of the dune erosion and overwash model XBeach (Roelvink *et al.*, 2009) in 2006. The model considers surfbeat, which makes it suitable for solving near-shore hydrodynamics accurately. The capabilities of XBeach to make overwash computations are internationally applicable in many situations. However, the availability of datasets that can be used for the validation of the overwash formulations in XBeach is limited.

The small-scale dune overwash experiments described in this report were executed with a dune profile representative for barrier islands that can be found in the United States. For example, the Chandeleur Islands near New Orleans.

## 1.2 Objective

The objectives of the experiments described in this report can be summarized as follows:

- The generation of a dataset in which erosion of dune profiles with a shallow foreshore during a storm surge is accurately described. The dataset is used to investigate the applicability of the DUROS+ model for Dutch sandy coasts for situations with shallow foreshores that compare well with the profiles found at Schiermonnikoog and Ameland. Moreover, the dataset might be used for the calibration and validation of an advanced assessment method for Dutch sandy coasts.
- The generation of a detailed dataset suitable for the validation of the dune overwash formulations in XBeach.

## 1.3 Demarcation

The initial cross-shore dune profile is an important parameter in dune erosion computations. Nevertheless, past experiments are often performed using a profile representative for the Holland coast. This profile is commonly known as the reference profile (Vellinga, 1986). The research of the influence of a shallow foreshore in the initial profiles is of recent date. The experiments discussed in the report should therefore be considered as pilot experiments. These experiments can be used to prepare future research on this topic.

Pilot experiments have a limited scope. During the experiments discussed, a single cross-shore dune profile was tested. It concerns a profile with a shallow foreshore at two meters above storm surge level, effectively being a wide beach (Figure 2.1). Conclusions drawn from these experiments are only valid for profiles that are well comparable with the tested profile. From computations made in ongoing research (Diermanse *et al.*, 2010) it is known that shallow foreshores below storm surge level also influence the amount of dune erosion largely. These kind of shallow foreshores are explicitly not investigated in the currently discussed experiments.

## 1.4 Reader's guide

This report consists of two parts: A and B. This part (B) is intended to contain a full description of the experiments performed. The detail in which some information is described, will exceed the need of many readers. This document should therefore be seen as a reference document. For a more aggregated description of the measurement results and the analysis performed on the dune erosion experiments is referred to part A of this report. For the dune overwash experiments is referred to McCall *et al.* (2011) and Appendix A.

In Chapter 2 the setup of the experiments is described. A description of the facilities and instrumentation is given. In addition, a description of the dune profiles and the measurement programme can be found in this chapter. Chapter 3 presents the measurement results. The bathymetric and hydrodynamic results are presented separately as well as the results for the dune erosion and overwash experiments. Chapter 4 contains a brief overview of the conclusions drawn and recommendations for further research. Most figures and tables are collected in the appendices and referred to from the different chapters.

Since the total amount of measurement data exceeded 5TB, it was not feasible to supply the full dataset along with this report. In Appendix D references to the original data sources can

be found to accommodate further analysis and research. This appendix also contains the naming conventions used throughout the project.

## 1.5 Realisation

This research is part of the program *Strength and Loads Water Defences – Dunes* (Sterkte en Belastingen Waterkeringen, SBW – Duinen) financed by the Dutch Directorate-General of Public Works and Watermanagement (Rijkswaterstaat – Waterdienst).

The experiments were executed in the Scheldt Flume at Deltares from the end of March until the end of May 2010. The model assistants involved were mainly F.J. van Eeden and T.J. Ammerlaan, occasionally supported or replaced by J.F. Coolegem, P.A. Pasterkamp and P.J. Alberts. The project management was provided by P.F.C. van Geer. The project engineers were B.M. Hoonhout and R.T. McCall. The internal quality review was performed by L.C. van Rijn.



## 2 Setup of the experiments

This chapter describes the facilities and instrumentation used. Also, the measurement programme and experiment setup are explained.

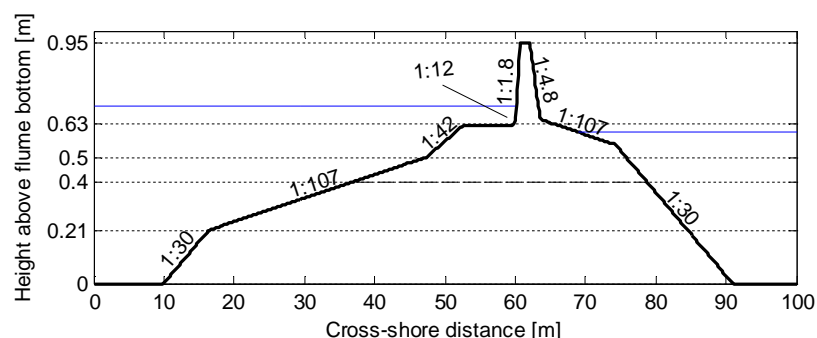
### 2.1 Description of the Scheldt Flume

The experiments were executed in the Scheldt Flume at Deltares. The flume has a length of 110m and is equipped with a wave paddle at each end. During the experiments, one wave paddle and over 100m of flume length was used. The width of the flume is 1m and its height 1.2m. The wave generator is capable of generating both regular and irregular waves. Depending on the water depth, waves with a frequency between 0.01Hz and 2Hz and a significant wave height up to 26.7cm can be generated. The wave generator is equipped with Active Reflection Compensation (ARC), which measures and absorbs waves reflected by the model in order to minimize the disturbance of the generated wave field due to re-reflections. The wave generator also uses second order steering to account for second order effects of lower harmonics of the wave field.

### 2.2 Dune profiles

The dune profiles used in the experiments are based on the reference profile, which is considered representative for the Holland coast. This reference profile was first published in Vellinga (1986) and was used in several past studies. Amongst those studies were WL|Delft Hydraulics (1981a, 1981b, 1982 and 2006) and Coeveld and De Vroeg (2004).

With respect to the reference profile, a shallow horizontal foreshore was added at a height of 2m+NAP in prototype scale (Figure 2.1). The foreshore started at the point where the dune toe reaches the foreshore level and runs 480m seaward. At the seaward border of the shallow foreshore, the original sloping foreshore was extended to meet the newly introduced shallow foreshore. For the overwash experiments, also a rear-side slope and hinterland was created in the flume.



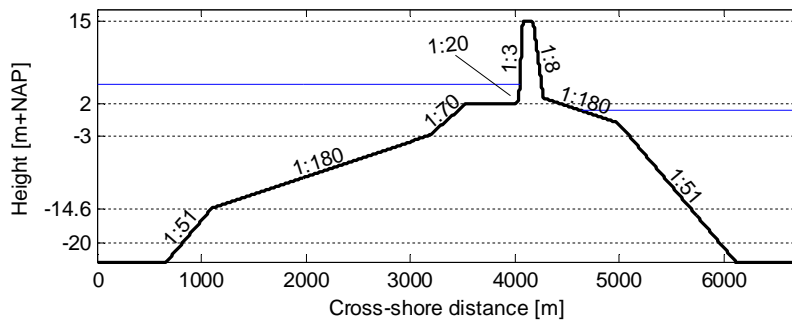


Figure 2.1 Dune profile with shallow foreshore in flume scale (upper) and prototype scale (lower)

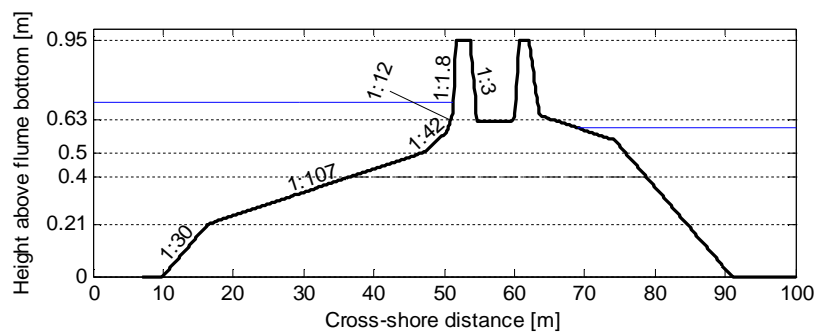


Figure 2.2 Dune profile used in reference experiment C1 experiment D1

Originally, a dune crest of 100m in prototype scale was created. To accommodate a relative fast failure of the dune, the crest width was reduced to 50m after the first overwash experiments. In addition, before the start of the overwash experiments, with the exception of experiment A2d, the height of the crest was reduced by 10cm in flume scale to meet the representative profile for barrier islands in the United States. During experiments C1 and D1 (see 2.4 *Measurement Programme*) an alternative profile with two dunes was used (Figure 2.2).

To fit the dune profile, including the shallow foreshore, in the Scheldt Flume, a scaling factor of  $n_d = 40$  was used. In correspondence with the 2004 experiments, the dune profile was horizontally contracted with a factor 1.68. The model time is, according to the scaling relations elaborated by Vellinga (1986), scaled by a factor of the square root of the depth scale:  $n_t = \sqrt{40}$ .

To reduce the reconstruction times between the different experiments, the part of the profile below the 40cm level with respect to the flume bottom was constructed out of concrete. In this area, no significant erosion was expected.

The sediment used was obtained from the same company as by Coeveld and De Vroeg (2004). It concerns sediment known as *Asserzand* with a grain size  $d_{50}$  of approximately 90 $\mu$ m from *Trip-Popken B.V.* in Assen. The desired grain size appeared not to be available. Therefore, a slightly larger grain size was used and an extra reference experiment (C-series) was performed to make comparison with the results of past experiments still possible (see 2.4 *Measurement Programme*). The sieve curves of the used sediment can be found in Figure C.2 and Figure C.3.

## 2.3 Instrumentation

Before, during and after the experiments, the following was measured:

- Cross-shore profile
- Wave climate
- Water levels
- Flow velocities
- Water and sediment layer thickness
- Grain size distribution
- Temperature of the water
- Three-dimensional bathymetry

This section discusses the instrumentation and methodology used for these measurements. Also the results obtained are discussed qualitatively. In Table B.2 and Table B.3 a detailed overview is given of the locations of all measurements.

### 2.3.1 Wheel profiler

The cross-shore profile was measured using a remote controlled vehicle, known as a wheel profiler. The wheel profiler had three profile followers mounted on it (Figure 2.3). One follower was located at the flume axis. The other two followers were located on both sides of the flume axis at a distance of 25cm. A follower follows the bathymetry using a wheel with a 2cm radius and a speed of 10cm/s. The followers were able to follow and measure bathymetric features on the scale of bed ripples, but the wheel size was large enough to prevent (frequent) hindrance of small bathymetric irregularities like gaps and lumps. The measurement frequency was set to 0.5cm for this purpose. The wheel profiler always starts from the dune crest downward to reduce pressures exerted on the bathymetry.

Before and after the experiments the entire profile was measured. At pre-determined intervals during the experiments (see 2.4 *Measurement Programme*), the active part of the profile was measured. Measurements that run from the hinterland to the wave paddles are done in two steps: first, the part from the dune crest to the hinterland was measured and then the part running from the dune crest to the wave paddles was measured. This was done to ensure a downward measuring direction of the followers.



Figure 2.3 Profile followers of the wheel profiler used to measure the cross-shore dune profile

### 2.3.2 Wave height and flow velocity meters

Wave height meters (WHM) based on electric resistance were used during the experiments. The accuracy of the instruments is  $\pm 2.5\text{mm}$ , which is  $\pm 0.5\%$  or  $1\%$  of the measurement reach. The three most offshore located WHM's had a range of  $1\text{m}$ , while the other WHM had a range of  $0.5\text{m}$ . The measurement frequency was  $25\text{Hz}$ .

Electromagnetic flow velocity meters of the type P-EMS were used during the experiments. The accuracy of the instruments was  $\pm 0.01\text{ m/s}$  or  $\pm 1\%$  of the measured value. The measurement frequency was  $25\text{Hz}$ .

The wave climate was measured using a collection of 16 wave height meters and 4 flow velocity meters (see Figure C.1). Three sets of three WHM and one EMS were used to measure incoming and reflecting short and long waves separately. One of these sets was located in front of the wave paddle to monitor the generated wave climate. The other sets were located just in front of the foreshore and just in front of the dune to measure the wave transformations from the wave paddle to the dune and back. Halfway the wave paddle and foreshore a set of three WHM were located. A set of one WHM and one EMS was located at the hinterland to measure incoming and reflecting overwash waves in this area. Two of the three WHM left were distributed evenly over the foreshore and the other was located at some distance from the foreshore to increase the spatial resolution of the wave transformation measurements.

### 2.3.3 Water level gauge

The water levels were measured at the start of each experiment using two gauges at both sides of the flume. Only during the A1 experiments, the water levels were measured during the experiments as well.

### 2.3.4 Layer thickness meters

Layer thickness meters (LTM) can be seen as reversed wave height meters. Two conducting wires were attached to the flume bottom and mounted on a beam on top of the flume and spanning the flume width (Figure 2.4). The wires therefore penetrated both the sediment and the water layer. The accuracy and measurement frequency were similar to the WHM.



Figure 2.4 Layer thickness meters mounted on the concrete lower part of the dune profile



Based on the resistance of the wires, the instantaneous water level, when wet, or bed level, when dry, at a certain location can be determined. The measurement signal will fluctuate on the time scale of the hydrodynamics. The signal can also fluctuate due to morphological changes. Therefore, if changes in the bathymetry are at a longer time scale than the hydrodynamic time scale, the two can be separated and the bathymetry can be monitored using the layer thickness meters.

Four layer thickness meters were used during the experiments. Two of them were located at the rear-side slope of the dune and two were located just behind the dune, making them only effective during the overwash experiments (Figure C.1). The meters were placed 10cm away from the flume axis to prevent obstruction of the wheel profiler (Figure 2.4).

### 2.3.5 Sieves

Before and during the experiments, the grain size of the sediment in the flume was measured using a sieving installation. The distribution curves can be found in Figure C.2 and Figure C.3.

### 2.3.6 Thermometer

A thermometer continuously recorded the temperature of the water in the flume during the experiments.

### 2.3.7 Cameras

Three video cameras were installed around the flume. Cameras #1 and #2 were positioned next to each other facing to the glass wall of the flume at the location of the dune (Figure 2.5 and Figure 2.6). These cameras were making snapshot and time-exposure images with a time interval of 10s. The images were used to obtain detailed measurements of the profile developments and monitor whether the dune front was leaning over or not. Camera #3 was mounted above the flume facing downward making planview images of the dune area (Figure 2.7). Camera #3 was only used during the overwash experiments and makes snapshot and time-exposure images with a frequency of 30Hz. The images were used to monitor the development of gullies at the rear-side slope of the dune and to track overtopping waves.

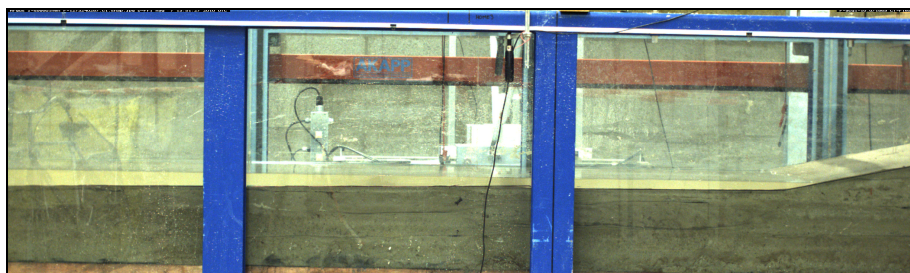


Figure 2.5 View camera #1

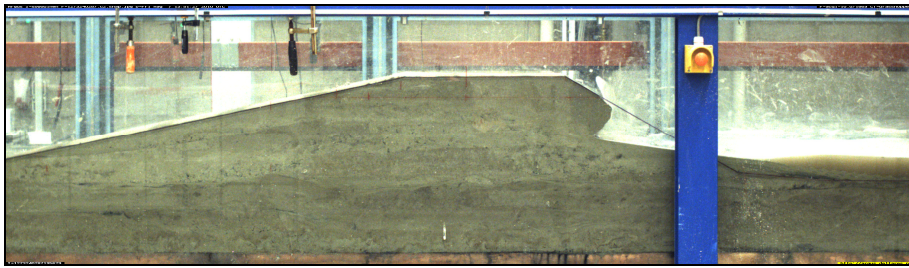


Figure 2.6 View camera #2

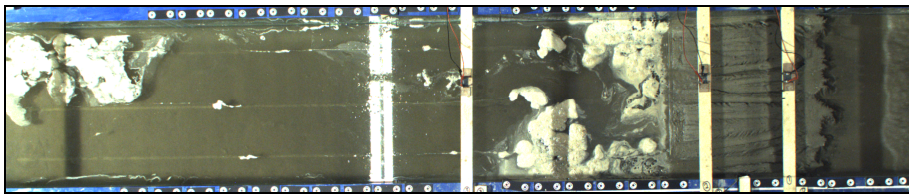


Figure 2.7 View camera #3

## 2.3.8 Stereo photography

The technique of stereo photography provides three-dimensional images of an arbitrary object. The technique is based on two spatially and temporally aligned cameras with a fixed distance in between (Figure 2.8). This camera unit provides stereo photographs. The object of interest is surrounded by physical markers with a unique identification code. The identification of the markers works similar to the well-known bar code system. By making a series of photographs with the camera unit that contain both (a part of) the object of interest and three or more markers, software can be used to extract the position of both the markers and the camera unit at the time the photographs are taken. From this information, a geometry of the markers can be solved.



Figure 2.8 Stereo photo camera on tripod

Another software package is subsequently able to find correlations between pixels found on different photographs based on the geometry of the markers. These correlations are then used to construct a three-dimensional image of the object of interest.

Stereo photography was used during the overwash experiments. Especially the morphological behaviour at the rear-side slope and hinterland showed considerable three-dimensional effects. These effects could not be measured using the regular profile measurements. Therefore, during these experiments stereo photographs were taken along with the regular profile measurements.

## 2.4 Measurement Programme

Four series of experiments were defined (A to D). Each series consists of one or more dune erosion experiments. The erosion experiments were followed by overwash experiments using the final dune profile of the erosion experiments. The wave height and period as well as the water level were changed between different experiments. The same sediment and a JONSWAP spectrum were used for all experiments. The measurement programme is presented in Table 2.1. A more detailed overview can be found in Table B.1.

Experiment	Prototype		Model		
	H <sub>m0</sub> [m]	T <sub>p</sub> [s]	h [m]	H <sub>m0</sub> [m]	T <sub>p</sub> [s]
A1a	Varying	Varying	Varying	Varying	Varying
A1d	9.0 – 10.7	14.2	0.71 – 0.75	0.225 – 0.267	2.25
A2a	9.0	14.2	0.70	0.225	2.25
A2d	9.0	14.2	0.78 – 0.82	0.225	2.25
B1a	10.7	14.2	0.70	0.267	2.25
B1d	10.7	14.2 – 18.9	0.70 – 0.74	0.267	2.25 – 3.00
B2a	9.0	18.9	0.70	0.225	3.00
B2d	9.0 – 10.7	14.2	0.70 – 0.74	0.225 – 0.267	2.25
C1a *	9.0	14.2	0.70	0.225	2.25
C1d *	9.0	14.2	0.70 – 0.74	0.225	2.25
D1d	5.0 – 9.0	10.6 – 14.2	0.74 – 0.79	0.125 – 0.225	1.68 – 2.25

Table 2.1 Measurement programme. In case of linearly increasing values, the range of values is given. Experiments marked with an asterisk (\*) were executed using the reference profile without shallow foreshore.

Experiments are labeled with an experiment identifier (first column Table 2.1). The first character indicates the experiment series (A to D). The number indicates the order of the experiment in a series. Identifiers ending with an “a” are dune erosion experiments. Experiment identifiers ending with a “d” are overwash experiments. See Appendix D.1 for a full description of the experiment identifiers.

The duration of the dune erosion experiments was 5 hours. The overwash experiments ran until breakthrough of the dune. A breakthrough was forced by a gradual increase either of the water level, the wave height or wave period. In case an increase of the wave height or period until the maximum value determined by the wave paddle, did not force a breakthrough, also the water level was increased. At set intervals, the wave paddle was stopped and the dune profile measured. For the erosion experiments, these intervals are presented in Table 2.2. For the overwash experiments, this interval was 20 minutes, except for experiment D1d where it was 10 minutes.

Interval #	Time [min]
1	0
2	5
3	16
4	52
5	156
6	312

Table 2.2 Measurement intervals dune erosion experiments

The following paragraphs discuss the four different series of experiments. Each series provides data for comparison with another series or past experiments.

#### 2.4.1 A-series

The A-series provide two erosion experiments. Experiment A1 models an entire storm surge as proposed by Vellinga (1986). During this experiment, the water level, wave height and wave period was frequently varied in order to approach the course presented in Figure C.4. The purpose of this experiment was to validate the assumption that the erosion due to a full storm surge can well be modelled using the maximum conditions for a period of 5 hours at prototype scale. This assumption is often used during dune erosion experiments, but was not yet validated for dune profiles with shallow foreshores.

Experiment A2 repeats the experiment using the maximum storm conditions only. The water level was set to 70cm above the flume bottom. A JONSWAP spectrum with a significant wave height  $H_{m0}$  set to 22.5cm and a peak wave period  $T_p$  set to 2.25s were used. These conditions are similar to the conditions during the T11 experiment of Coeveld and De Vroeg (2004), although they used a Pierson-Moskowitz spectrum (see 2.4.3 C-series). Comparison between experiments A1 and A2 provided insight in the validity of the assumption of the use of maximum storm conditions during a 5-hour period. Furthermore, experiment A2 provided a basis for comparison with the B-series experiments.

During the overwash experiments in the A-series, a breakthrough was forced by a gradual increase of the water level. During the overwash experiment A1d, the significant wave height was finally increased to a value of 26.7cm as well.

#### 2.4.2 B-series

The B-series provide variations on the A2 experiment in wave height and period. During the B1 experiment, the significant wave height was increased to a value of 26.7cm. During the B2 experiment, the peak wave period was increased to 3.0s, which is in agreement with the T12 experiment of Coeveld and De Vroeg (2004). From both experiments, the sensitivity of the erosion volumes for the wave height and period are obtained.

During the overwash experiment B1d, a breakthrough was forced by a gradual increase of the wave period, followed by the water level. During the overwash experiment B2d, first the water level and then the wave height was gradually increased.

#### 2.4.3 C-series

Compared to past experiments, the major difference during the experiments presented in this report is the introduction of a shallow foreshore. However, also some small differences can be

observed in the experiment setup. The most important are the use of a JONSWAP spectrum instead of a Pierson-Moskowitz spectrum and the use of a slightly different grain size. In order to investigate the influence of these differences and to ensure a valid comparison between different series of experiments, a reference experiment was performed.

The reference experiment C1a was a repetition of the T11 experiment of Coeveld and De Vroeg (2004), including the dune profile without shallow foreshore (Figure 2.2), but excluding the differences in grain size and spectrum shape. A comparison between the T11 and other past experiments and experiment A2a, provided insight in the possibilities to compare both series of experiments and the influence of the differences in experiment setup.

During the overwash experiment C1d, a breakthrough was forced by a gradual increase of the water level, followed by a gradual increase of the wave height.

#### 2.4.4 D-series

For the C-series experiments, an alternative dune profile without a shallow foreshore was constructed (Figure 2.2). This dune profile was simply obtained by adding a second dune to the original profile starting from the most seaward point of the foreshore. Consequently, a profile configuration with two dunes was obtained. This opportunity was used to perform a single exploring experiment where a primary dune has failed, but a second dune row is present. This experiment on its own is referred to experiment D1d and was the only experiment in the D-series.

The experiment continued with the final profile of experiment C1d. First, the first dune was fully eroded using constant maximum storm conditions for 2 hours model scale. A situation with a large shallow bar at the location of the first dune was obtained. In between this bar and the second dune, the original shallow foreshore was located. In order to prevent a run-up overwash regime at the location of the former primary dune and force an inundation overwash situation at this location, the wave induced water level set-up was limited by decreasing the wave height and period. Run-up overwash was not aimed at since complex three-dimensional morphological behaviour can be expected. First, the wave height and period were gradually increased, followed by a gradual increase of the water level. During the experiment, the erosion of the second dune and the development of the bar and former primary dune were observed.



### 3 Measurements

This chapter presents the results of the measurements. The results are presented at the scale they are measured in the physical model.

#### 3.1 Hydrodynamics

An analysis of the hydrodynamic measurements is given in this section. For all experiments, the hydrodynamic conditions were inferred from the wave height meter (WHM) and flow velocity meter (EMS) data. Data from the four layer thickness meters (LTM) and camera #3 were added to the analysis of the hydrodynamic conditions during the overwash experiments.

##### 3.1.1 Hydrodynamics during erosion experiments

During the erosion experiments, hydrodynamic data were collected by 15 WHM and 3 EMS. The total low frequency and high frequency wave heights at all 15 WHM were calculated from the measured water surface elevation variance density spectra, assuming a split frequency between low frequency waves and high frequency waves of half the incident peak frequency. These high and low frequency wave heights are shown in Figure C.56 to Figure C.86. These figures show that the high frequency waves decreased in height from the wave board and have already lost most of their energy by the start of the shallow foreshore due to breaking. In contrast, the low frequency waves increased in height (shoal) until the start of the shallow foreshore, after which they lost height due to breaking and bed friction (Figure 3.1). The total low frequency wave height on the shallow foreshore was equal to or greater than the total high frequency wave height on the foreshore.

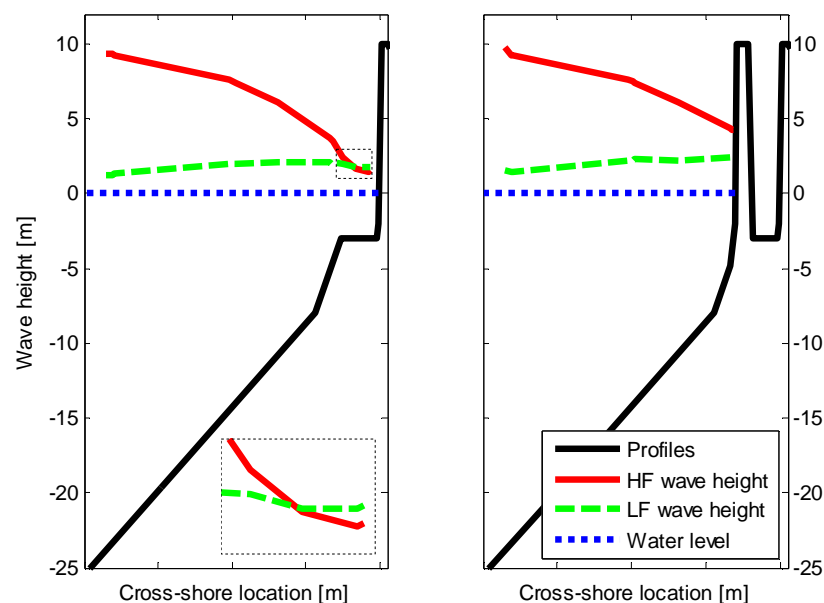


Figure 3.1 Change of high- and low frequency wave height over the tested dune profiles with and without wide beach. The inset provides a detailed view on the wave heights at the wide beach.

Three sets of three WHM and one EMS were used to separate incident and reflected wave spectra, using the relation presented by Guza *et al.* (1984). These spectra are shown in Figure C.87 to Figure C.97. These data are summarized as incident and reflected high frequency and low frequency wave heights in Table B.6. The results show that the high frequency wave energy of the reflected signal was approximately 4% of the high frequency wave energy of the incident signal at WHM01. The reflected low frequency wave energy was approximately 30% of the incident low frequency wave energy at WHM01.

Time-averaged cross-shore velocities and standard deviation of the velocity, measured at the four EMS, are shown in Figure C.98 through Figure C.130 and summarized in Table B.7. The results show that the time-averaged velocities at all three EMS between the wave board and the dune were directed offshore, varying between 0-5 cm/s. The standard deviation of the velocity at EMS1 was in the order of 20 cm/s.

### 3.1.2 Hydrodynamics during overwash experiments

Data from the WHM and EMS instruments were analysed to determine total, incident and reflected wave heights and time-averaged flows in an identical manner to those of the erosion experiments. The results can be found in Figure C.56 through Figure C.130 and Table B.6 and Table B.7.

The time series of the four layer thickness meters (LTM) were analysed to investigate overtopping frequencies and discharges. The LTM data show a voltage level that relates to the water level when wet, and the bed level when dry. Since the LTM were not calibrated, an estimate of the calibration factor of the LTM was made by comparison of the trend of the water level increase and by considering constant wave energy flux between LDM04 and WHM16 during tests D1d\_4 through D1d\_7. An example of a LTM time series is shown in Figure 3.2.

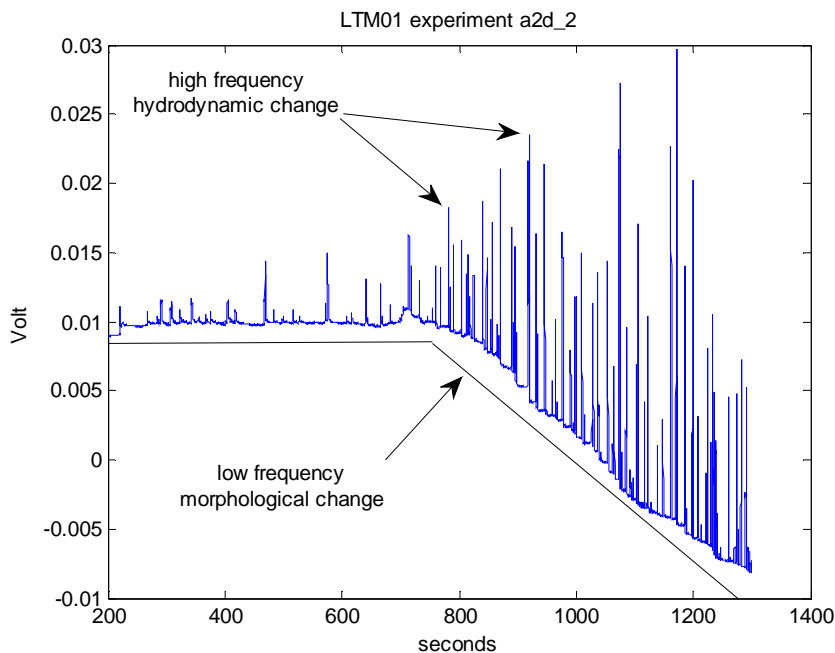


Figure 3.2 Example of a LTM data time series with the high-frequency hydrodynamic and low-frequency morphodynamic change

In many experiments the morphological change was related directly to individual bore or overwash events, see for instance Figure 3.2. In these experiments, each successive bore



eroded the bed at the LTM and little bed level change occurred in the inter-bore periods. In these cases it was not possible to fully decouple the morphological time scale from the hydrodynamic time scale.

The results from the LTM measurements are represented as water level and bed level density spectra in Figure C.131 through Figure C.135. These spectra are obtained by a Fourier Transform. The figures show that the LTM-spectra were dominated by frequencies lower than the split frequency between the high frequency and low frequency waves. This indicates that the hydrodynamics and morphodynamics on the dune do not occur at the same frequency as the peak frequency of the incident waves. Note that no data are shown for experiment C1d, as the LTM were not in a position to measure overtopping on that profile.

### *Camera image results*

From camera #3 plan view images with approximately a 30Hz frequency were obtained. The images were used to track the waves overtopping the dune crest during the overwash experiments. Based on the results from experiment A1d, the bores appeared to have travelled more or less with a constant speed over the dune crest. Once they reached the rear-side slope, the bores started to accelerate and the bore speed tripled from about 0.26m/s to about 0.76m/s (Figure C.29). The standard deviation of the measurements was respectively 0.1m/s and 0.16m/s or 38% and 21%. Several differences were observed in the B2d experiment results. Reliable measurements of bore celerities were only available at the end of the experiment. The dune was eroded away largely and large gullies were visible at the rear-side slope. The clear distinction between crest and rear-side slope had disappeared. This was also visible in the measurements. The overall average bore celerity was 0.67m/s without acceleration (Figure C.30). The time-averaged bore speeds for the different experiments are summarized in Table B.5.

## **3.2 Bathymetry measurements**

The results of the morphological measurements obtained from the wheel profiler, video cameras #1 and #2 and stereo photography are presented in this section. The results for the erosion and overwash experiments are presented separately.

### **3.2.1 Morphology during erosion experiments**

The wheel profiler measurements during the dune erosion experiments provided the cross-shore profiles averaged over the flume width. These profiles are presented in Figure C.6 to Figure C.15. For each experiment two figures are given. The first figure provides the desired profile, the realized profile at the start of the experiment and the final profile at the end of the experiment. The second figure provides a more detailed view on the profile developments at the active part of the dune and foreshore. Erosion volumes derived from the measured profiles are summarized in Table B.4 and Figure C.5. The realized profiles were reasonably in agreement with the desired profiles. The maximum deviation was 1.5cm in vertical direction.

A generic behaviour of the dune can be discerned from the figures (Figure 3.3). The dune front steepened at the beginning of each experiment, followed by a gradual retreat. The sediment eroded from the dune settled on the foreshore. This results in an increase of the bed level at the foreshore, in front of the dune. More seaward, the foreshore showed considerable erosion resulting in a smoother transition from deep water to the shallow foreshore. The sediment eroded from the foreshore settled in deep water near the wave paddle. Regularly, the dune front showed non-uniformities over the flume width. The non-uniformities were mainly situated at the higher parts of the dune front near the flume walls.

Due to adhesion of the sediment at the flume wall, the erosion appeared to be less at these locations. Consequently, the adhesive effects caused the erosion to be slightly delayed.

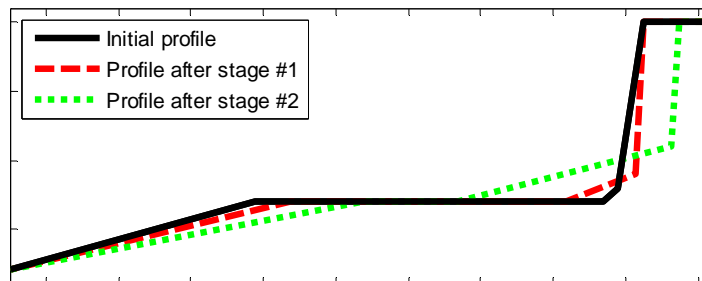


Figure 3.3 Schematic representation of two stages of erosion of the dune front and shallow foreshore observed during the dune erosion experiments.

### Dune fronts leaning over

The increased capillary effect, due to the downscaled grain size, caused additional adhesion of the sediment. A corresponding delay of the erosion and a dune front leaning over were consequently observed. The same effect is observed in past studies (e.g. Boers *et al.*, 2008; Coeveld and De Vroeg, 2004). By performing additional measurements, both studies concluded that the effect on the observed erosion volumes is insignificant. However, the profiles measured by the wheel profiler sometimes show a perfectly vertical dune front. Most likely, such situation was caused by a dune front leaning over. After all, the profiler wheels were not obstructed in their fall downward from the dune crest to the foreshore. Therefore, the erosion volumes are slightly underestimated at some points in time. Images from video camera #1 and #2 provided insight in the actual situation.

The images obtained from these cameras provided information on the profile development in a much higher temporal resolution. Since the adhesive sediment lumps at the flume walls were more pronounced in this dataset, it could be used to cut off the dune fronts leaning over artificially (Figure C.26 to Figure C.28).

### 3.2.2 Morphology during overwash experiments

The wheel profiler measurements during the dune overwash experiments provided the cross-shore profiles averaged over the flume width. These profiles are presented in Figure C.16 to Figure C.25. The figures show the end profile of the preceding erosion experiment and the subsequent profile measurements during the overwash experiment.

After overtopping and overwash started to occur, the uniformity of the dune over the flume width started to decrease rapidly. Three-dimensional morphological behaviour was observed especially at the rear-side slope of the dune where gullies were formed. Measurements obtained from the wheel profiler are therefore not in all cases representative. Moreover, due to the development of large meandering gullies, measuring the entire cross-shore profile using the wheel profiler was not always possible. Again, the images from video camera #1 and #2 provided insight in the more advanced morphological behaviour. Stereo photography was used to record the three-dimensional features like lumps, gullies and overwash fans.

From the camera images, three stages of erosion were discerned after overtopping starts (Figure 3.4). These stages are in agreement with the stages discerned by Steetzel and Visser (1992). Steetzel and Visser performed overflow experiments over a sand dike without waves. The first stage involved steepening of the rear-side slope. The second stage involved the

decrease of the crest due to a seaward retreat of the rear-side slope. The third stage started when the crest width was almost zero. In this stage, the crest lowered until the dune was completely eroded away. Once overtopping started, sediments were deposited more and more landward. Once inundation started, the sediment transports were entirely directed landward.

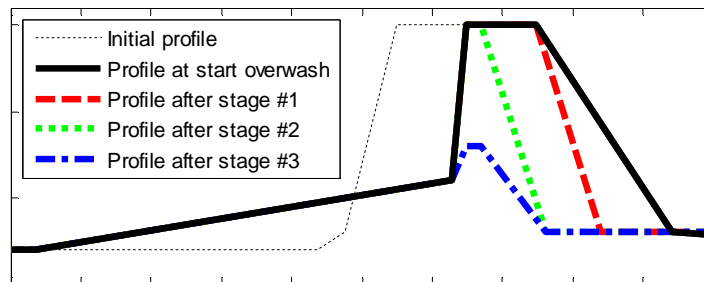


Figure 3.4 Schematic representation of three stages of erosion of the dune observed during the dune overwash experiments.

#### Stereo photo results

During the dune overwash experiments, three-dimensional bathymetric measurements were obtained from series of stereo photos. Since the use of stereo photography in dune experiments was still experimental, not from all experiments are stereo photos available. Table 3.1 shows the moments successful stereo photographs were taken. Figure C.31 to Figure C.50 present the bathymetries around the dune obtained from these photographs. Figure C.51 to Figure C.55 show the difference plots for the successive series of experiments.

Test	Stereo photos
A1d	4, 7, 8
B1d	2, 5, 6, 7
B2d	1, 5, 7, 8
C1d	2, 3, 4, 5
D1d	2, 5, 6, 7, 8

Table 3.1 Available series of stereo photos for different series of experiments. The numbers refer to the subtest following the moment the photo was taken (see Appendix D.1 and Table B.1)

Qualitatively the measurements support the stages discerned by Steetzel and Visser (1992): the steepening and erosion of the rear-side slope in the first two stages (Figure 3.4). The erosion rapidly turned into a highly three-dimensional process due to the formation of gullies at the rear-side slope. In the third stage, the dune crest lowered until and beyond the surrounding bed level.



## 4 Conclusions

The experiments described in this report were performed to provide insight in the effects of a shallow foreshore on the amount of dune erosion. These experiments elaborated on the T11 experiment performed by Coeveld and De Vroeg (2004) and the WL|Delft Hydraulics (2006) study. This report is restricted to the factual description of the experiments and its results. The analysis of the results is described in part A of this report.

### *Nearshore hydrodynamics*

The hydrodynamics at the foot of the dune measured during these experiments correspond closely to the conditions that were expected and described in the introduction of this report. The measurements show that the incident high frequency wave height decreases quickly on the shallow foreshore and that the incident low frequency wave height is dominant at the dune foot and across the shallow foreshore. The experiments also show that the incident low frequency wave height slowly decreases on the shallow foreshore, indicating breaking or energy loss due to bed friction. This effect was not anticipated at the start of the experiments.

### *Dune erosion and model sensitivity*

The introduction of the shallow foreshore or wide beach resulted in a decrease of the erosion volumes of about 85%. An increase of the peak wave period of 34% results in an increase of the erosion volume of 18%. Comparison with Coeveld and De Vroeg (2004) after 3 hours of modeling, the maximum modelling time during the 2004 experiments, shows the same figures. An increase of the wave height of 19% resulted in an increase of the erosion volume of 25% after 5 hours of modeling.

### *Dune overwash*

During the overwash experiments, similar stages of erosion as in Steetzel and Visser (1992) were observed. Moreover, rapid formation of channels and gullies at the rear-side slope were observed resulting in large overwash fans in the hinterland area. The dune front eroded in these situations fairly uniform, often more than during the erosion experiments. Flow velocities ranging approximately from 0.65 to 0.75m/s were found at the rear-side slope of the dune, based on video images. As long as the crest of the dune was still intact, the flow velocities at the crest were limited around 0.25m/s.

### *Further research*

A single cross-shore profile was tested during the discussed experiments. The shallow foreshore, or wide beach, in this profile reduced the amount of dune erosion significantly. This reduction probably depends on the exact profile used. Further research is necessary to determine whether this is true. More recommendations on further research can be found in part A of this report.



## References

- Boers, M., Van der Werf, I.M. and Van Geer, P.F.C. (2008). *Dunes and Dikes – Lab experiments in the Vinjé Wave Basin*. Deltares, report H5019, draft.
- Coeveld, E.M. and De Vroeg, J.H. (2004). *Modelonderzoek duinafslag: meetverslag kleinschalige gidsproeven*. WL|Delft Hydraulics, report H4265.
- Diermanse, F.L.M., Walstra, D.J.R., Smale, A.J. (2010). *Detailtoets voor duinafslag*. Report, project 1202124, ongoing research.
- Guza, R.T., Thornton, E.B. and Holman, R.A. (1984). *Swash on steep and shallow beaches*. 19<sup>th</sup> International Conference on Coastal Engineering, Houston, pp. 708-723.
- Hoonhout, B.M., Van Geer, P.F.C., McCall, R.T., Boers, M. (2010). *Duinafslag en –overslag bij brede stranden – Deel A: toepasbaarheid DUROS voor kustprofielen met een breed strand*. Deltares, report 1202124-007-HYE-0002.
- McCall, R.T., Van Geer, P.F.C, Hoonhout, B.M. (2011). *Physical modeling of storm-induced erosion and overwash*. Proc. Seventh International Symposium on Coastal Engineering and Science of Coastal Sediment Processes, Miami, Florida. In press.
- Roelvink, J.A., Reniers, A.J.H.M., Van Dongeren, A.R., Van Thiel de Vries, J.S.M., McCall, R.T. and Lescinski, J.M. (2009). *Modelling storm impacts on beaches, dunes and barrier islands*. Journal of Coastal Engineering, Vol. 56 p. 1133 – 1152, doi:10.1016/j.coastaleng.2009.08.006.
- Steezel, H.J. and Visser P.J. (1992). *Profile development of dunes due to overflow*. Proceedings 23<sup>rd</sup> Coastal Engineering Conference, ASCE, 2669-2679.
- Vellinga, P. (1986). *Beach and dune erosion during storm surges*. Delft University of Technology, PhD thesis.
- WL|Delft Hydraulics (1981a). *Schaalserie duinafslag*. Meetrapport, project M1263-II.
- WL|Delft Hydraulics (1981b). *Onderzoek naar duinafslag tijdens superstormvloed*. Meetrapport, project M1653.
- WL|Delft Hydraulics (1982). *Systematisch onderzoek naar kenmerkende factoren voor duinafslag*. Report, project M1819-I.
- WL|Delft Hydraulics (2006). *Dune erosion – Product 2: Large-scale model tests and dune erosion prediction method*. Report, project H4357.
- WL|Delft Hydraulics (2007). *Technisch Rapport Duinafslag*. Report, project H4357.





## A Analysis of overwash experiments

This part of the report (B) is intended to contain a full description of the experiments performed. The analysis and interpretation of the results is described in part A of the report as far as it concerns the dune erosion experiments. Analysis and interpretation of the dune overwash experiments are mainly described in the paper of McCall *et al.* (2011). However, some interpretations that went in too much detail for this paper are collected in this appendix.

### Layer Thickness Meters

The layer thickness meters (LTM) were installed in order to measure both the hydrodynamic as well as the morphodynamic change at the rear-side slope of the dune during the overwash experiments (Figure A.1).

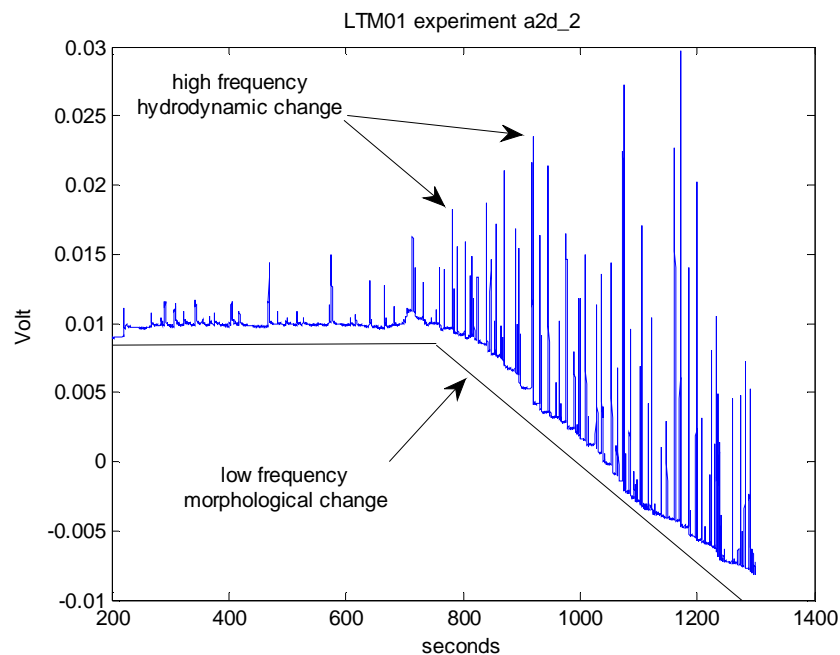


Figure A.1 Example of a LTM data time series with the high-frequency hydrodynamic and low-frequency morphodynamic change

The spectra obtained from the LTM were dominated by frequencies lower than the split frequency between the high frequency and low frequency waves. This indicates that the hydrodynamics and morphodynamics on the dune do not occur at the same frequency as the peak frequency of the incident waves. However, the maximum variance density estimated from the LTM data in the low frequency part of the spectrum was approximately 5-10 times less than the incident low frequency wave energy measured at WHM15. The estimated variance density in the LTM data in the high frequency part of the spectrum was higher than the incident high frequency wave energy at WHM15. These differences may be explained by taking into account wave energy dissipation, wave reflection, the effect of morphological developments and the wave energy shift towards high frequencies due to wave steepening (bores) over the dune profile.

In general was the morphological change related directly to individual bore or overwash events in many experiments. In these experiments, each successive bore eroded the bed at

the LTM and little bed level change occurred in the inter-bore periods. In these cases it was not possible to fully decouple the morphological time scale from the hydrodynamic time scale.

### Camera images

From camera #3 plan view images with approximately a 30Hz frequency were obtained. The images were used to track the waves overtopping the dune crest during the overwash experiments. In order to make the processing of the large amount of images feasible, first the images showing an overtopping wave were selected from the dataset. The variability of the signal from the layer thickness meters was used to discern the moments an overtopping wave passes (Figure A.2).

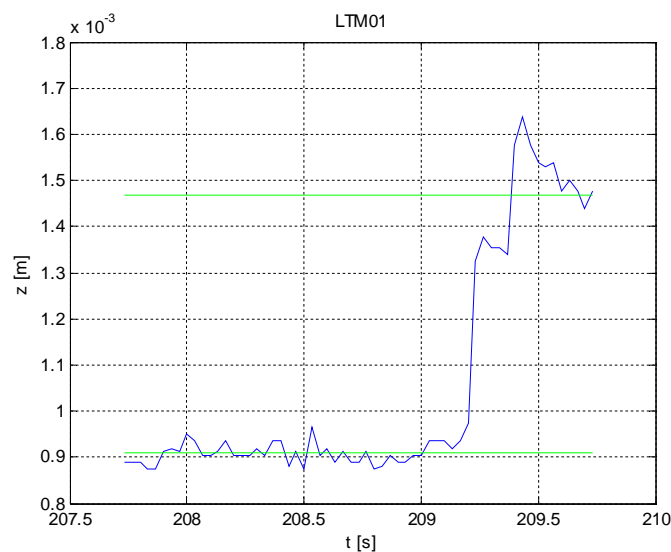


Figure A.2 Overtopping wave detected in layer thickness meter #1 (LTM01) and determination bore height based on averages.

In the selected images, the bore front was detected using a simple algorithm that subtracts two consecutive images. The area where the absolute result of the subtraction was significantly larger than zero, the image had changed. It was assumed that the bore had passed this area. From this information the location of the bore front could be detected. Averaging the location over the flume width and dividing by the time interval between the consecutive images gave an average bore speed (Figure A.3). The detection algorithm was not flawless. Lighting conditions and unexpected movements made a good detection sometimes impossible. Outliers in the averaged bore speed or detection location were neglected (approximately 30% of the bores).

The time-averaged bore speeds for the different experiments are given in Table B.5. Due to synchronisation problems between the layer thickness meter signal and the cameras during the first experiments, it was decided to synchronise the measurements using a light pulse. During the first experiments, the light pulse was absent and thus synchronisation and analysis of the camera images not possible. Only results for experiments A1d and B2d are available.

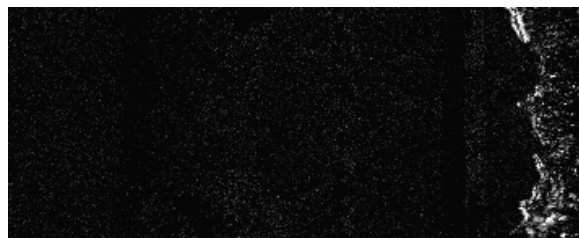
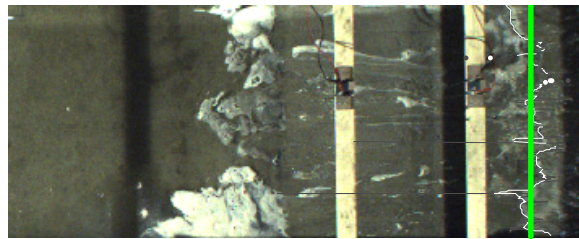


Figure A.3 Above: original image with detected bore front and average location (green). Below: difference image with respect to previous camera image.



## **B Tables**

Experiment		t	h (front)	h (back)	H <sub>m0</sub>	T <sub>p</sub>	order	profiler
		[min]	[m]	[m]	[m]	[s]		
A1a	1	5	0,60	0,60	0,192	2,08	2	✓
	2	9	0,61	0,61	0,195	2,09	2	
	3	9	0,63	0,63	0,198	2,11	2	
	4	9	0,64	0,64	0,202	2,13	2	
	5	19	0,65	0,65	0,207	2,16	2	
	6	9	0,65	0,65	0,211	2,18	2	✓
	7	9	0,64	0,64	0,214	2,19	2	
	8	28	0,63	0,63	0,218	2,21	2	
	9	9	0,64	0,64	0,222	2,23	2	✓
	10	9	0,66	0,66	0,223	2,24	2	
	11	10	0,67	0,67	0,224	2,24	2	
	12	9	0,69	0,69	0,224	2,25	2	
	13	9	0,70	0,70	0,225	2,25	2	
	14	10	0,70	0,70	0,225	2,25	2	
	15	9	0,70	0,70	0,225	2,25	2	✓
	16	9	0,69	0,69	0,224	2,25	2	
	17	10	0,67	0,67	0,224	2,24	2	
	18	9	0,66	0,66	0,223	2,24	2	
	19	9	0,64	0,64	0,222	2,23	2	
	20	28	0,63	0,63	0,218	2,21	2	
	21	9	0,64	0,64	0,214	2,19	2	✓
	22	9	0,65	0,65	0,211	2,18	2	
	23	19	0,65	0,65	0,207	2,16	2	
	24	9	0,64	0,64	0,202	2,13	2	✓
	25	9	0,63	0,63	0,198	2,11	2	✓
A1d	1	19	0,71	0,74	0,225	2,25	2	✓
	2	19	0,72	0,74	0,225	2,25	2	✓
	3	19	0,73	0,74	0,225	2,25	2	✓
	4	19	0,74	0,74	0,225	2,25	2	✓
	5	19	0,74	0,74	0,246	2,25	2	✓
	6	19	0,74	0,74	0,267	2,25	2	✓
	7	19	0,75	0,74	0,267	2,25	2	✓✓
A2a	1	5	0,70	0,63	0,225	2,25	2	✓
	2	10	0,70	0,63	0,225	2,25	2	✓
	3	36	0,70	0,63	0,225	2,25	2	✓
	4	104	0,70	0,63	0,225	2,25	2	✓
	5	156	0,70	0,63	0,225	2,25	2	✓✓
A2d	1	19	0,78	0,63	0,225	2,25	2	✓
	2	19	0,80	0,63	0,225	2,25	2	✓
	3	19	0,82	0,63	0,225	2,25	2	✓✓
B1a	1	5	0,70	0,70	0,267	2,25	2	✓
	2	10	0,70	0,70	0,267	2,25	2	✓
	3	36	0,70	0,70	0,267	2,25	2	✓
	4	104	0,70	0,70	0,267	2,25	2	✓
	5	156	0,70	0,70	0,267	2,25	2	✓✓
B1d	1	19	0,70	0,63	0,267	2,25	2	✓
	2	19	0,70	0,63	0,267	2,63	2	✓
	3	19	0,70	0,63	0,267	3,00	1	✓
	4	19	0,71	0,63	0,267	3,00	1	✓

continues on next page...

Experiment		t	h (front)	h (back)	H <sub>m0</sub>	T <sub>p</sub>	order	profiler
	5	19	0,72	0,63	0,267	3,00	1	✓
	6	19	0,73	0,63	0,267	3,00	1	✓
	7	19	0,74	0,63	0,267	3,00	1	✓✓
B2a	1	5	0,70	0,70	0,225	3,00	1	✓
	2	10	0,70	0,70	0,225	3,00	2	✓
	3	36	0,70	0,70	0,225	3,00	2	✓
	4	104	0,70	0,70	0,225	3,00	2	✓
	5	156	0,70	0,70	0,225	3,00	2	✓✓
B2d	1	19	0,7	0,63	0,225	2,25	2	✓
	2	19	0,71	0,63	0,225	2,25	2	✓
	3	19	0,72	0,63	0,225	2,25	2	✓
	4	19	0,73	0,63	0,225	2,25	2	✓
	5	19	0,74	0,63	0,225	2,25	2	✓
	6	19	0,74	0,63	0,246	2,25	2	✓
	7	19	0,74	0,63	0,267	2,25	2	✓✓
C1a	1	5	0,70	0,70	0,225	2,25	2	✓
	2	10	0,70	0,70	0,225	2,25	2	✓
	3	36	0,70	0,70	0,225	2,25	2	✓
	4	104	0,70	0,70	0,225	2,25	2	✓
	5	156	0,70	0,70	0,225	2,25	2	✓✓
C1d	1	19	0,70	0,63	0,225	2,25	2	✓
	2	19	0,71	0,63	0,225	2,25	2	✓
	3	19	0,72	0,63	0,225	2,25	2	✓
	4	19	0,73	0,63	0,225	2,25	2	✓
	5	19	0,74	0,63	0,225	2,25	2	✓✓
D1d	1	120	0,74	0,74	0,225	2,25	2	✓
	2	9	0,74	0,78	0,125	1,678	2	✓
	3	9	0,74	0,78	0,175	1,985	2	✓
	4	9	0,74	0,78	0,225	2,25	2	✓
	5	9	0,75	0,78	0,225	2,25	2	✓
	6	9	0,76	0,78	0,225	2,25	2	✓
	7	13	0,79	0,78	0,225	2,25	2	✓✓

Table B.1 Measurement programme. Experiment identifiers ending with an "a" are dune erosion experiments. Experiment identifiers ending with a "d" are overwash experiments. The side of the waveboard is indicated as "front", side of the hinterland is indicated as "back". Rows without spectrum information and duration indicate a measurement of a final profile.

Instrument	x	y	
	[m]	[m]	
TEMP	-2,40	-0,05	
WHM01	9,47	-0,50	clustered
EMS01	10,00	-0,50	
WHM02	10,73	-0,50	
WHM03	11,17	-0,50	
WHM04	34,26	-0,50	clustered
WHM05	34,99	-0,50	
WHM06	35,44	-0,50	
WHM07	44,06	-0,50	
WHM08	54,56	-0,50	clustered
EMS02	54,56	-0,50	
WHM09	54,82	-0,50	
WHM10	55,08	-0,50	
WHM11	57,14	-0,50	
WHM12	59,66	-0,50	
WHM13	62,26	-0,50	clustered
EMS03	62,26	-0,25	
WHM14	62,42	-0,50	
WHM15	62,58	-0,50	
LTM01	65,81	-0,60	
LTM02	66,31	-0,60	
LTM03	67,71	-0,60	
LTM04	70,73	-0,60	
EMS04	84,23	-0,60	clustered
WHM16	84,41	-0,50	

Table B.2 Locations of instruments in flume. Coordinate system: x-axis runs from wave board along flume length with south to north positive, y-axis runs from inner side west flume wall along flume width with east to west positive, z-axis runs from flume bottom positive upward.

Camera	experiments	x	y	z	resolution	frequency
		[m]	[m]	[m]	[px]	[hz]
CAM01	A,B,D	67,85	8,37	1,04	2448x720	0.1
	C	56,66	7,06	0,94	2448x720	0.1
CAM02	A,B,D	65,28	8,40	1,03	2448x720	0.1
	C	55,82	7,02	0,94	2448x720	0.1
CAM03	A,B,D	67,53	-0,17	9,46	2448x500	30
	C	59,32	-0,24	9,50	2448x500	30

Table B.3 Locations of cameras. Coordinate system: x-axis runs from wave board along flume length with south to north positive, y-axis runs from inner side west flume wall along flume width with east to west positive, z-axis runs from flume bottom positive upward.

Experiment	H <sub>m0</sub>	T <sub>p</sub>	Dune erosion [dm <sup>3</sup> /m]						Increase
			0.1h	0.25h	1h	2.5h	4h	5h	
	m	s							%
A2a	0.225	2.25	1.00	1.29	2.33	3.44	4.06	4.44	0
B1a	0.267	2.25	1.22	1.81	3.09	4.10	4.98	5.54	24.8
B2a	0.225	3.00	0.78	1.12	2.57	4.08	4.78	5.17	16.5
C1a	0.225	2.25	5.51	8.49	15.35	21.02	24.65	26.92	506.2

Table B.4 Erosion volumes above mean sea level measured using the wheel profiler, interpolated to fixed model times. Increase in erosion volume is given with respect to experiment A2a at 5h model time.



Exp.	nr of bores	avg. speed crest	avg. speed slope	std. deviation speed crest	std. deviation speed slope
		[m/s]	[m/s]	[m/s]	[m/s]
A1d	15	0.26	0.76	0.10	0.16
B2d	17	-	0.67	-	0.14

Table B.5 Overtopping wave celerities. Speeds are based on planview images and not corrected for any slopes.

Experiment	Hrms hi incident (m)			Hrms hi reflected (m)			Hrms lo incident (m)			Hrms lo reflected (m)		
	WHM01	WHM08	WHM13	WHM01	WHM08	WHM13	WHM01	WHM08	WHM13	WHM01	WHM08	WHM13
a1a_1	0.158	0.037	0.004	0.039	0.029	0.004	0.024	0.021	0.015	0.008	0.013	0.015
a1a_6	0.158	0.043	0.006	0.033	0.017	0.006	0.024	0.027	0.011	0.007	0.008	0.015
a1a_9	0.168	0.042	0.005	0.034	0.016	0.005	0.027	0.026	0.010	0.007	0.008	0.013
a1a_15	0.164	0.062	0.014	0.031	0.022	0.010	0.025	0.025	0.019	0.011	0.014	0.018
a1a_21	0.164	0.043	0.003	0.034	0.018	0.003	0.026	0.023	0.008	0.008	0.007	0.008
a1a_24	0.155	0.043	0.003	0.034	0.018	0.003	0.023	0.023	0.008	0.006	0.006	0.008
a1a_26	0.154	0.033	0.001	0.036	0.015	0.001	0.023	0.020	0.002	0.008	0.010	0.002
a1d_1	0.165	0.075	0.021	0.032	0.027	0.013	0.025	0.028	0.023	0.011	0.017	0.023
a1d_2	0.161	0.080	0.025	0.032	0.030	0.015	0.024	0.029	0.024	0.011	0.018	0.024
a1d_3	0.161	0.084	0.028	0.032	0.031	0.016	0.023	0.030	0.025	0.013	0.019	0.025
a1d_4	0.161	0.087	0.030	0.033	0.031	0.017	0.024	0.030	0.026	0.013	0.020	0.026
a1d_5	0.174	0.089	0.031	0.035	0.032	0.017	0.027	0.032	0.027	0.014	0.022	0.027
a1d_6	0.185	0.089	0.032	0.038	0.032	0.017	0.031	0.032	0.027	0.015	0.021	0.027
a1d_7	NaN	NaN	NaN	NaN	NaN	NaN	NaN	NaN	NaN	NaN	NaN	NaN
a2a_1	0.165	0.071	0.021	0.033	0.033	0.018	0.025	0.029	0.021	0.011	0.017	0.021
a2a_2	0.166	0.071	0.019	0.031	0.029	0.013	0.027	0.031	0.022	0.013	0.017	0.022
a2a_3	0.158	0.068	0.019	0.030	0.027	0.012	0.024	0.031	0.022	0.011	0.017	0.022
a2a_4	0.161	0.068	0.018	0.031	0.026	0.011	0.026	0.030	0.022	0.011	0.017	0.022
a2a_5	0.160	0.070	0.019	0.030	0.026	0.011	0.025	0.029	0.022	0.010	0.016	0.023
a2d_1	0.172	0.109	0.045	0.034	0.039	0.023	0.026	0.035	0.031	0.016	0.025	0.029
a2d_2	0.171	0.117	0.051	0.034	0.039	0.022	0.026	0.036	0.032	0.017	0.026	0.029
a2d_3	0.162	0.118	0.054	0.033	0.036	0.020	0.025	0.038	0.032	0.013	0.019	0.020
b1a_1	0.184	0.070	0.021	0.036	0.032	0.018	0.031	0.030	0.023	0.012	0.018	0.023
b1a_2	0.183	0.068	0.020	0.035	0.028	0.013	0.033	0.034	0.024	0.014	0.018	0.025
b1a_3	0.178	0.068	0.019	0.034	0.027	0.012	0.032	0.031	0.023	0.013	0.017	0.023
b1a_4	0.179	0.067	0.019	0.035	0.026	0.012	0.032	0.031	0.023	0.013	0.017	0.024
b1a_5	0.179	0.068	0.020	0.034	0.025	0.012	0.031	0.030	0.023	0.012	0.017	0.025
B1d_1	0.179	0.069	0.020	0.035	0.026	0.013	0.031	0.029	0.024	0.012	0.016	0.026
B1d_2	0.182	0.067	0.021	0.031	0.024	0.014	0.033	0.031	0.026	0.013	0.018	0.029
B1d_3	0.175	0.063	0.021	0.030	0.024	0.016	0.022	0.031	0.027	0.013	0.018	0.029
B1d_4	0.178	0.068	0.025	0.031	0.025	0.018	0.023	0.032	0.029	0.014	0.020	0.030
B1d_5	0.176	0.071	0.028	0.030	0.027	0.018	0.023	0.033	0.031	0.014	0.021	0.029
B1d_6	0.178	0.077	0.033	0.032	0.029	0.020	0.023	0.034	0.032	0.015	0.023	0.031
B1d_7	0.178	0.080	0.036	0.032	0.028	0.020	0.023	0.034	0.033	0.015	0.023	0.030
B2a_1	0.160	0.065	0.020	0.028	0.027	0.019	0.020	0.034	0.023	0.011	0.017	0.025
B2a_2	0.165	0.064	0.019	0.027	0.025	0.016	0.027	0.035	0.024	0.011	0.017	0.026
B2a_3	0.163	0.065	0.019	0.026	0.024	0.015	0.026	0.033	0.023	0.011	0.017	0.024
B2a_4	0.165	0.065	0.020	0.027	0.024	0.014	0.027	0.032	0.024	0.012	0.018	0.025
B2a_5	0.165	0.065	0.021	0.027	0.024	0.015	0.026	0.031	0.025	0.011	0.018	0.027
b2d_1	0.164	0.071	0.019	0.032	0.026	0.012	0.024	0.028	0.023	0.010	0.015	0.025
b2d_2	0.162	0.076	0.023	0.031	0.028	0.014	0.023	0.029	0.025	0.011	0.016	0.025
b2d_3	0.160	0.081	0.027	0.031	0.030	0.016	0.023	0.029	0.026	0.011	0.018	0.025
b2d_4	0.160	0.087	0.030	0.032	0.032	0.018	0.022	0.030	0.028	0.012	0.020	0.026
b2d_5	0.146	0.083	0.031	0.029	0.030	0.017	0.021	0.028	0.025	0.012	0.019	0.024
b2d_7	0.177	0.088	0.032	0.035	0.031	0.016	0.029	0.031	0.028	0.013	0.020	0.024
C1a_1	0.164	0.080	NaN	0.040	0.057	NaN	0.025	0.029	NaN	0.019	0.027	NaN
C1a_2	0.164	0.080	NaN	0.036	0.040	NaN	0.026	0.032	NaN	0.018	0.029	NaN
C1a_3	0.163	0.079	NaN	0.034	0.035	NaN	0.025	0.032	NaN	0.017	0.029	NaN
C1a_4	0.162	0.079	NaN	0.033	0.034	NaN	0.026	0.033	NaN	0.017	0.029	NaN
C1a_5	0.162	0.080	NaN	0.033	0.034	NaN	0.025	0.033	NaN	0.016	0.028	NaN
C1d_1	0.163	0.082	NaN	0.033	0.039	NaN	0.025	0.033	NaN	0.016	0.027	NaN
C1d_2	0.162	0.089	NaN	0.033	0.050	NaN	0.024	0.032	NaN	0.016	0.027	NaN
C1d_3	0.161	0.098	NaN	0.033	0.058	NaN	0.024	0.033	NaN	0.016	0.028	NaN
C1d_4	0.161	0.106	NaN	0.032	0.064	NaN	0.024	0.033	NaN	0.017	0.028	NaN
C1d_5	0.160	0.101	NaN	0.031	0.056	NaN	0.023	0.033	NaN	0.012	0.021	NaN
D1d_1	0.160	0.069	0.015	0.031	0.030	0.010	0.023	0.025	0.019	0.011	0.017	0.019
D1d_2	0.090	0.099	0.010	0.026	0.049	0.005	0.008	0.017	0.011	0.005	0.009	0.011
D1d_3	0.124	0.089	0.013	0.028	0.036	0.008	0.014	0.025	0.017	0.009	0.013	0.017
D1d_4	0.210	0.211	0.011	0.182	0.169	0.006	0.016	0.022	0.011	0.008	0.010	0.011
D1d_5	0.159	0.085	0.017	0.031	0.031	0.010	0.023	0.030	0.021	0.012	0.017	0.022
D1d_6	0.159	0.091	0.019	0.032	0.032	0.011	0.022	0.030	0.022	0.013	0.019	0.023
D1d_7	0.155	0.104	0.027	0.032	0.036	0.013	0.021	0.032	0.024	0.014	0.019	0.022

Table B.6 High-frequency and low-frequency incident and reflected wave heights at three locations in the cross shore

Experiment	Mean (m/s)				Standard deviation (m/s)			
	EMS1	EMS2	EMS3	EMS4	EMS1	EMS2	EMS3	EMS4
a1a_1	-0.044	-0.062	NaN	0.000	0.182	0.160	NaN	0.005
a1a_2	-0.045	-0.035	NaN	-0.000	0.175	0.058	NaN	0.005
a1a_3	-0.043	-0.010	NaN	0.001	0.175	0.039	NaN	0.005
a1a_4	-0.040	-0.006	0.182	0.001	0.175	0.032	0.118	0.005
a1a_5	-0.040	-0.005	-0.053	0.000	0.171	0.033	0.117	0.005
a1a_6	-0.042	-0.002	-0.028	0.000	0.180	0.031	0.116	0.005
a1a_7	-0.042	-0.003	-0.021	-0.000	0.183	0.032	0.110	0.005
a1a_8	-0.044	-0.006	0.015	-0.001	0.186	0.034	0.083	0.005
a1a_9	-0.045	-0.004	-0.026	-0.000	0.191	0.028	0.103	0.005
a1a_10	-0.059	-0.009	-0.079	0.000	0.187	0.032	0.123	0.005
a1a_11	-0.045	-0.005	-0.023	-0.001	0.187	0.029	0.123	0.005
a1a_12	-0.045	-0.006	-0.032	0.004	0.186	0.034	0.129	0.004
a1a_13	-0.047	-0.006	-0.007	0.003	0.183	0.030	0.133	0.005
a1a_14	-0.044	-0.004	-0.025	0.007	0.183	0.029	0.135	0.004
a1a_15	-0.042	-0.005	-0.016	0.001	0.183	0.032	0.133	0.005
a1a_16	-0.043	-0.003	-0.006	0.006	0.186	0.031	0.131	0.004
a1a_17	-0.045	-0.002	-0.010	0.001	0.186	0.028	0.125	0.005
a1a_18	-0.044	-0.004	0.056	-0.005	0.187	0.028	0.125	0.004
a1a_19	-0.047	-0.007	0.001	0.002	0.189	0.028	0.106	0.005
a1a_20	-0.046	-0.005	0.000	-0.002	0.188	0.033	0.088	0.005
a1a_21	-0.048	-0.000	NaN	-0.001	0.189	0.029	NaN	0.005
a1a_22	-0.046	-0.002	NaN	-0.000	0.181	0.028	NaN	0.005
a1a_23	-0.045	-0.004	NaN	-0.001	0.177	0.028	NaN	0.005
a1a_24	-0.043	-0.004	NaN	-0.001	0.173	0.029	NaN	0.005
a1a_25	-0.042	-0.004	NaN	-0.001	0.174	0.033	NaN	0.005
a1a_26	-0.045	-0.019	NaN	-0.001	0.174	0.040	NaN	0.005
a1d_1	-0.042	-0.006	-0.152	-0.002	0.180	0.029	0.136	0.005
a1d_2	-0.040	-0.003	-0.012	0.000	0.175	0.030	0.143	0.005
a1d_3	-0.039	-0.001	-0.019	0.001	0.173	0.031	0.148	0.005
a1d_4	-0.039	-0.006	-0.019	-0.000	0.172	0.029	0.147	0.005
a1d_5	-0.043	-0.006	-0.027	-0.001	0.186	0.030	0.152	0.005
a1d_6	-0.047	-0.004	-0.032	-0.001	0.198	0.030	0.155	0.007
a1d_7	NaN	NaN	NaN	NaN	NaN	NaN	NaN	NaN
a2a_1	-0.039	-0.055	0.001	0.000	0.190	0.173	0.145	0.005
a2a_2	-0.043	-0.059	-0.014	-0.002	0.188	0.183	0.134	0.005
a2a_3	-0.040	-0.056	-0.014	-0.000	0.178	0.172	0.136	0.005
a2a_4	-0.041	-0.047	-0.024	0.004	0.182	0.168	0.140	0.004
a2a_5	-0.043	-0.045	-0.011	-0.001	0.182	0.166	0.142	0.005
a2d_1	-0.044	-0.058	-0.038	0.001	0.185	0.200	0.167	0.005
a2d_2	-0.041	-0.058	-0.057	-0.002	0.181	0.205	0.171	0.005
a2d_3	-0.036	-0.037	-0.027	-0.013	0.169	0.199	0.157	0.034
b1a_1	-0.045	-0.045	-0.004	-0.001	0.210	0.174	0.155	0.005
b1a_2	-0.048	-0.054	-0.007	0.001	0.209	0.180	0.146	0.005
b1a_3	-0.048	-0.047	-0.014	-0.000	0.202	0.171	0.141	0.005
b1a_4	-0.048	-0.048	-0.010	0.002	0.203	0.167	0.146	0.005
b1a_5	-0.050	-0.044	-0.013	-0.000	0.203	0.163	0.152	0.005
B1d_1	-0.050	-0.045	-0.018	0.000	0.203	0.165	0.161	0.005
B1d_2	-0.049	-0.040	-0.004	-0.001	0.213	0.172	0.171	0.005

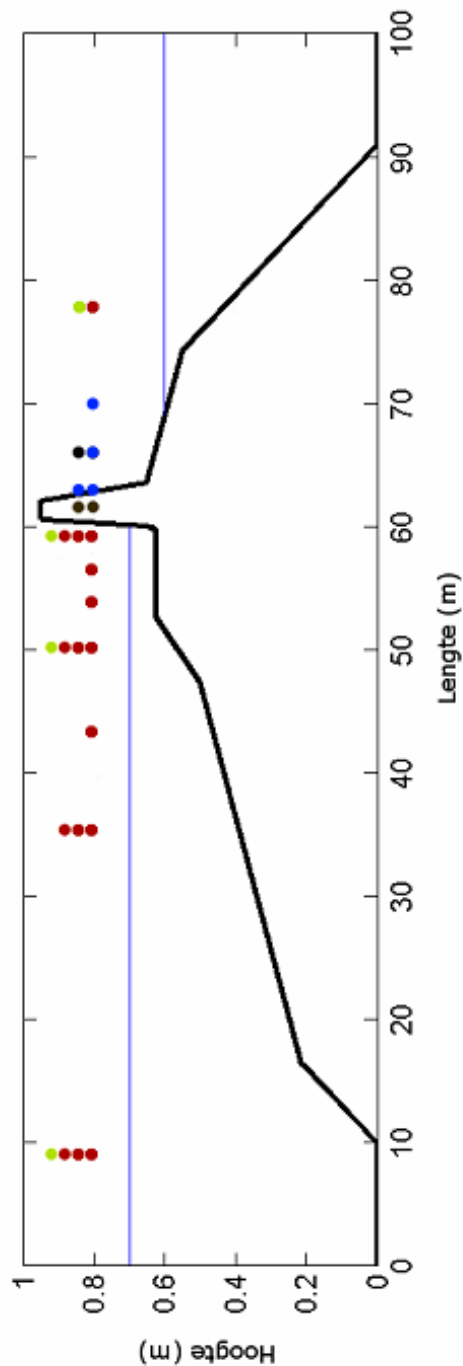
continues on next page...

	Mean (m/s)				Standard deviation (m/s)			
B1d_3	-0.046	-0.040	-0.011	0.001	0.202	0.165	0.178	0.005
B1d_4	-0.045	-0.044	-0.036	0.001	0.204	0.173	0.183	0.005
B1d_5	-0.047	-0.041	-0.022	-0.000	0.202	0.177	0.183	0.006
B1d_6	-0.046	-0.047	-0.029	0.001	0.200	0.183	0.186	0.006
B1d_7	-0.042	-0.037	-0.031	-0.001	0.199	0.183	0.190	0.010
B2a_1	-0.034	-0.053	0.007	-0.003	0.183	0.181	0.161	0.005
B2a_2	-0.033	-0.049	-0.004	-0.002	0.193	0.188	0.153	0.005
B2a_3	-0.036	-0.049	-0.007	-0.004	0.191	0.180	0.148	0.005
B2a_4	-0.034	-0.047	-0.007	0.000	0.192	0.175	0.154	0.005
B2a_5	-0.040	-0.044	-0.004	-0.000	0.192	0.171	0.162	0.005
b2d_1	-0.045	-0.047	0.000	-0.000	0.181	0.169	0.154	0.007
b2d_2	-0.041	-0.046	-0.008	-0.001	0.178	0.173	0.157	0.007
b2d_3	-0.040	-0.053	-0.021	0.001	0.175	0.177	0.158	0.006
b2d_4	-0.039	-0.053	-0.027	-0.001	0.172	0.183	0.162	0.006
b2d_5	-0.0335	-0.0438	-0.0235	0.0006	0.1570	0.1703	0.1482	0.0065
b2d_7	-0.0431	-0.0453	-0.0255	-0.0021	0.1905	0.1821	0.1579	0.0139
C1a_1	-0.038	-0.000	-0.146	-0.002	0.184	0.038	0.261	0.005
C1a_2	-0.040	-0.000	-0.286	-0.002	0.183	0.034	0.345	0.005
C1a_3	-0.039	-0.002	0.044	-0.000	0.180	0.035	0.248	0.005
C1a_4	-0.041	-0.003	0.167	0.003	0.180	0.036	0.260	0.004
C1a_5	-0.039	-0.005	0.056	-0.001	0.179	0.036	0.220	0.005
C1d_1	-0.042	-0.006	-0.024	-0.001	0.180	0.047	0.020	0.005
C1d_2	-0.040	-0.006	-0.496	-0.001	0.178	0.063	0.069	0.005
C1d_3	-0.040	-0.006	-0.522	-0.001	0.176	0.061	0.351	0.005
C1d_4	-0.040	-0.008	0.255	-0.001	0.174	0.060	0.222	0.005
C1d_5	-0.039	-0.008	0.027	-0.001	0.172	0.052	0.079	0.005
D1d_1	-0.040	0.001	-0.003	-0.001	0.171	0.049	0.093	0.005
D1d_2	-0.015	-0.001	-0.003	-0.002	0.083	0.023	0.058	0.005
D1d_3	-0.026	-0.003	-0.004	-0.002	0.126	0.028	0.085	0.005
D1d_4	-0.020	-0.001	-0.006	-0.002	0.099	0.027	0.060	0.005
D1d_5	-0.039	-0.004	-0.000	-0.002	0.169	0.031	0.105	0.005
D1d_6	-0.039	-0.051	0.001	-0.002	0.168	0.184	0.110	0.006
D1d_7	-0.035	-0.042	-0.000	-0.003	0.161	0.192	0.114	0.016

Table B.7 Time-average cross shore velocities and standard deviation of the velocity as measured by the four EMS



## **C Figures**

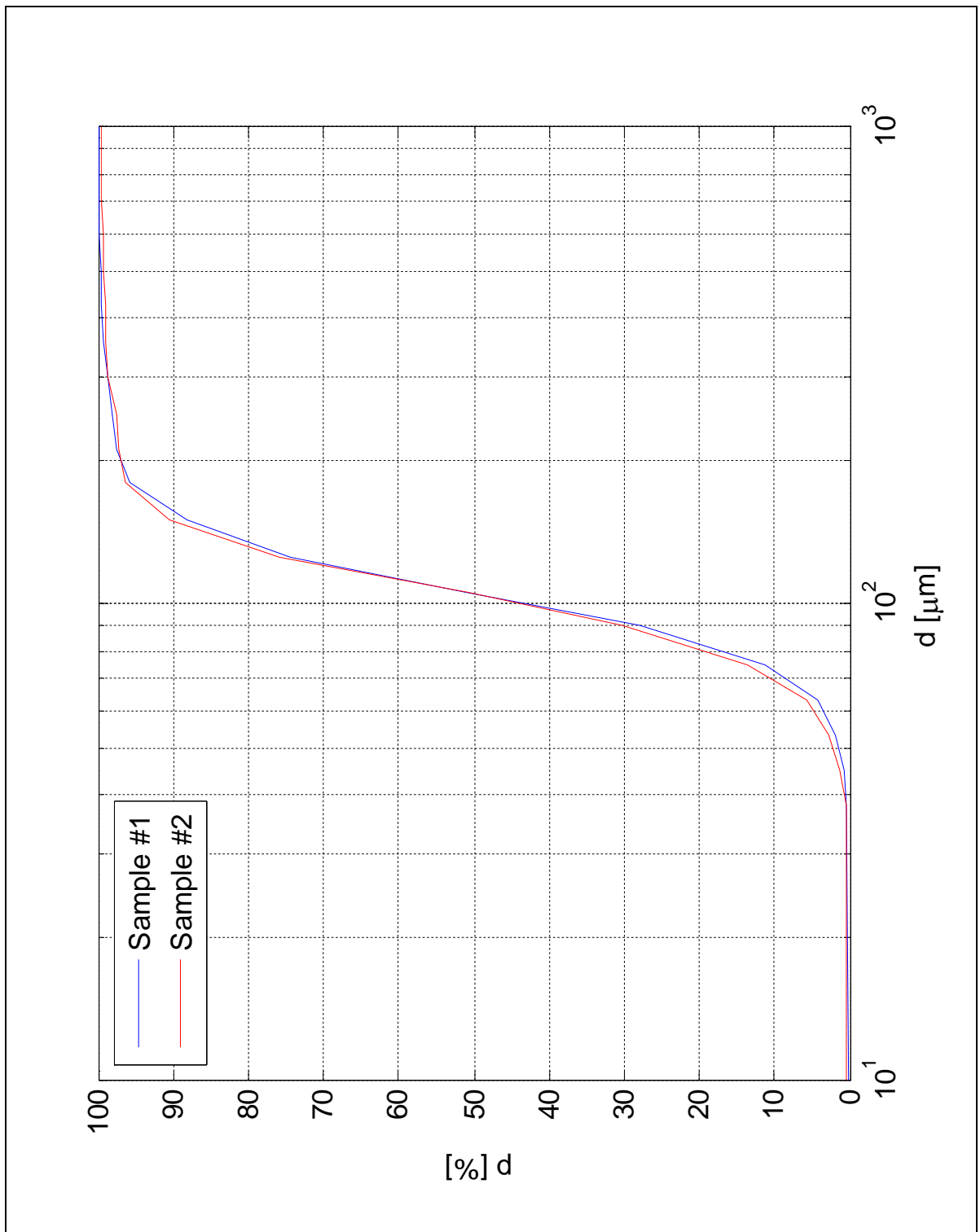


Location of instrumentation during the experiments: 16 wave height meters (red), 4 flow velocity meters (green), 3 layer thickness meters (blue) and three camera's (black).

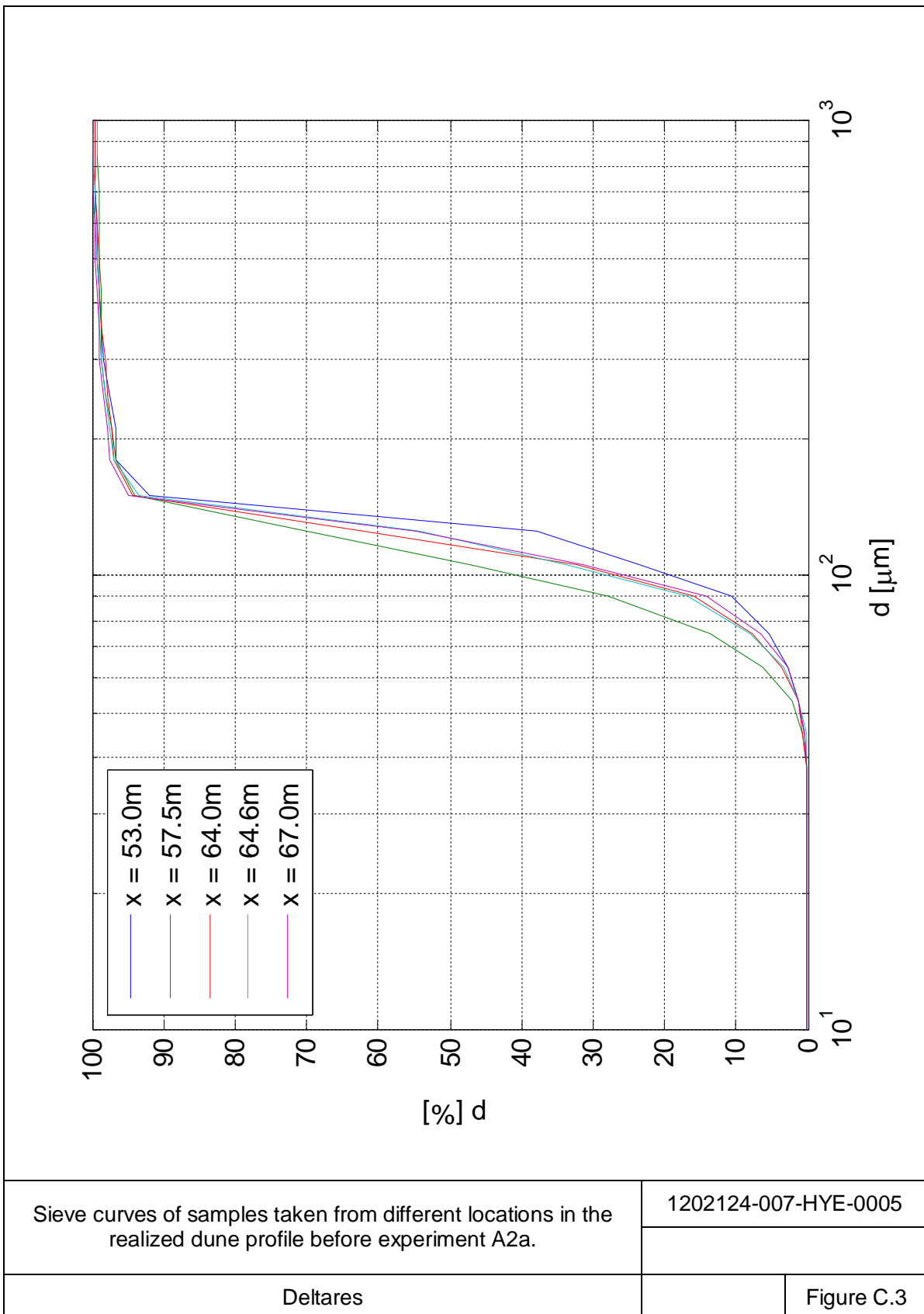
1202124-007-HYE-0005

Deltares

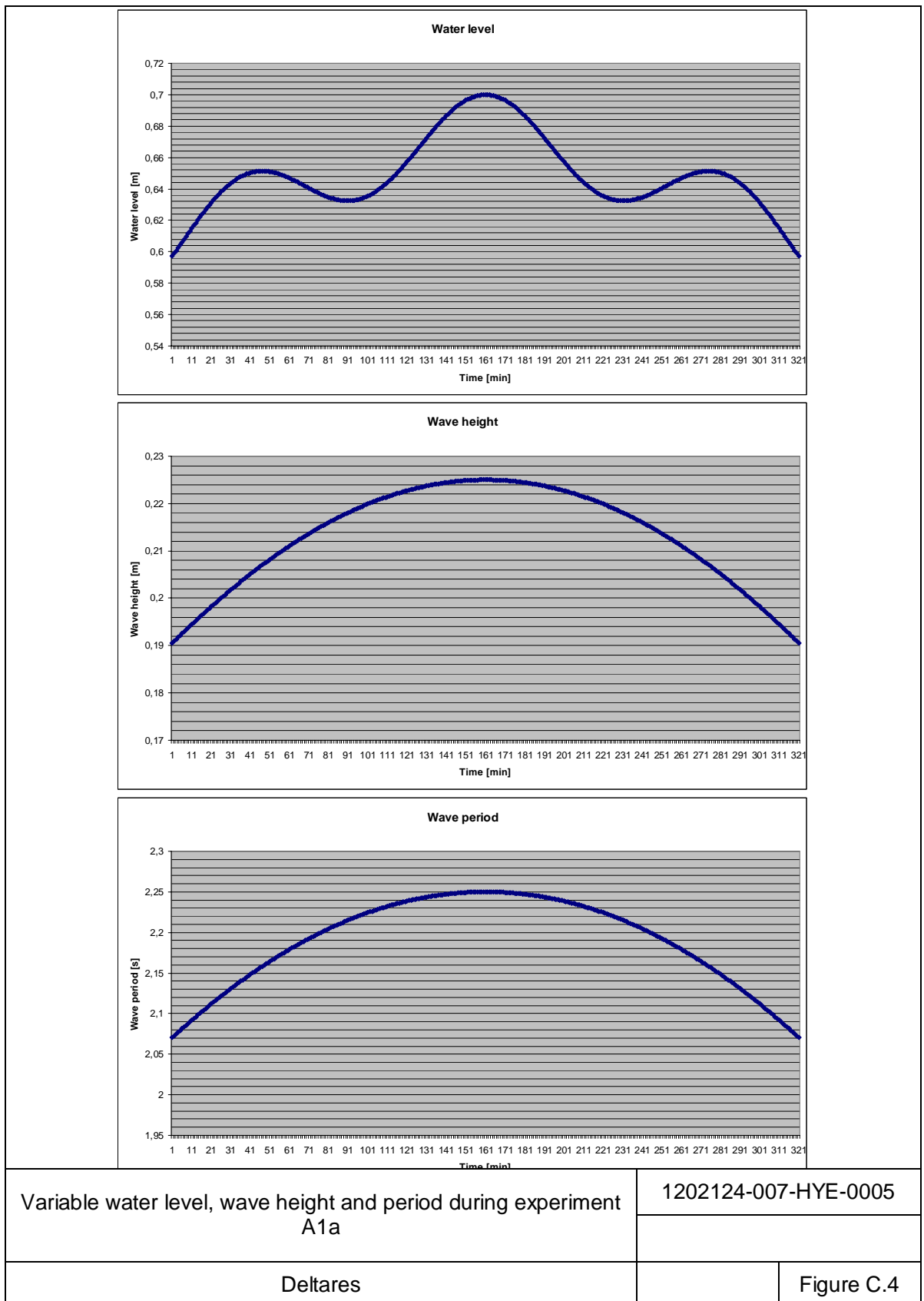
Figure C.1

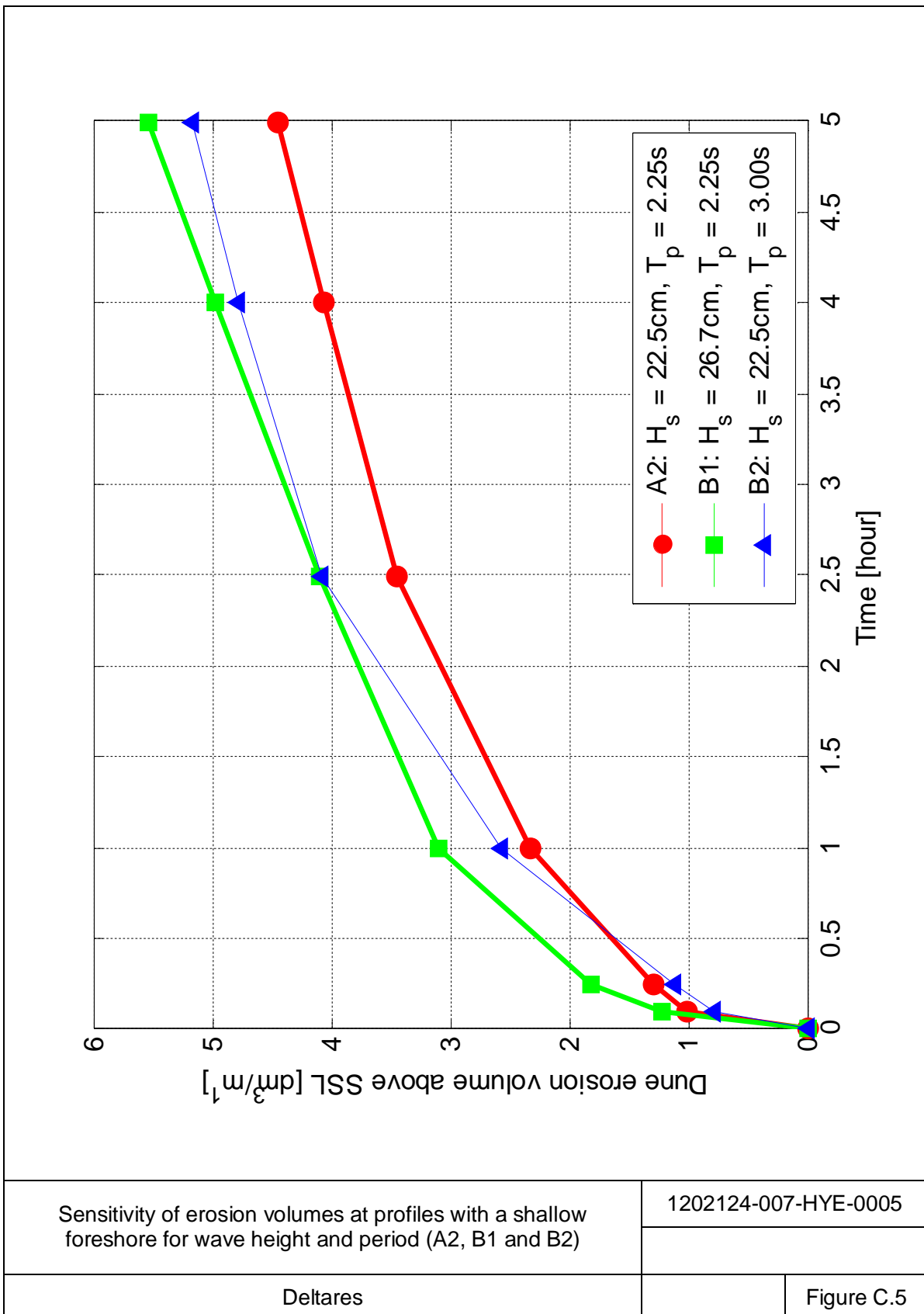


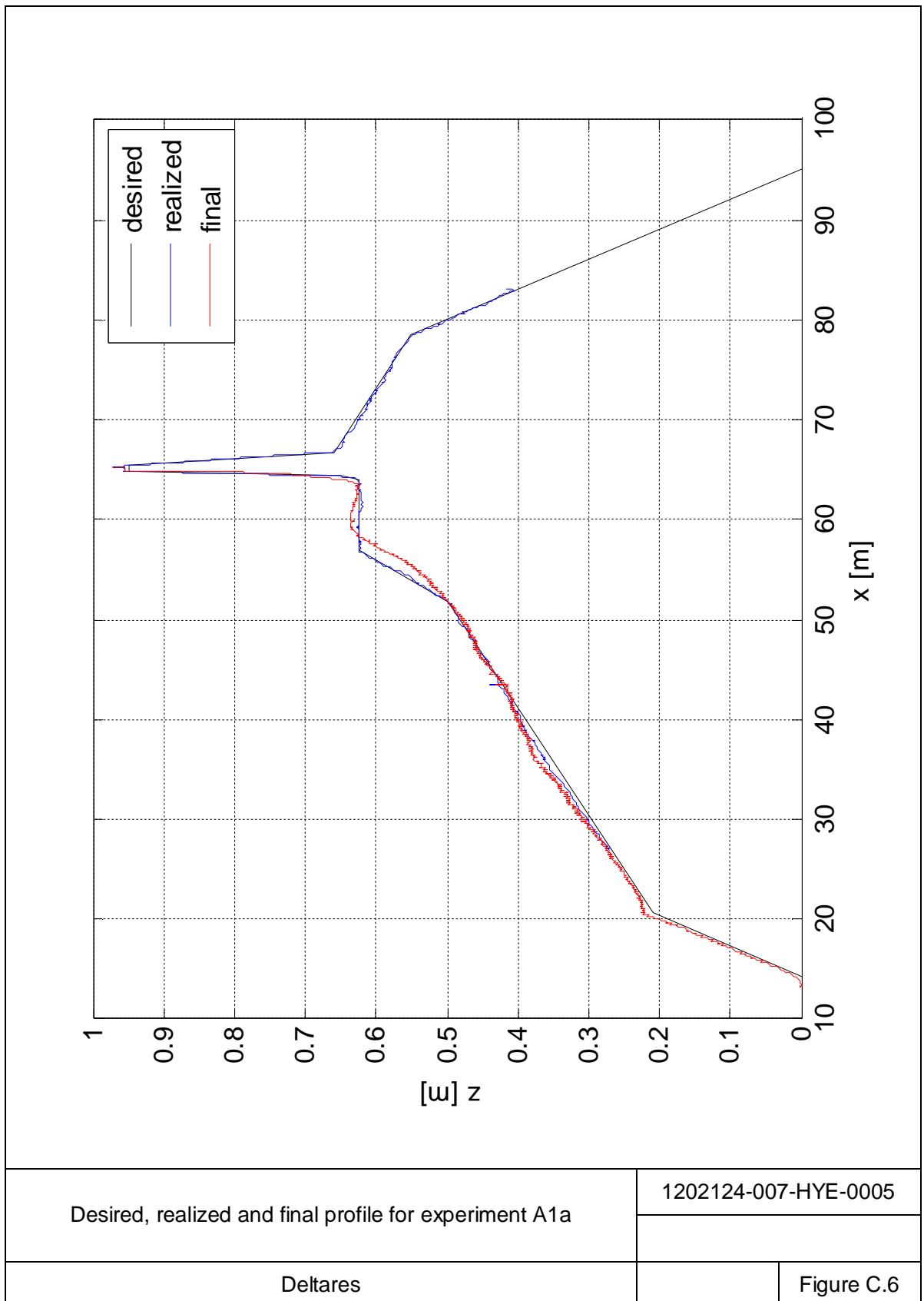
Sieve curves of samples taken from the sediment delivered by <i>Trip-Popken B.V.</i> in Assen.	1202124-007-HYE-0005
Deltares	Figure C.2

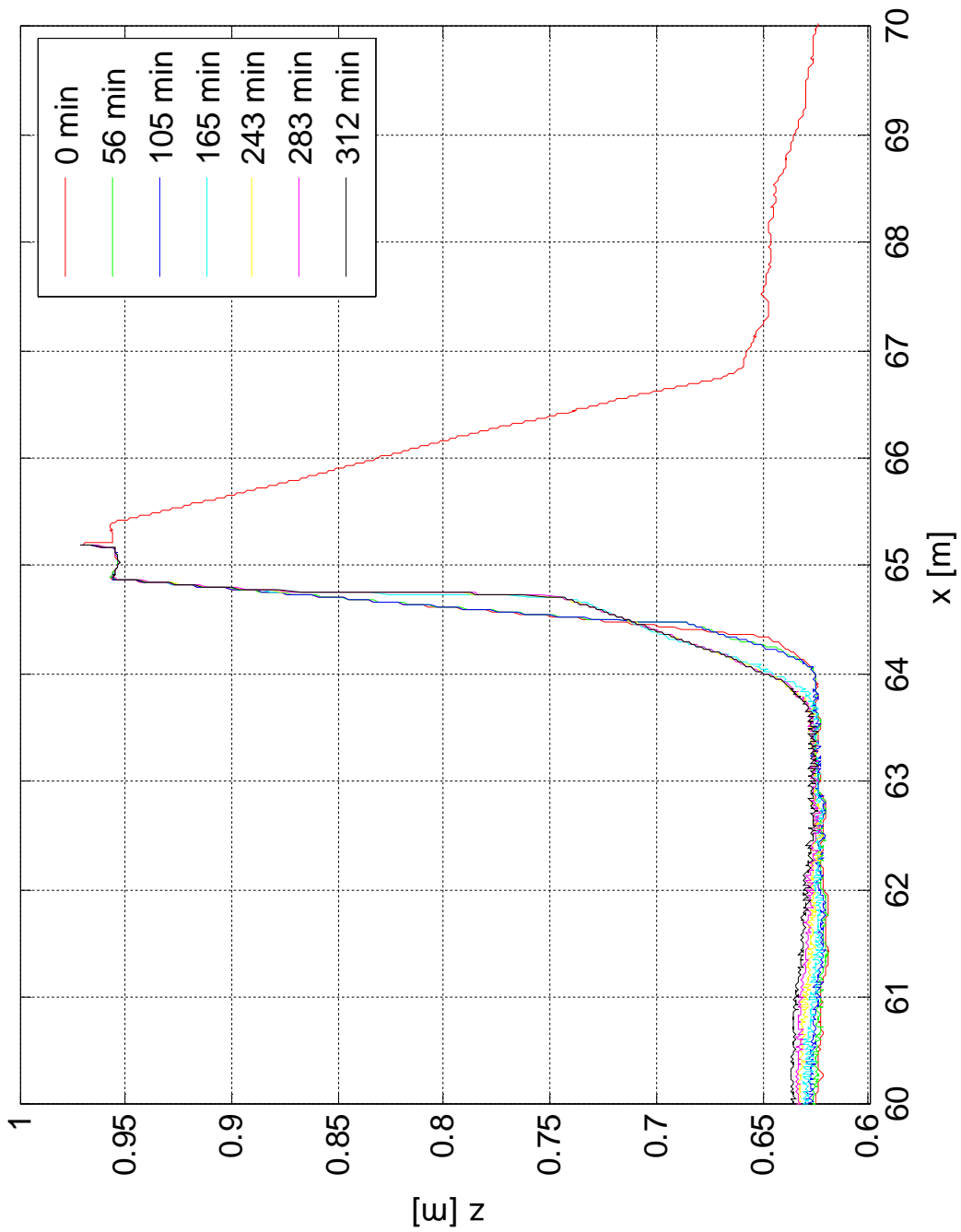






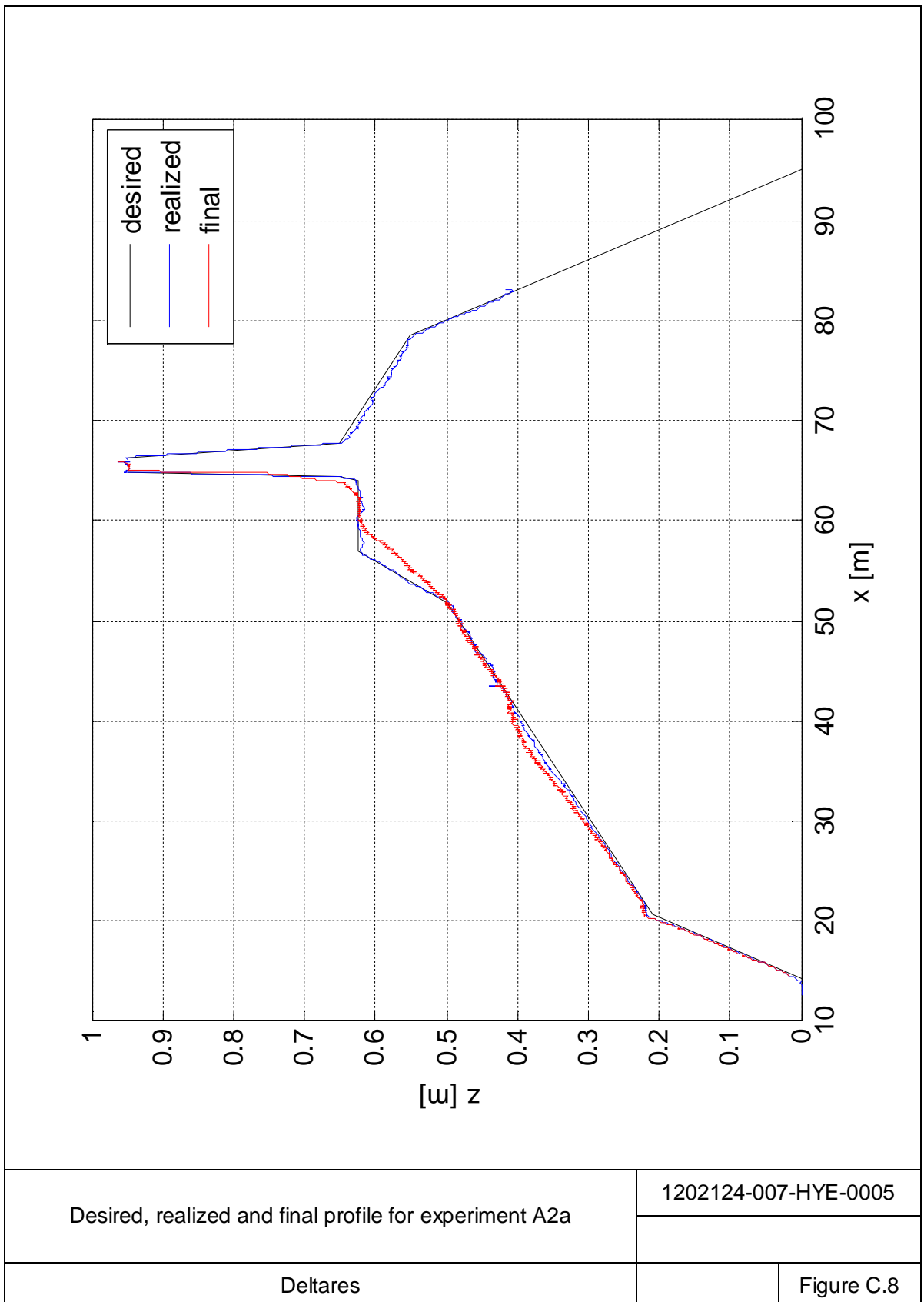






Dune profile development during experiment A1a

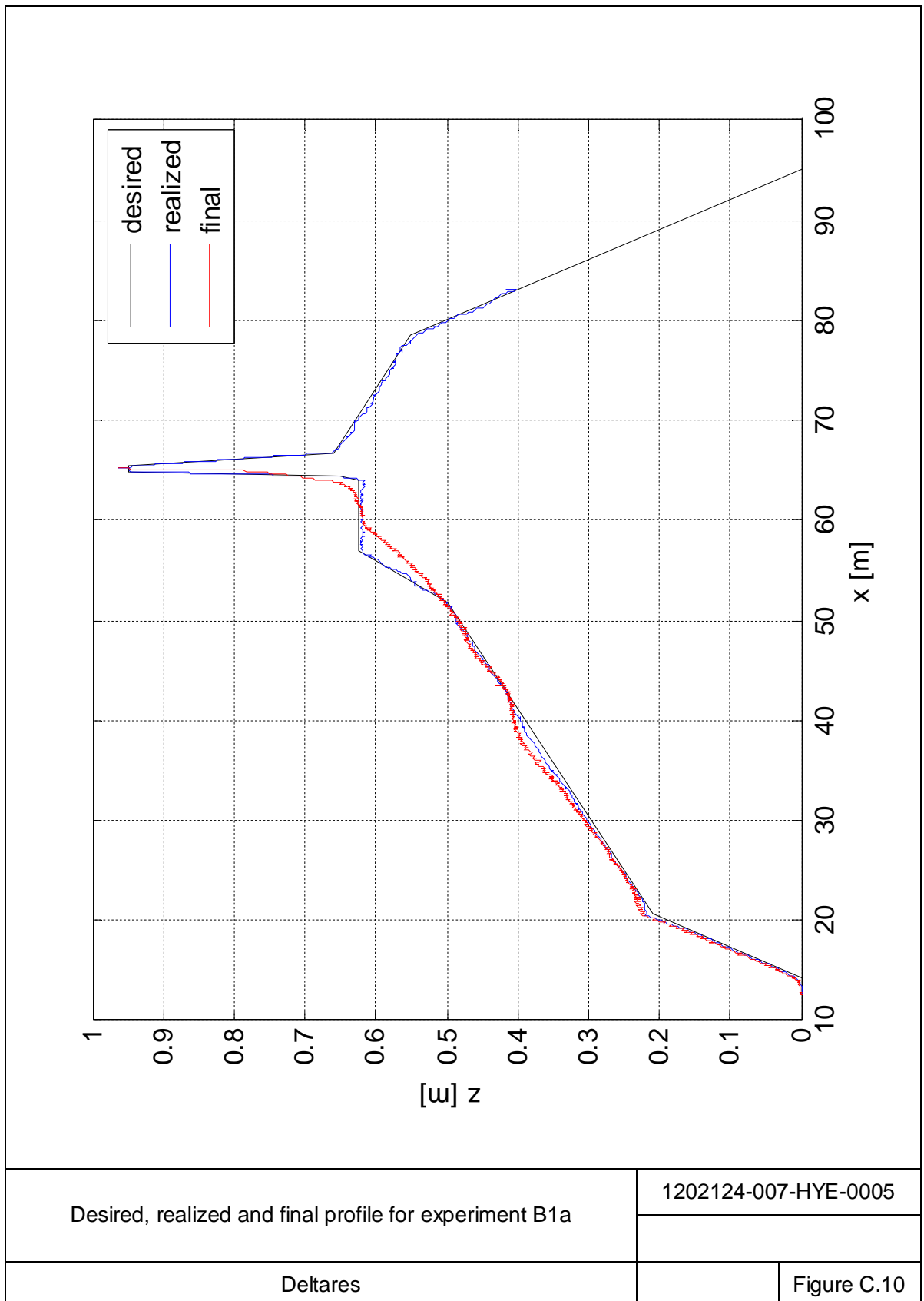
1202124-007-HYE-0005

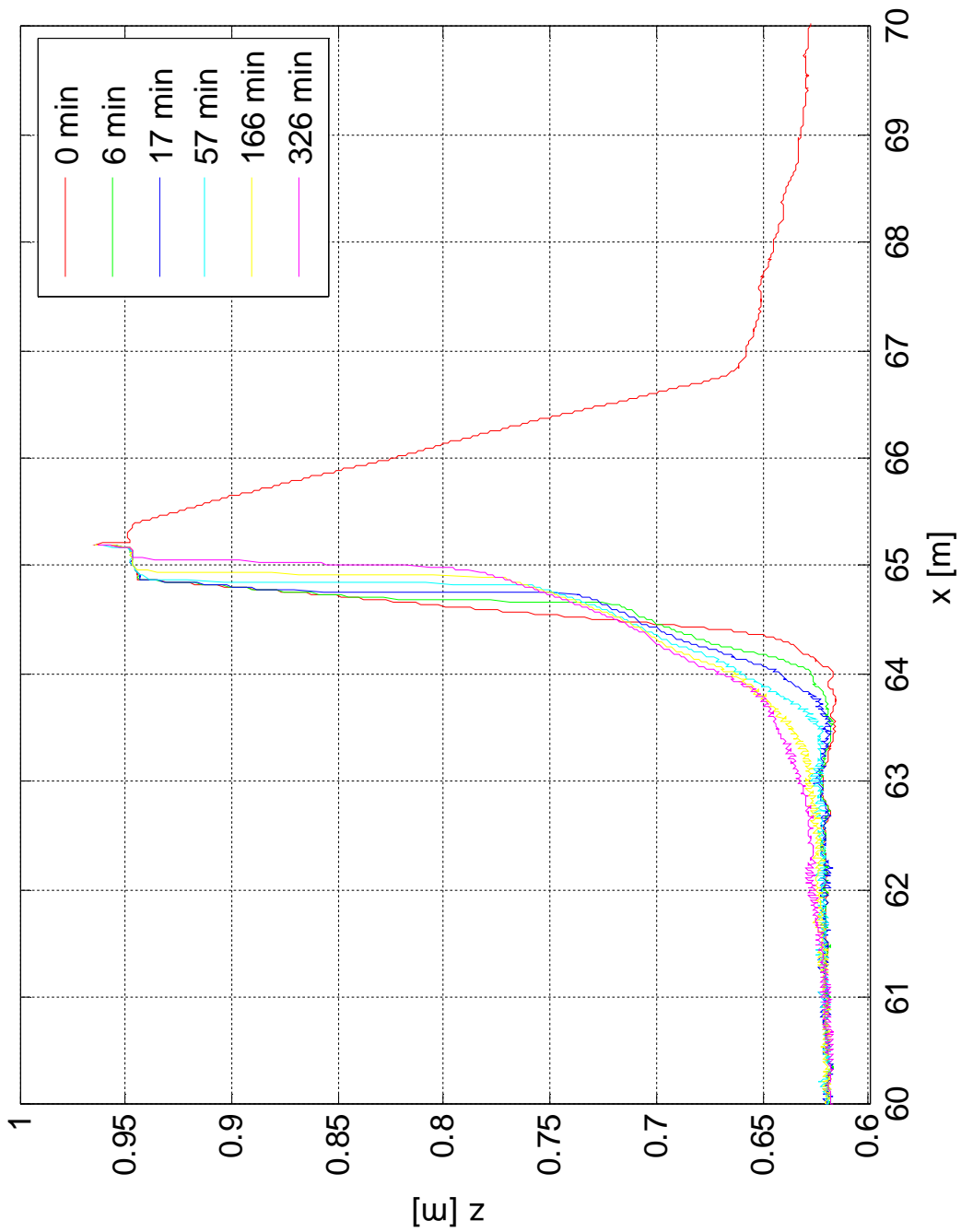




Dune profile development during experiment A2a

1202124-007-HYE-0005

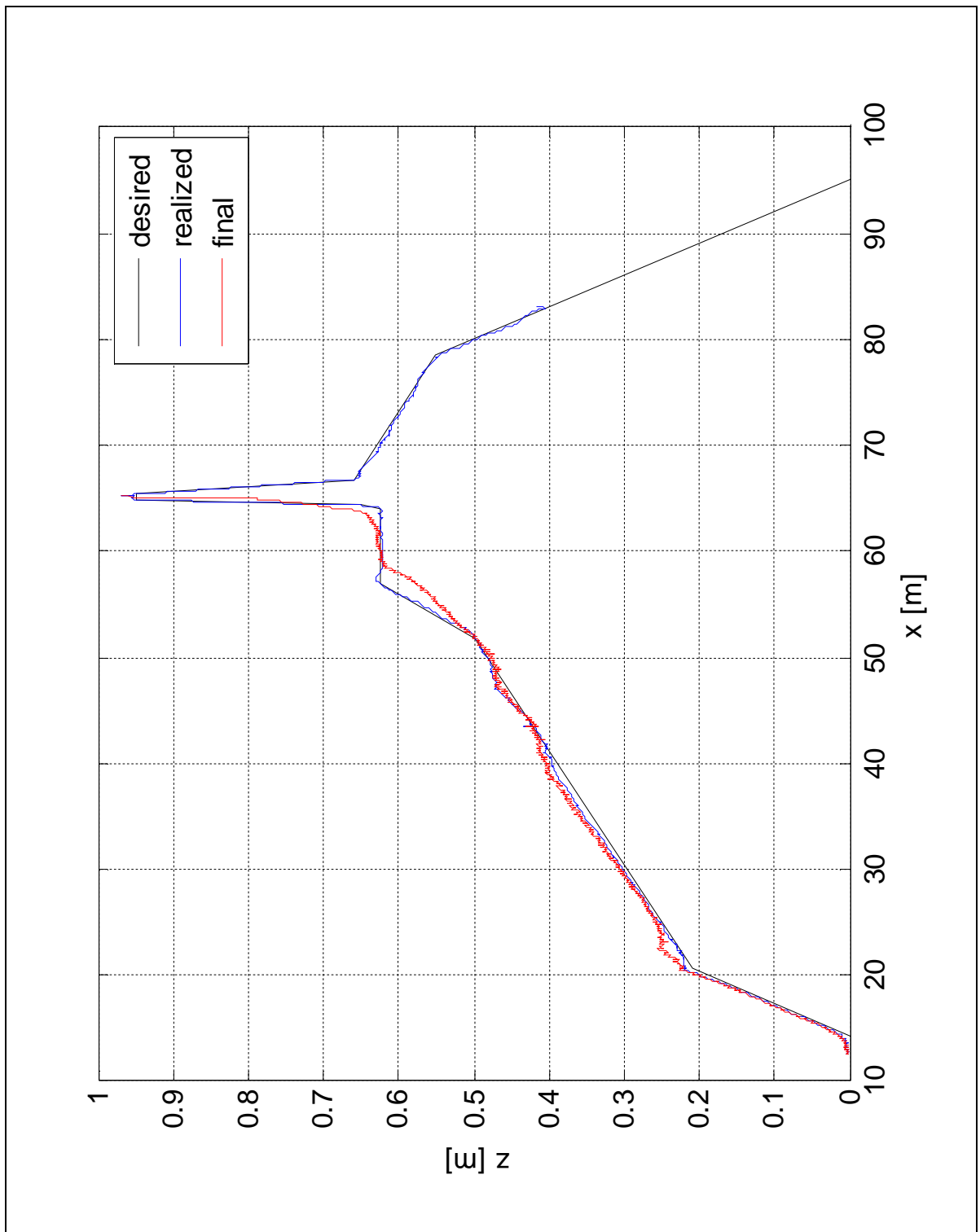




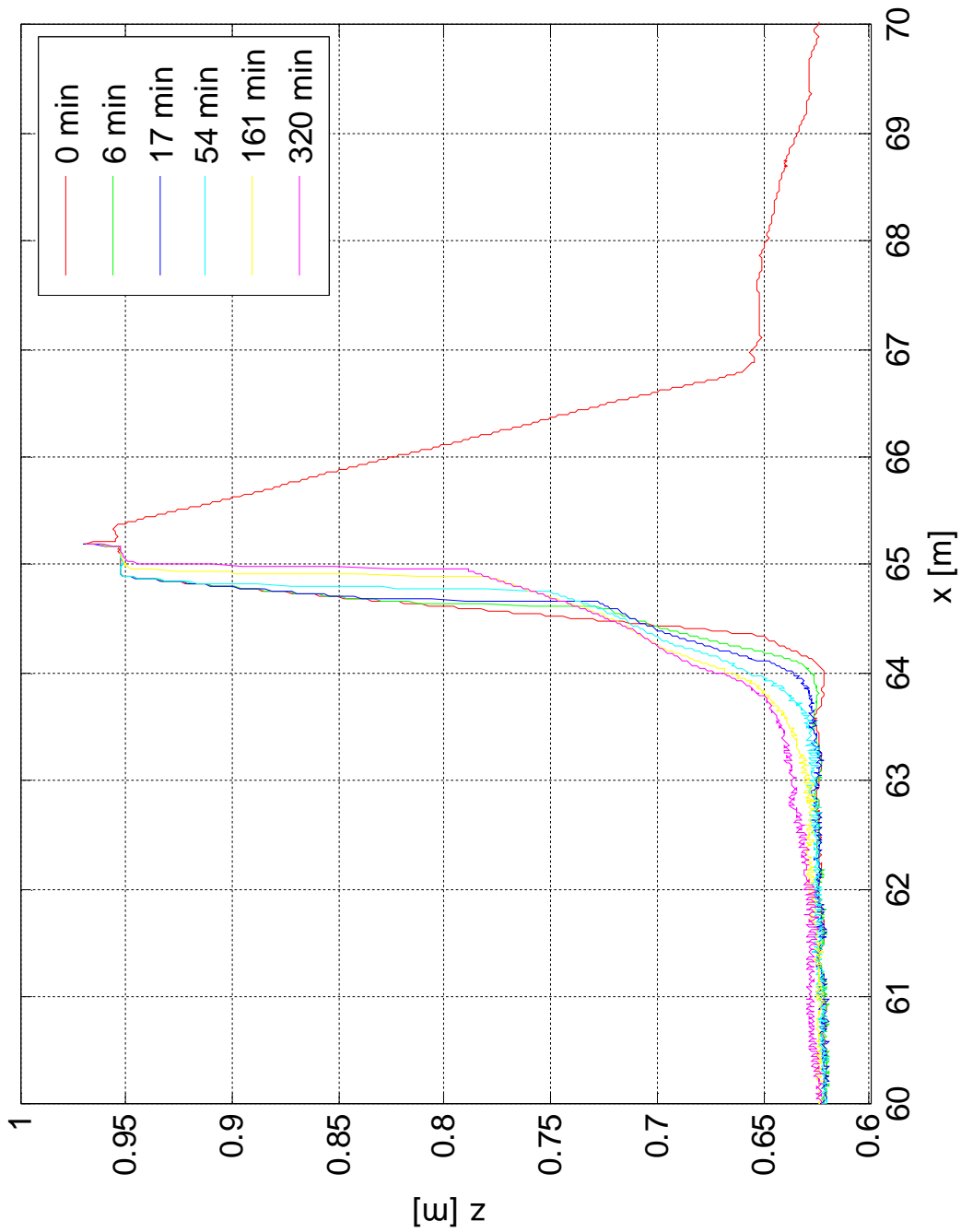
Dune profile development during experiment B1a

1202124-007-HYE-0005



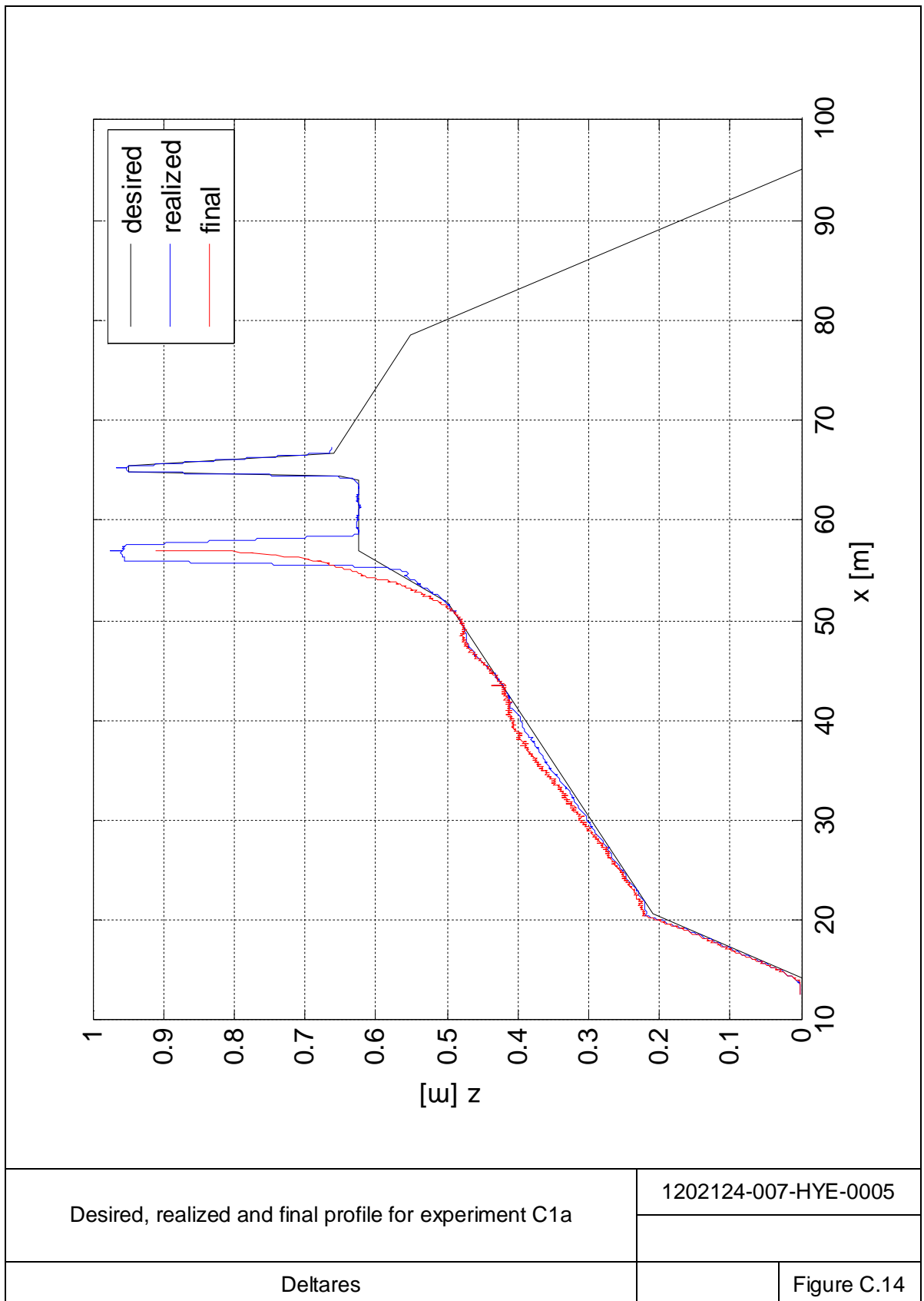


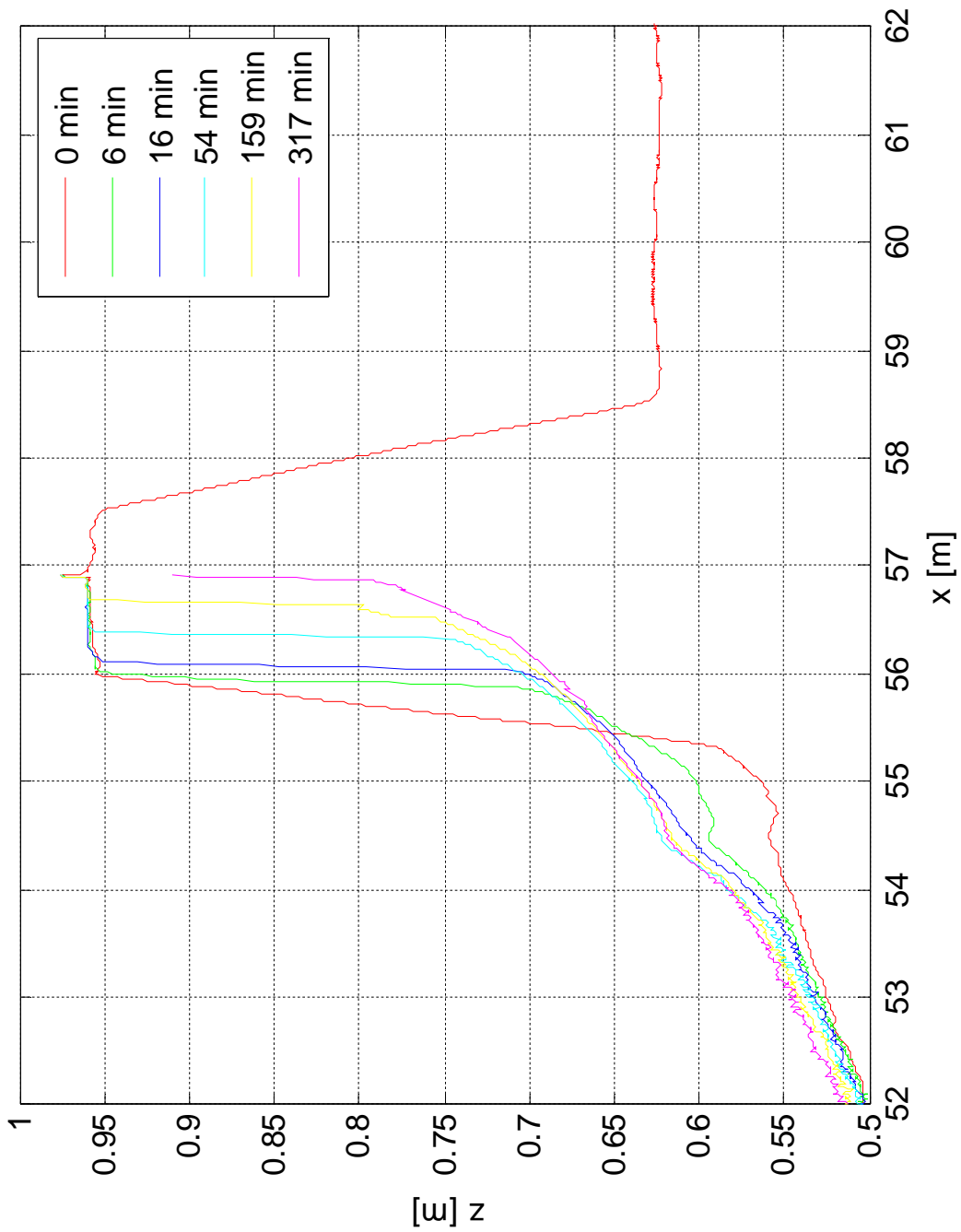
Desired, realized and final profile for experiment B2a	1202124-007-HYE-0005	
Deltares		Figure C.12



Dune profile development during experiment B2a

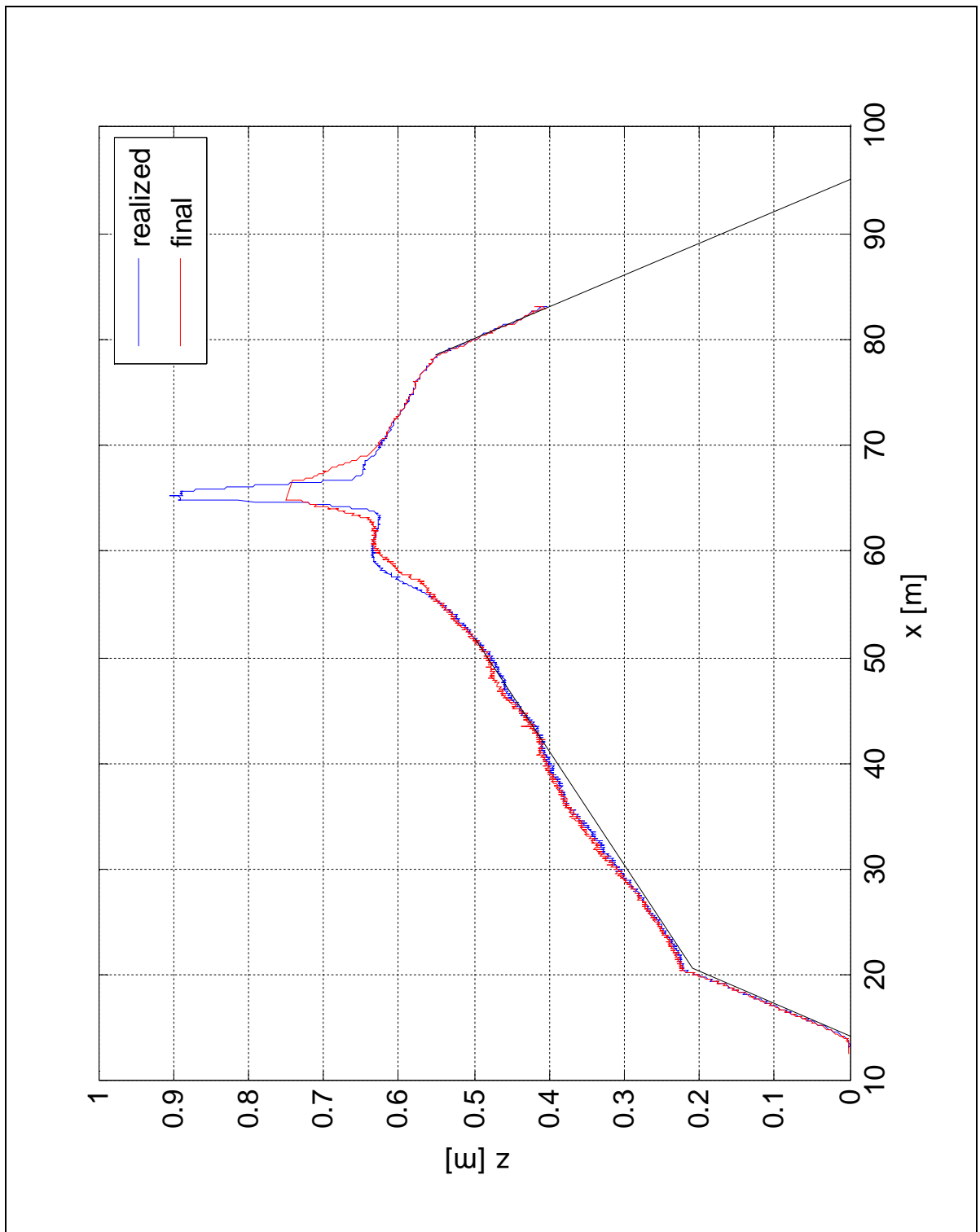
1202124-007-HYE-0005



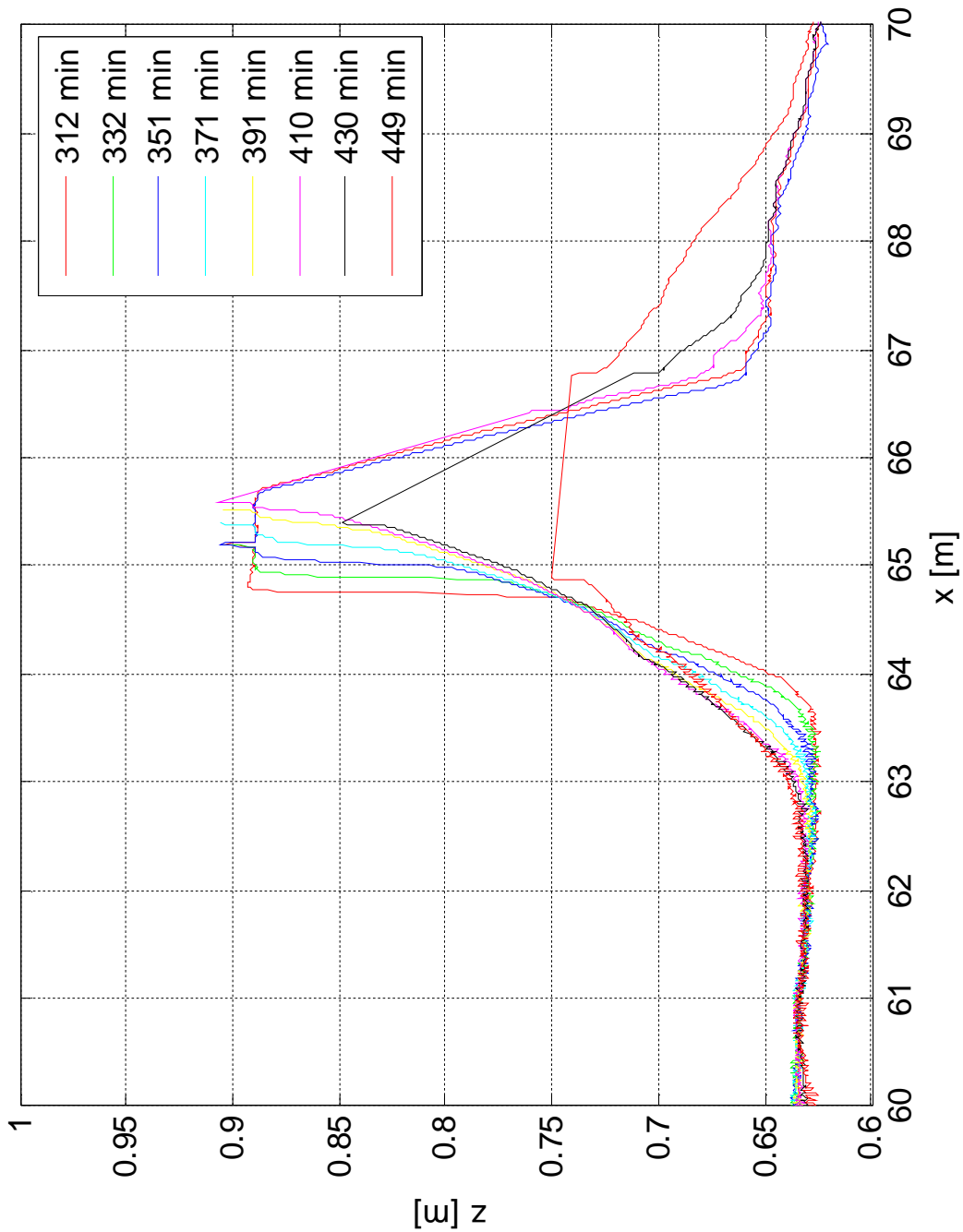


Dune profile development during experiment C1a

1202124-007-HYE-0005

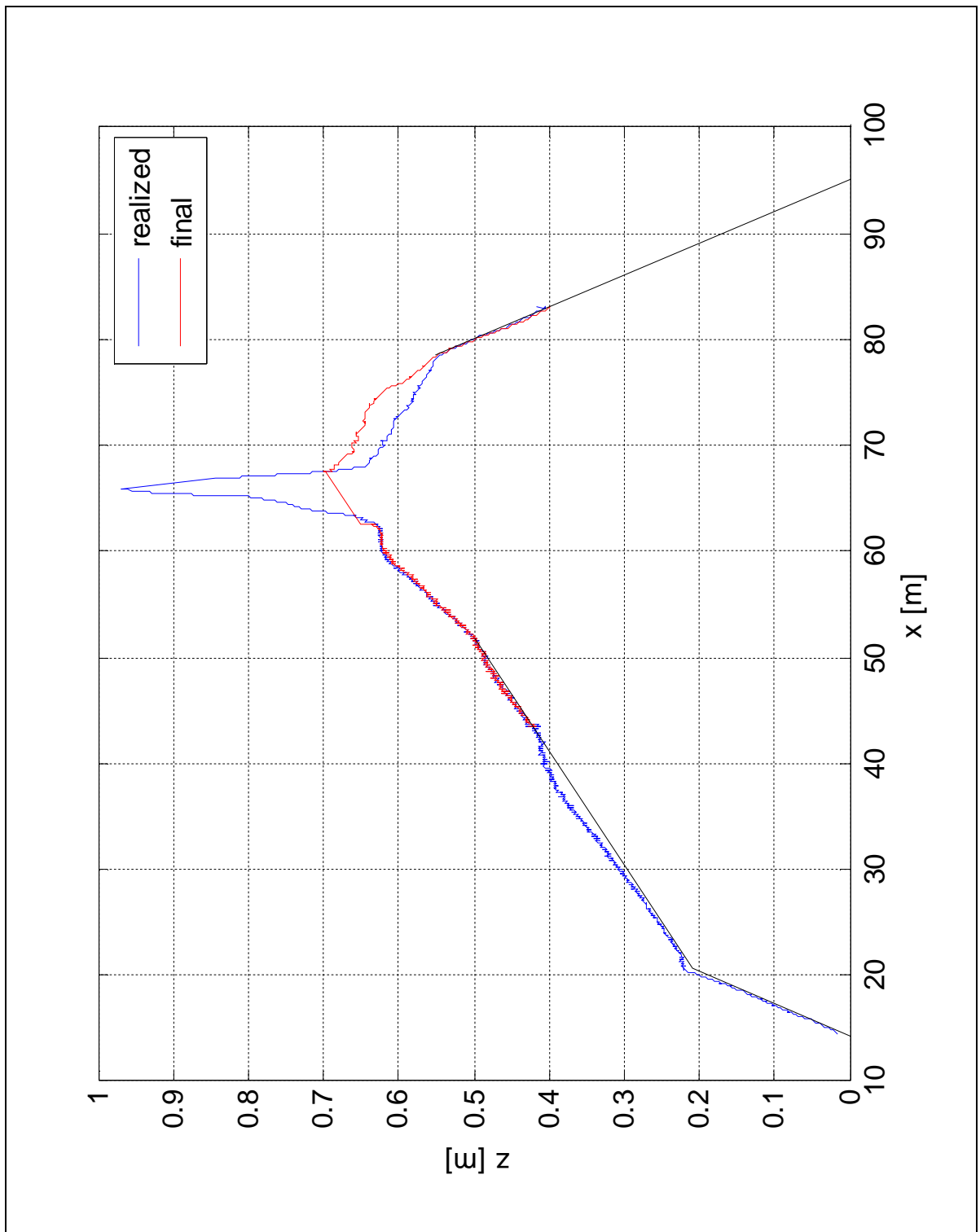


Realized starting profile and final profile for experiment A1d	1202124-007-HYE-0005	
Deltares		Figure C.16

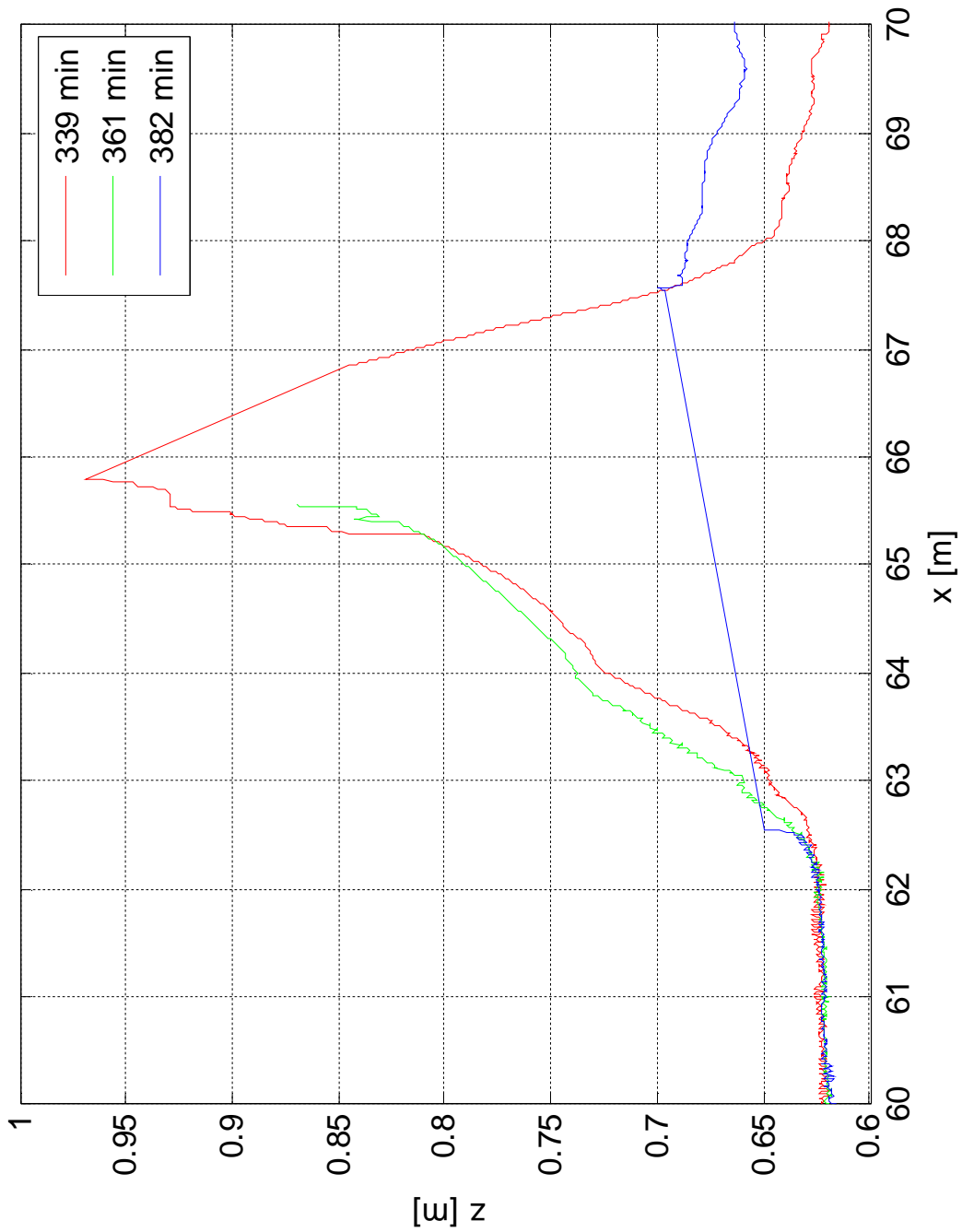


Dune profile development during experiment A1d

1202124-007-HYE-0005



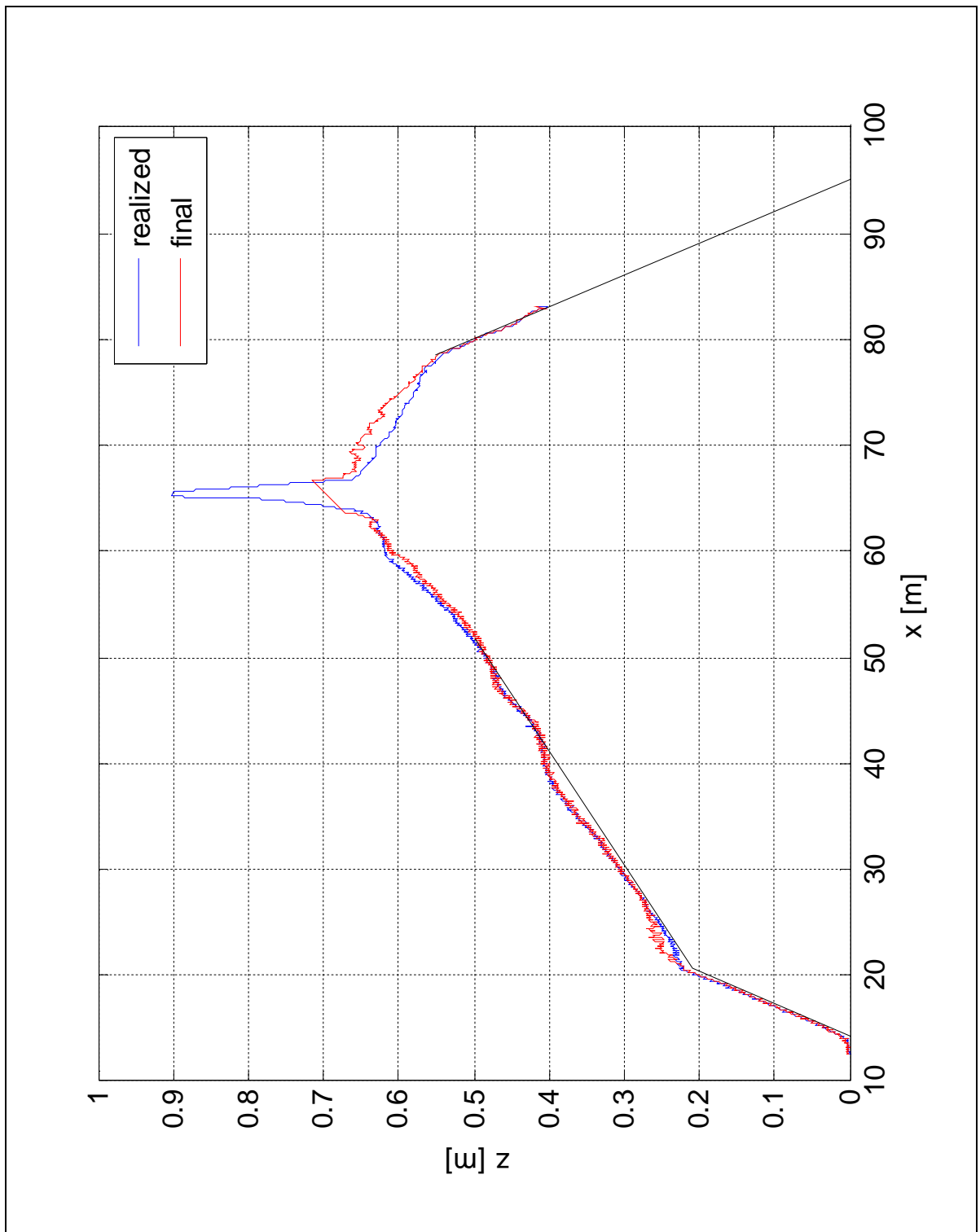
Realized starting profile and final profile for experiment A2d	1202124-007-HYE-0005	
Deltares		Figure C.18



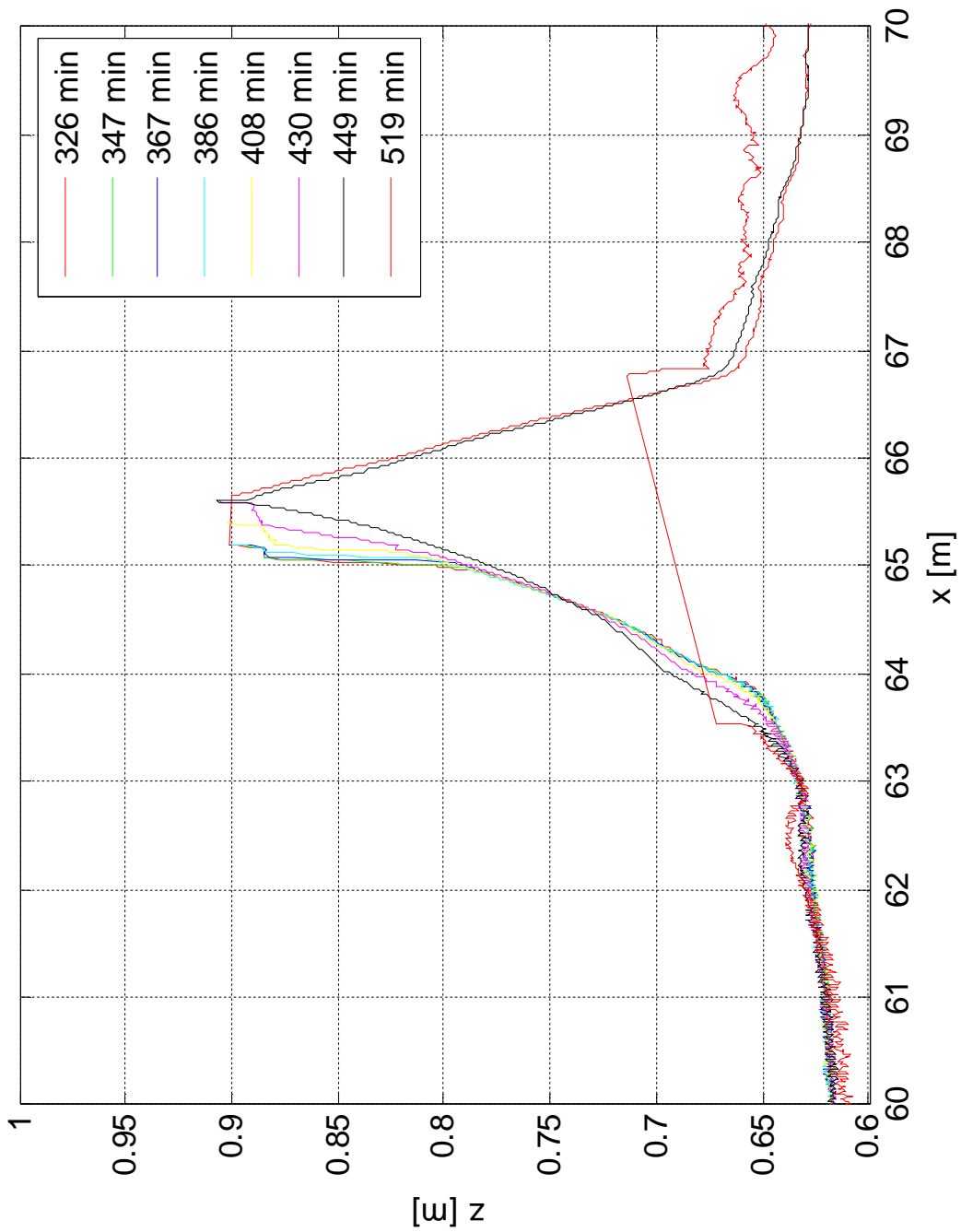
Dune profile development during experiment A2d

1202124-007-HYE-0005



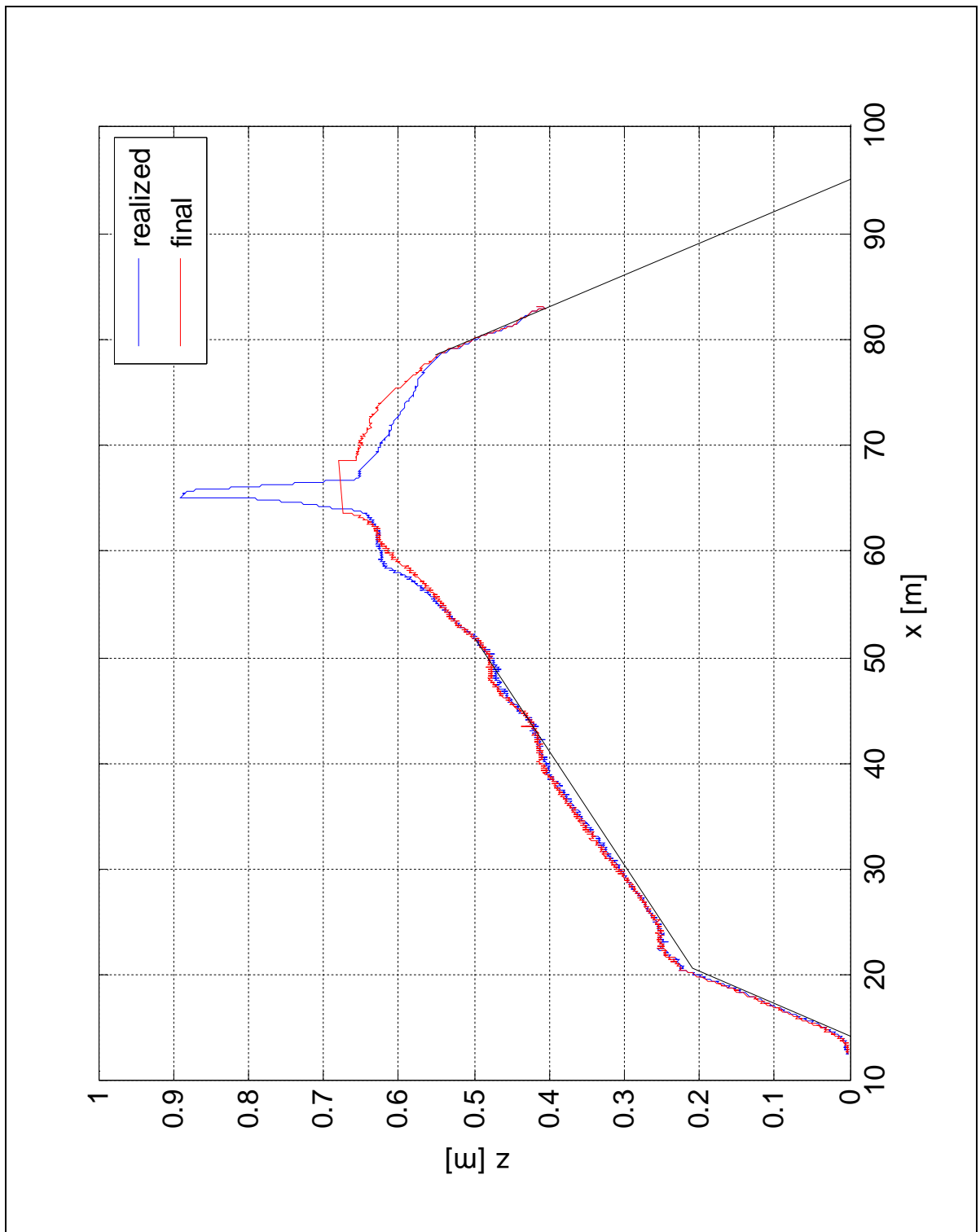


Realized starting profile and final profile for experiment B1d	1202124-007-HYE-0005	
Deltares		Figure C.20

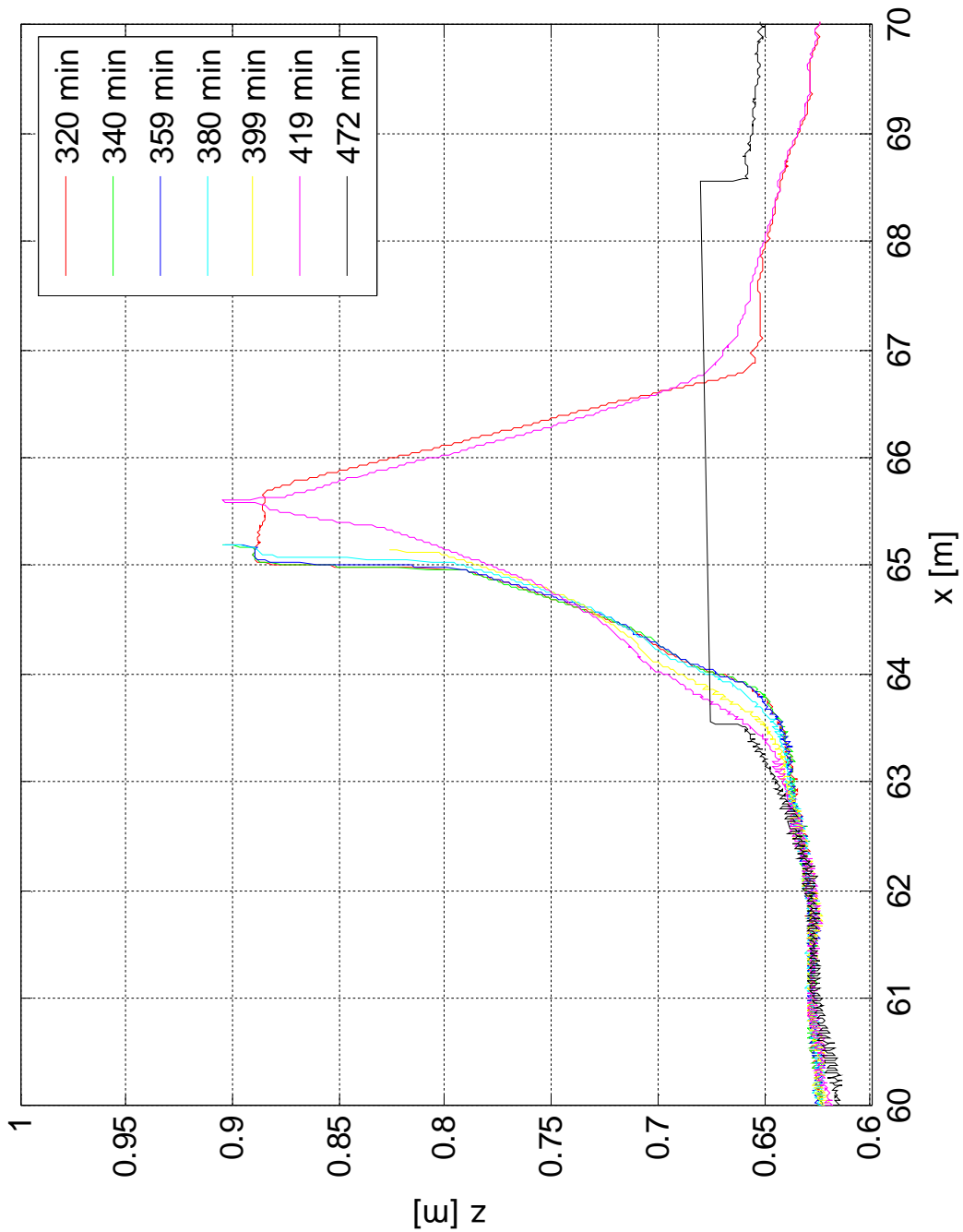


Dune profile development during experiment B1d

1202124-007-HYE-0005

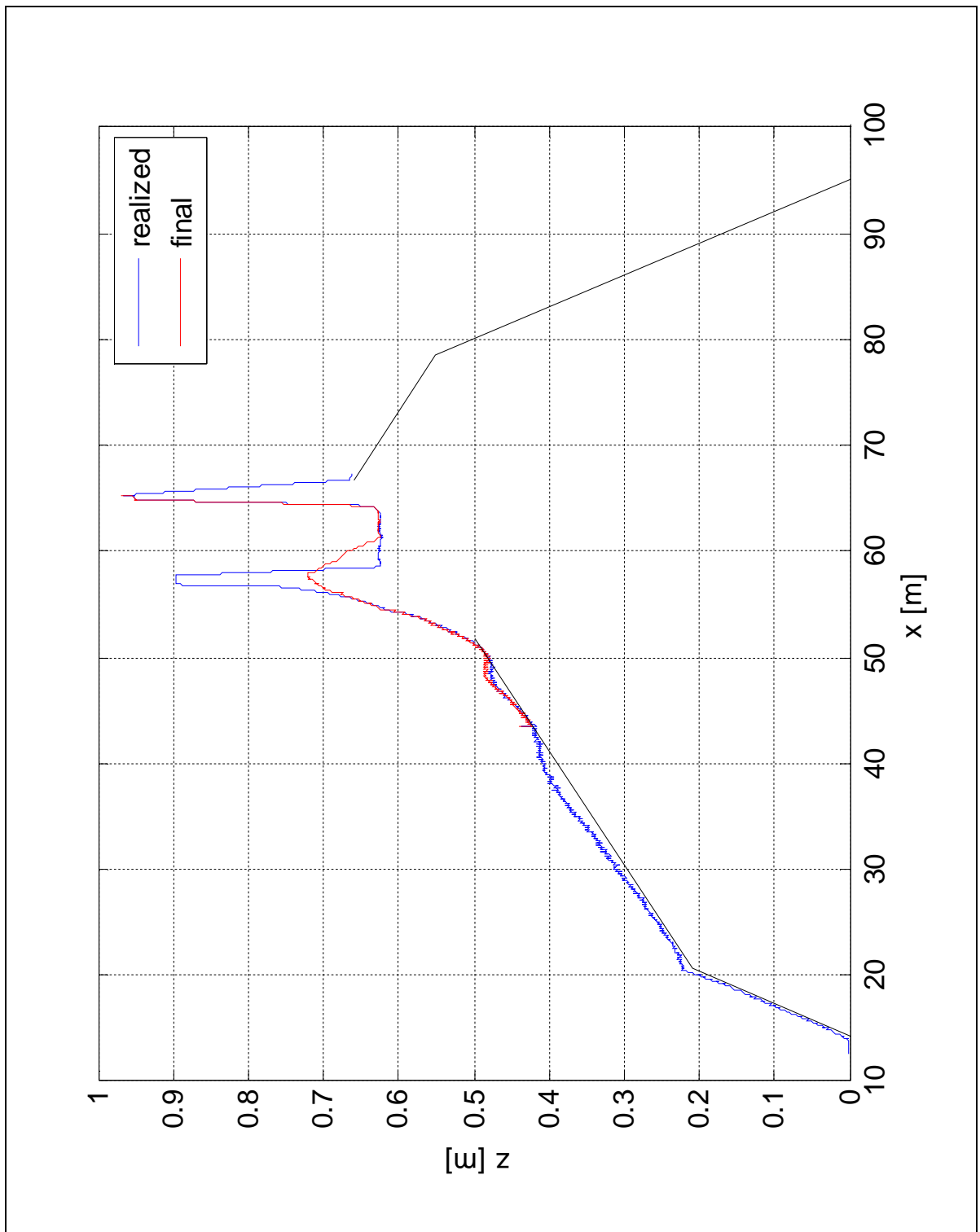


Realized starting profile and final profile for experiment B2d	1202124-007-HYE-0005	
Deltares		Figure C.22

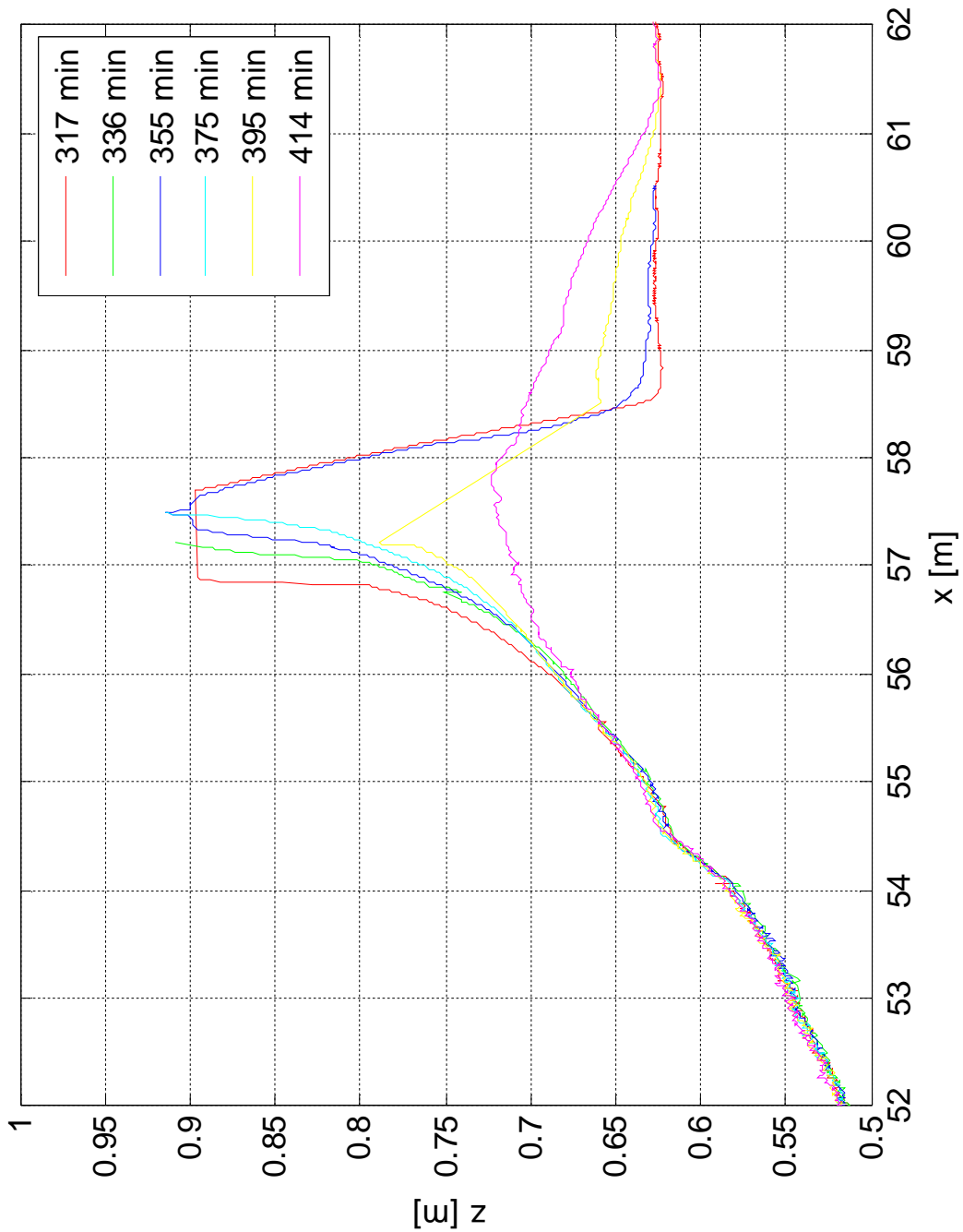


Dune profile development during experiment B2d

1202124-007-HYE-0005

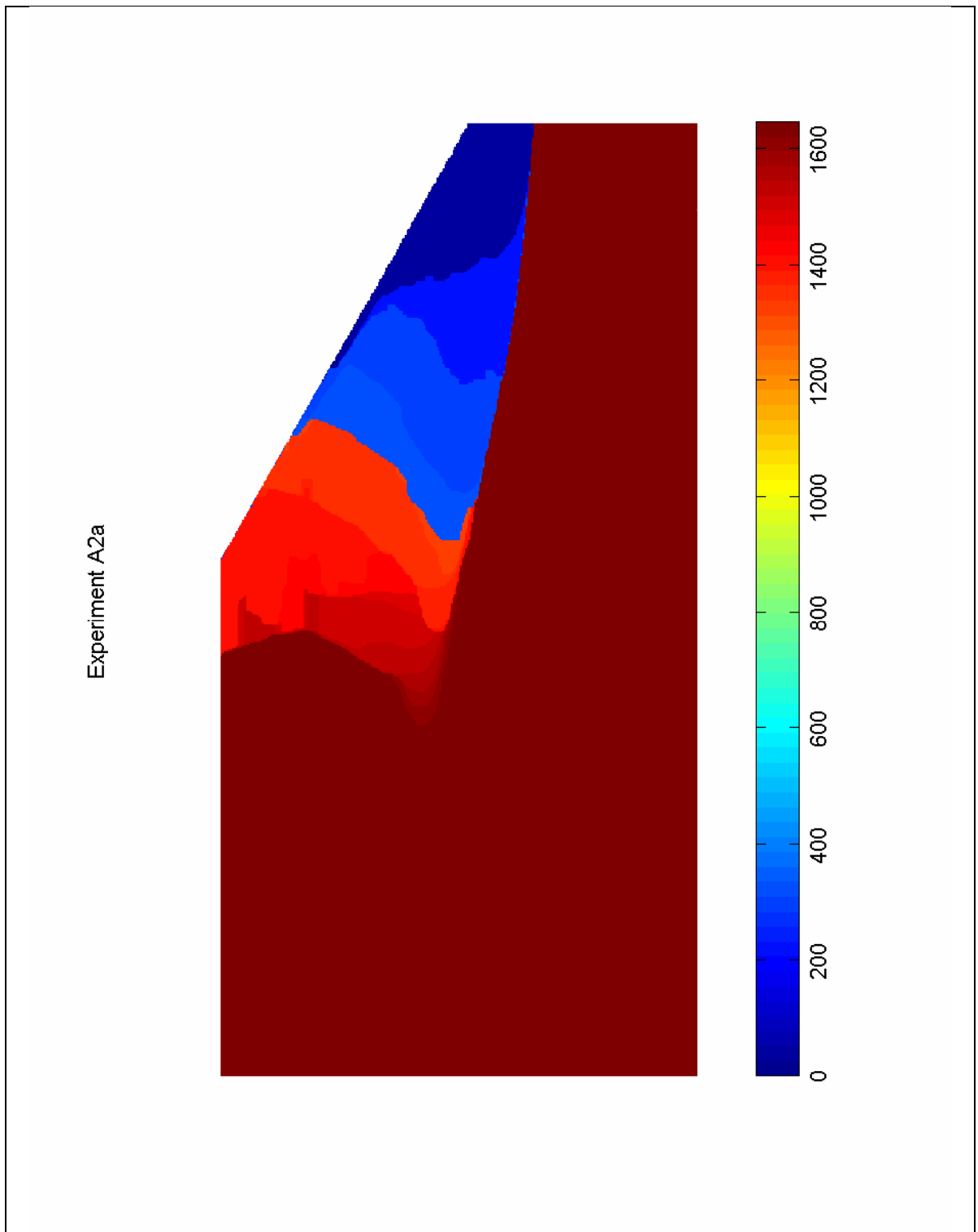


Realized starting profile and final profile for experiment C1d	1202124-007-HYE-0005	
Deltares		Figure C.24

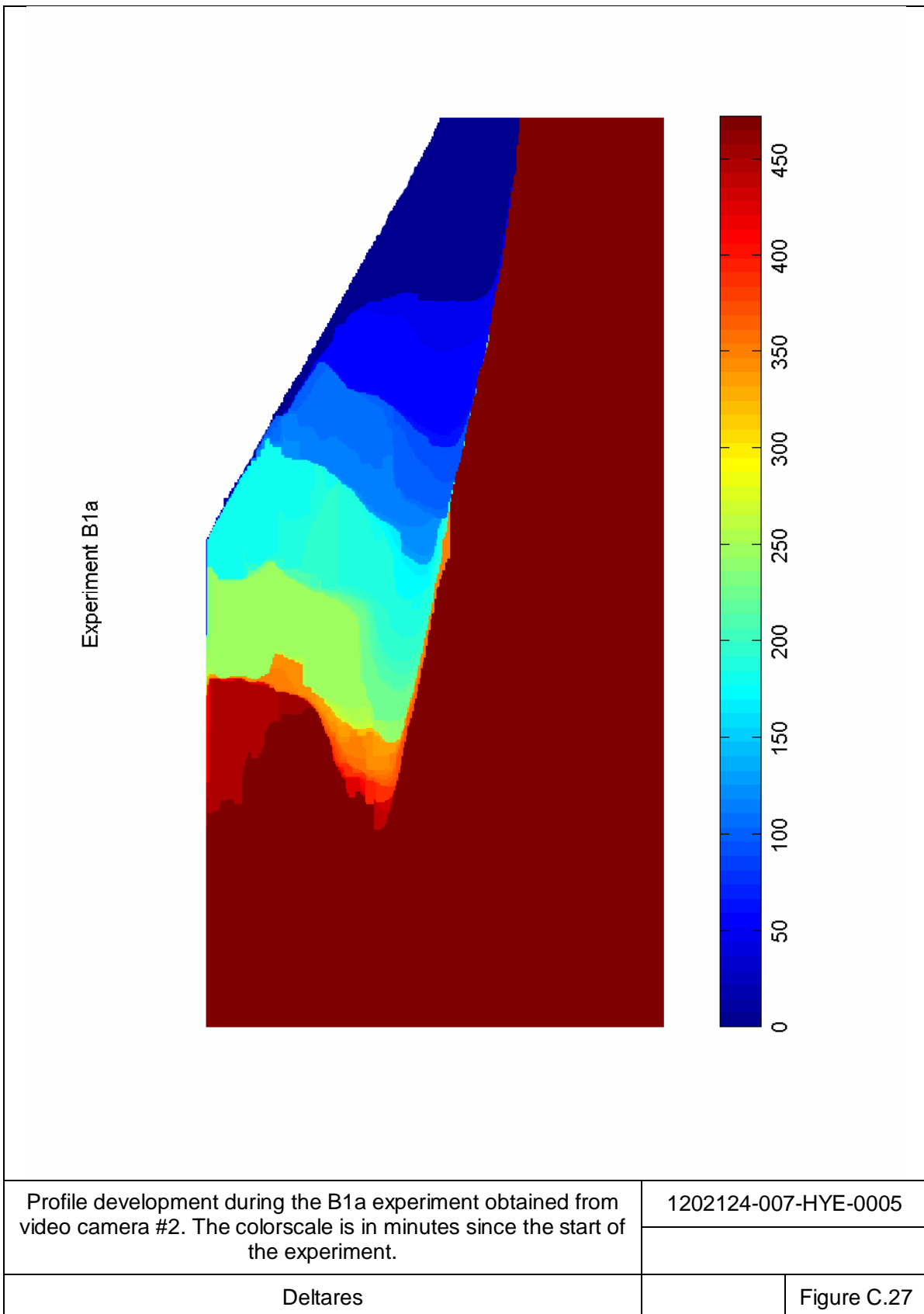


Dune profile development during experiment C1d

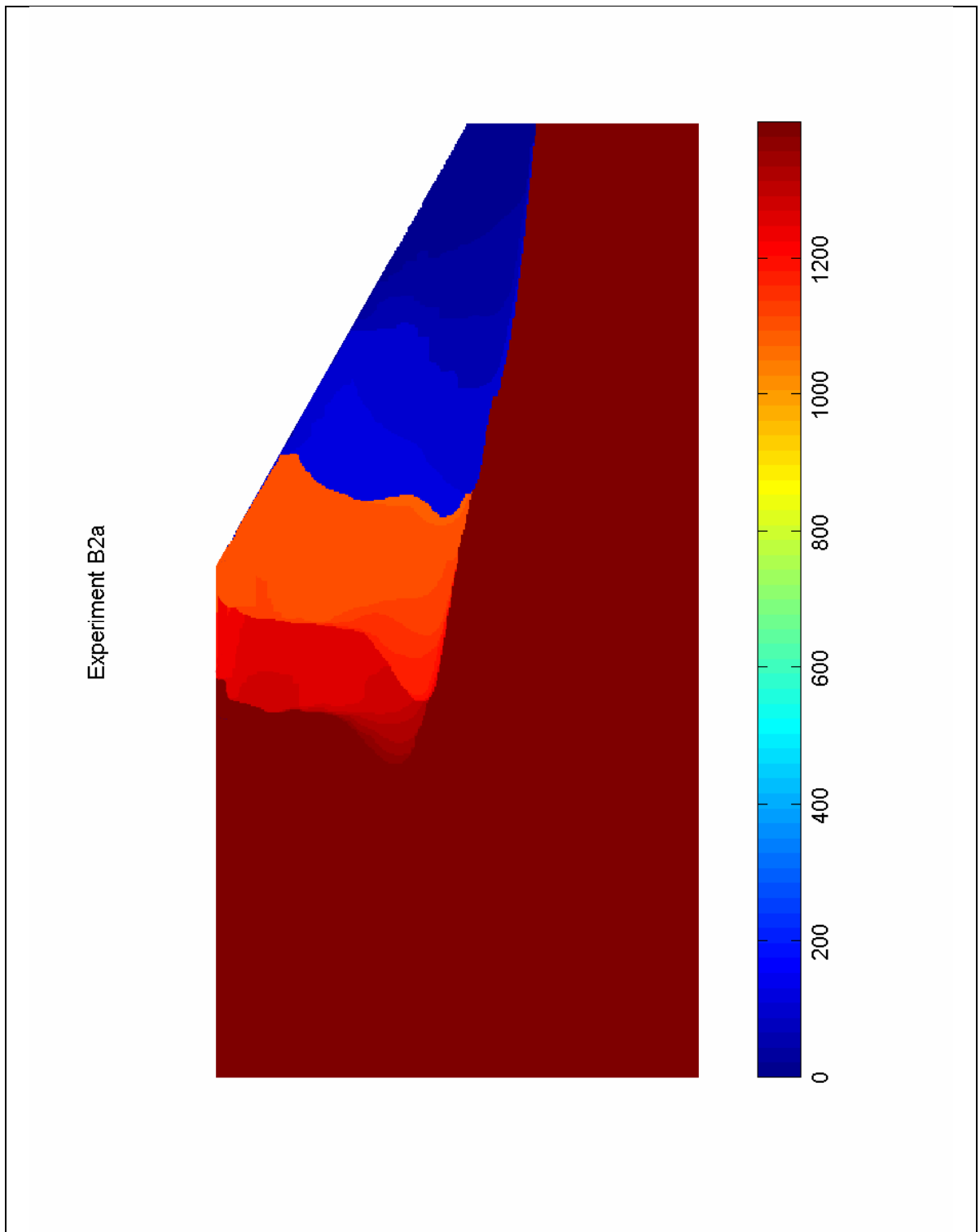
1202124-007-HYE-0005



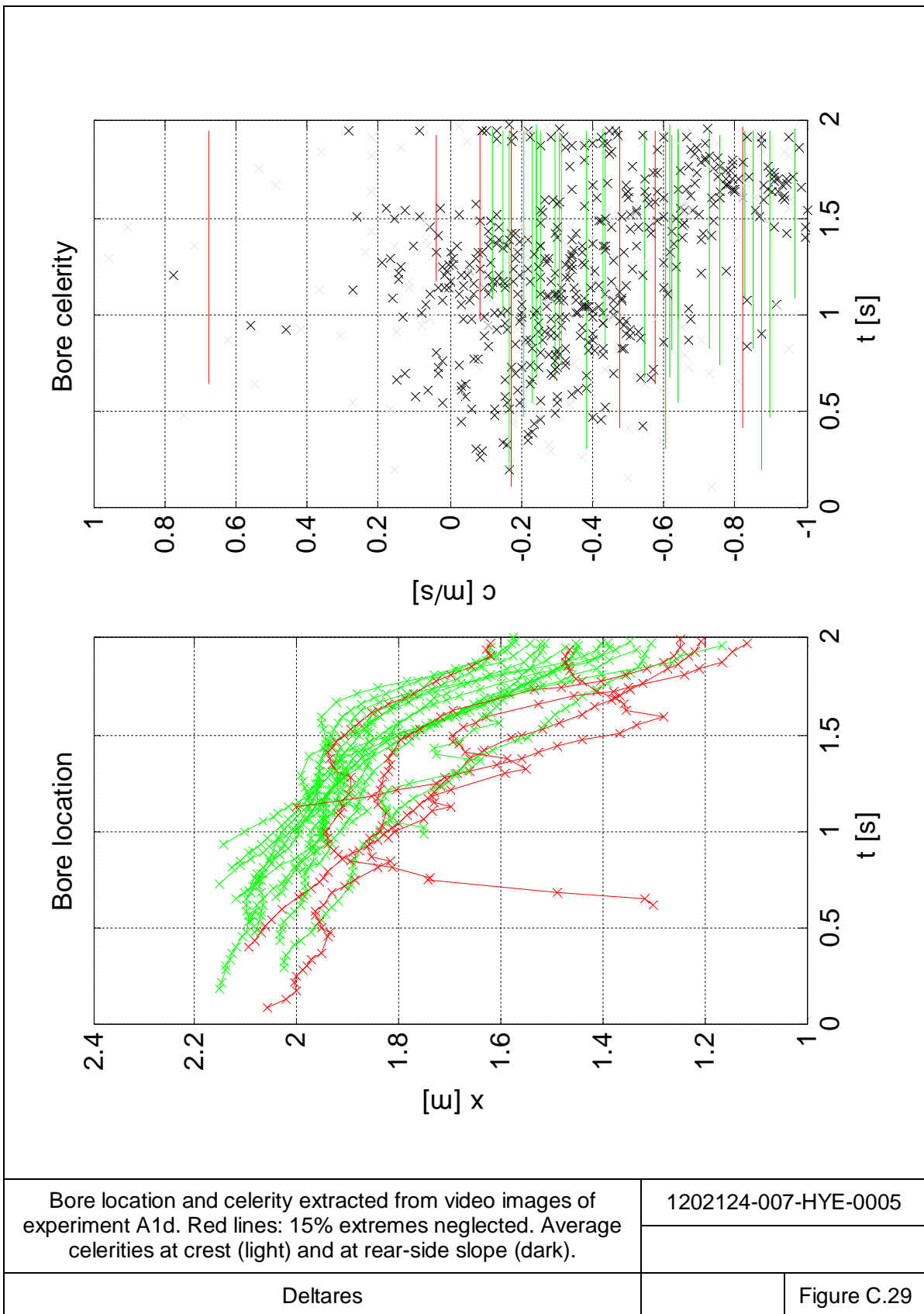
Profile development during the A2a experiment obtained from video camera #2. The colorscale is in minutes since the start of the experiment.	1202124-007-HYE-0005	
	Deltares	Figure C.26

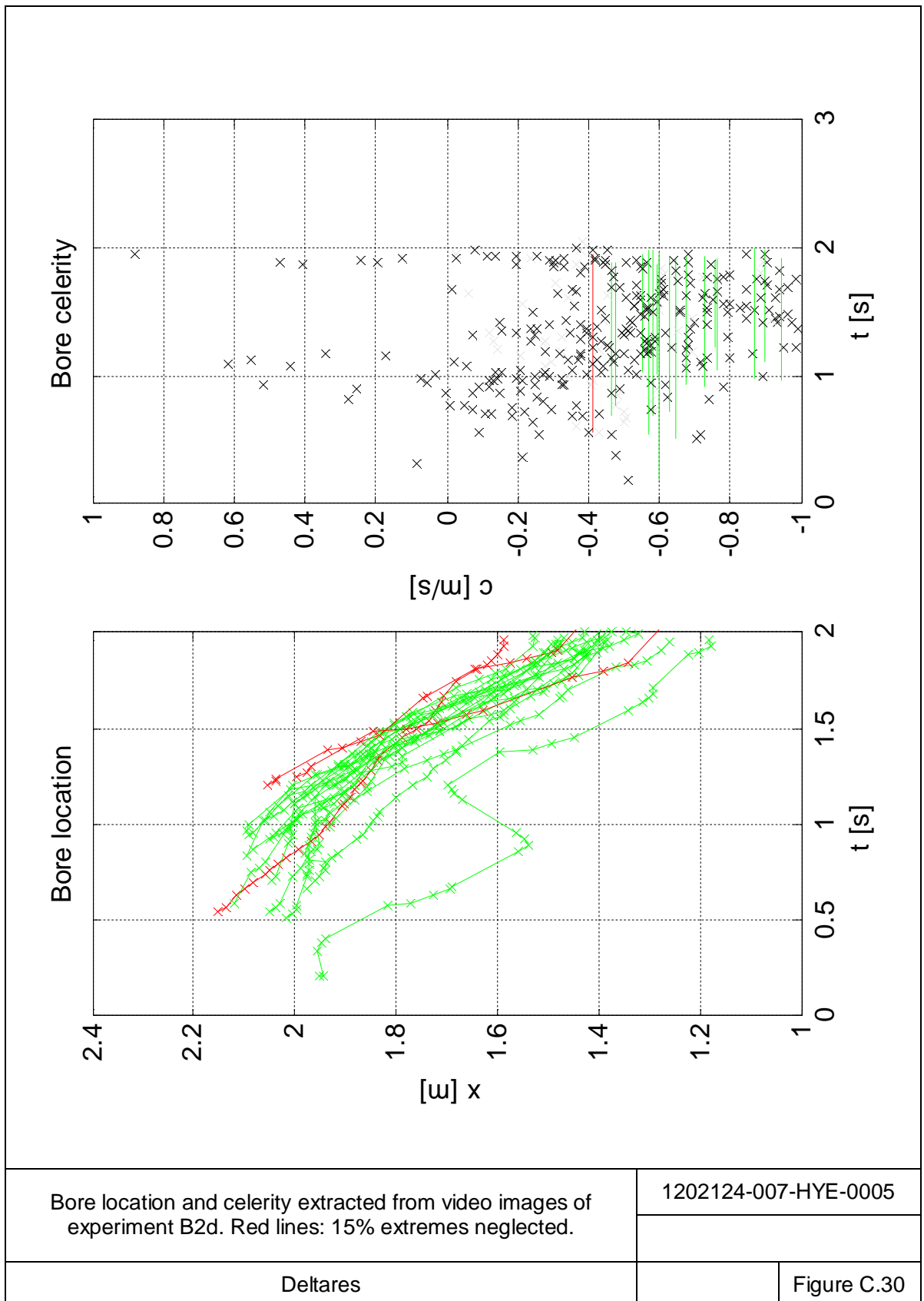


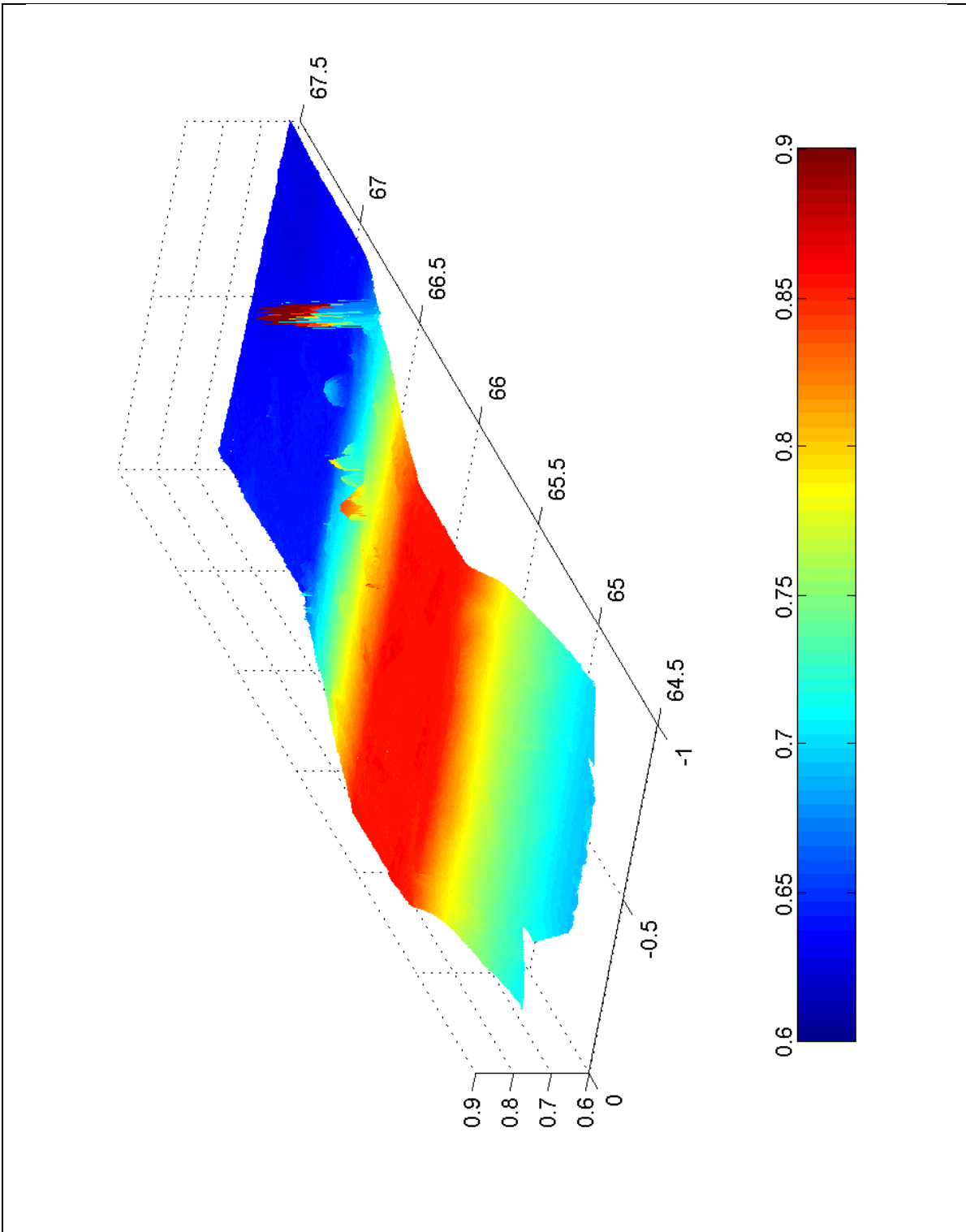




Profile development during the B2a experiment obtained from video camera #2. The colorscale is in minutes since the start of the experiment.	1202124-007-HYE-0005	
	Deltares	Figure C.28





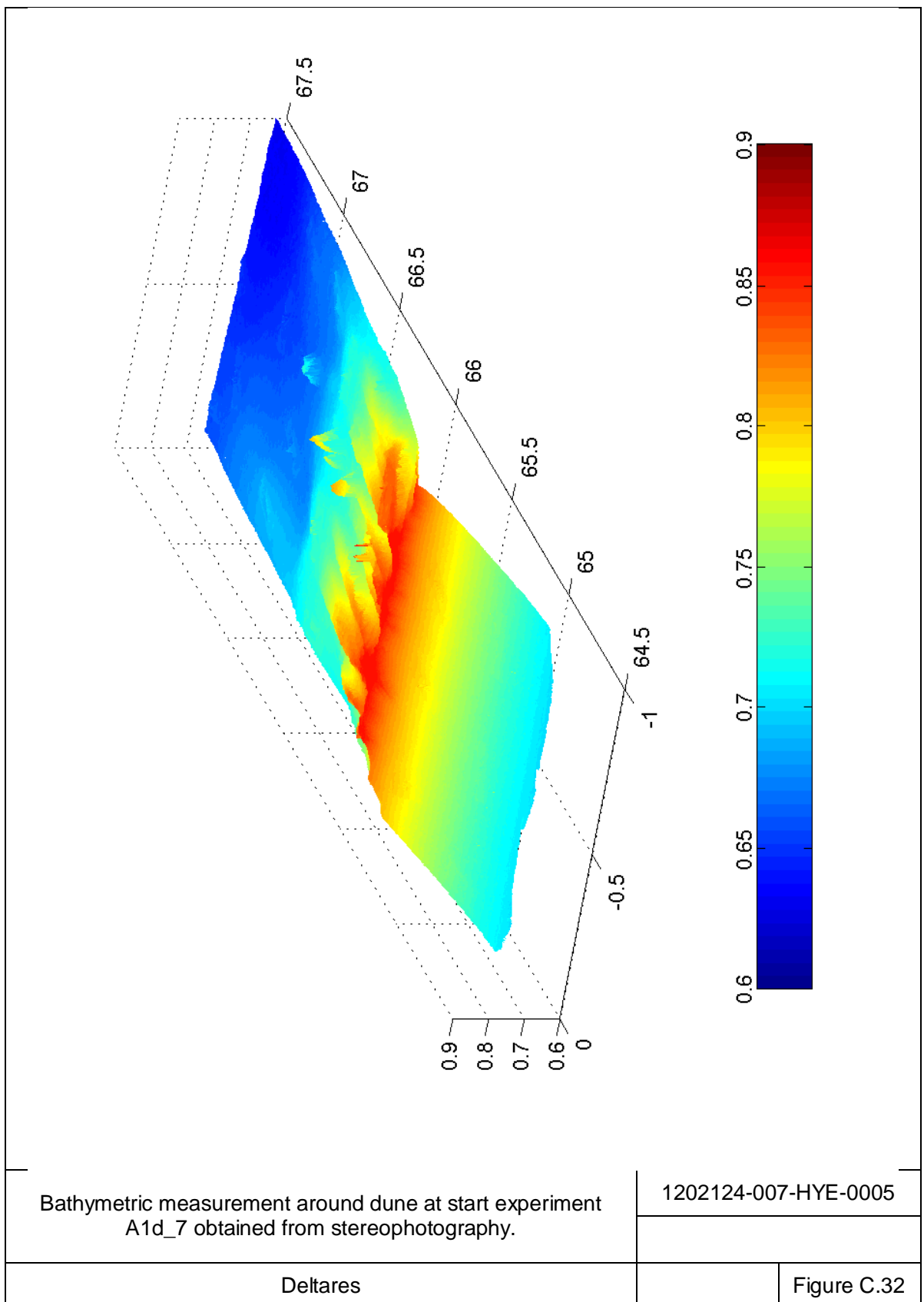


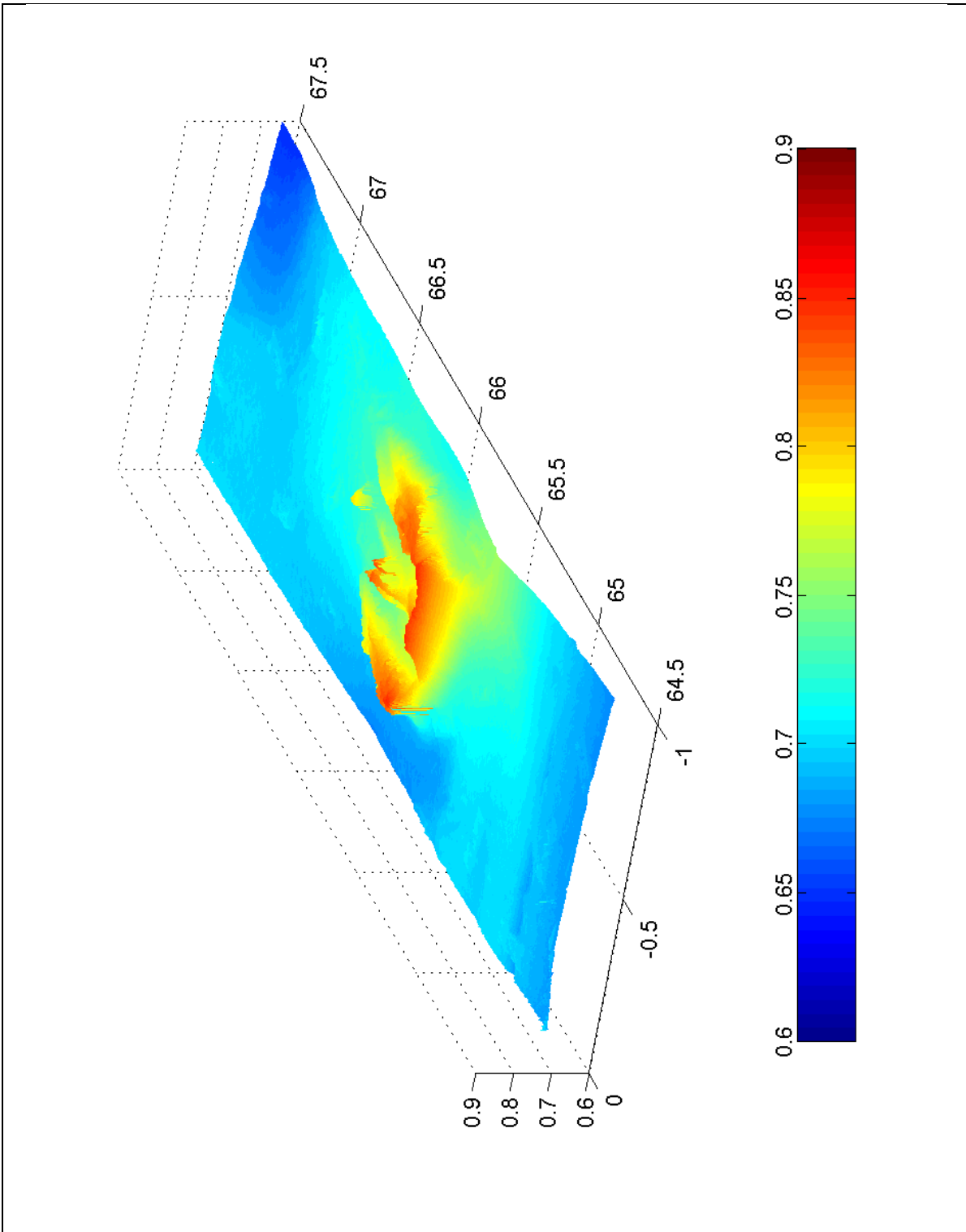
Bathymetric measurement around dune at start experiment A1d\_4 obtained from stereophotography.

1202124-007-HYE-0005

Deltares

Figure C.31



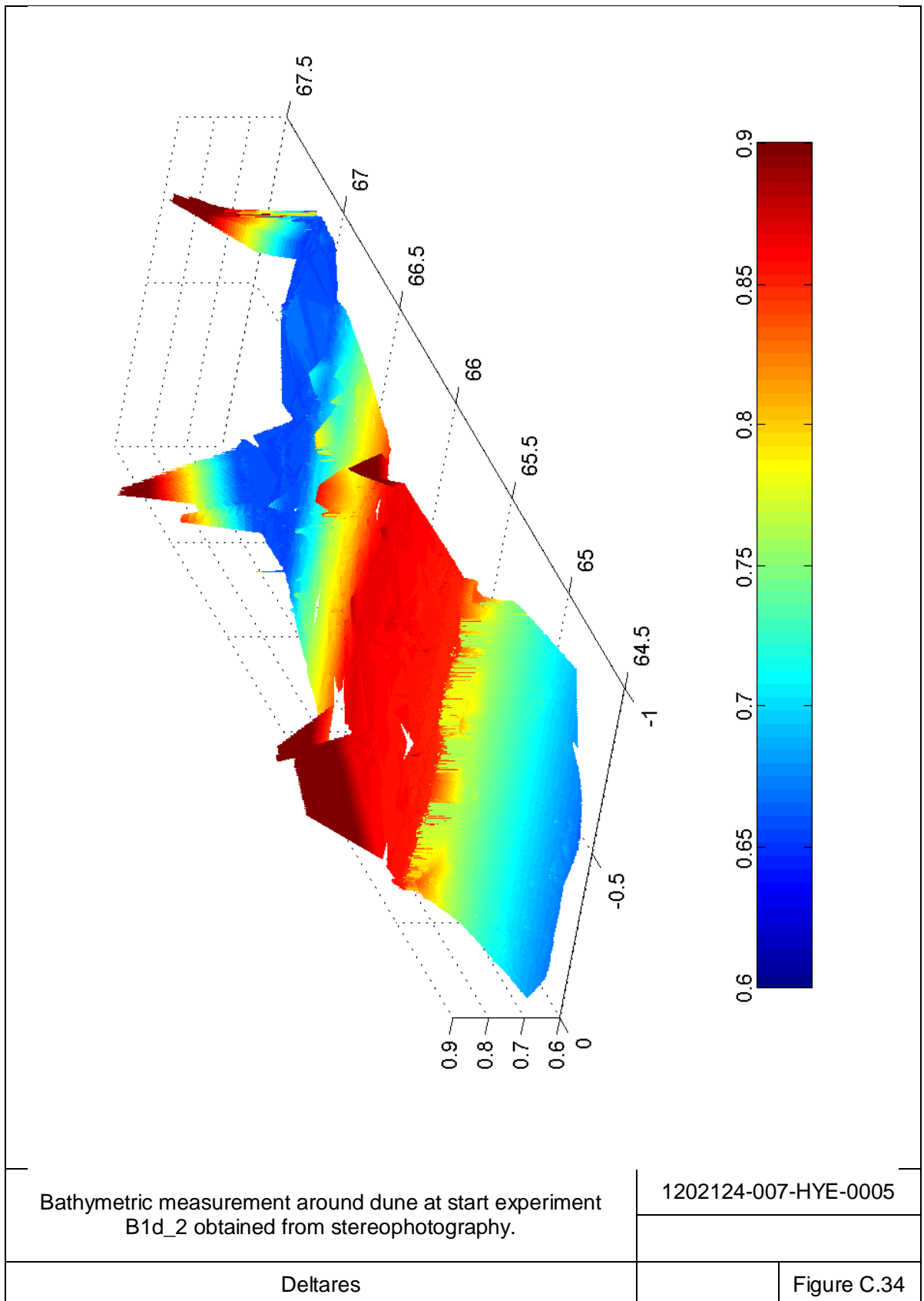


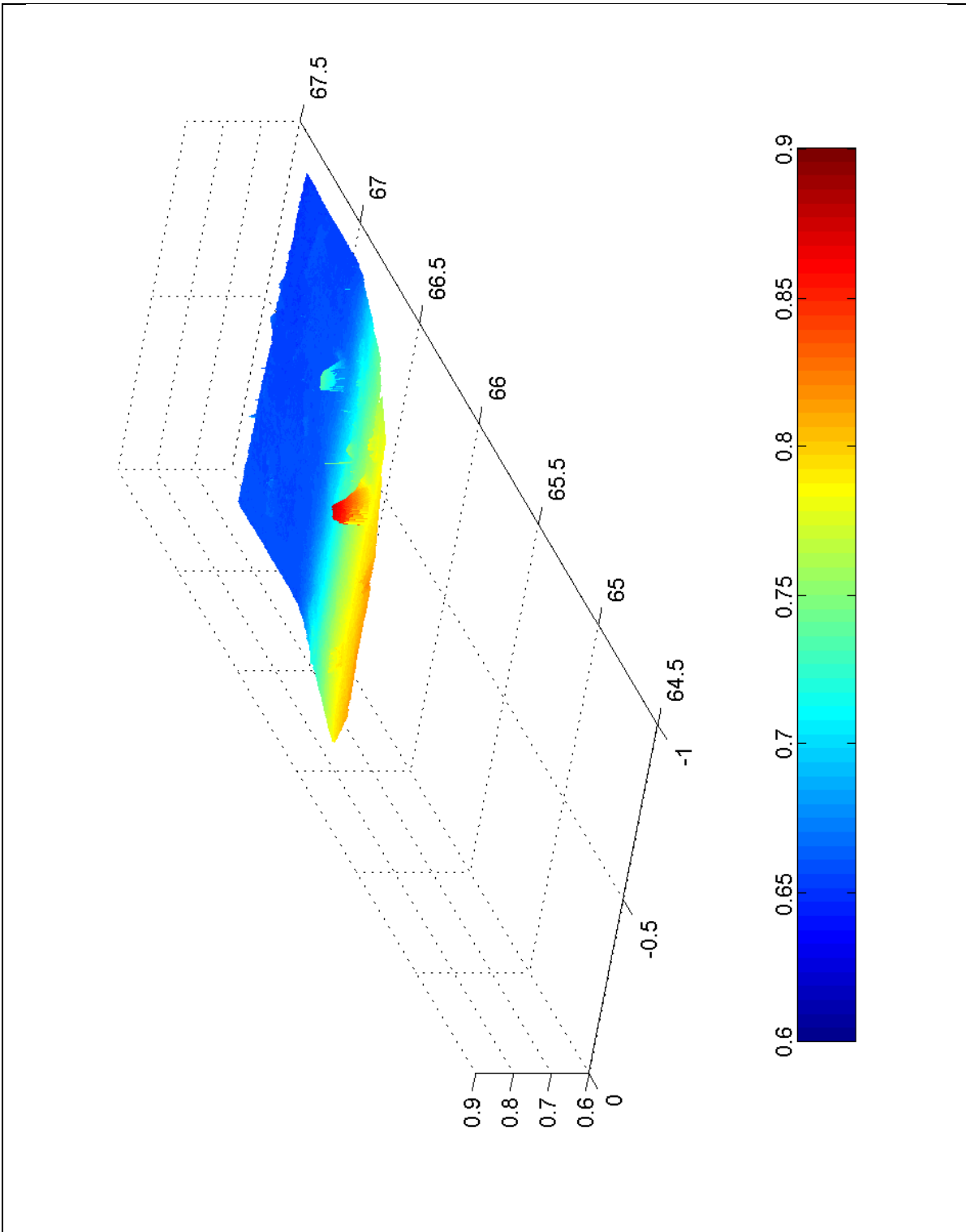
Bathymetric measurement around dune at start experiment  
A1d\_8 obtained from stereophotography.

1202124-007-HYE-0005

Deltares

Figure C.33





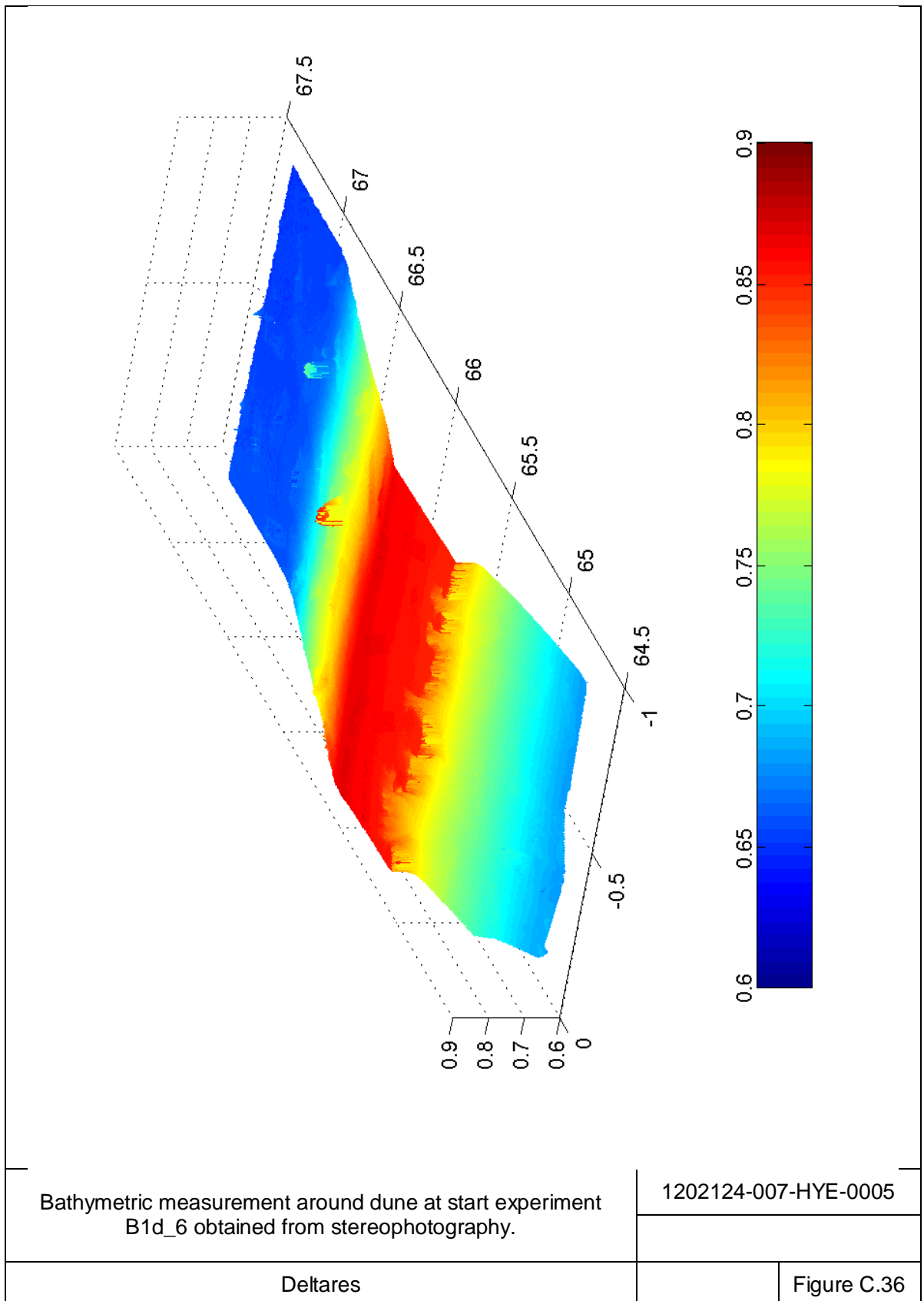
Bathymetric measurement around dune at start experiment B1d\_5 obtained from stereophotography.

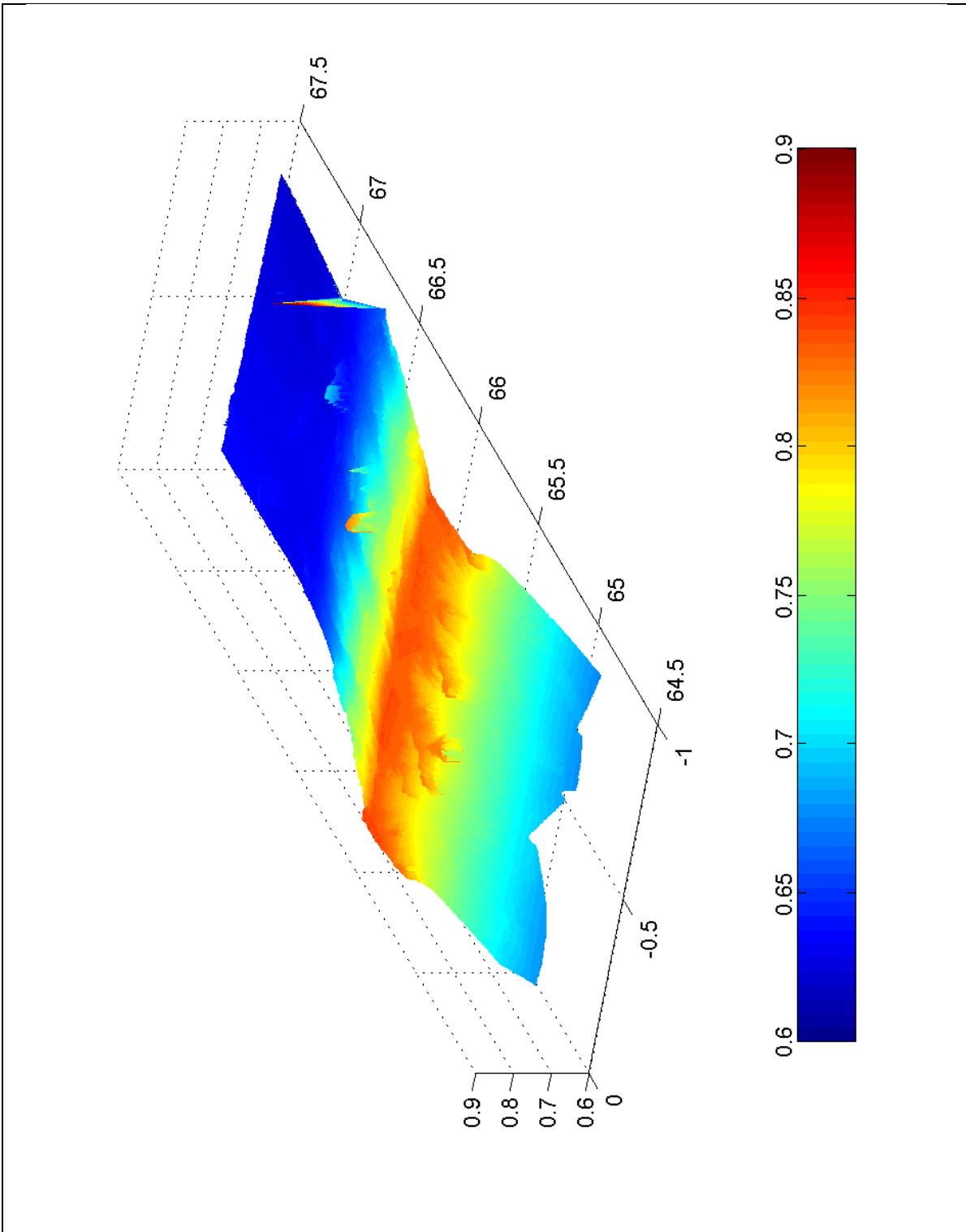
1202124-007-HYE-0005

Deltares

Figure C.35





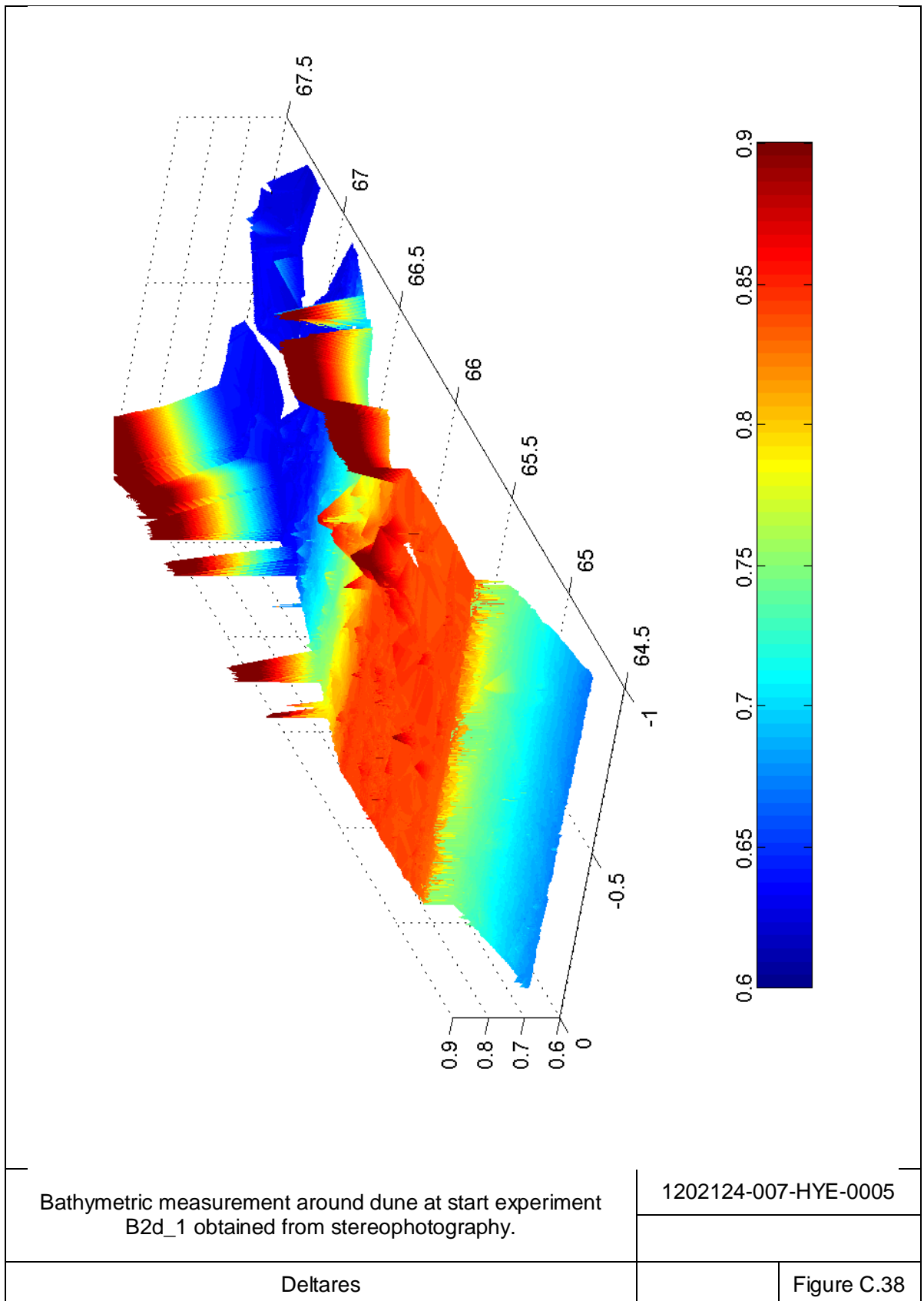


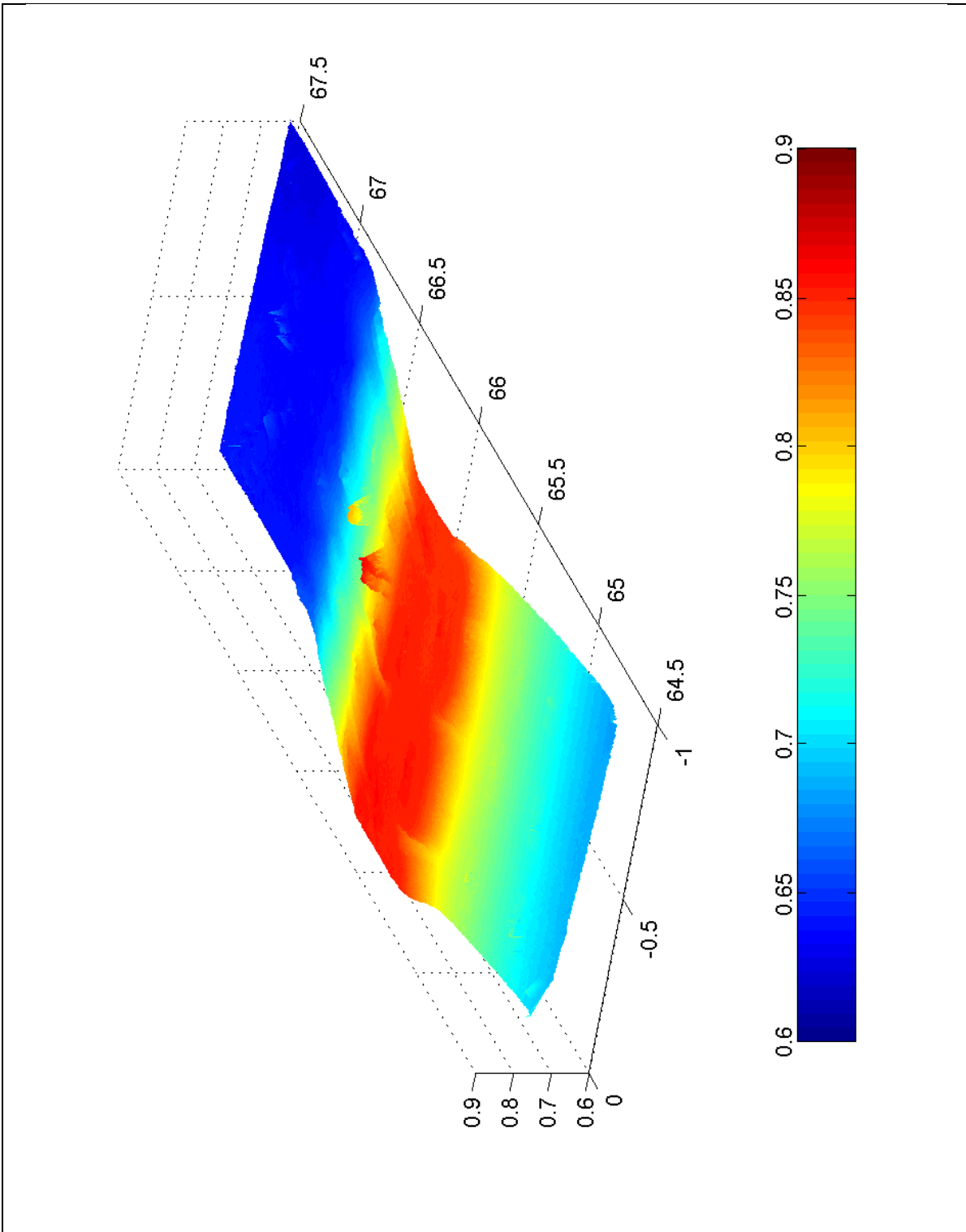
Bathymetric measurement around dune at start experiment B1d\_7 obtained from stereophotography.

1202124-007-HYE-0005

Deltares

Figure C.37



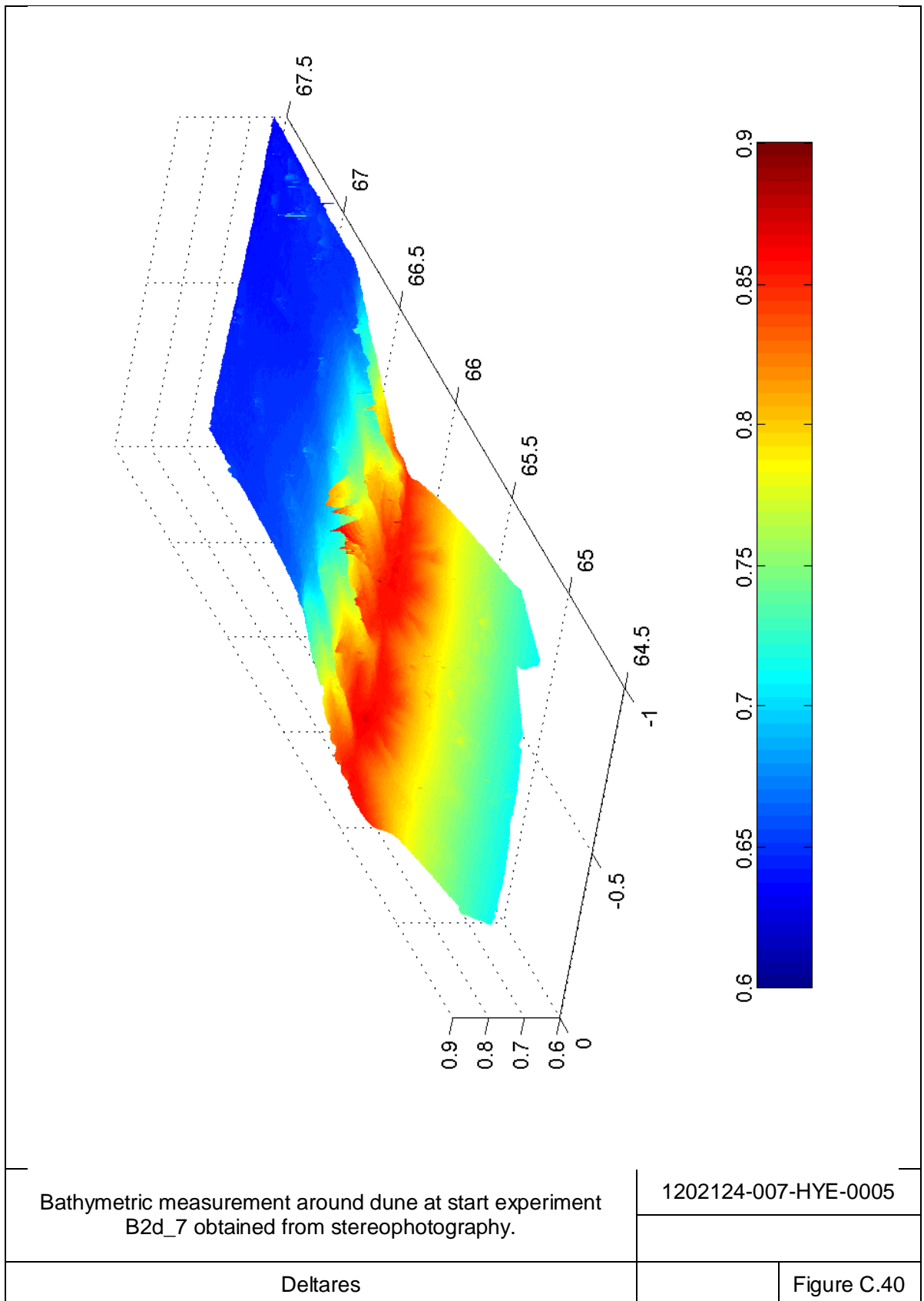


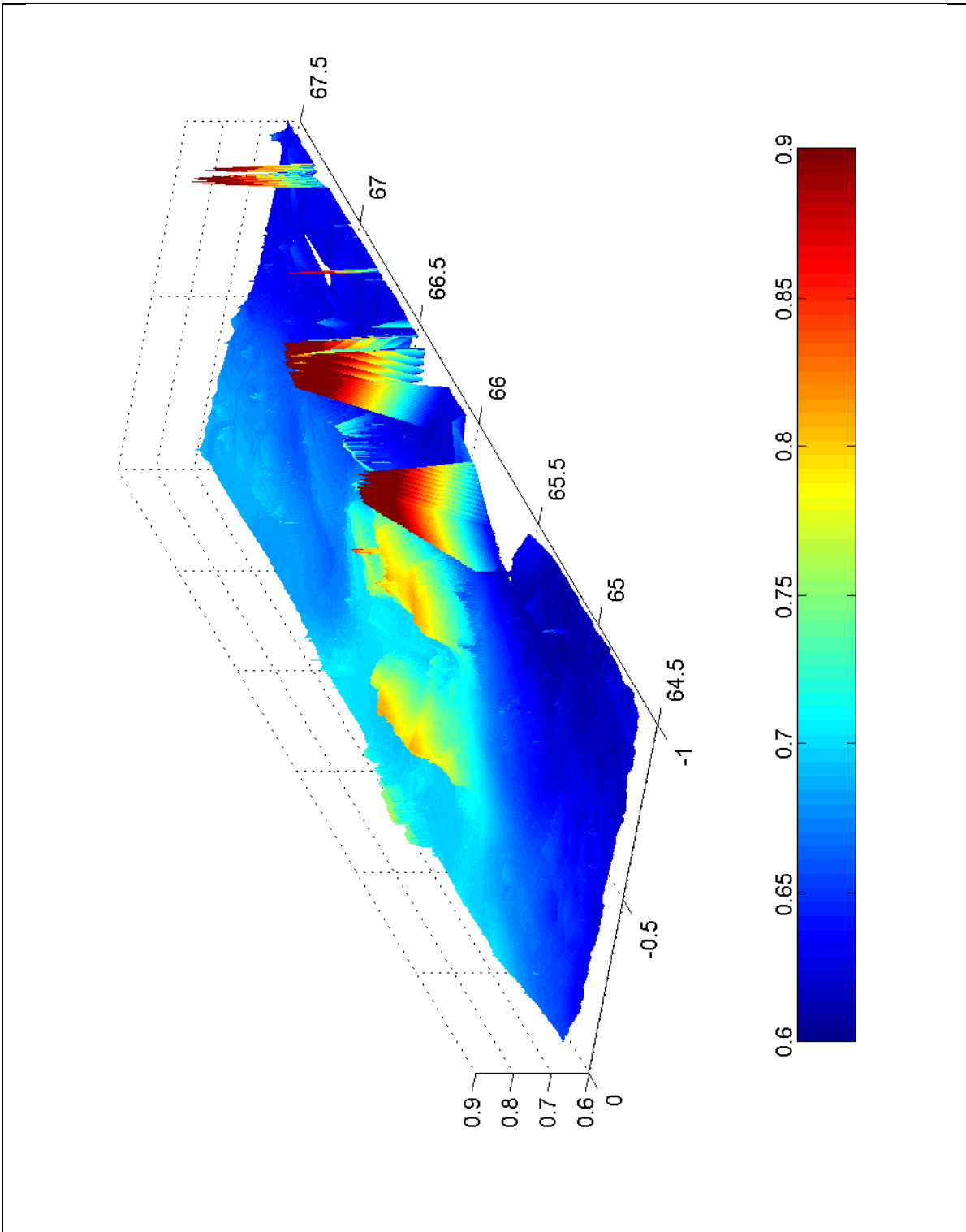
Bathymetric measurement around dune at start experiment B2d\_5 obtained from stereophotography.

1202124-007-HYE-0005

Deltares

Figure C.39



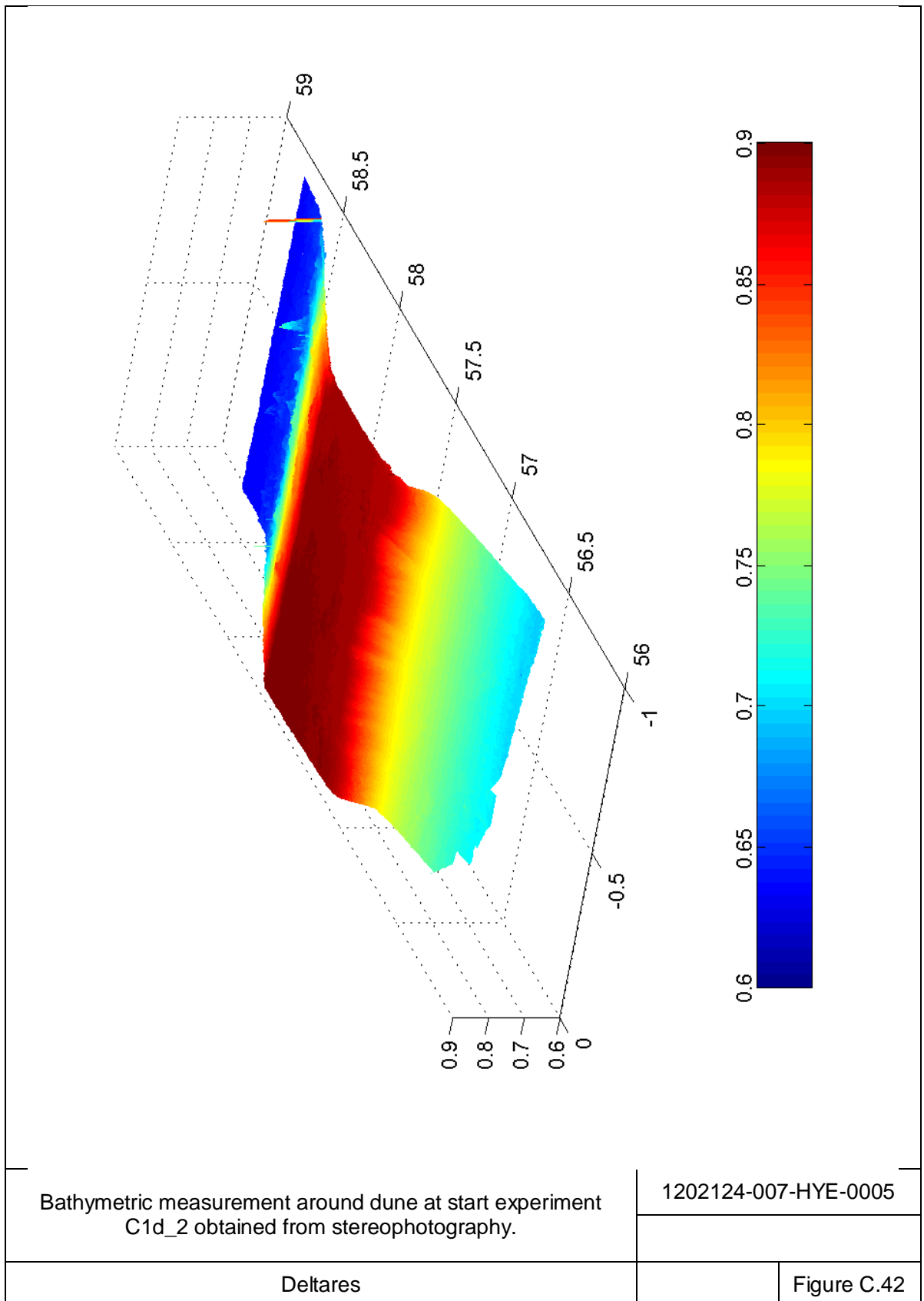


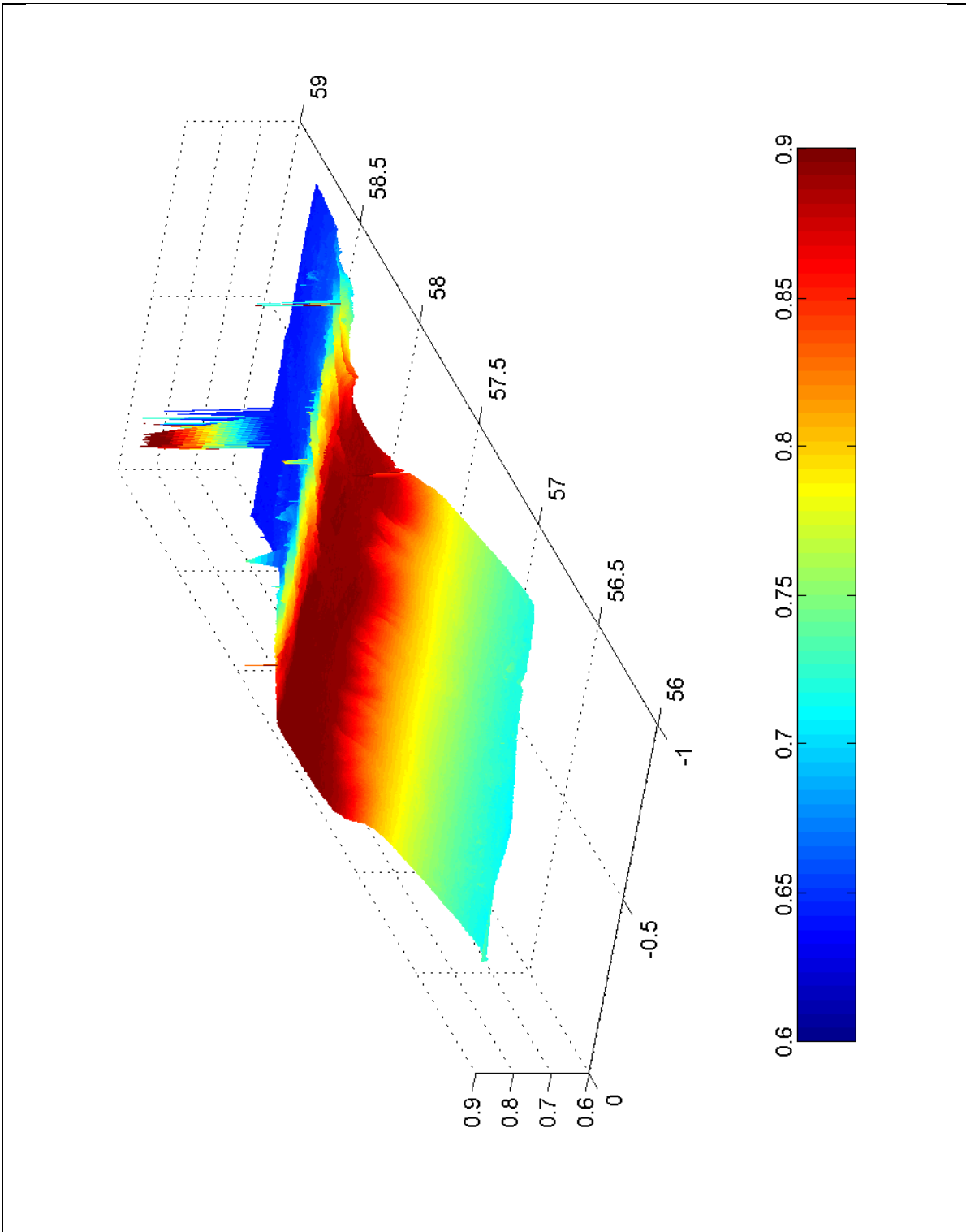
Bathymetric measurement around dune at start experiment B2d\_8 obtained from stereophotography.

1202124-007-HYE-0005

Deltares

Figure C.41





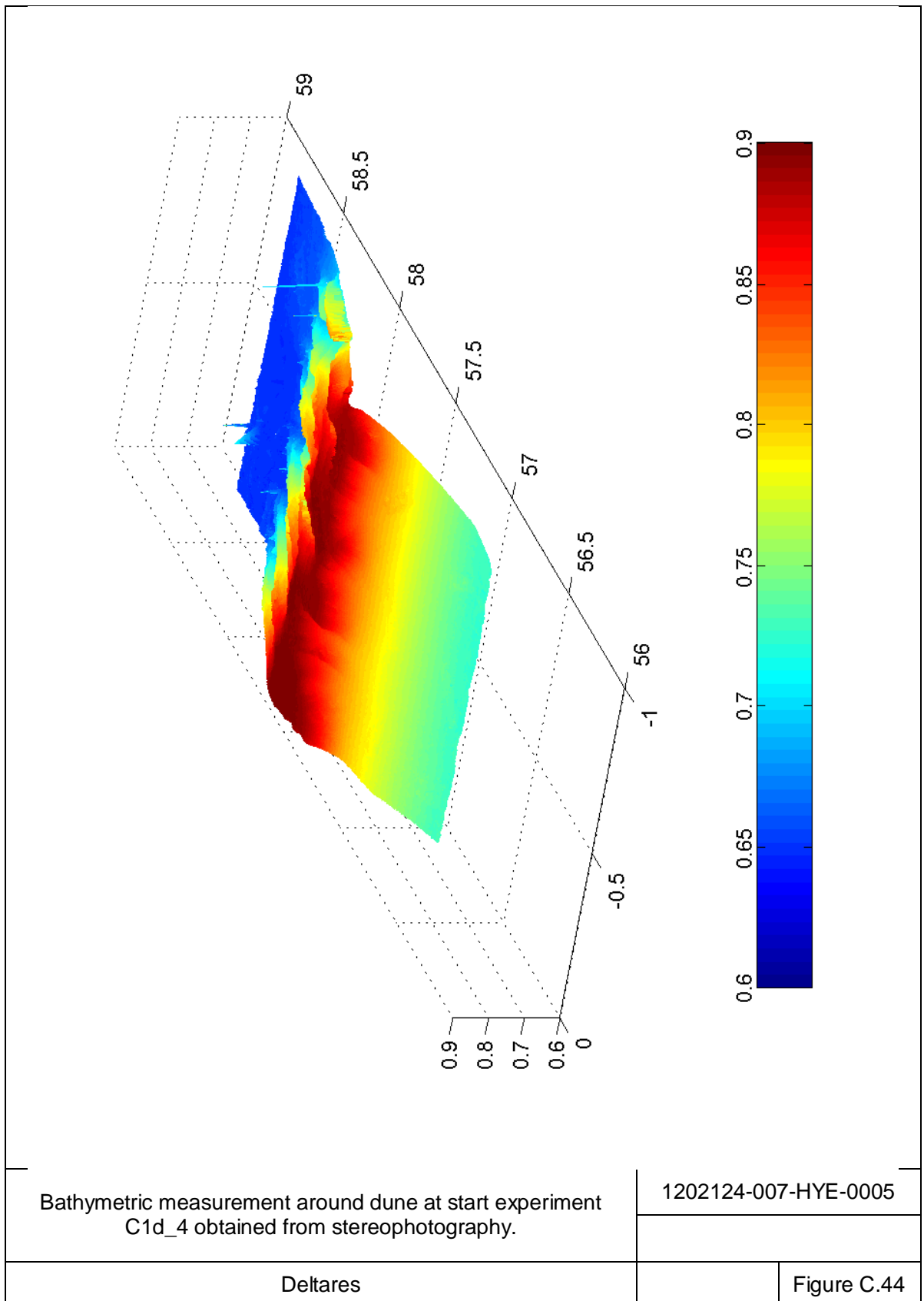
Bathymetric measurement around dune at start experiment C1d\_3 obtained from stereophotography.

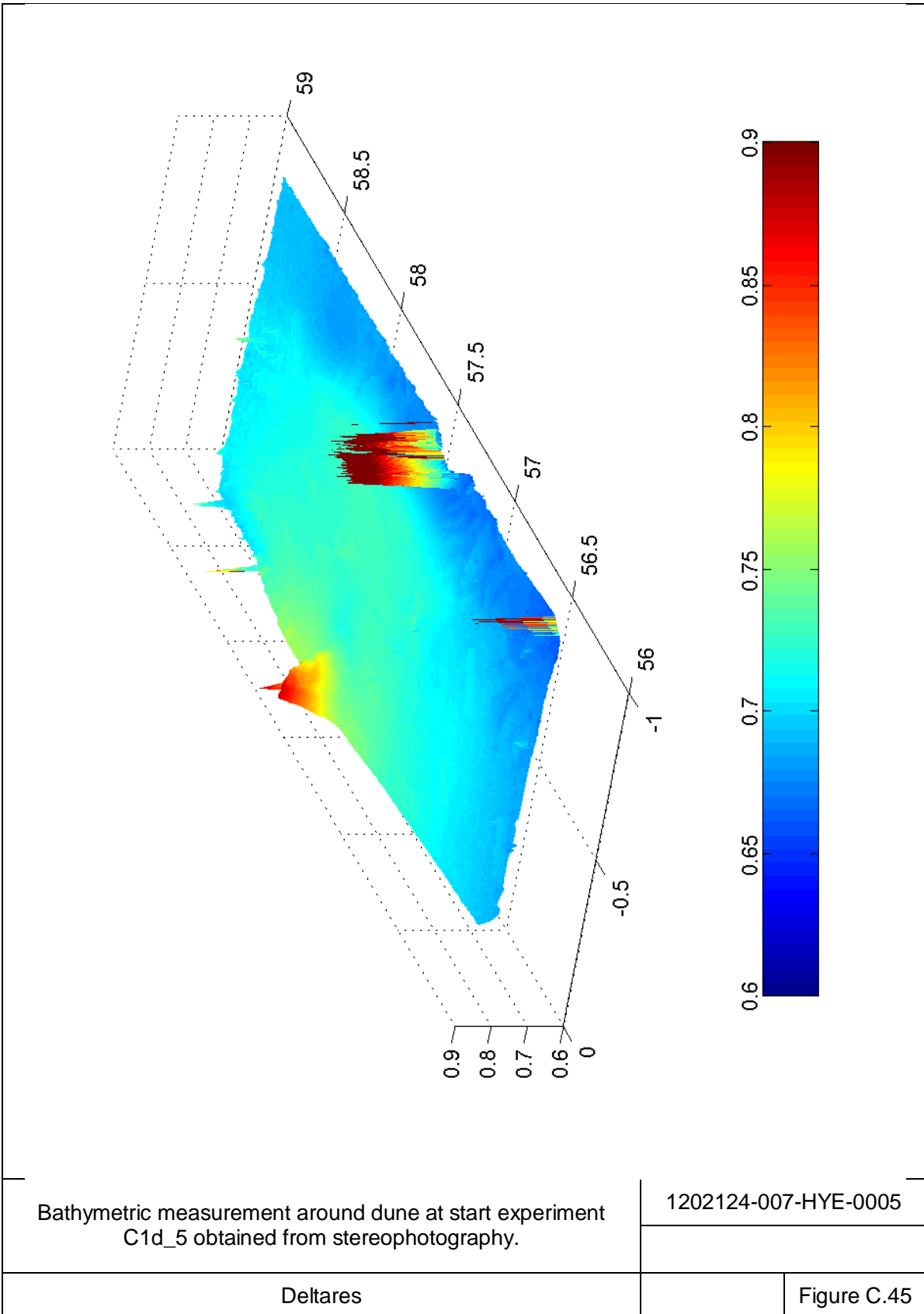
1202124-007-HYE-0005

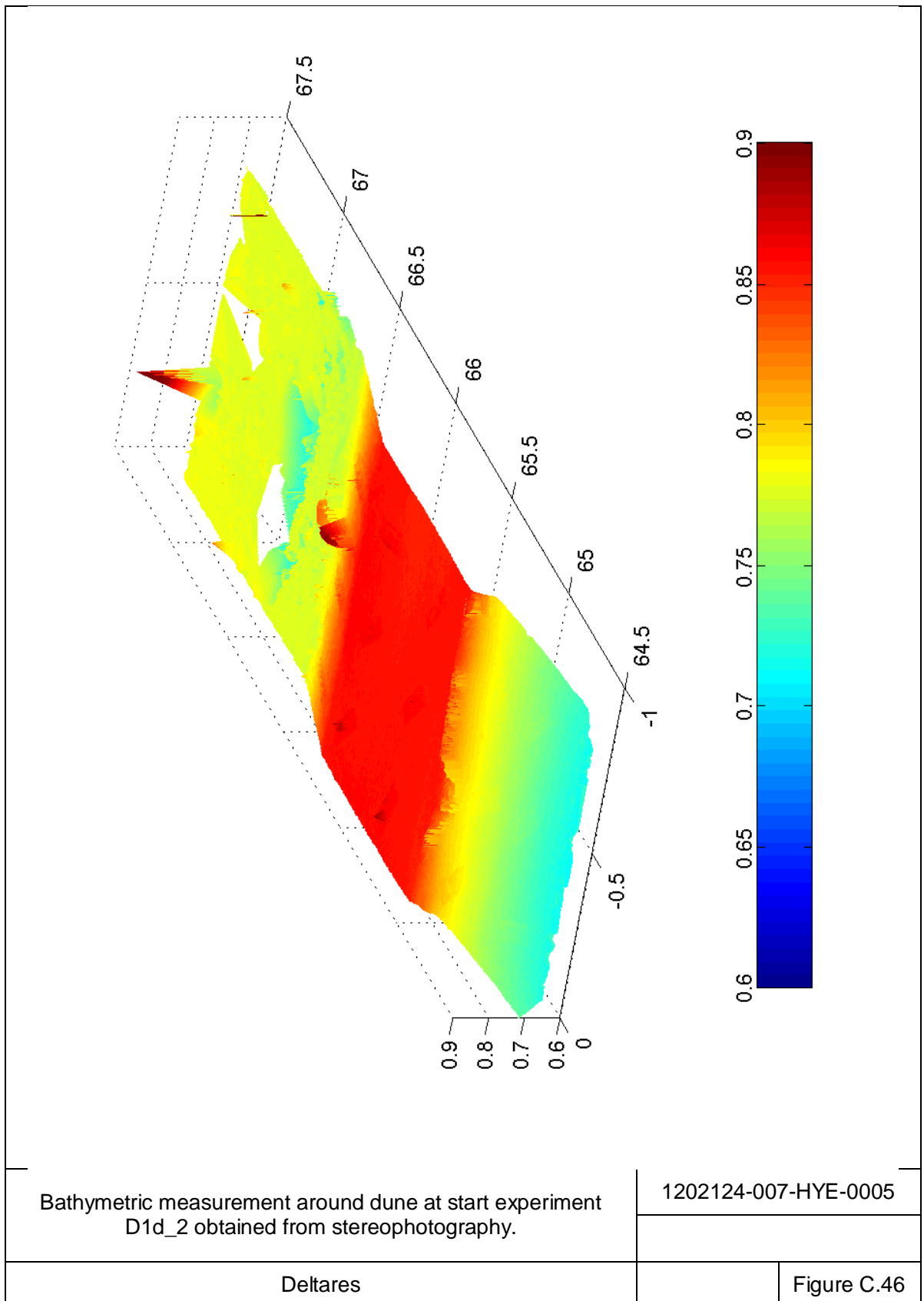
Deltares

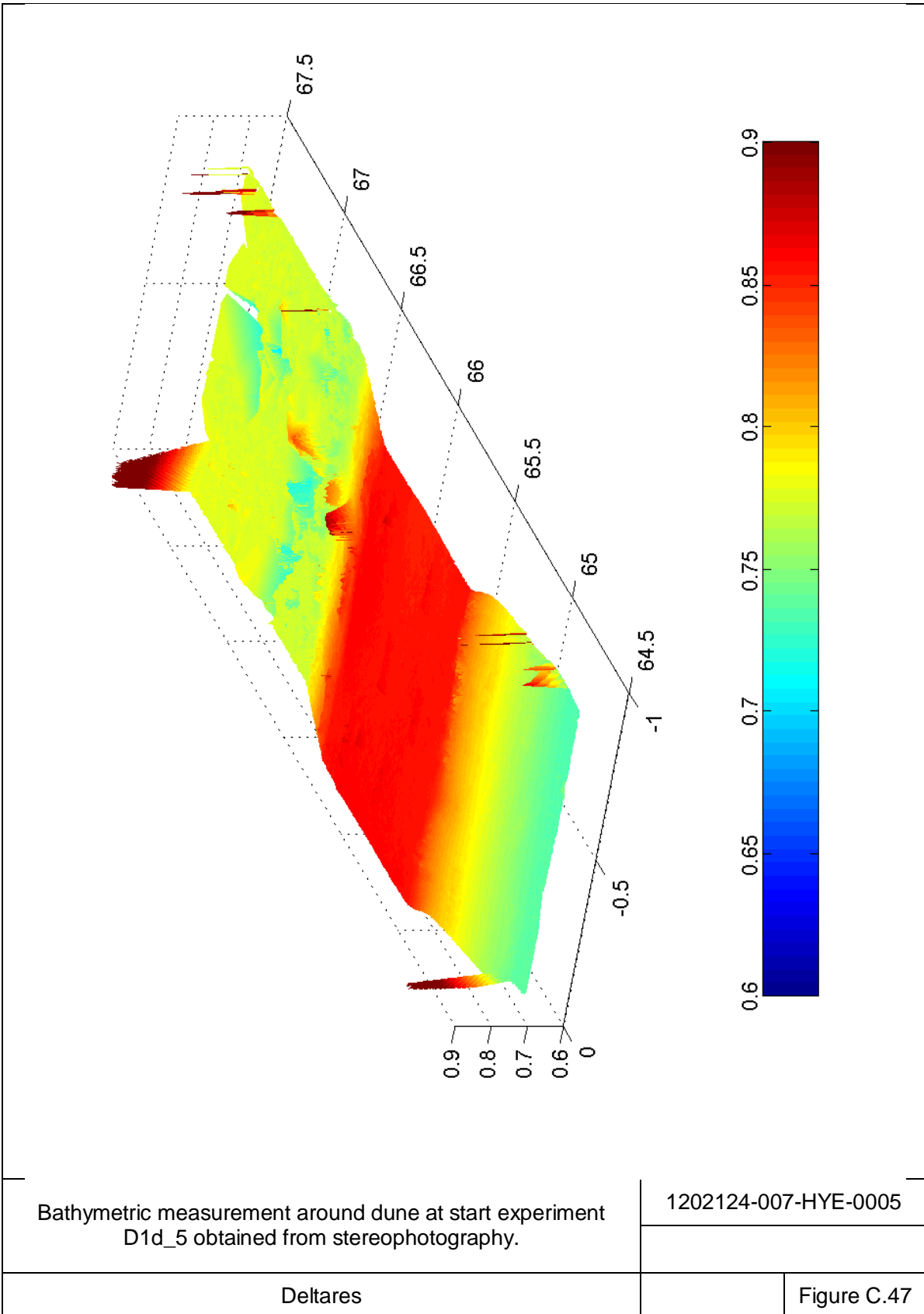
Figure C.43

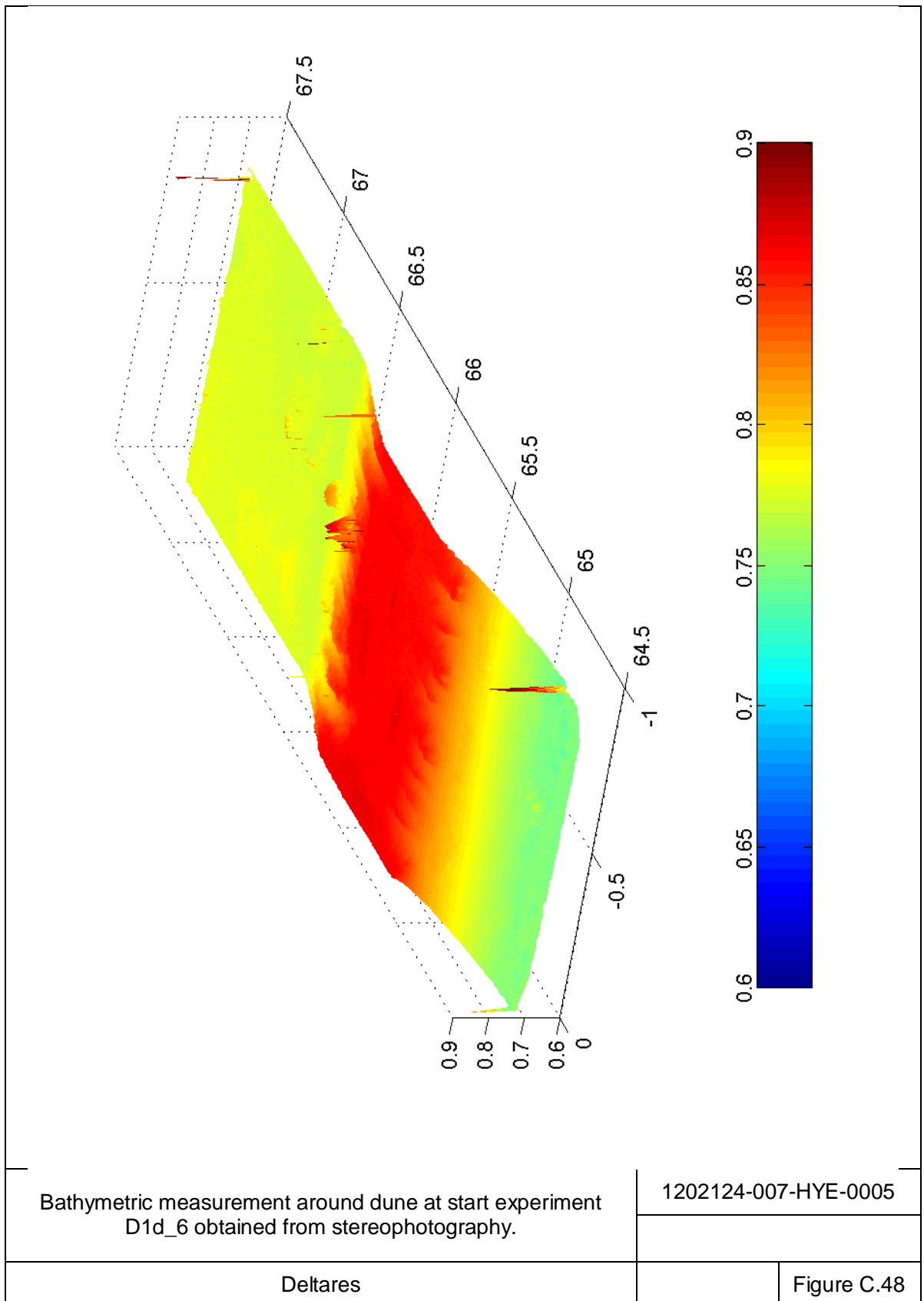


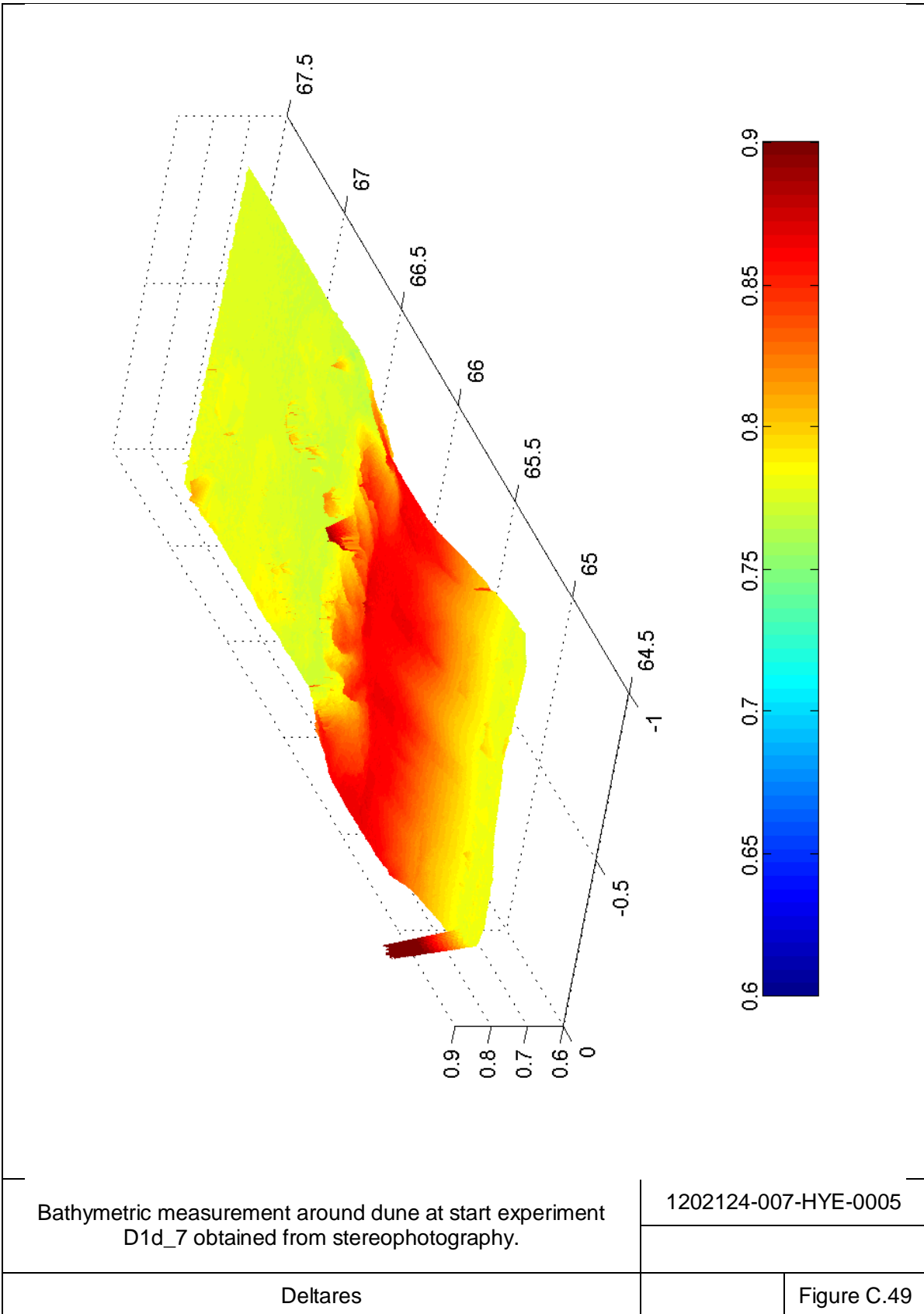


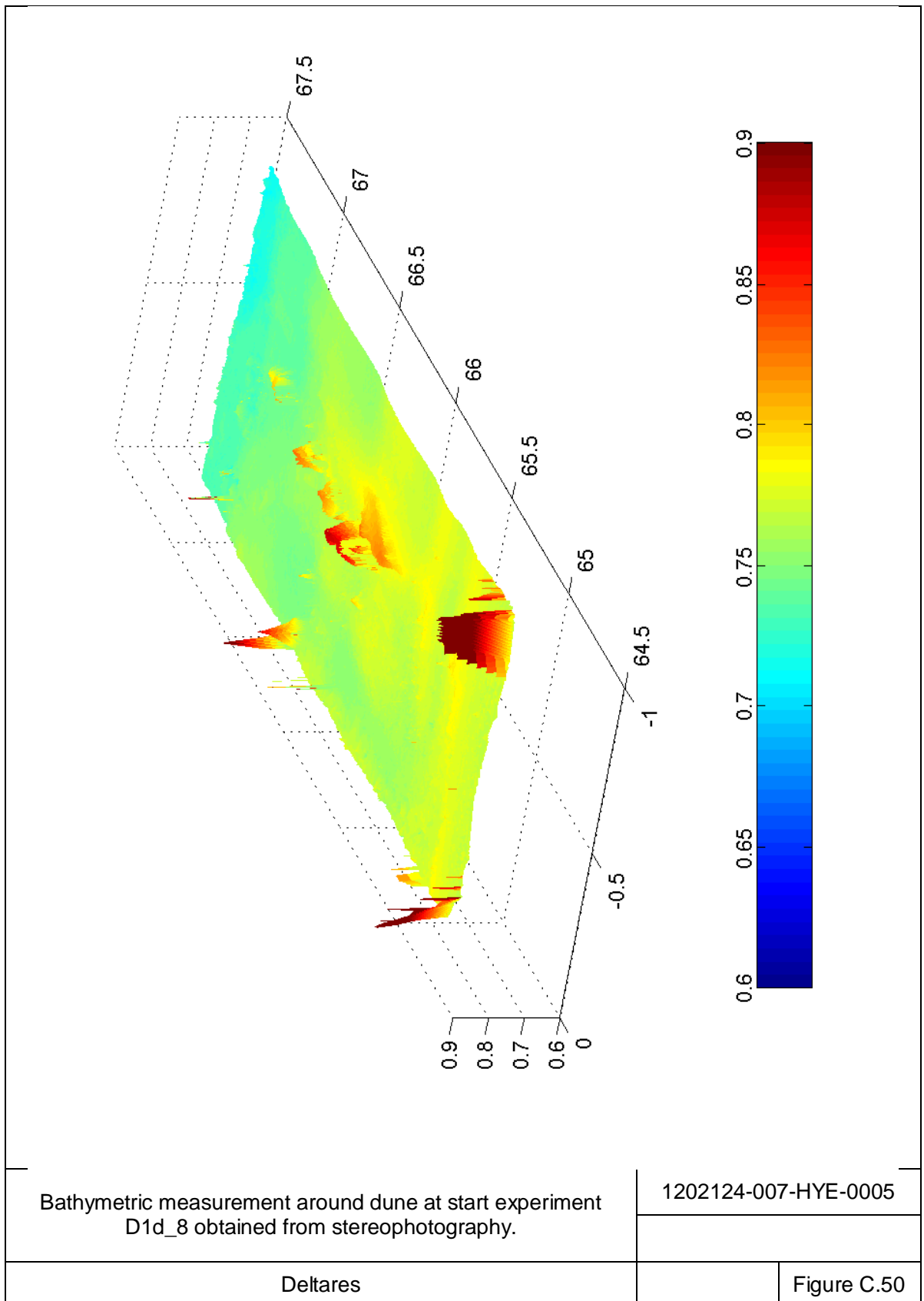


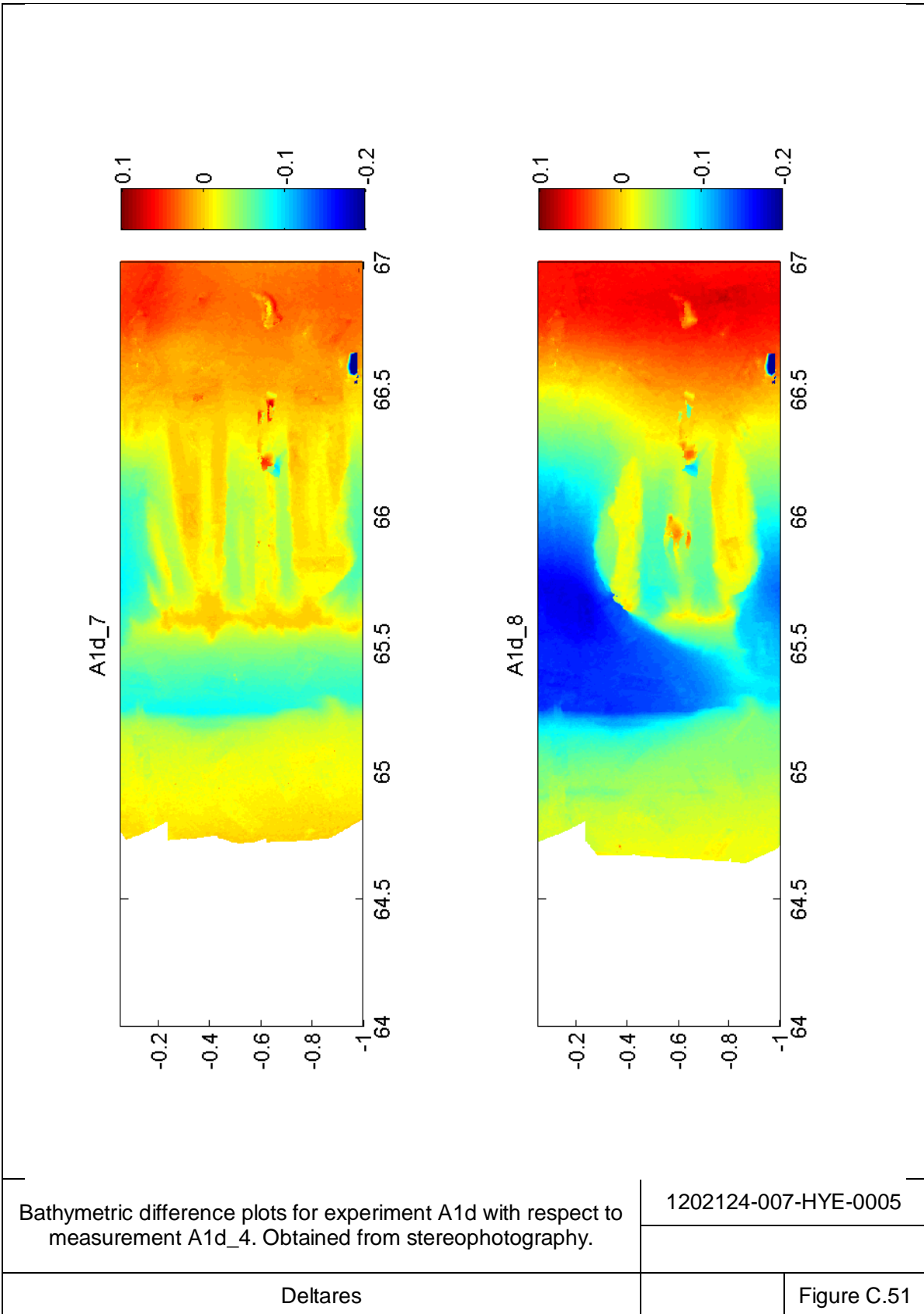




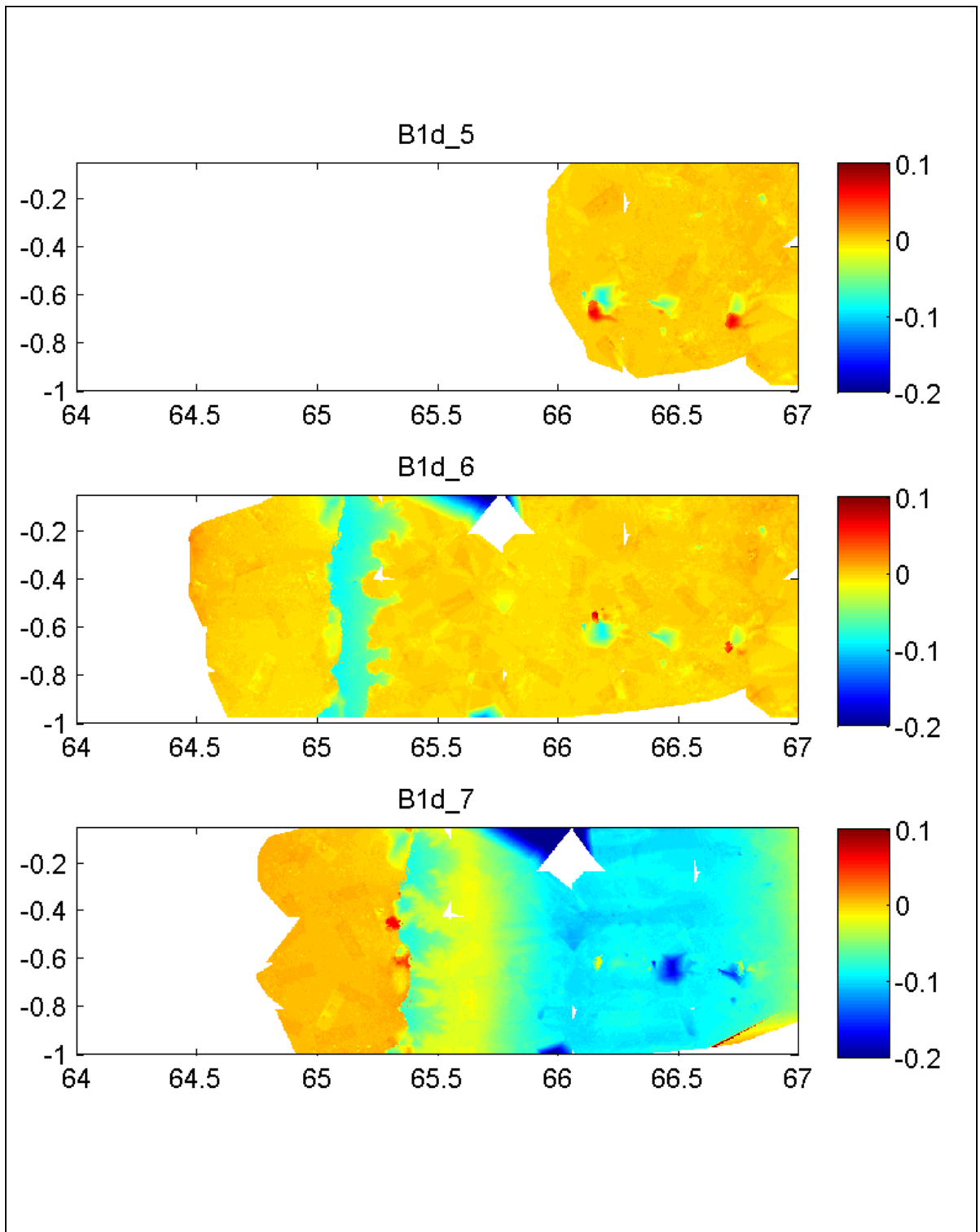




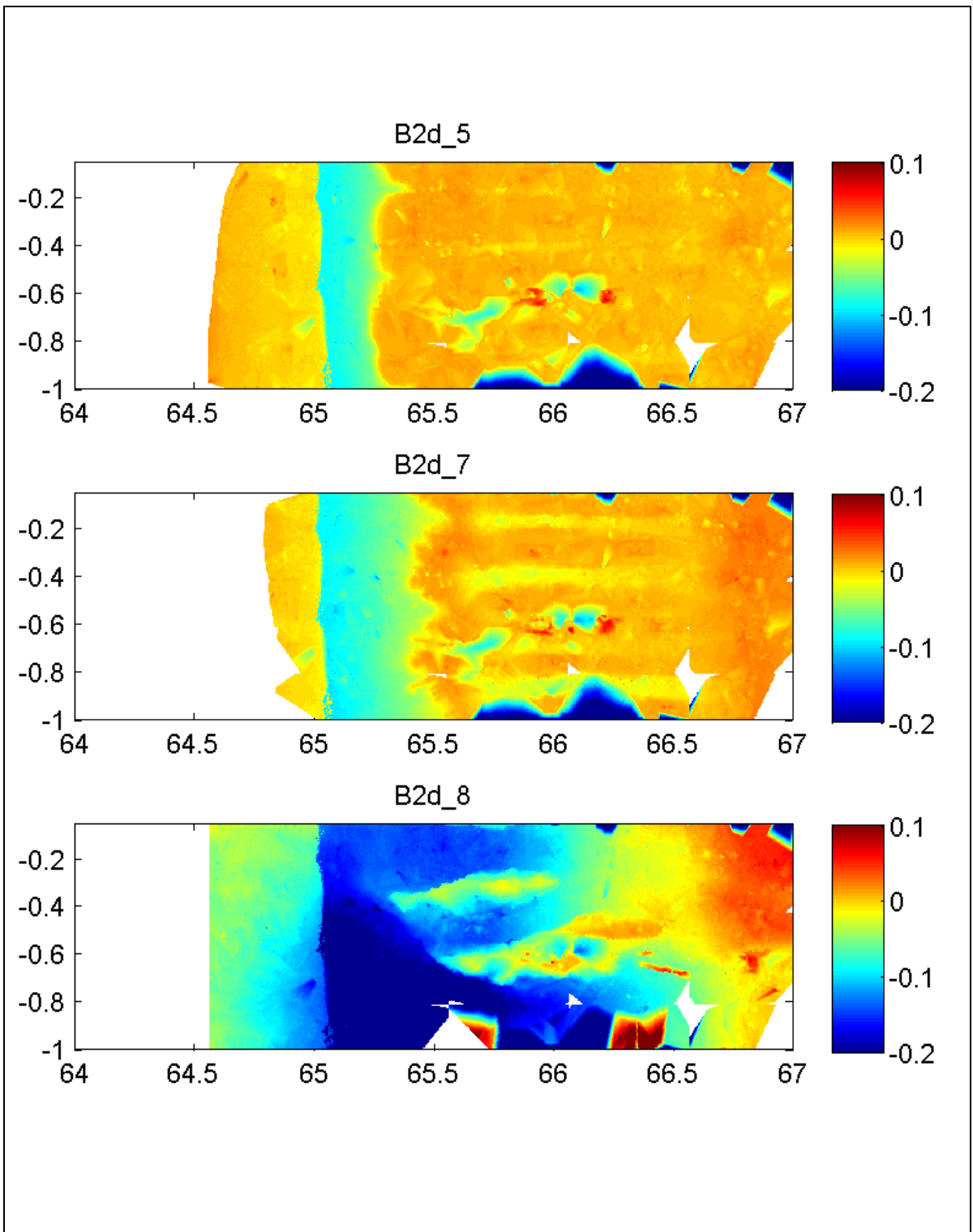




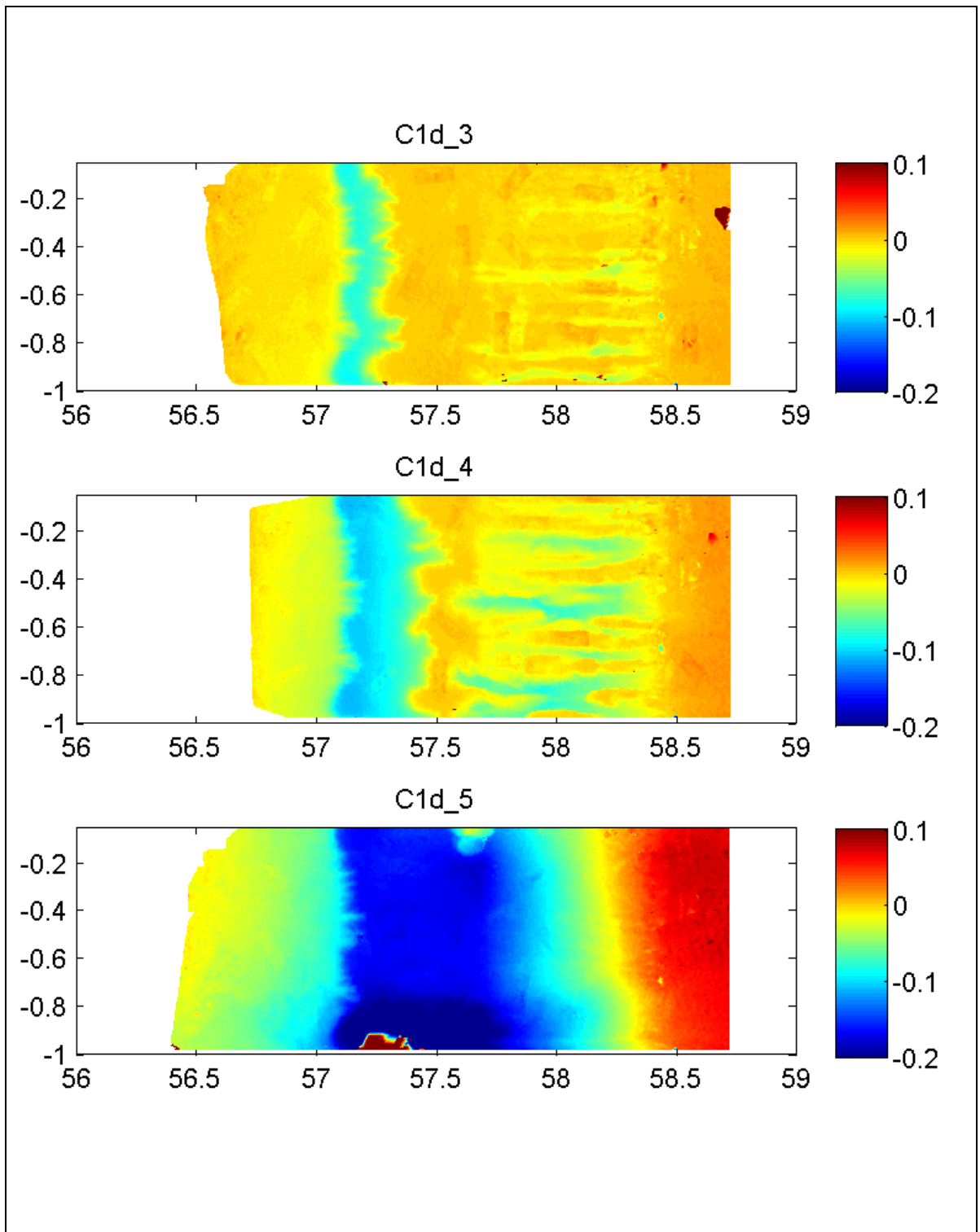




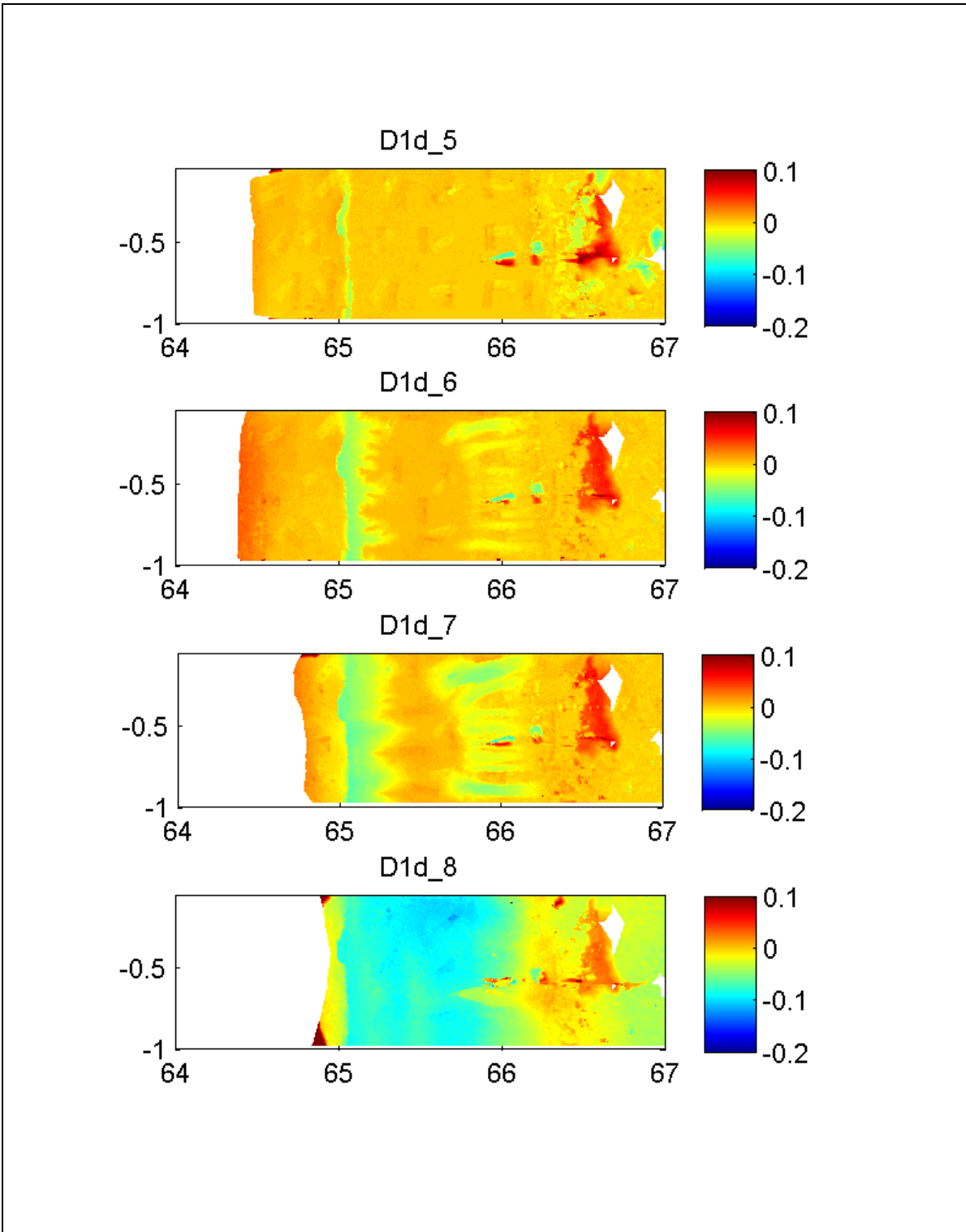
Bathymetric difference plots for experiment B1d with respect to measurement B1d_2. Obtained from stereophotography.	1202124-007-HYE-0005	
	Deltares	Figure C.52



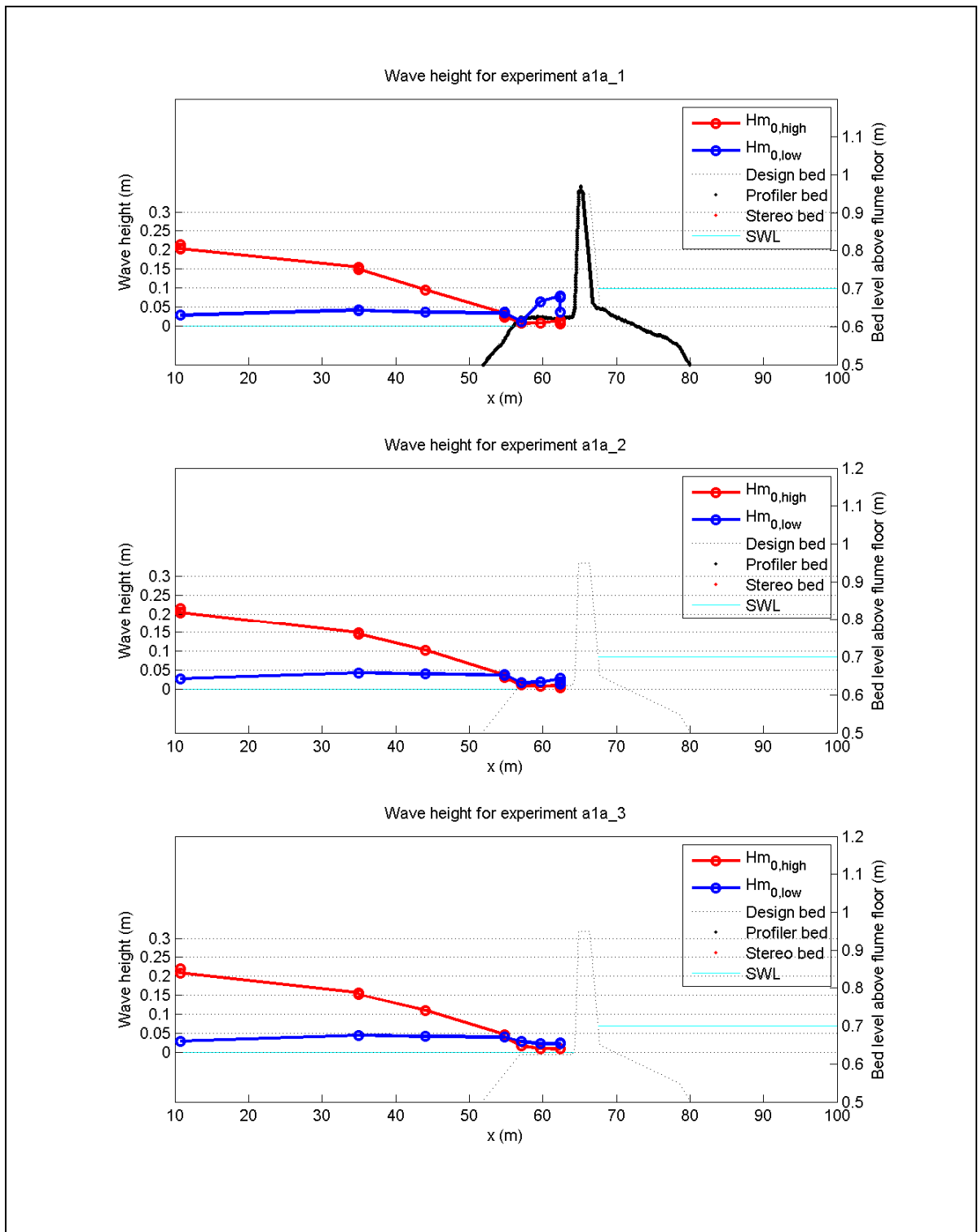
Bathymetric difference plots for experiment B2d with respect to measurement B2d_1. Obtained from stereophotography.	1202124-007-HYE-0005	
Deltares		Figure C.53



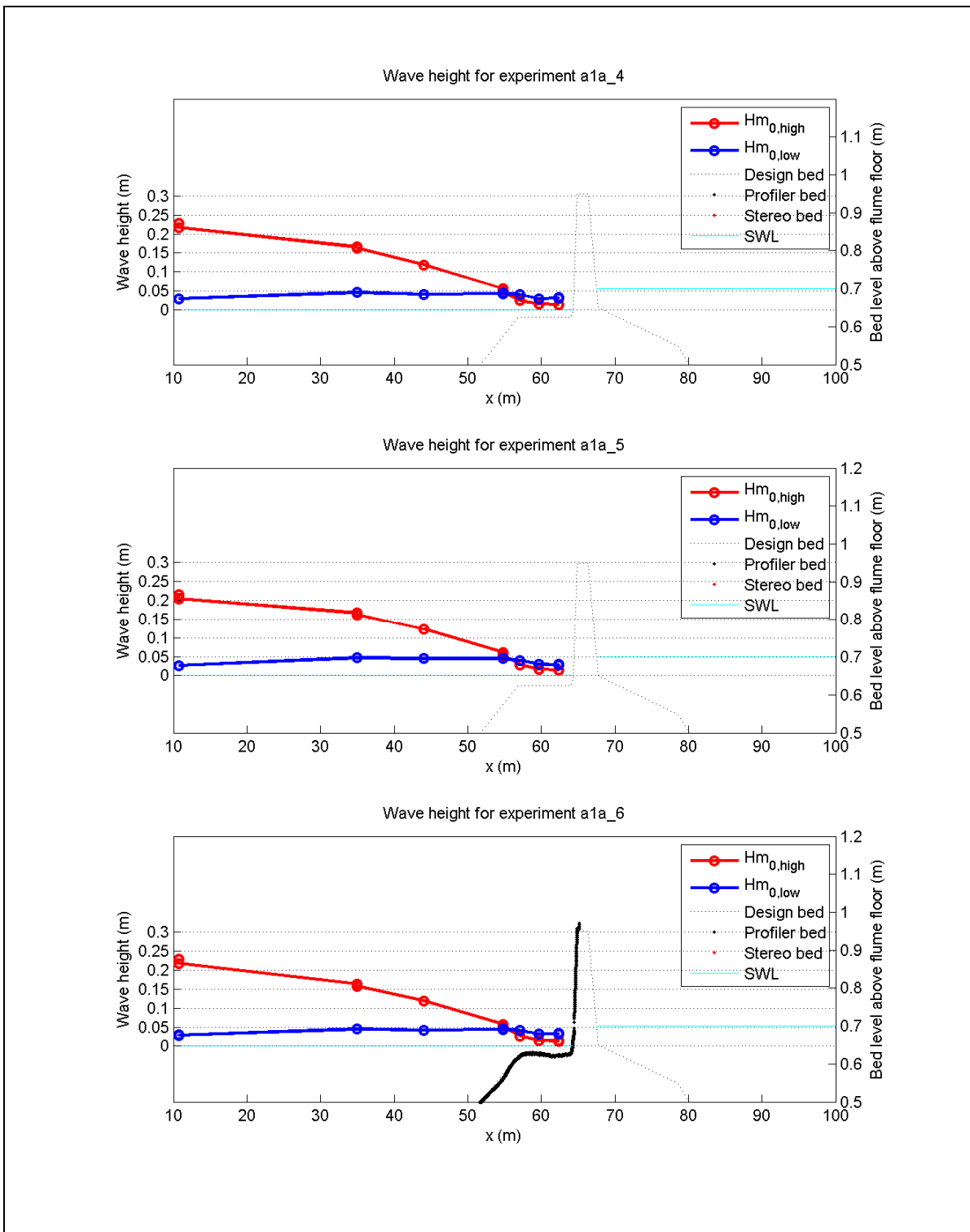
Bathymetric difference plots for experiment C1d with respect to measurement C1d_2. Obtained from stereophotography.	1202124-007-HYE-0005	
	Deltares	Figure C.54



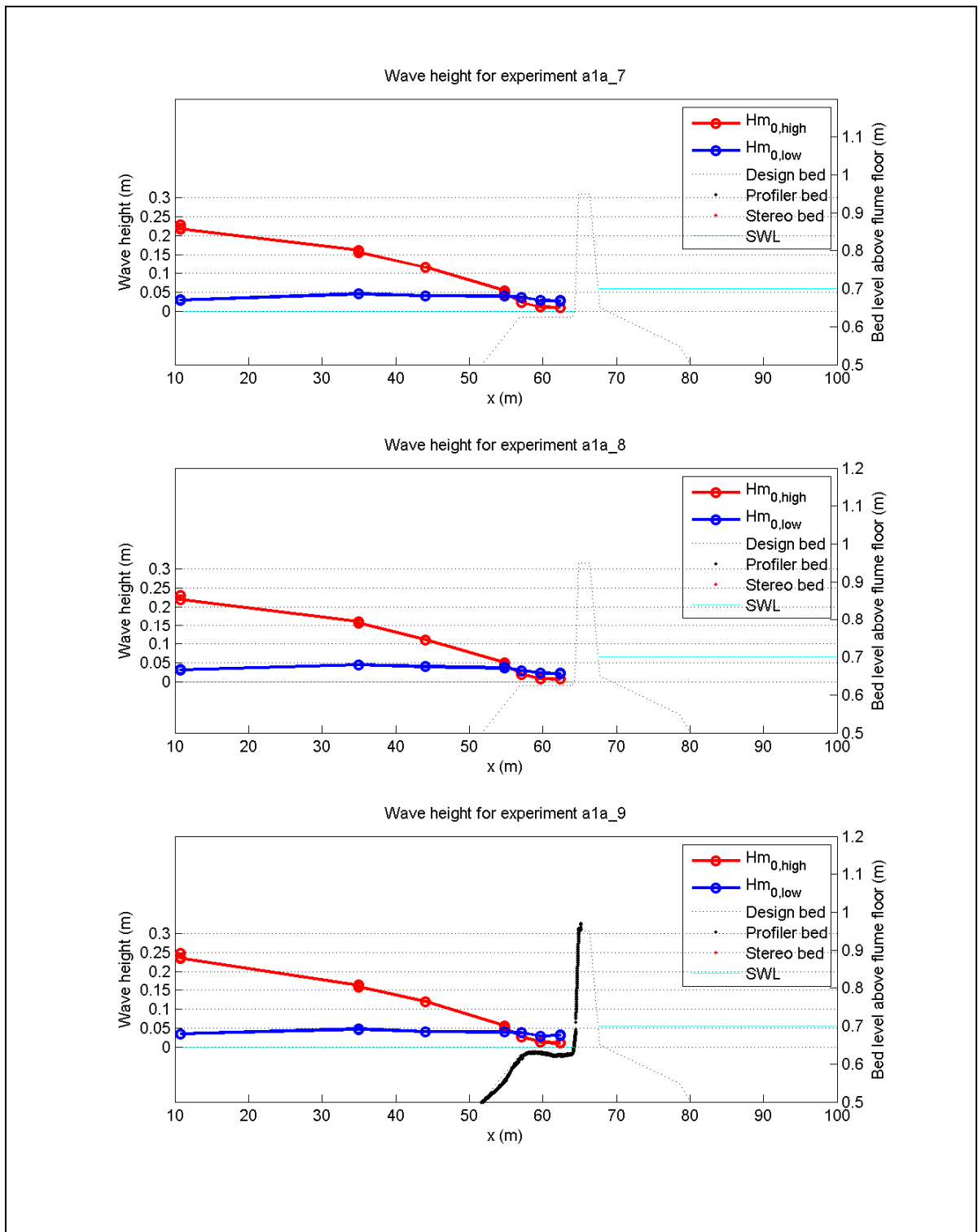
Bathymetric difference plots for experiment D1d with respect to measurement D1d_2. Obtained from stereophotography.	1202124-007-HYE-0005	
Deltares		Figure C.55



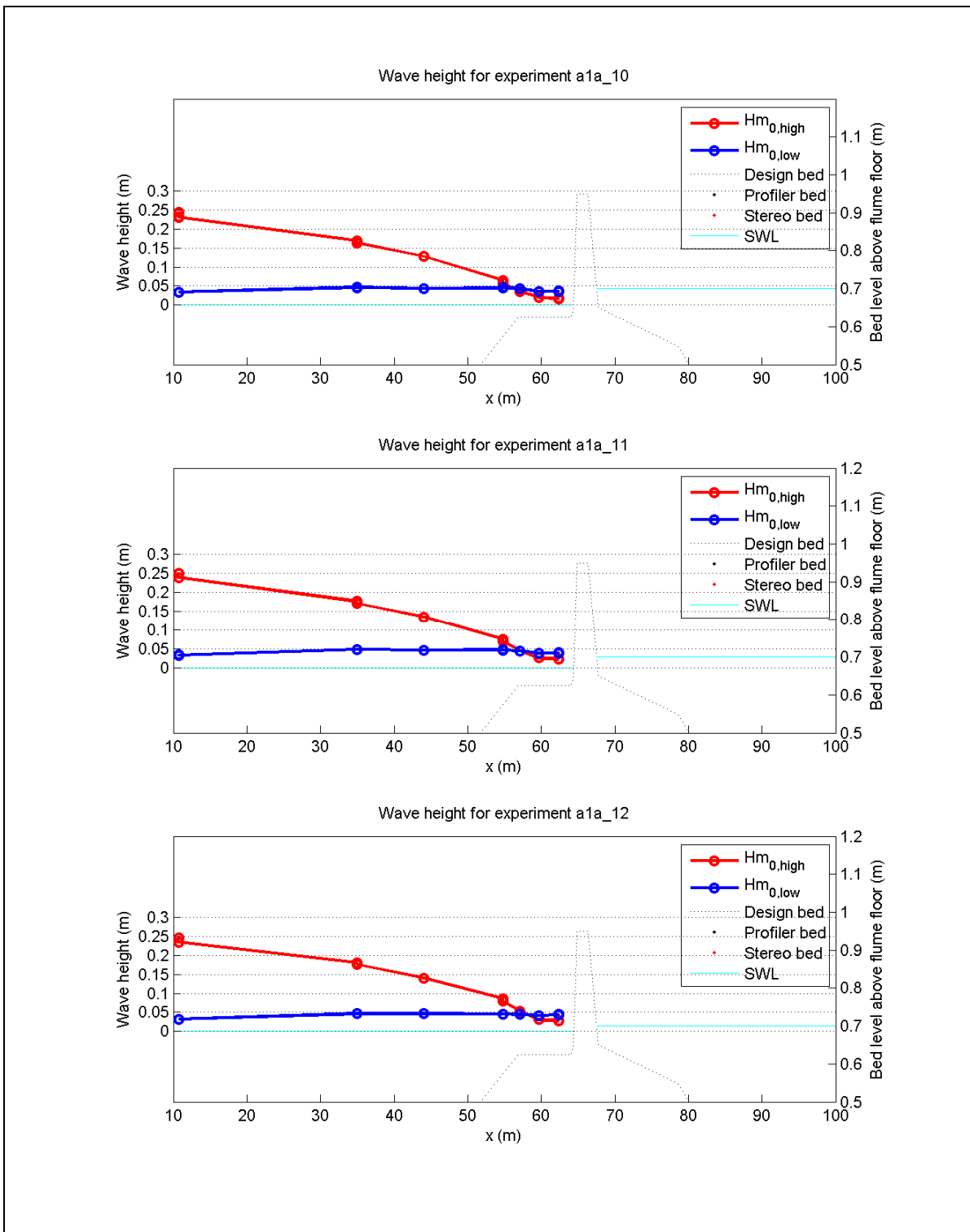
Measured high frequency and low frequency $H_{m0}$ wave height during experiment A1a.	1202124-007-HYE-0005	
	Deltares	Figure C.56



Measured high frequency and low frequency $H_{m0}$ wave height during experiment A1a.	1202124-007-HYE-0005
	Figure C.57

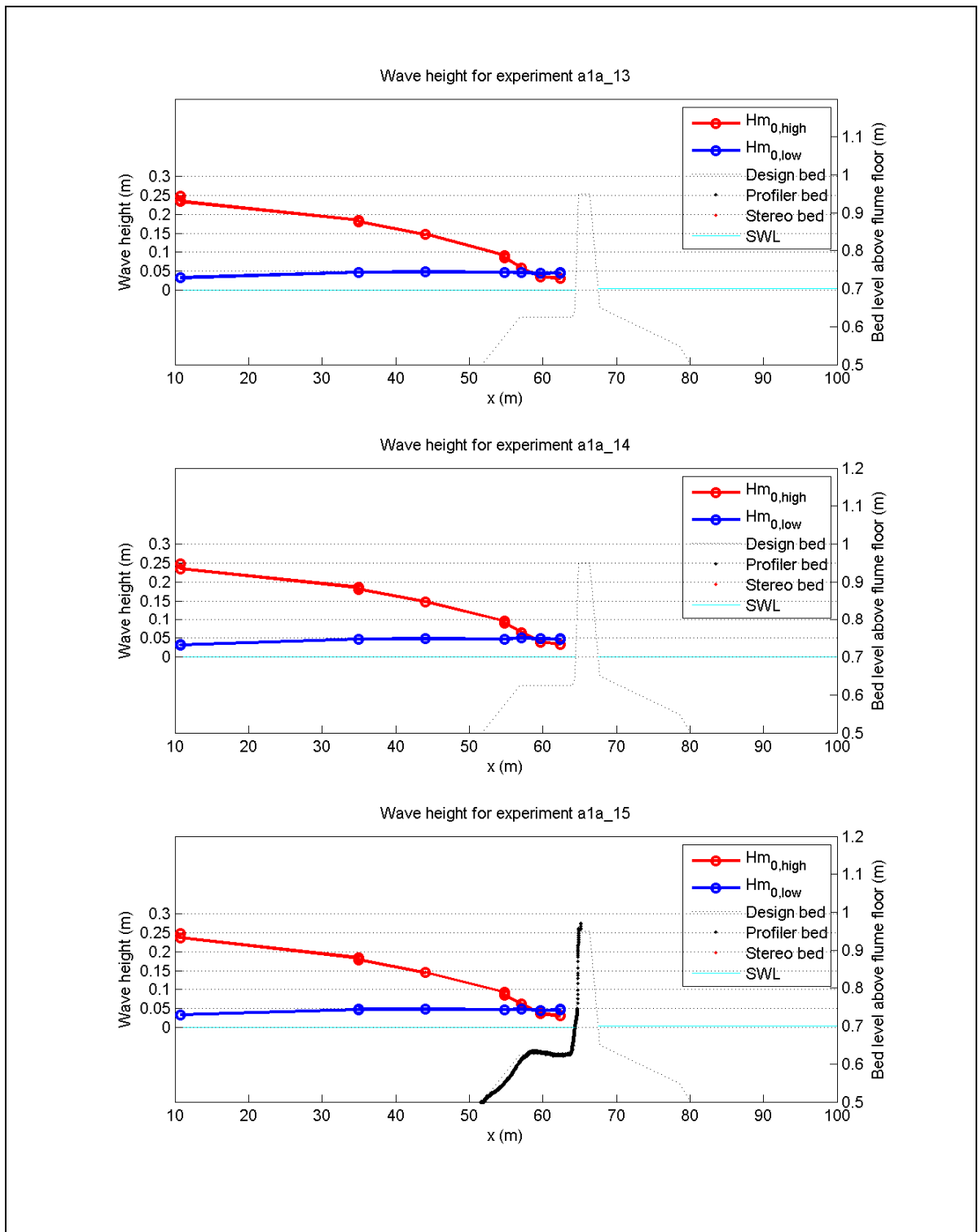


Measured high frequency and low frequency $H_{m0}$ wave height during experiment A1a.	1202124-007-HYE-0005	
	Deltares	Figure C.58

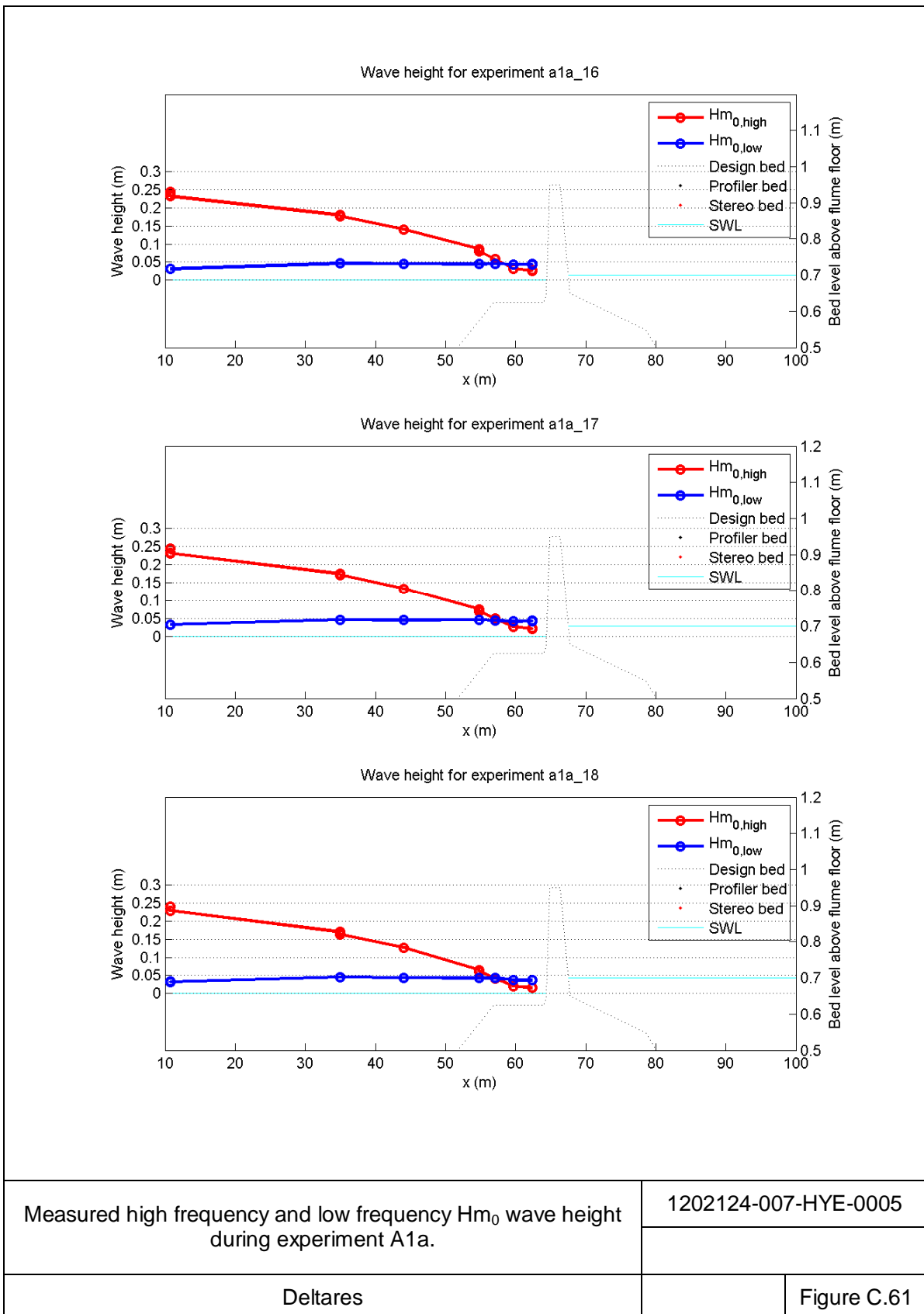


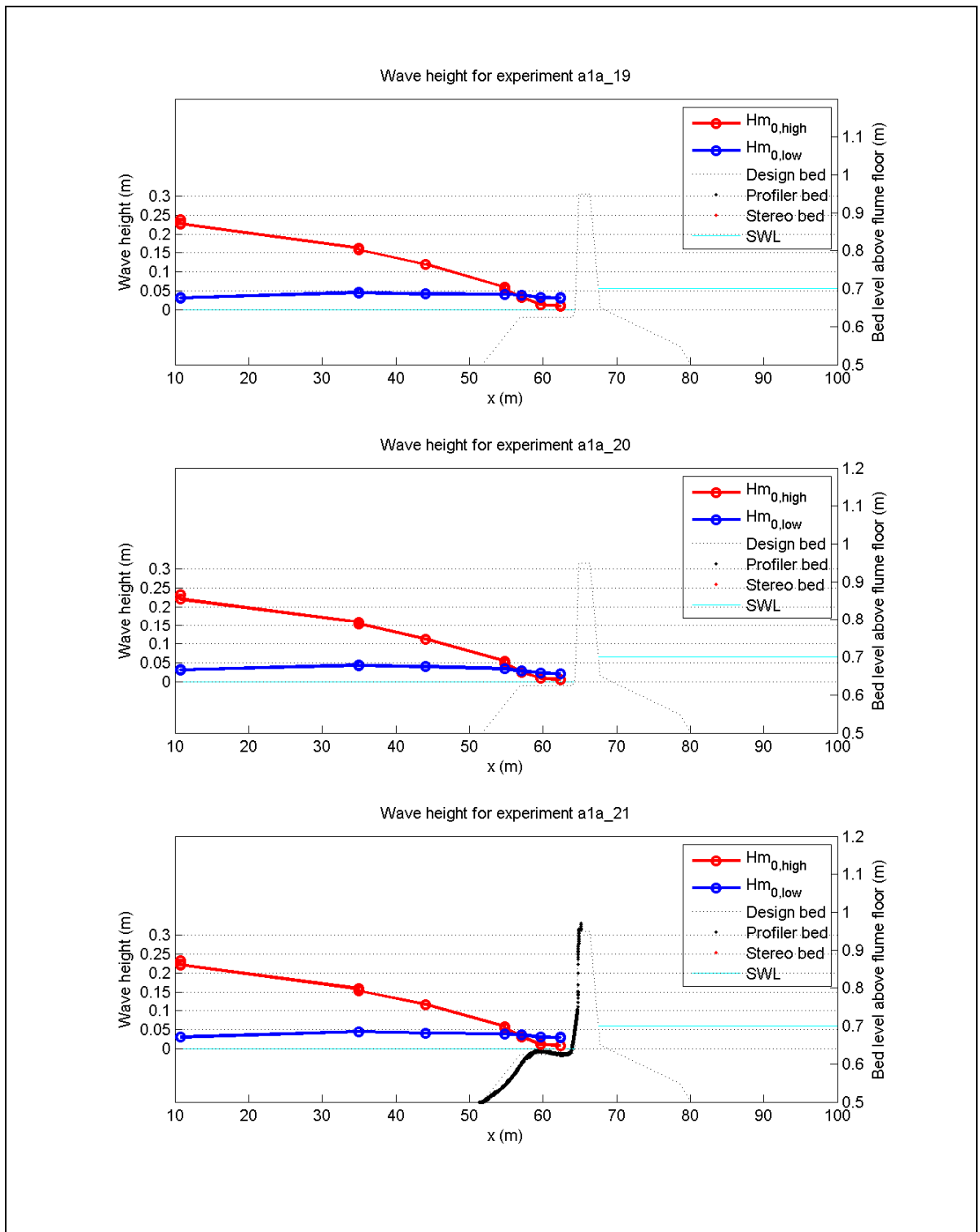
Measured high frequency and low frequency Hm <sub>0</sub> wave height during experiment A1a.	1202124-007-HYE-0005	
	Deltares	Figure C.59



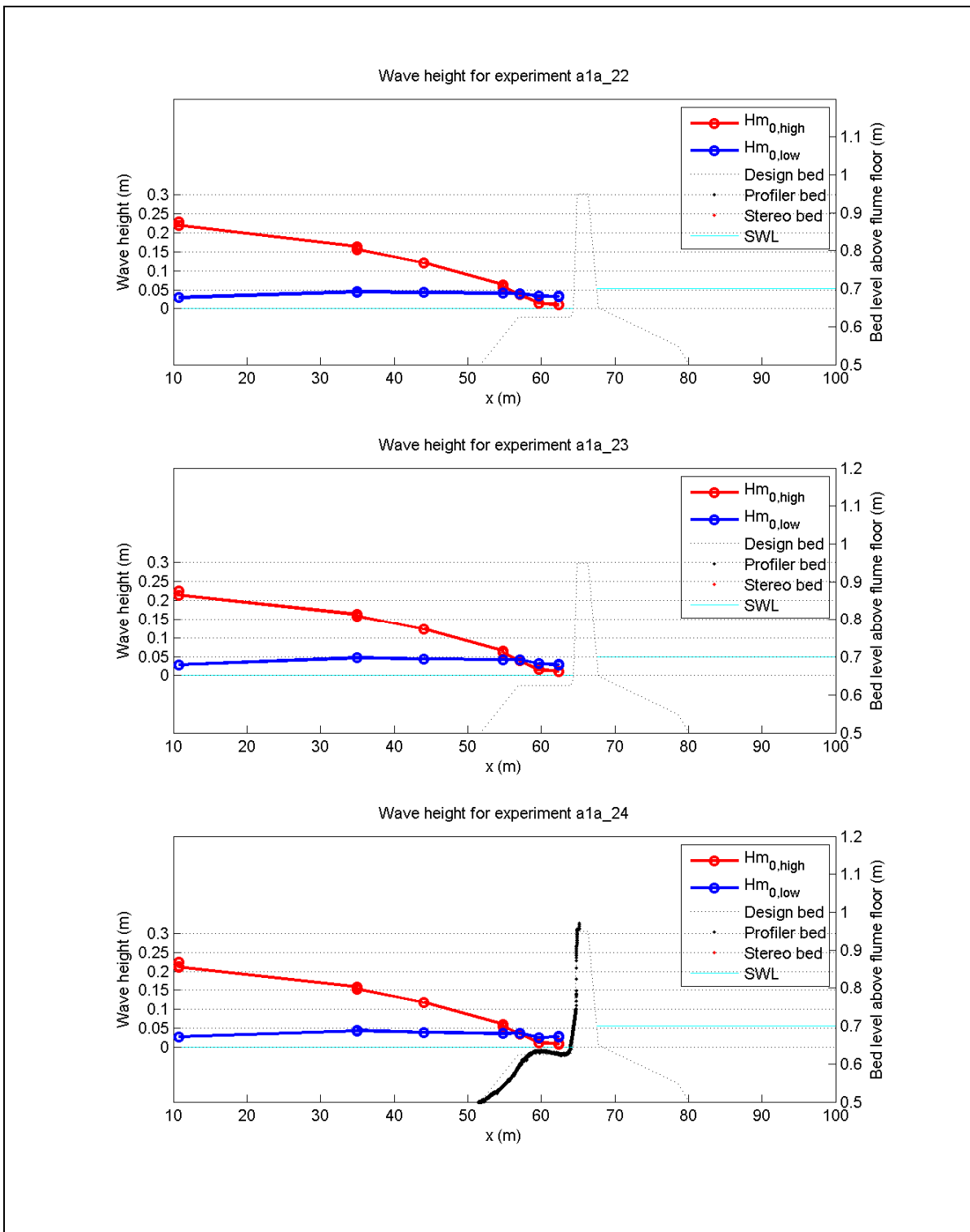


Measured high frequency and low frequency $H_{m0}$ wave height during experiment A1a.	1202124-007-HYE-0005	
	Deltares	Figure C.60

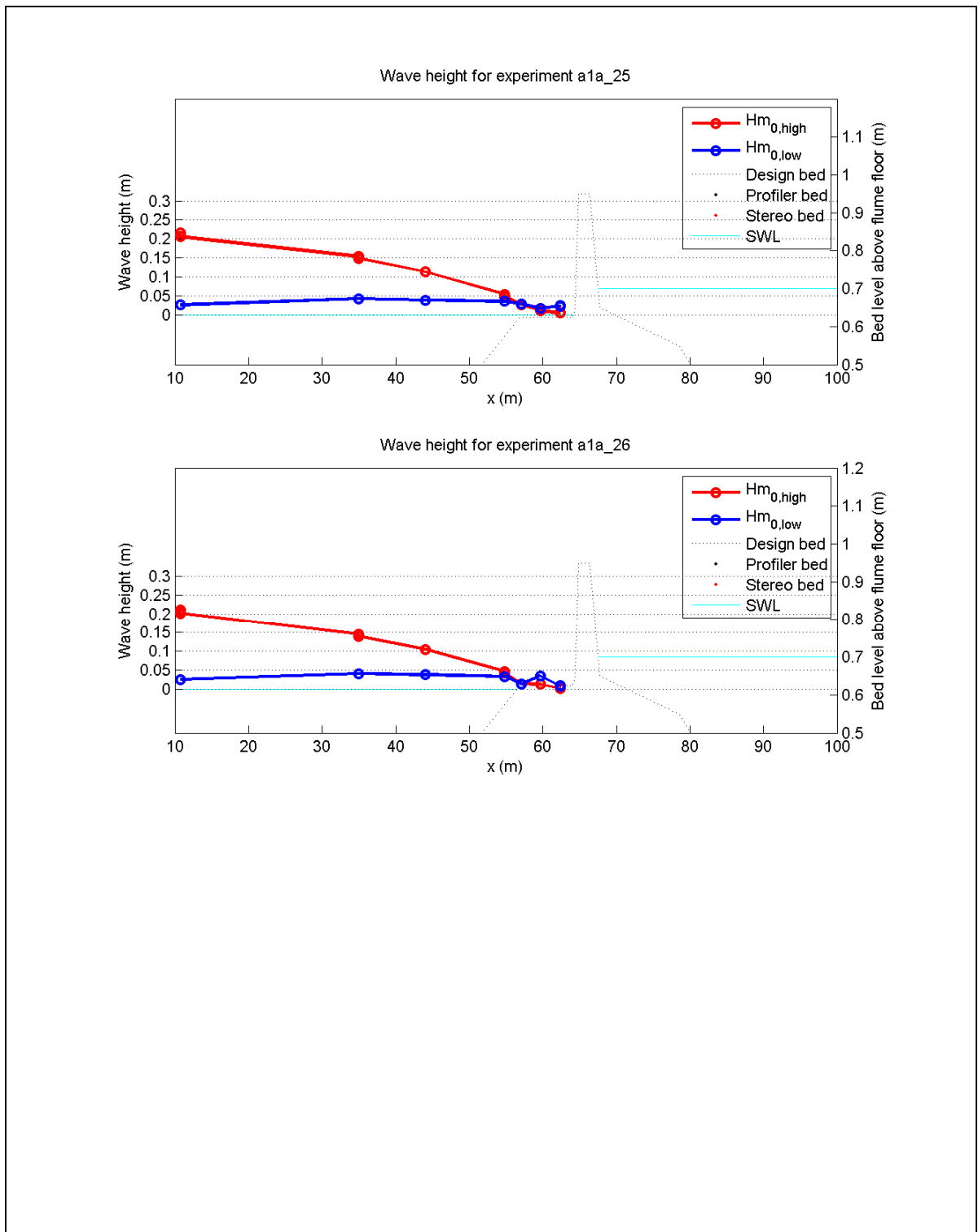




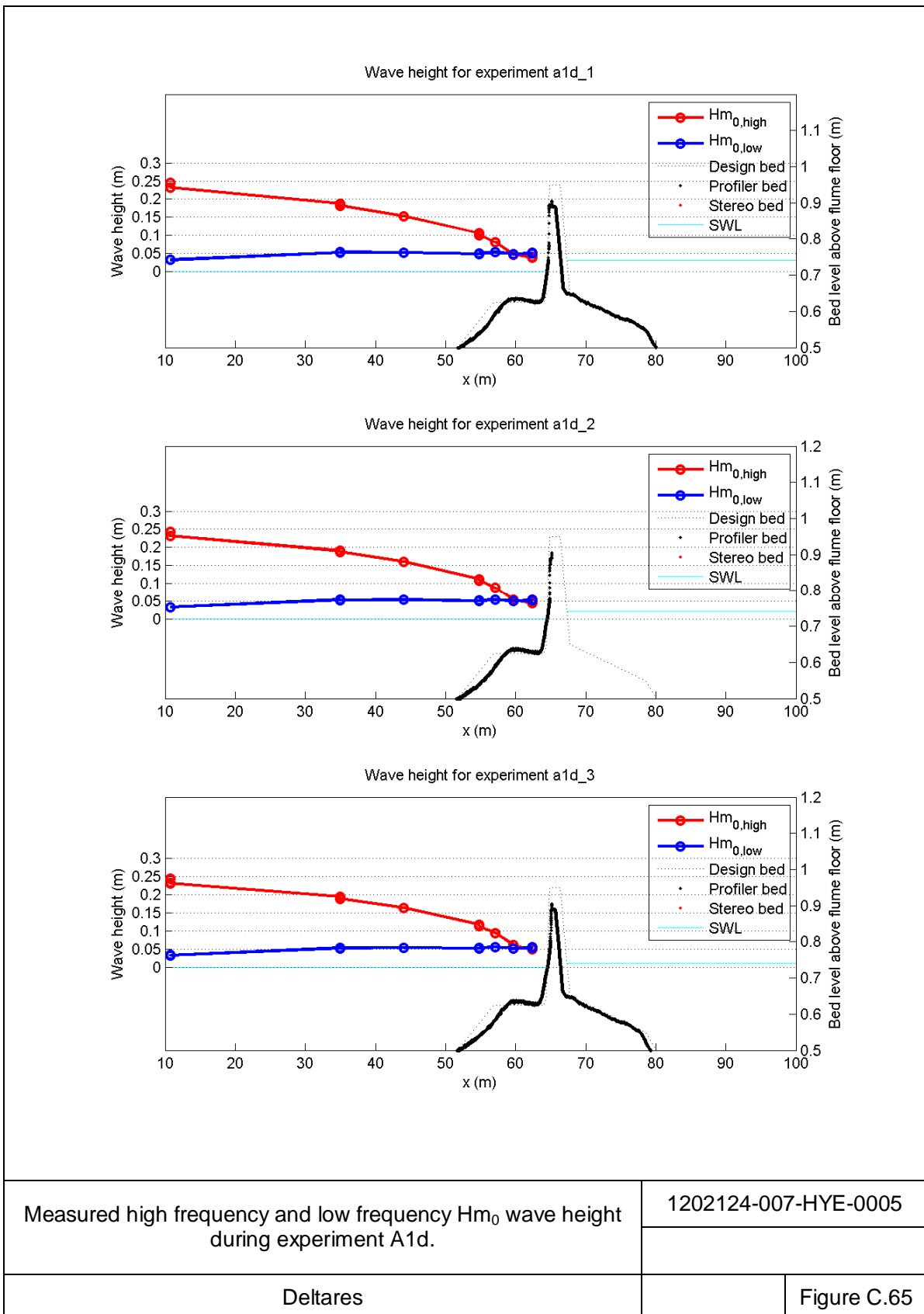
Measured high frequency and low frequency $H_{m0}$ wave height during experiment A1a.	1202124-007-HYE-0005	
	Deltares	Figure C.62

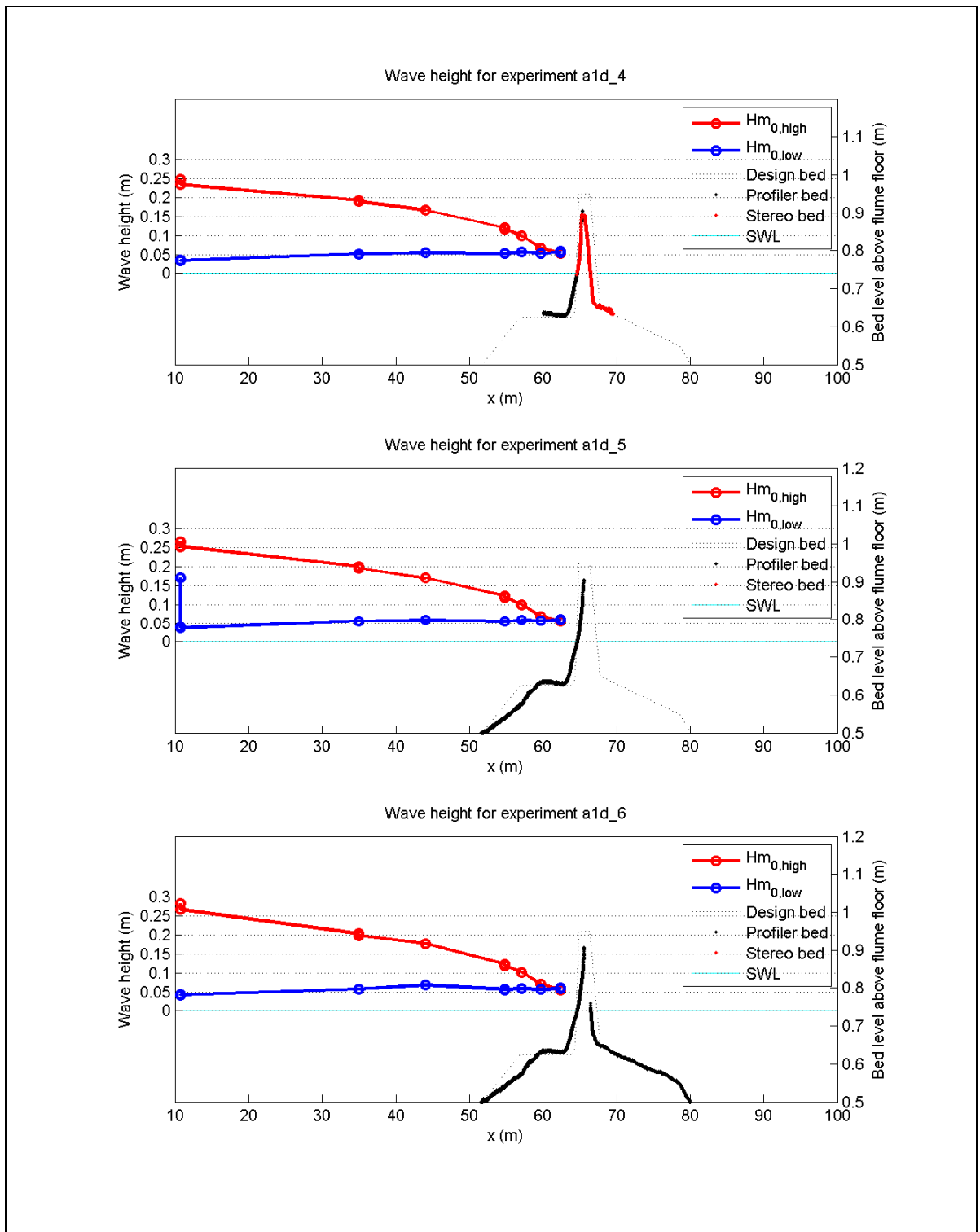


Measured high frequency and low frequency $H_{m0}$ wave height during experiment A1a.	1202124-007-HYE-0005	
	Deltares	Figure C.63

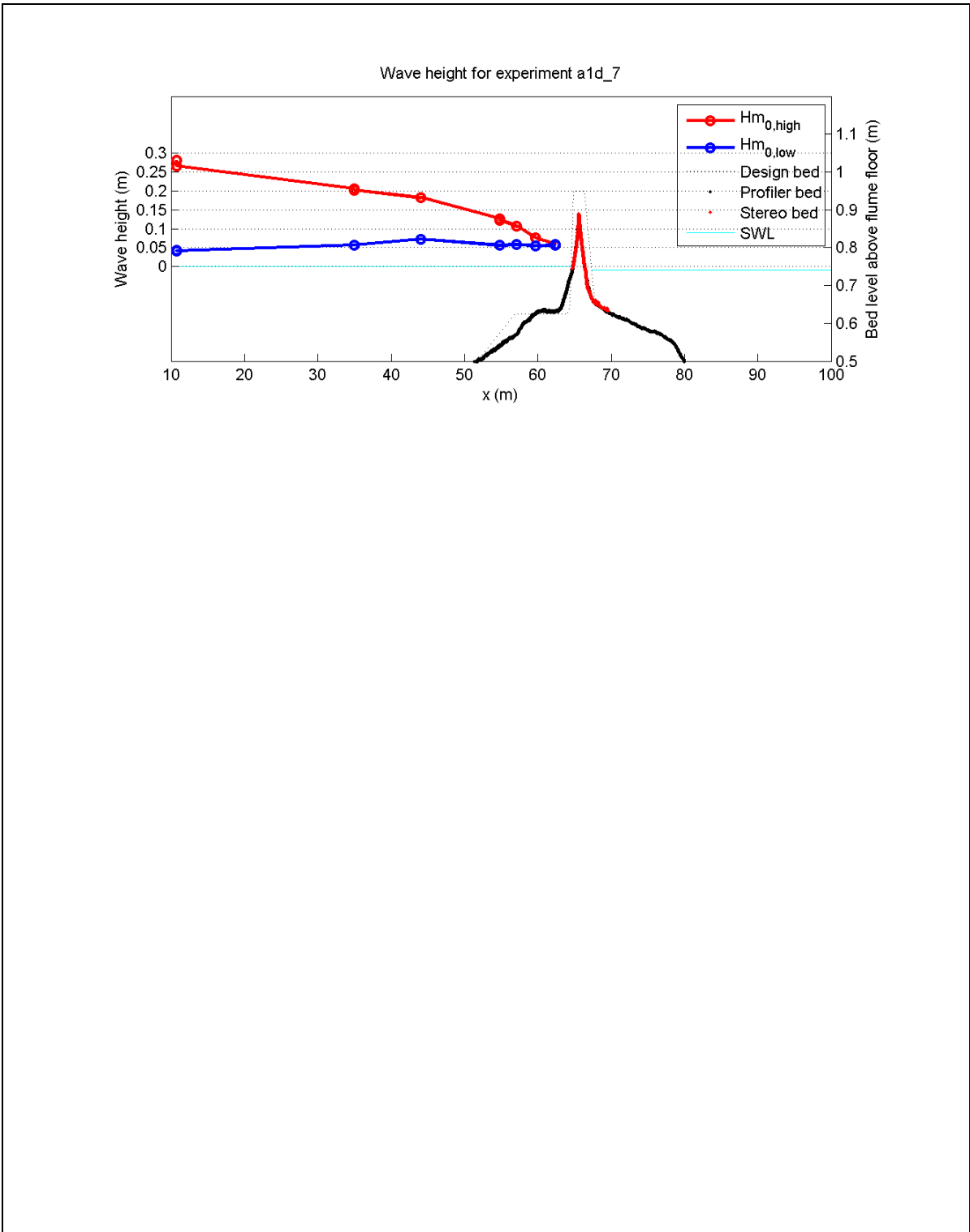


Measured high frequency and low frequency $H_{m0}$ wave height during experiment A1a.	1202124-007-HYE-0005	
Deltares		Figure C.64



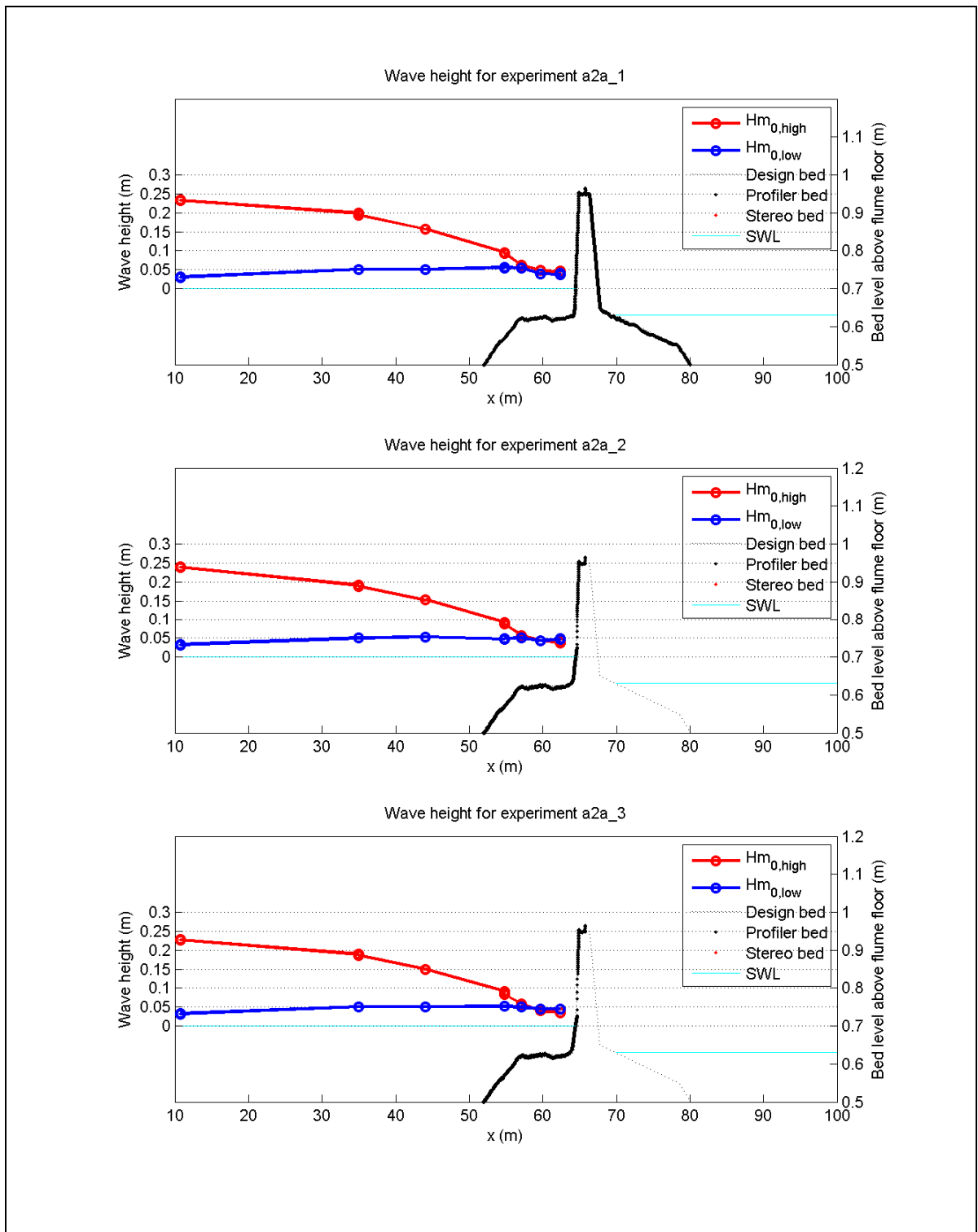


Measured high frequency and low frequency $H_{m0}$ wave height during experiment A1d.	1202124-007-HYE-0005	
	Deltares	Figure C.66

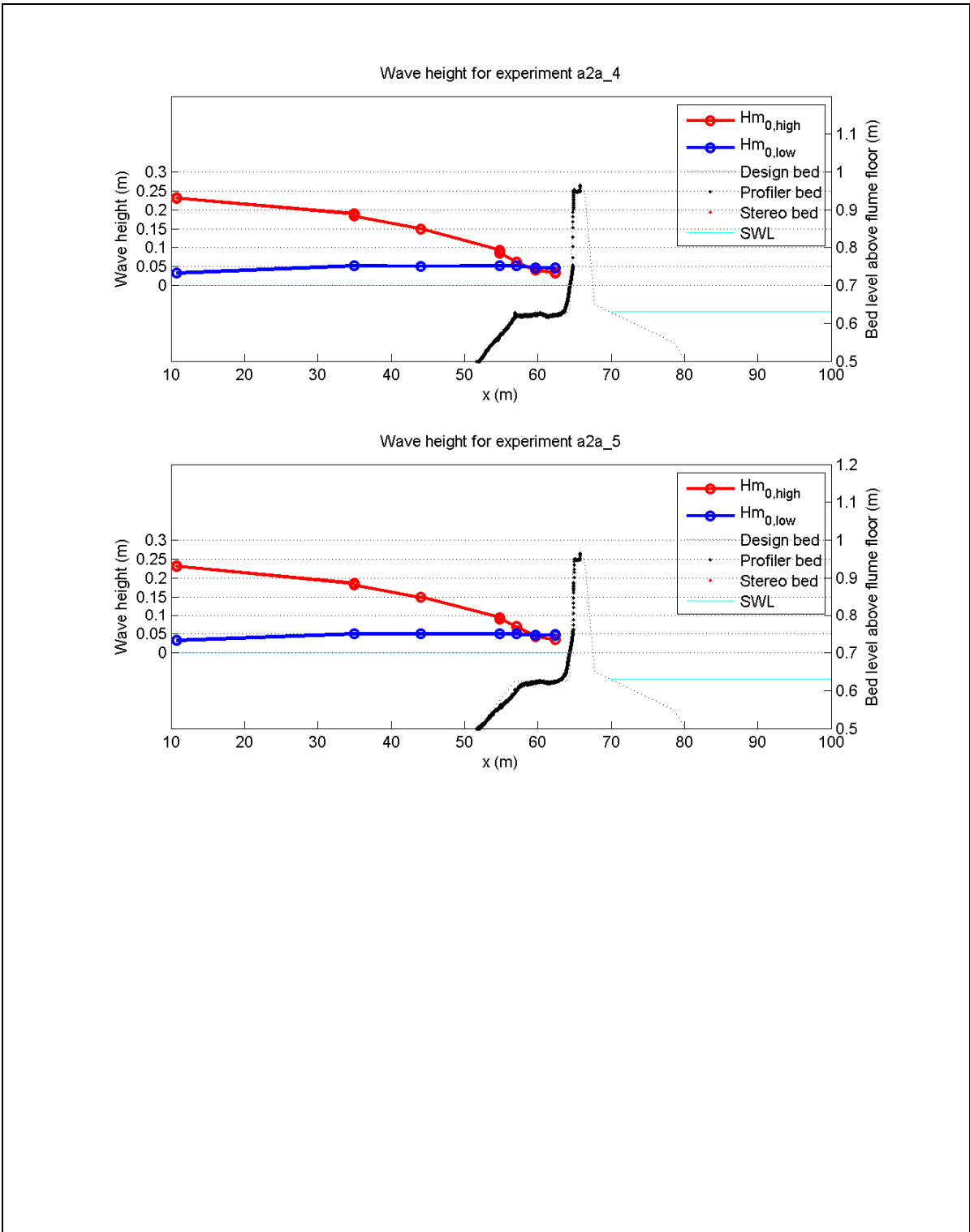


Measured high frequency and low frequency Hm <sub>0</sub> wave height during experiment A1d.	1202124-007-HYE-0005	
Deltares		Figure C.67

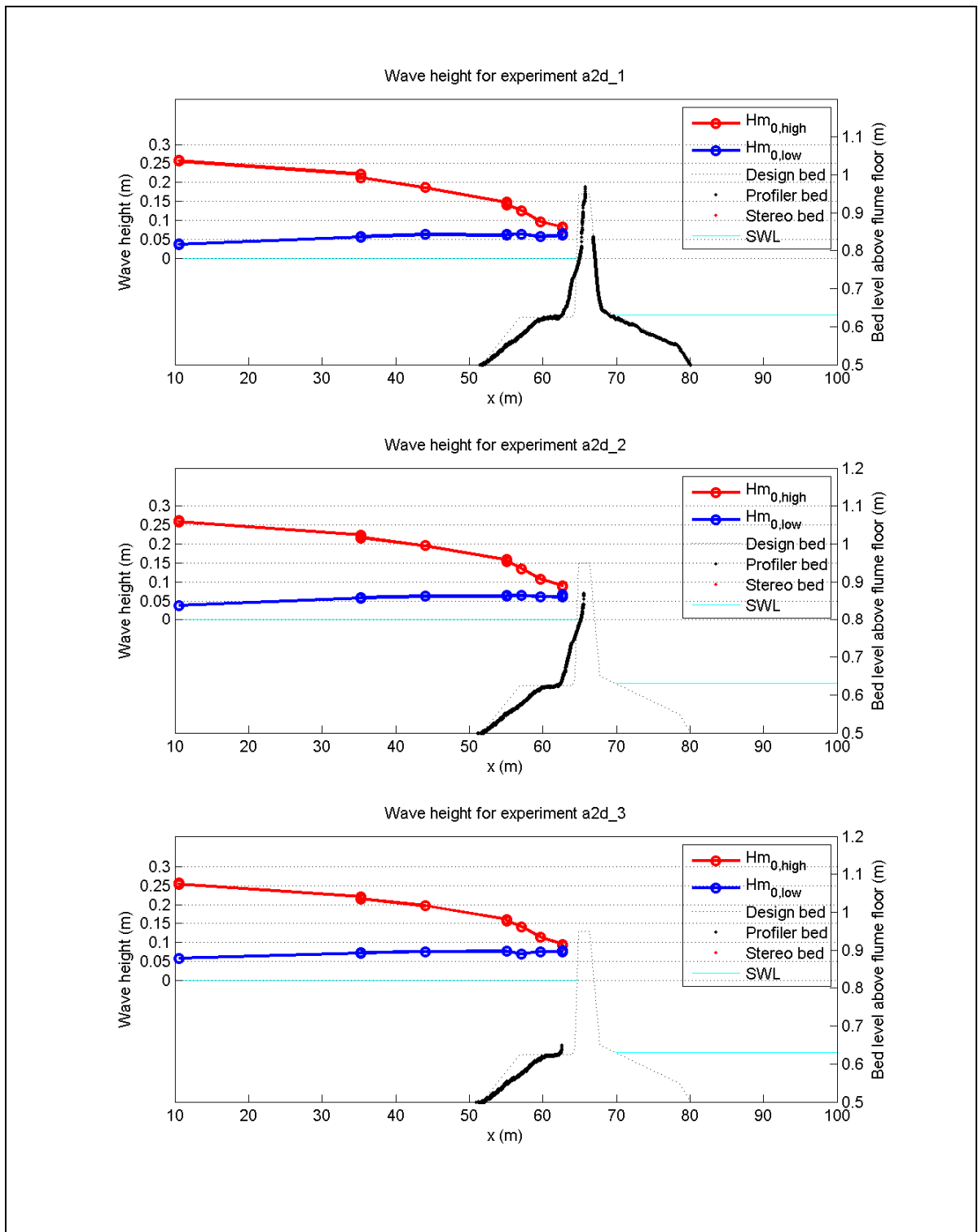




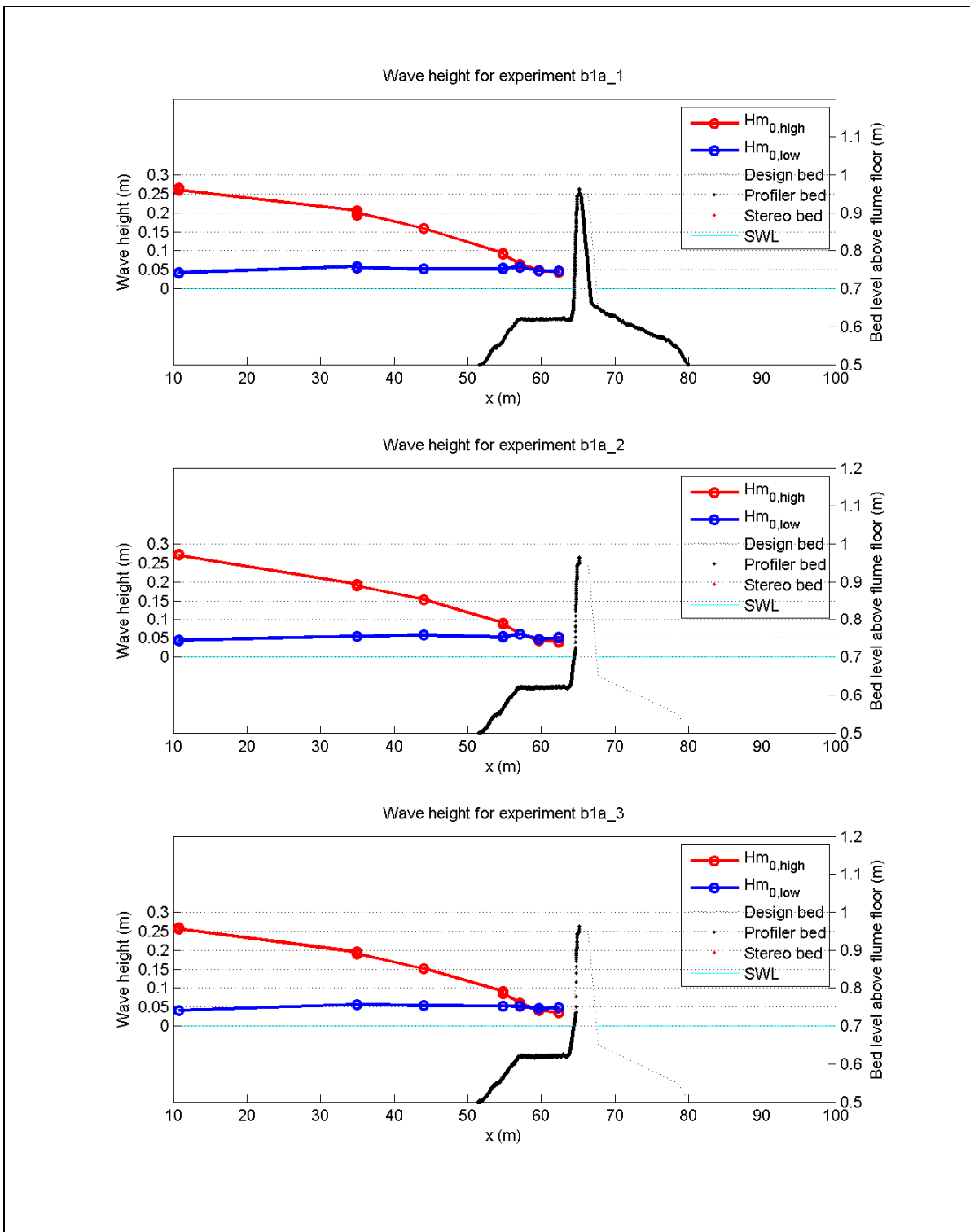
Measured high frequency and low frequency $H_{m0}$ wave height during experiment A2a.	1202124-007-HYE-0005	
	Deltares	Figure C.68



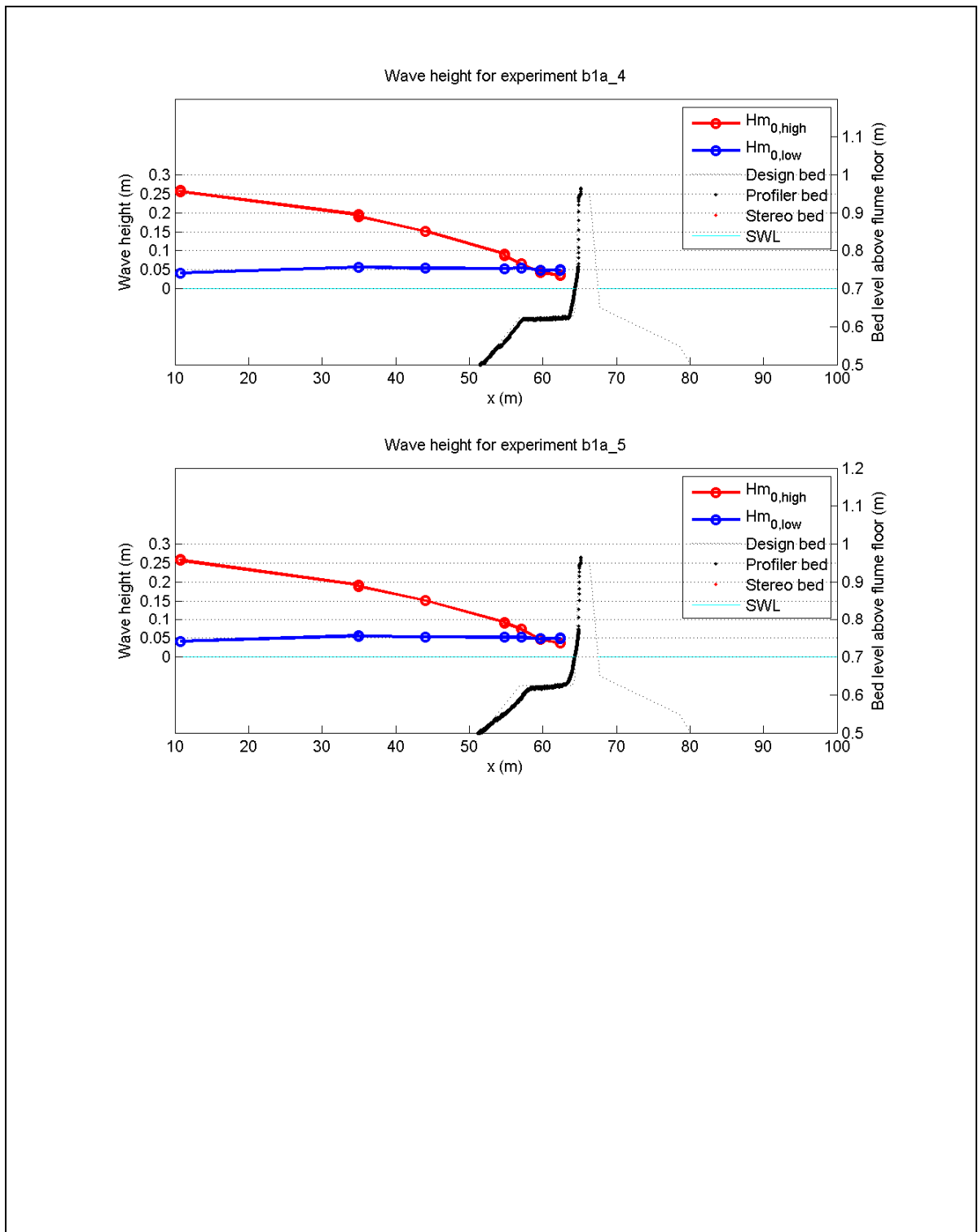
Measured high frequency and low frequency Hm <sub>0</sub> wave height during experiment A2a.	1202124-007-HYE-0005	
	Deltares	Figure C.69



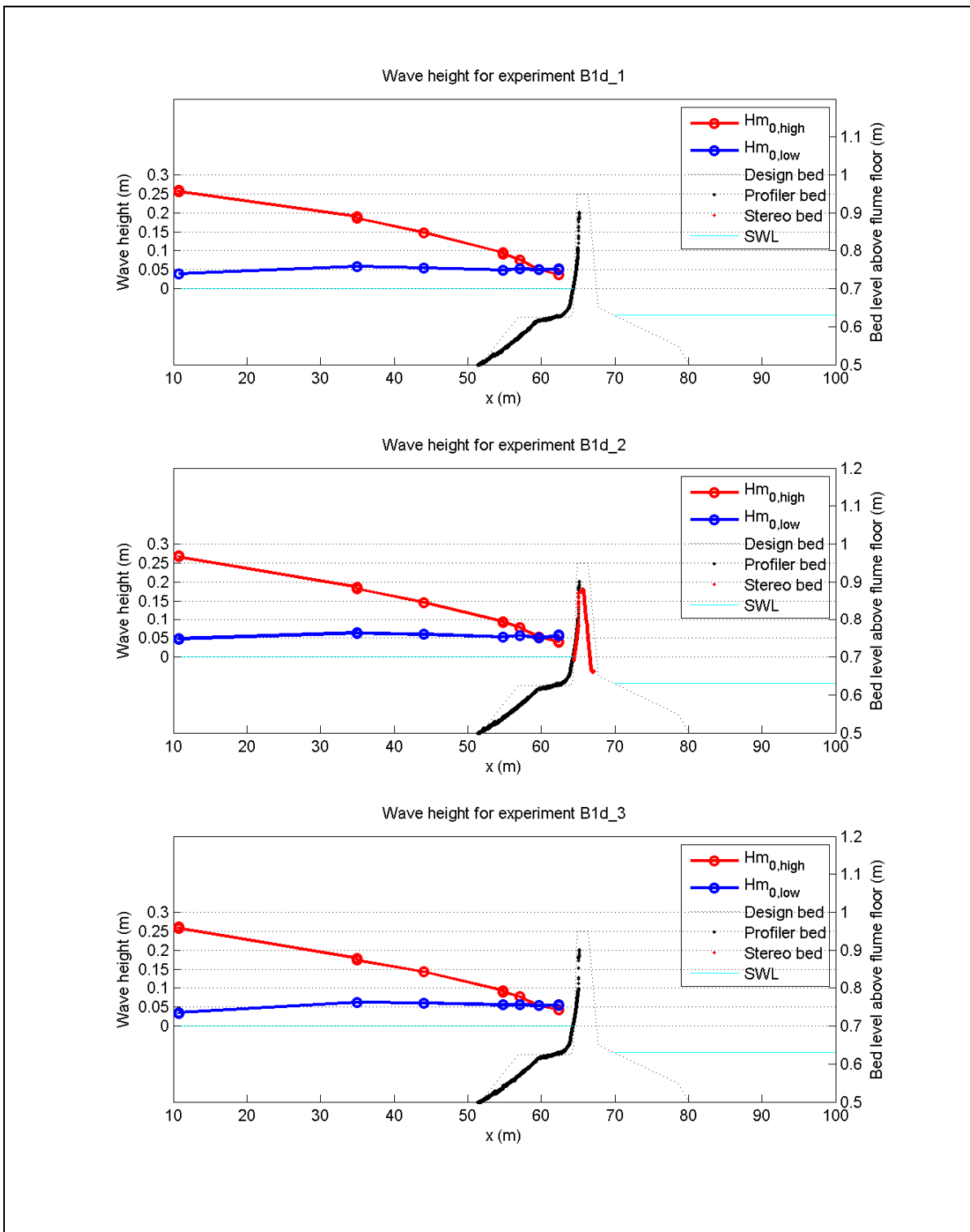
Measured high frequency and low frequency $H_{m0}$ wave height during experiment A2d.	1202124-007-HYE-0005	
	Deltares	Figure C.70



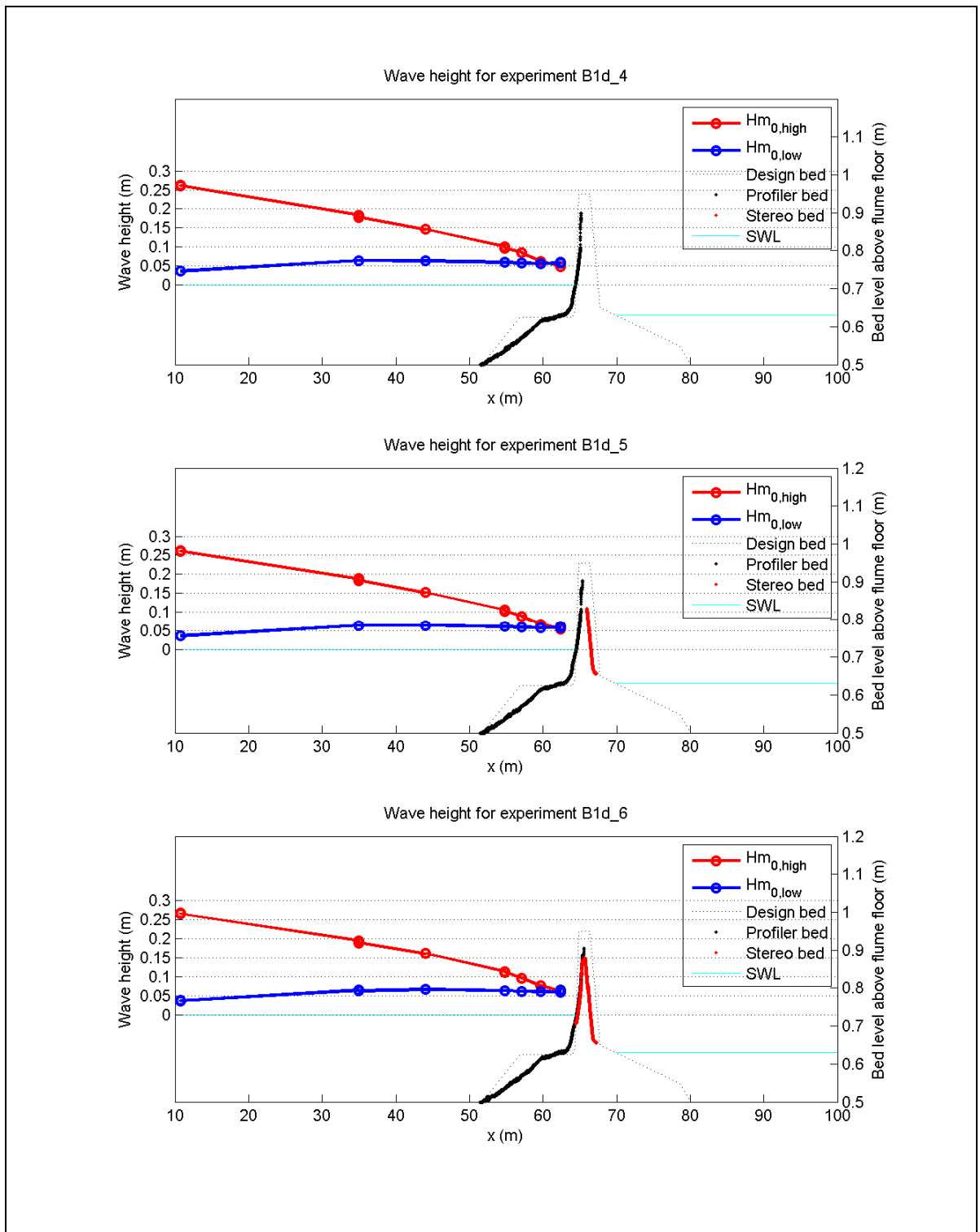
Measured high frequency and low frequency $Hm_0$ wave height during experiment B1a.	1202124-007-HYE-0005	
	Deltares	Figure C.71



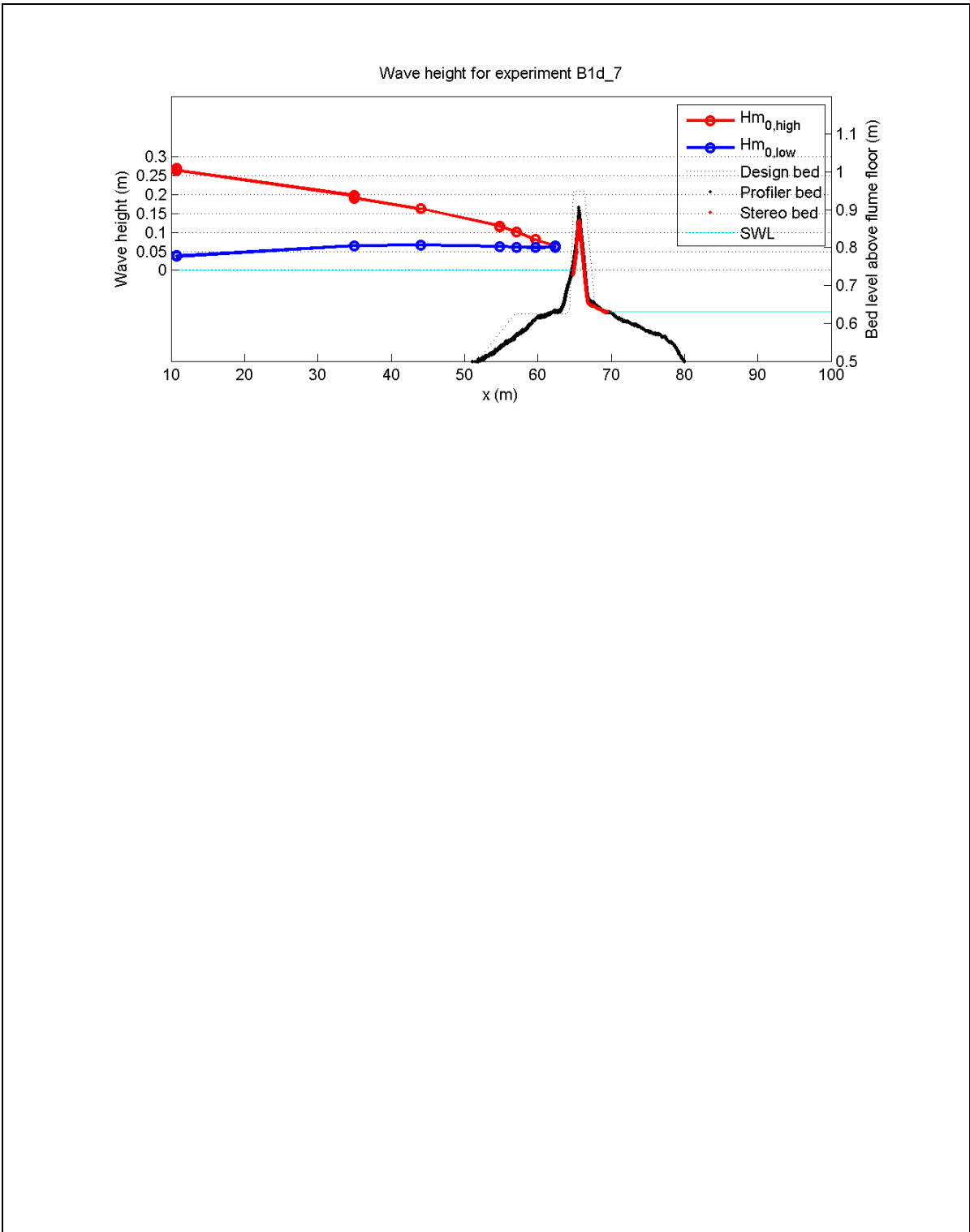
Measured high frequency and low frequency $H_{m0}$ wave height during experiment B1a.	1202124-007-HYE-0005	
	Deltares	Figure C.72



Measured high frequency and low frequency $H_{m0}$ wave height during experiment B1d.	1202124-007-HYE-0005	
	Deltares	Figure C.73

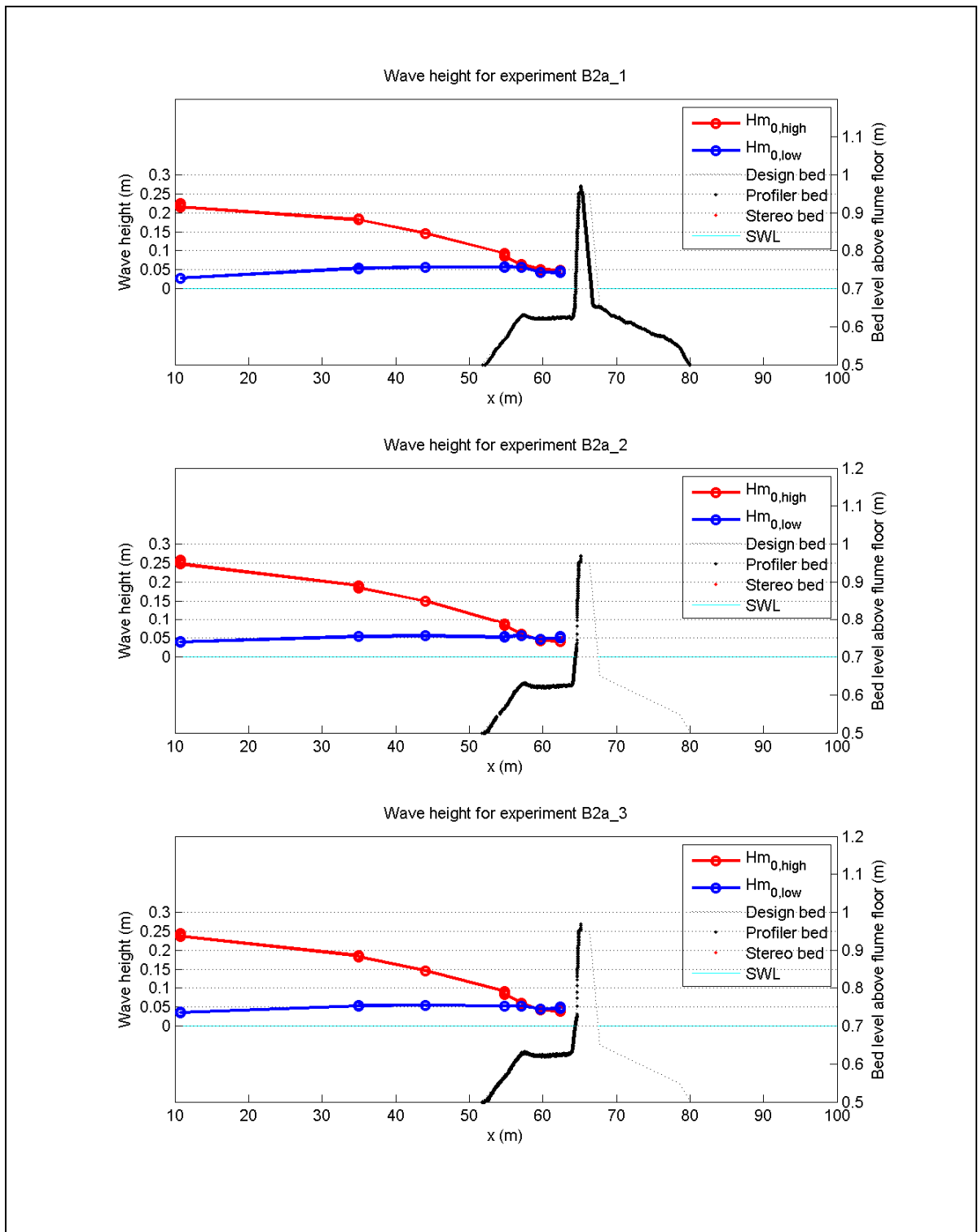


Measured high frequency and low frequency $H_{m0}$ wave height during experiment B1d.	1202124-007-HYE-0005	
	Deltares	Figure C.74

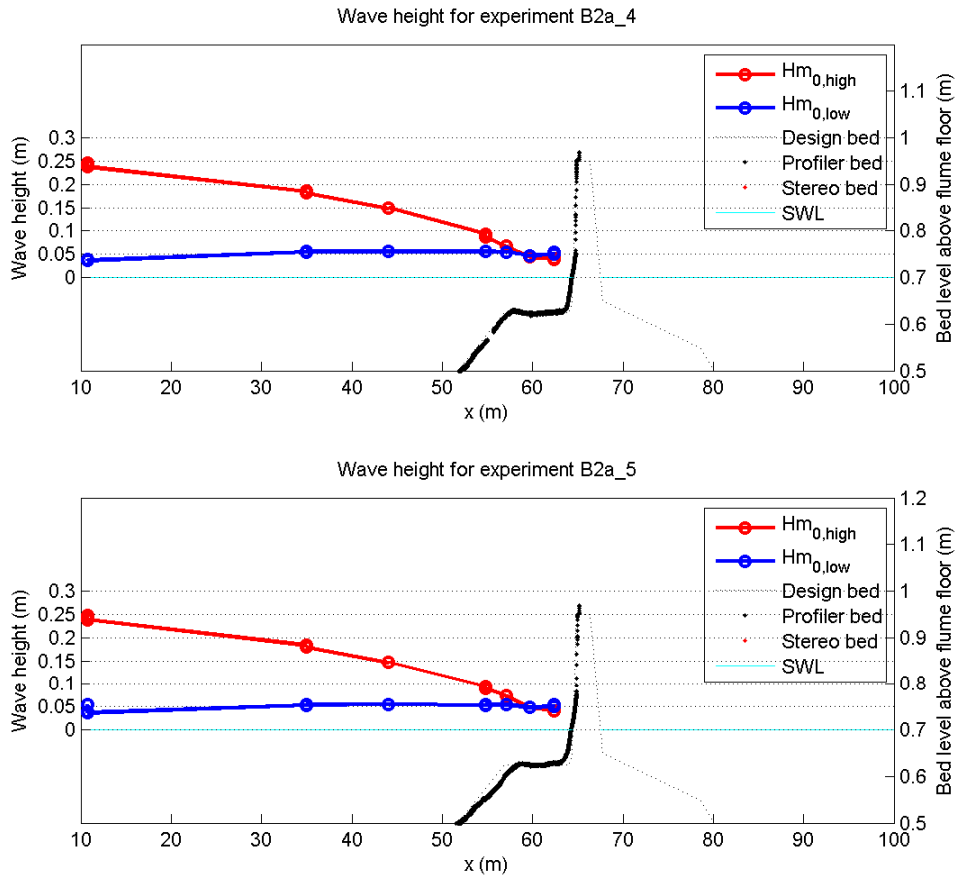


Measured high frequency and low frequency Hm <sub>0</sub> wave height during experiment B1d.	1202124-007-HYE-0005	
Deltares		Figure C.75





Measured high frequency and low frequency $H_{m0}$ wave height during experiment B2a.	1202124-007-HYE-0005	
	Deltares	Figure C.76

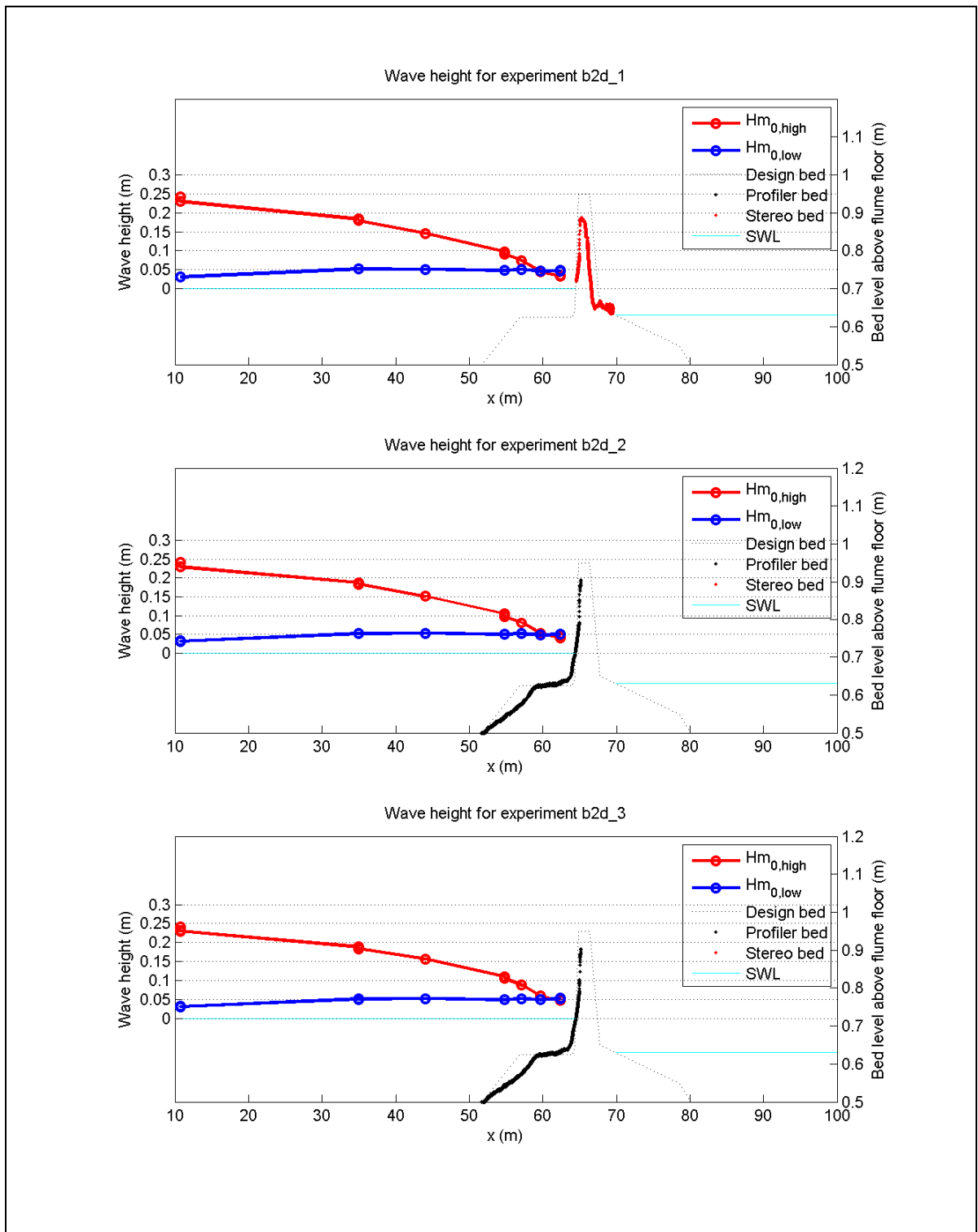


Measured high frequency and low frequency  $H_{m0}$  wave height during experiment B2a.

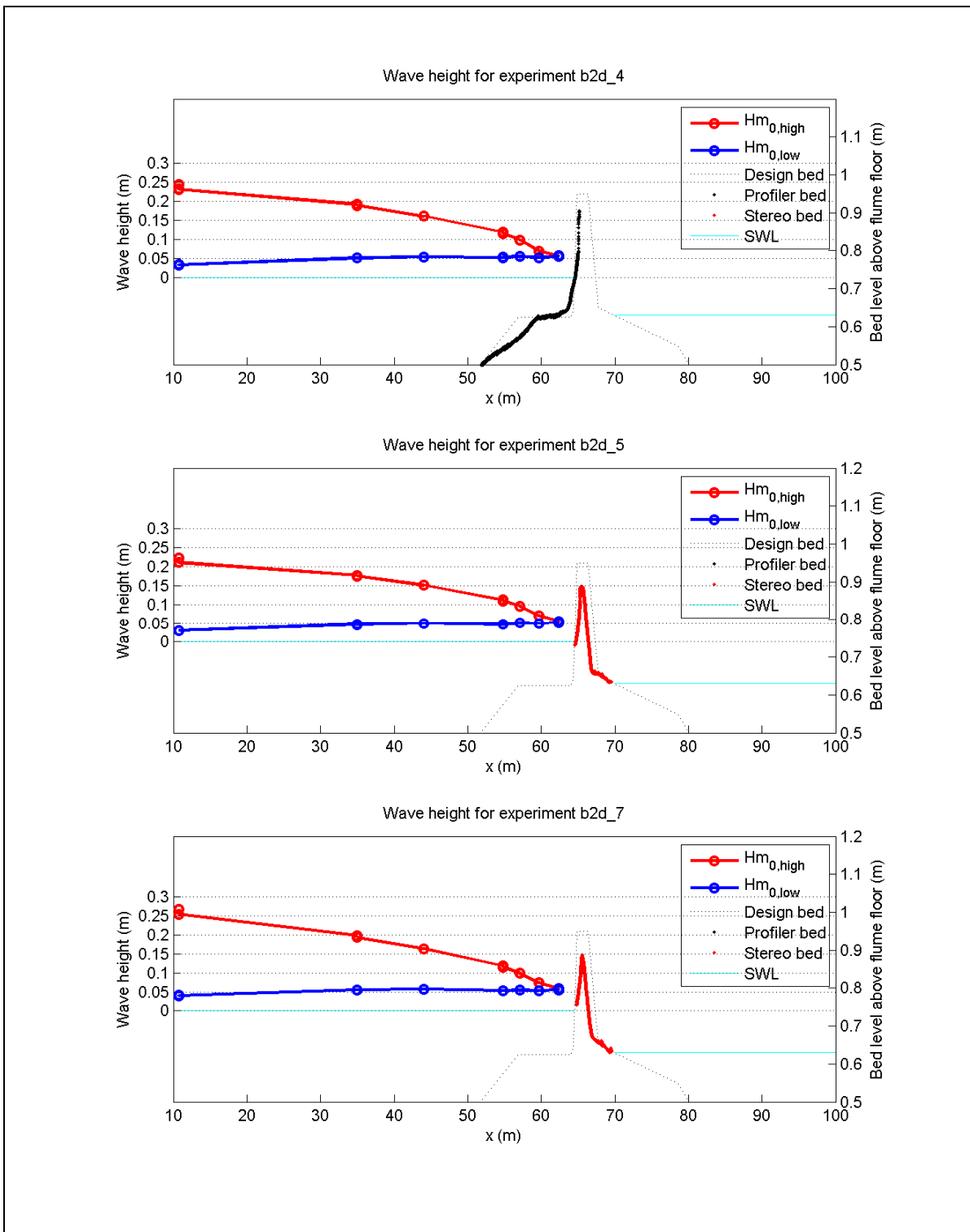
1202124-007-HYE-0005

Deltares

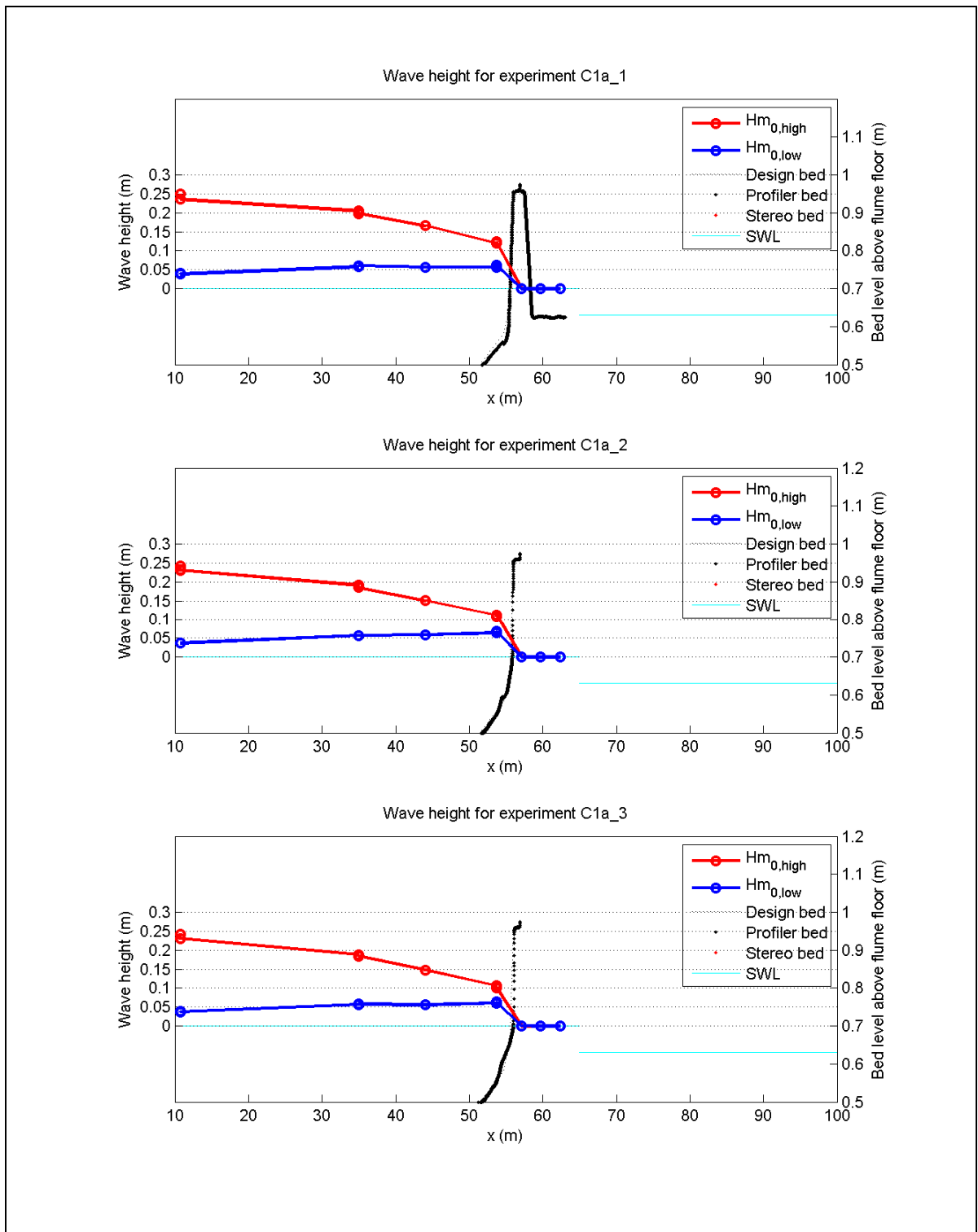
Figure C.77



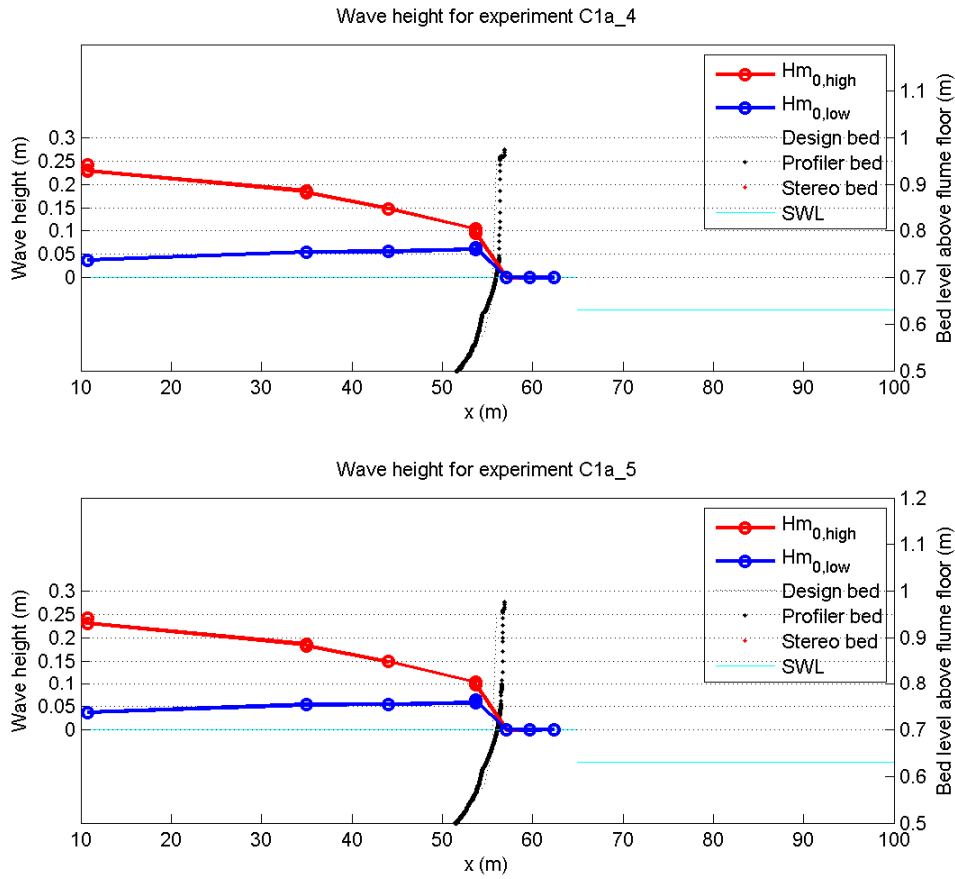
Measured high frequency and low frequency $H_{m0}$ wave height during experiment B2d.	1202124-007-HYE-0005	
	Deltares	Figure C.78



Measured high frequency and low frequency $Hm_0$ wave height during experiment B2d.	1202124-007-HYE-0005	
	Deltares	Figure C.79



Measured high frequency and low frequency $H_{m0}$ wave height during experiment C1a.	1202124-007-HYE-0005	
	Deltares	Figure C.80

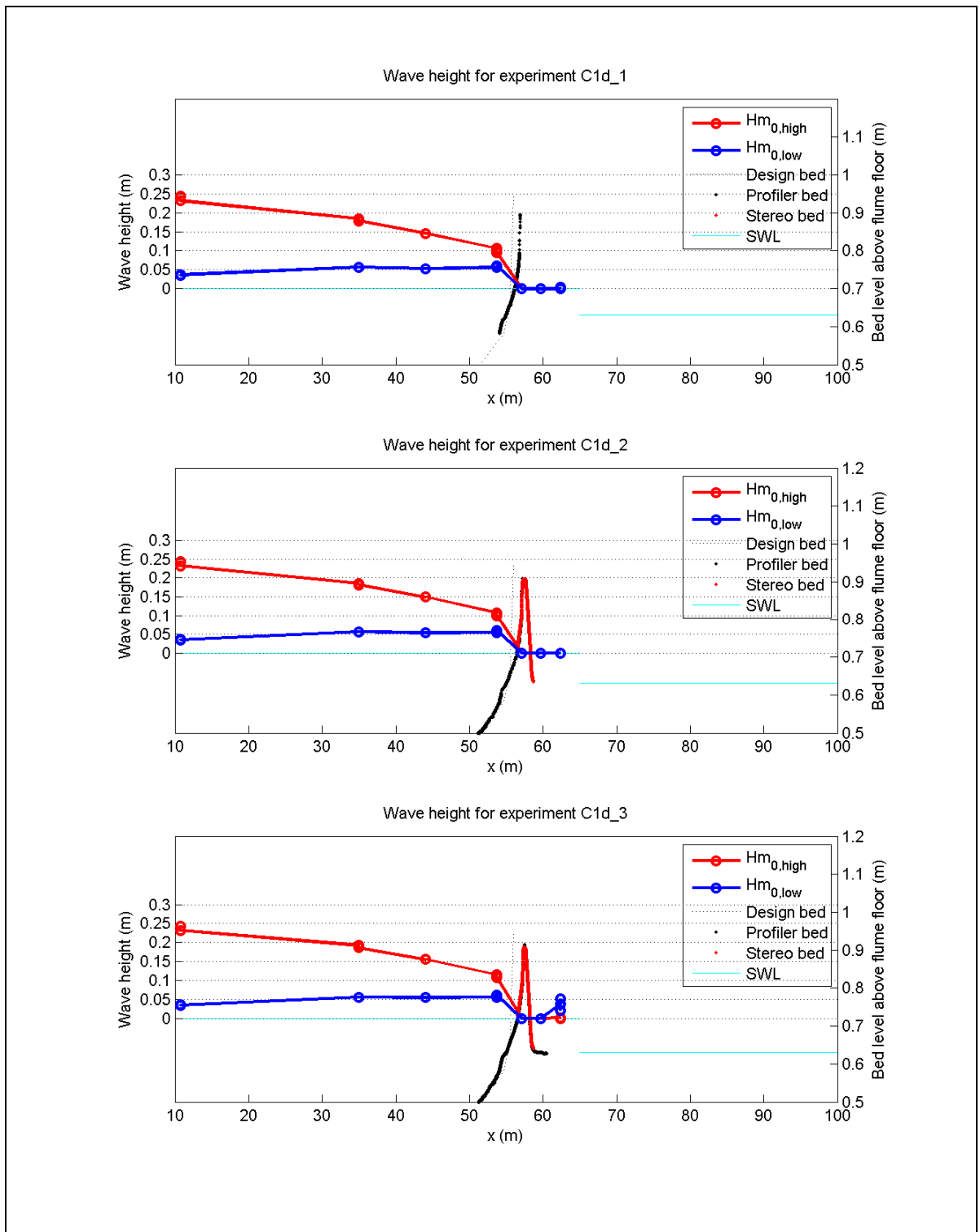


Measured high frequency and low frequency  $H_{m0}$  wave height during experiment C1a.

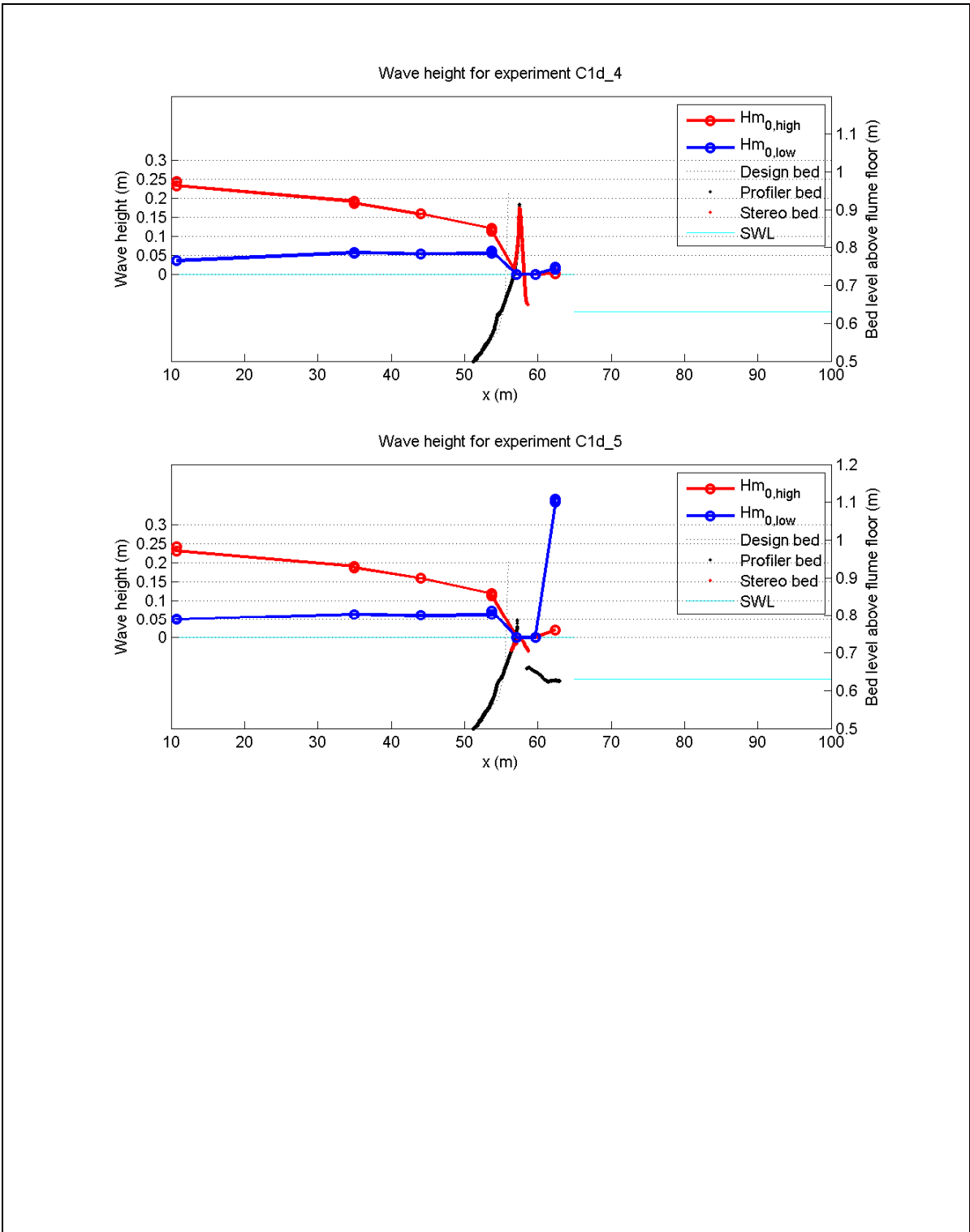
1202124-007-HYE-0005

Deltares

Figure C.81

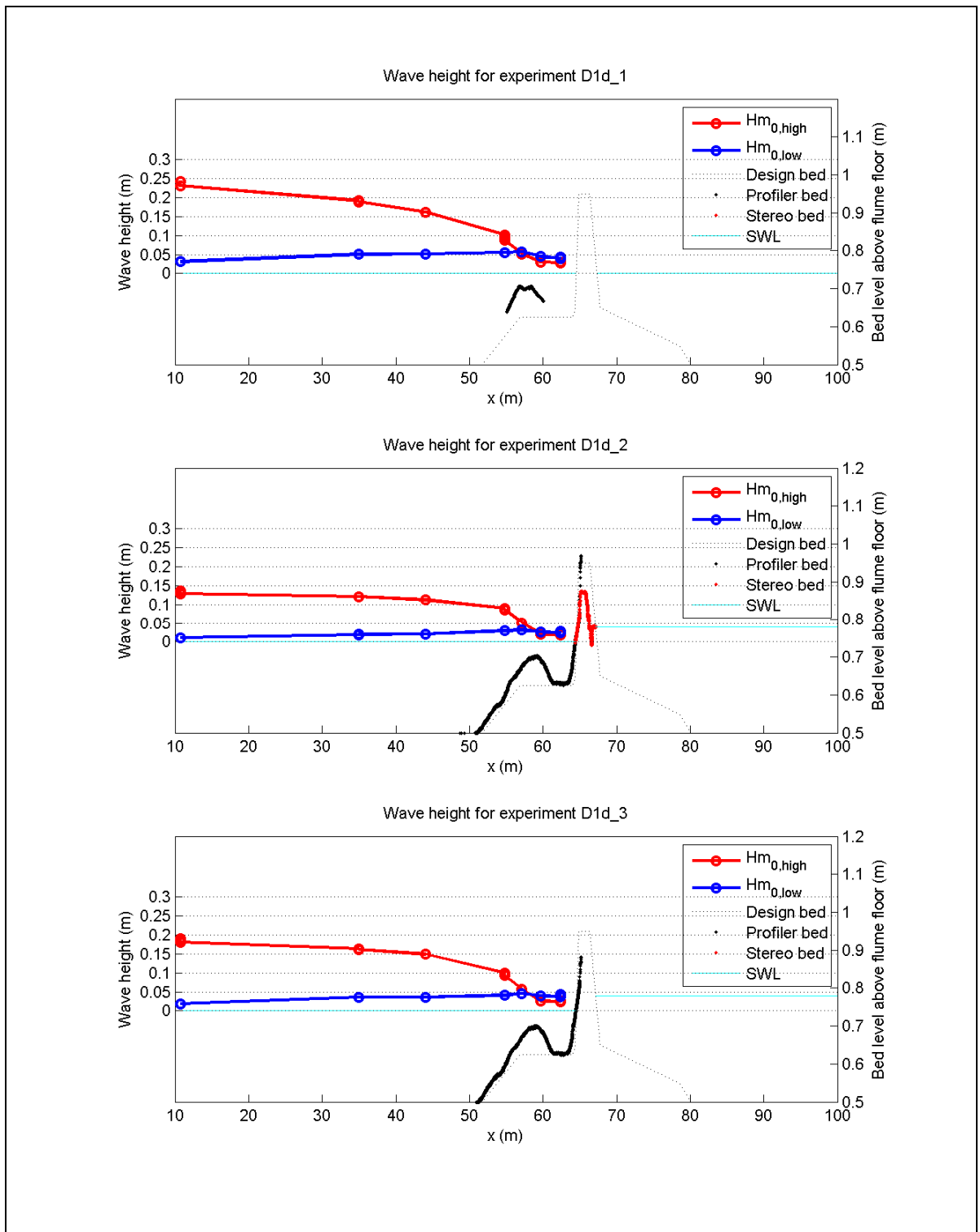


Measured high frequency and low frequency $H_{m0}$ wave height during experiment C1d.	1202124-007-HYE-0005	
	Deltares	Figure C.82

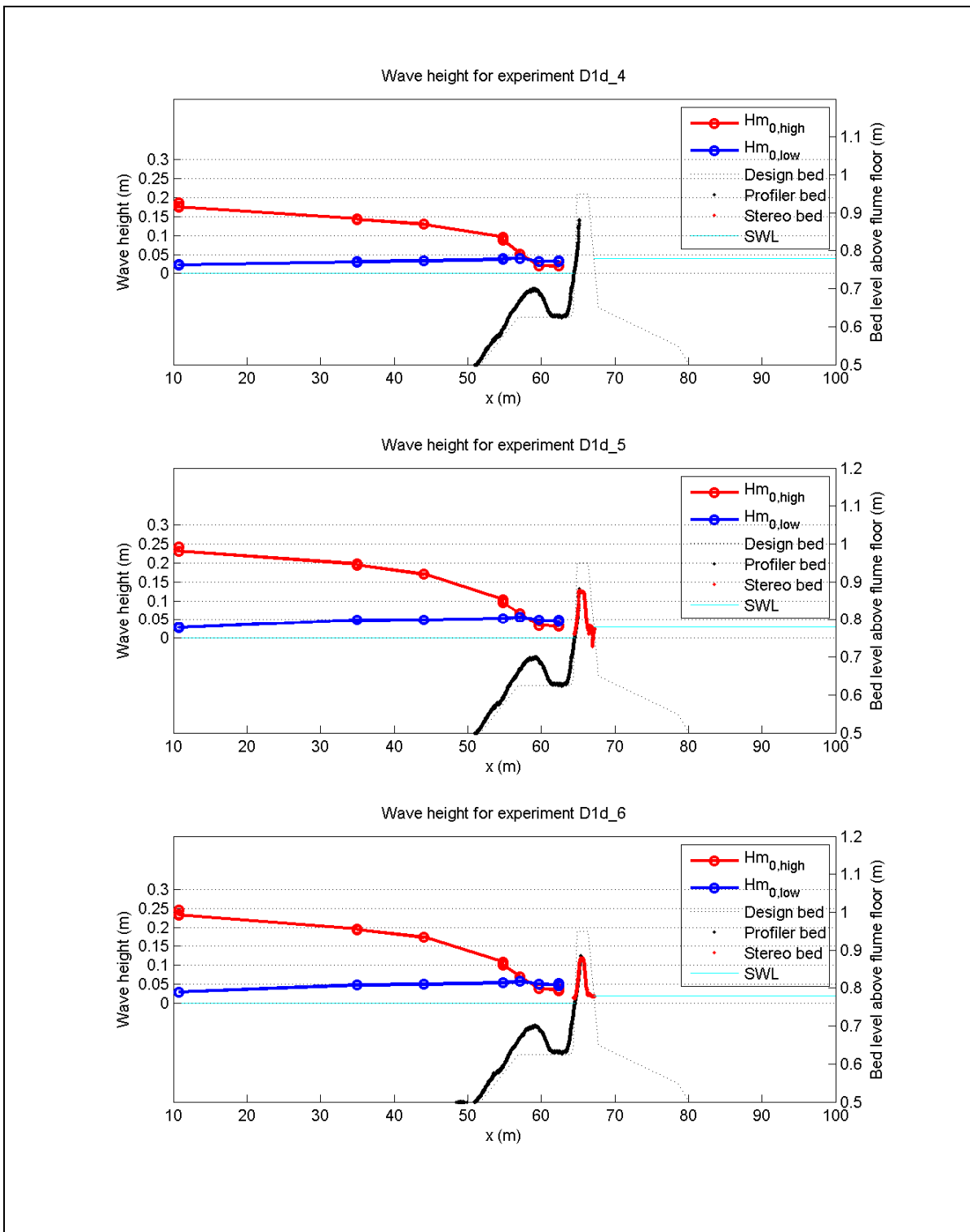


Measured high frequency and low frequency $H_{m0}$ wave height during experiment C1d.	1202124-007-HYE-0005	
	Deltares	Figure C.83

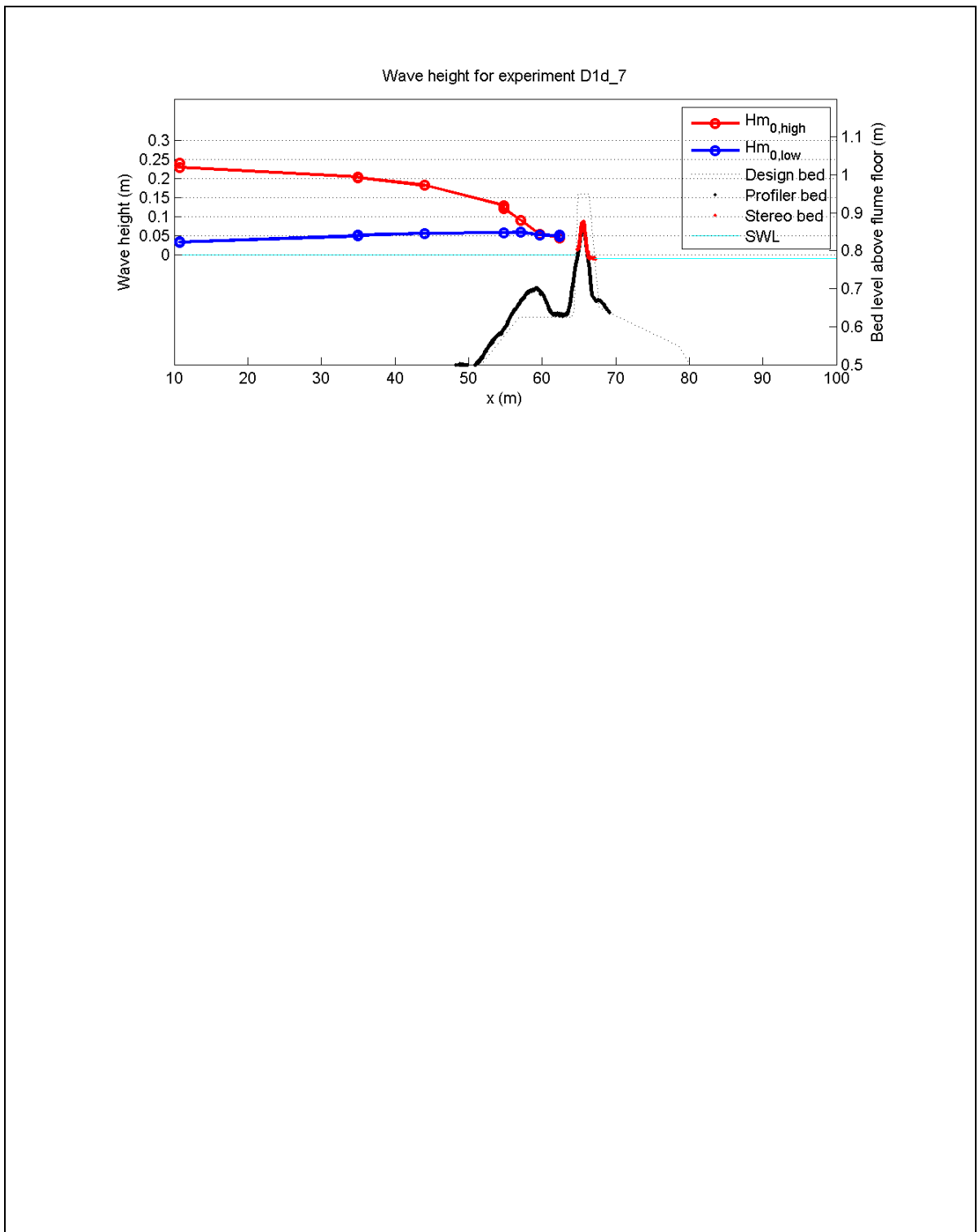




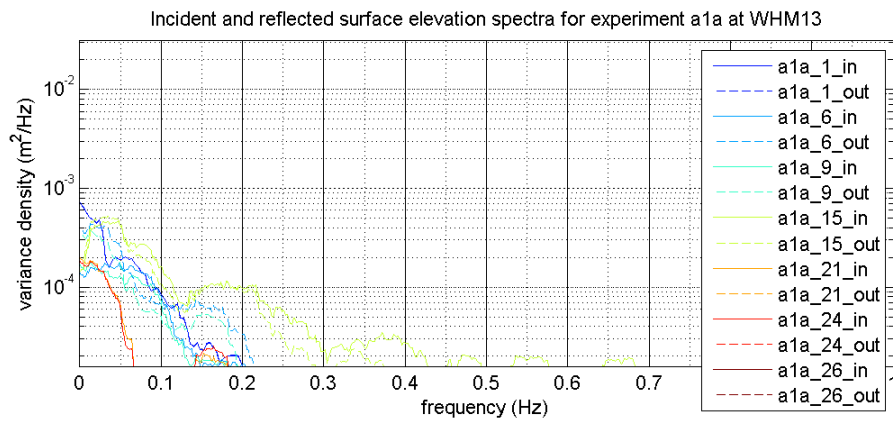
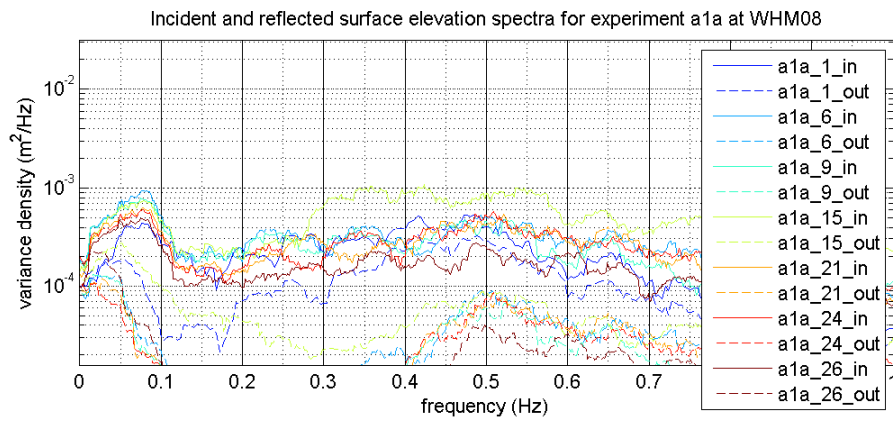
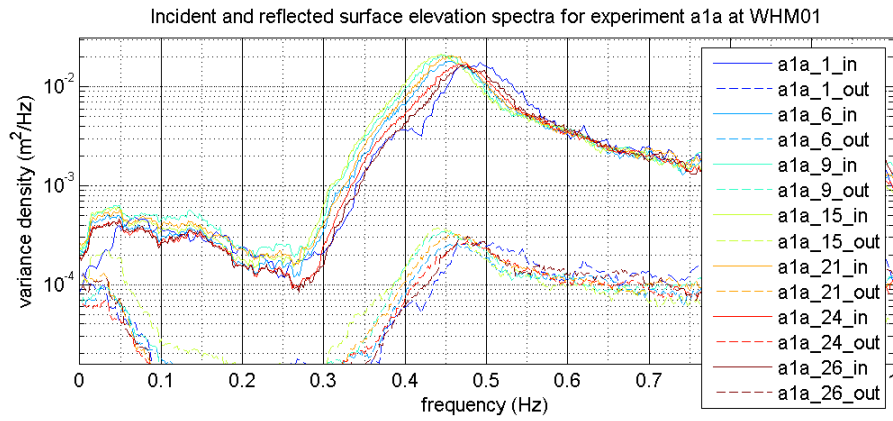
Measured high frequency and low frequency $H_{m0}$ wave height during experiment D1d.	1202124-007-HYE-0005	
	Deltares	Figure C.84



Measured high frequency and low frequency $H_{m0}$ wave height during experiment D1d.	1202124-007-HYE-0005	
	Deltares	Figure C.85



Measured high frequency and low frequency $H_{m0}$ wave height during experiment D1d.	1202124-007-HYE-0005	
Deltares		Figure C.86

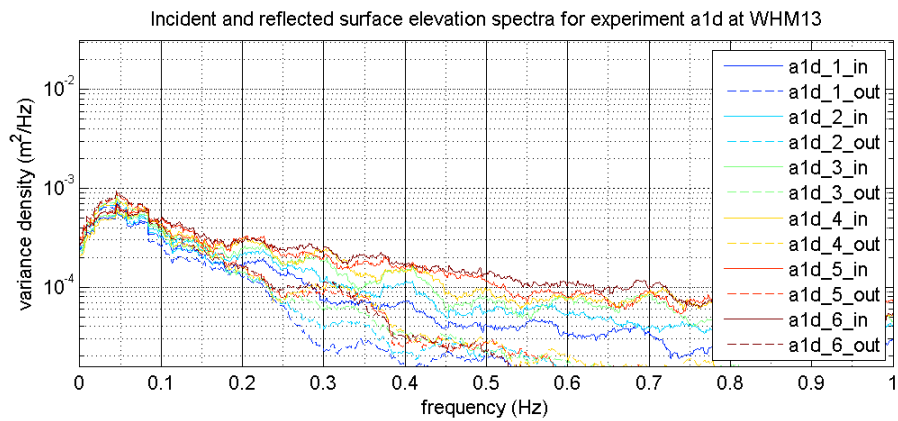
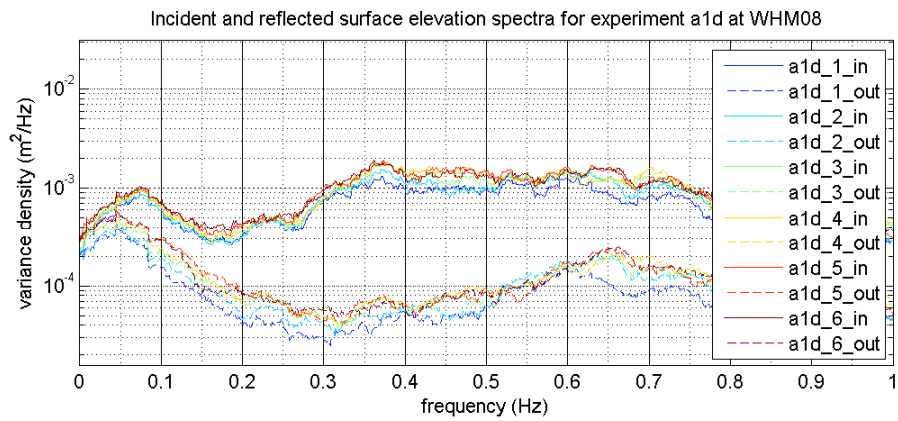
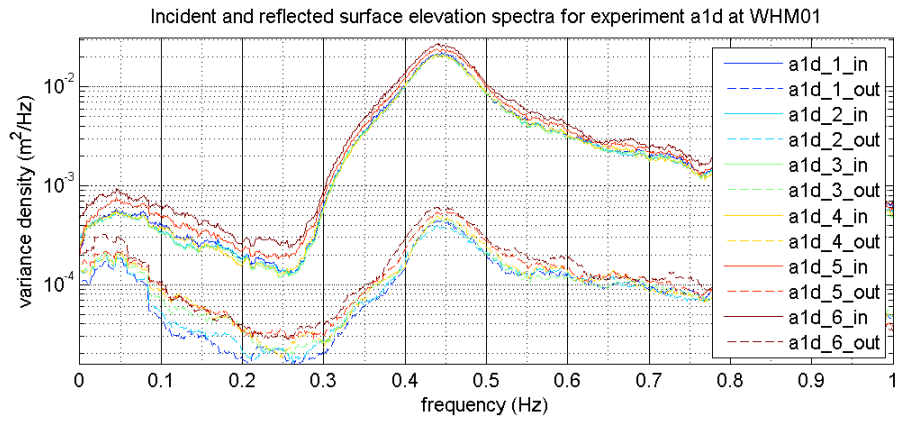


Measured incident and reflected wave spectra at WHM01, WHM08 and WHM13 during experiment A1a.

1202124-007-HYE-0005

Deltares

Figure C.87

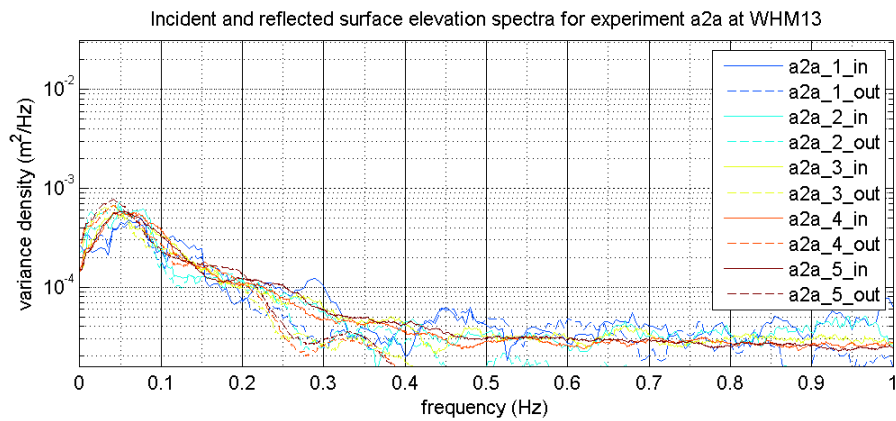
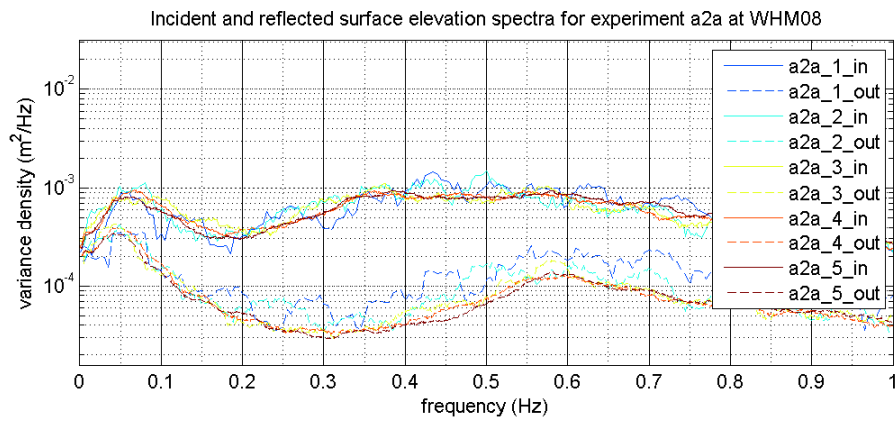
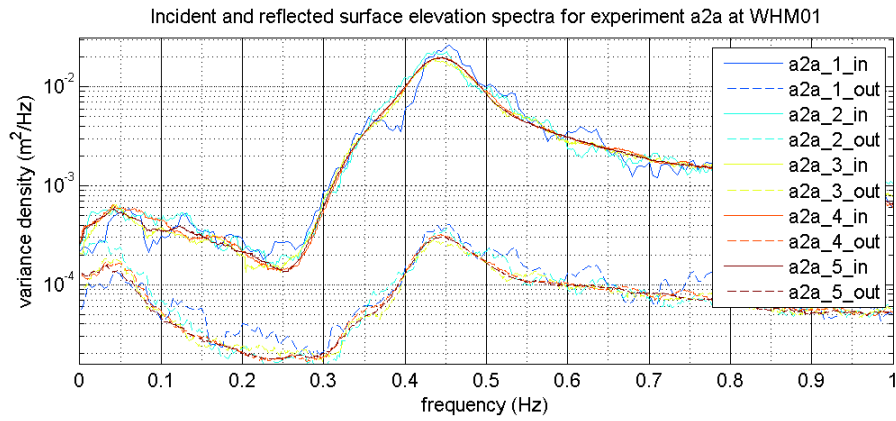


Measured incident and reflected wave spectra at WHM01, WHM08 and WHM13 during experiment A1d.

1202124-007-HYE-0005

Deltares

Figure C.88

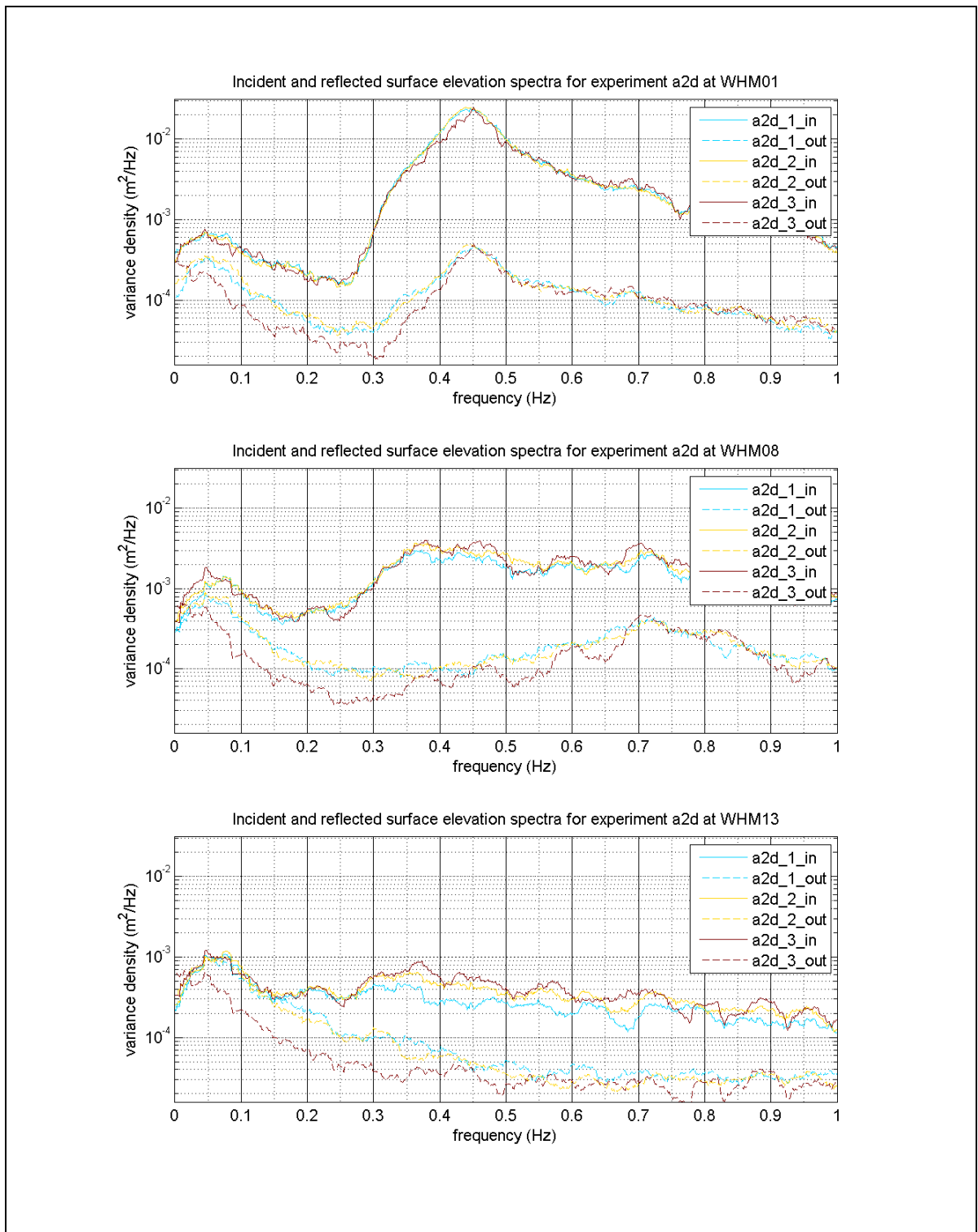


Measured incident and reflected wave spectra at WHM01, WHM08 and WHM13 during experiment A2a.

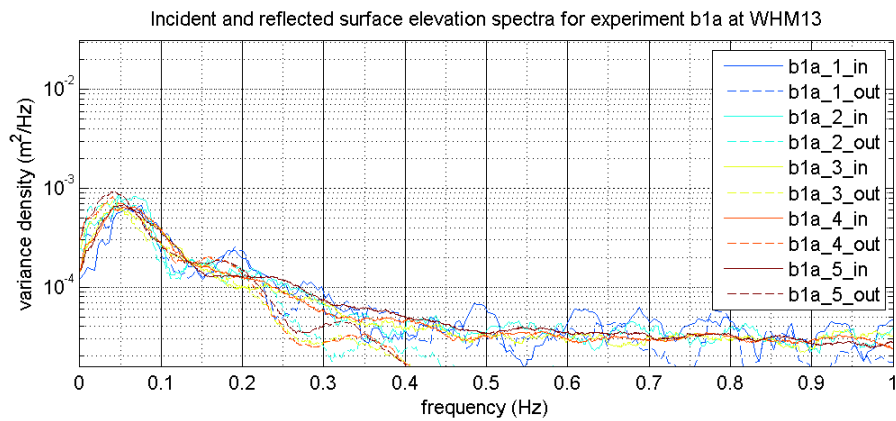
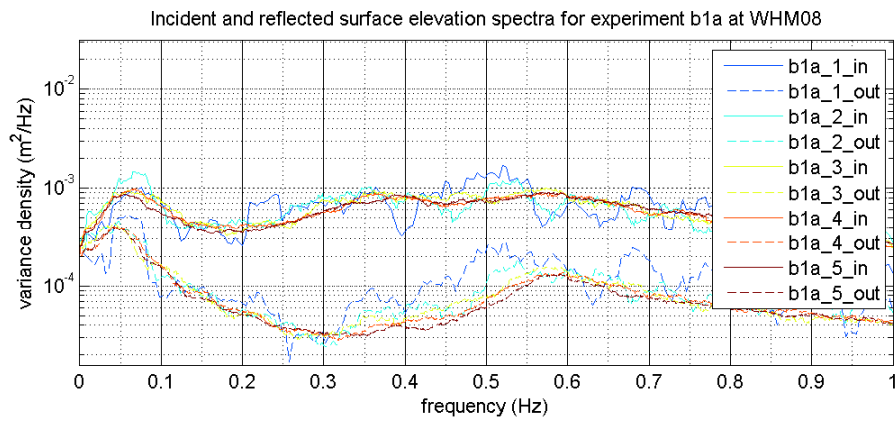
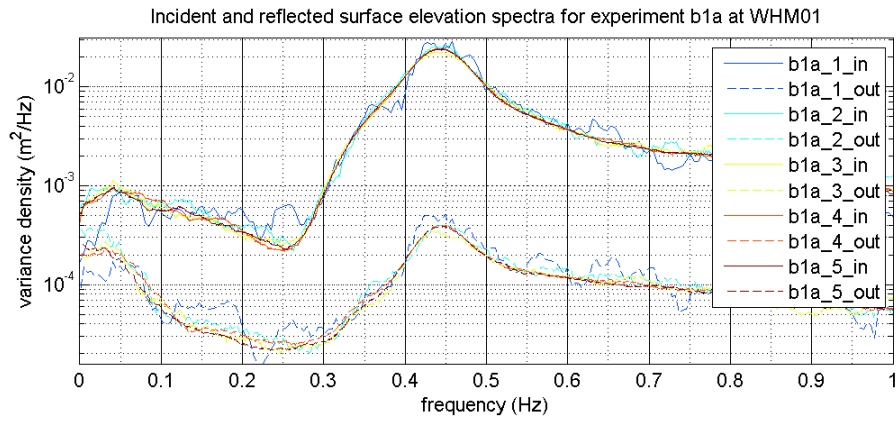
1202124-007-HYE-0005

Deltares

Figure C.89



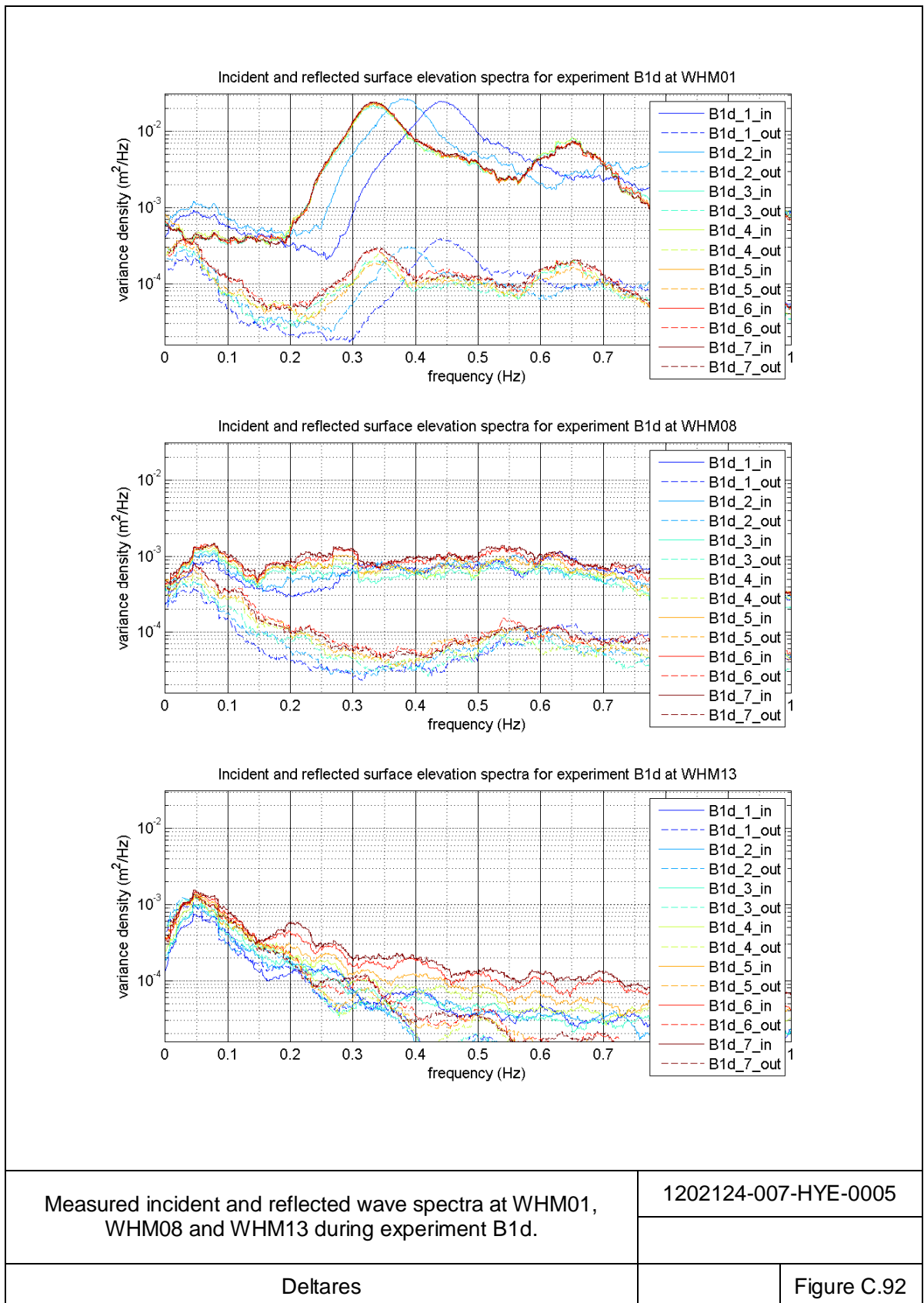
Measured incident and reflected wave spectra at WHM01, WHM08 and WHM13 during experiment A2d.	1202124-007-HYE-0005	
	Deltares	Figure C.90

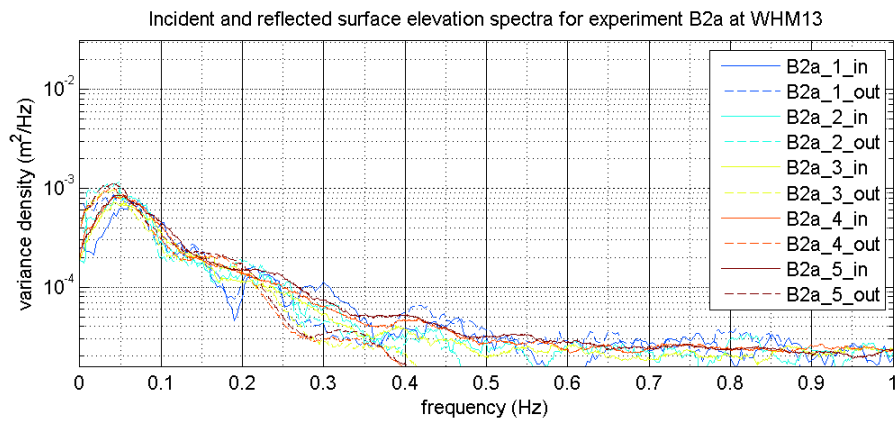
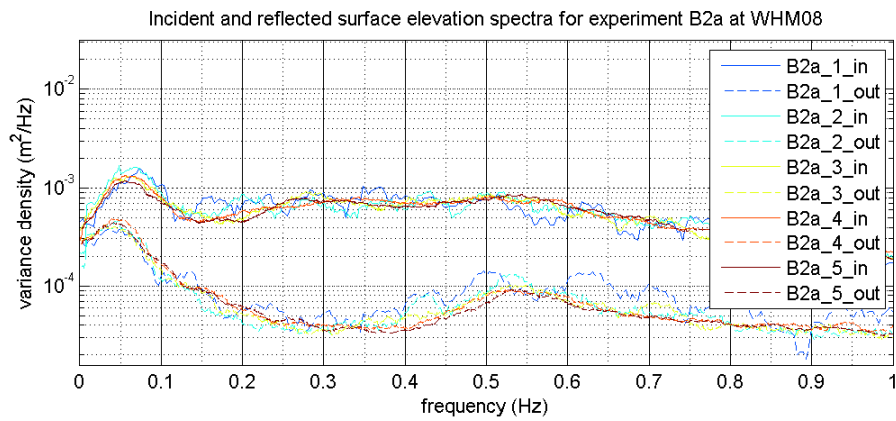
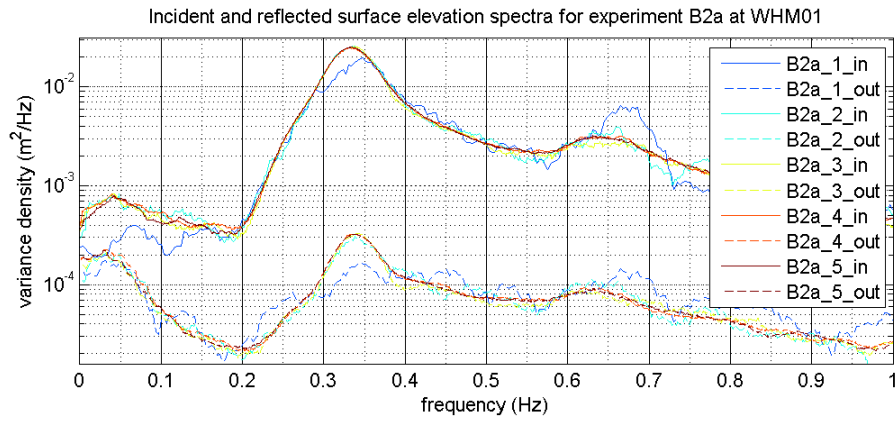


Measured incident and reflected wave spectra at WHM01, WHM08 and WHM13 during experiment B1a.

1202124-007-HYE-0005





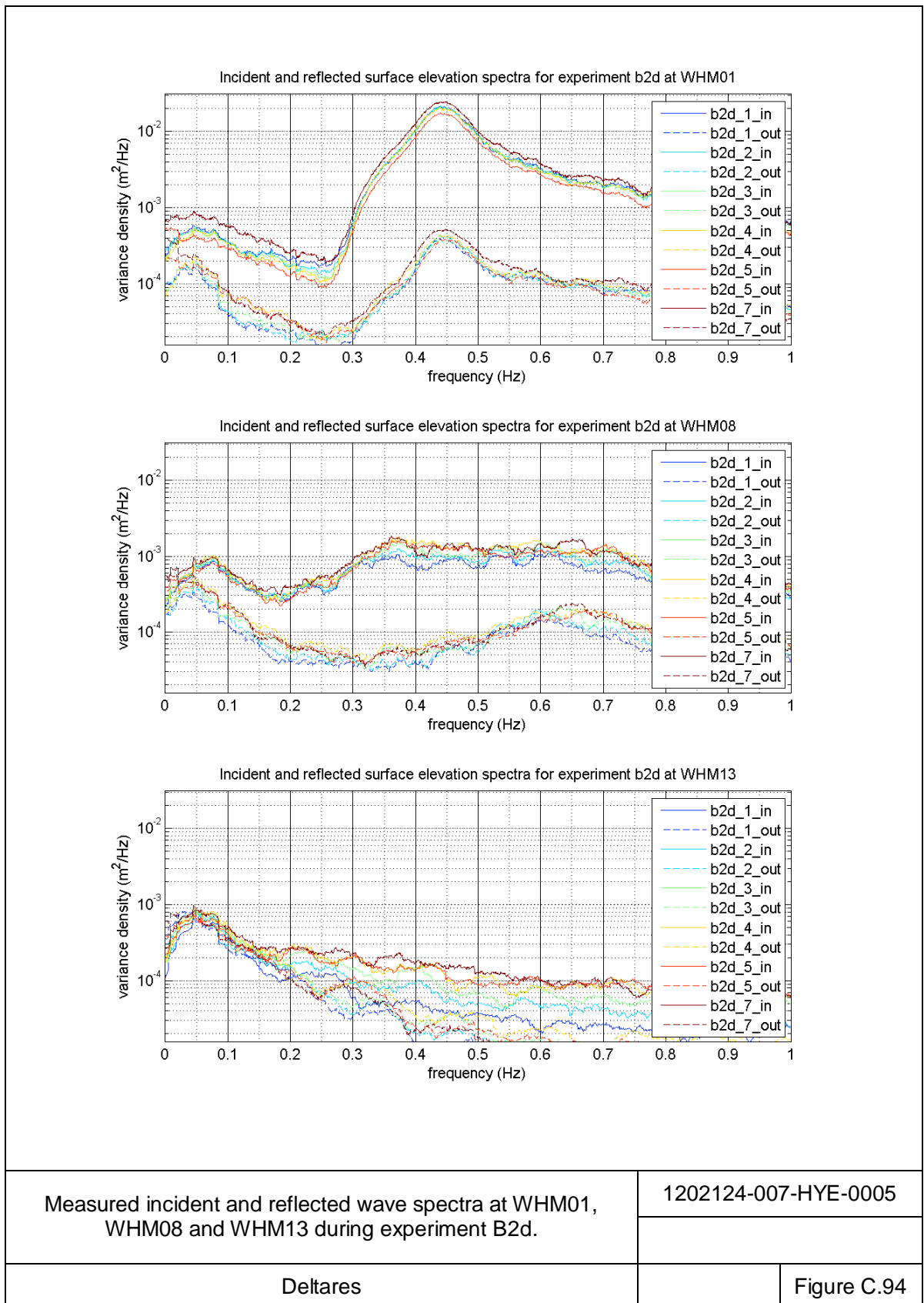


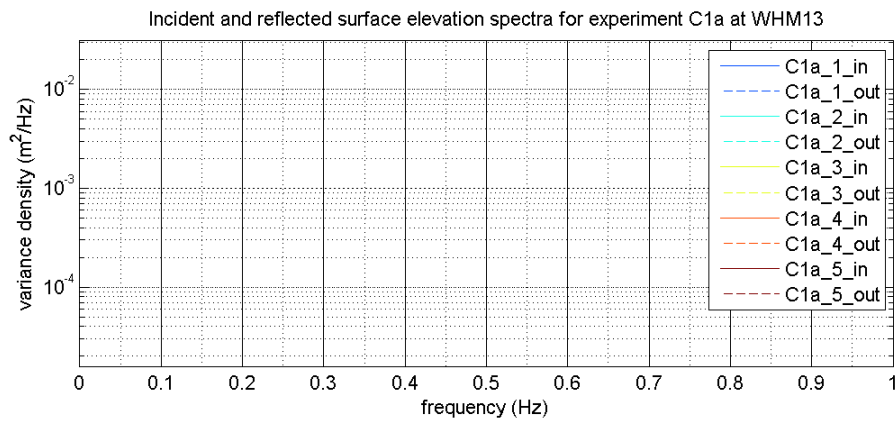
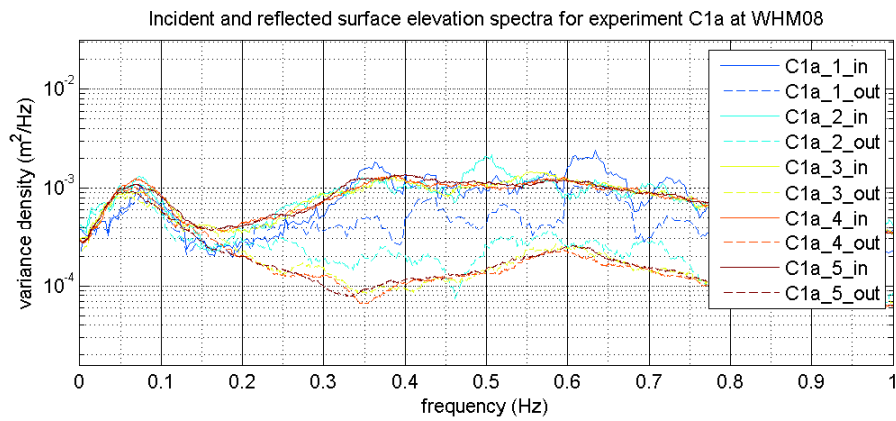
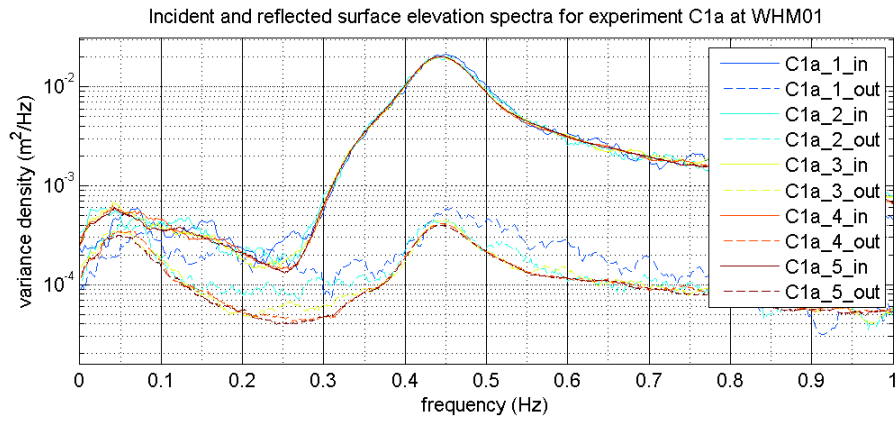
Measured incident and reflected wave spectra at WHM01, WHM08 and WHM13 during experiment B2a.

1202124-007-HYE-0005

Deltares

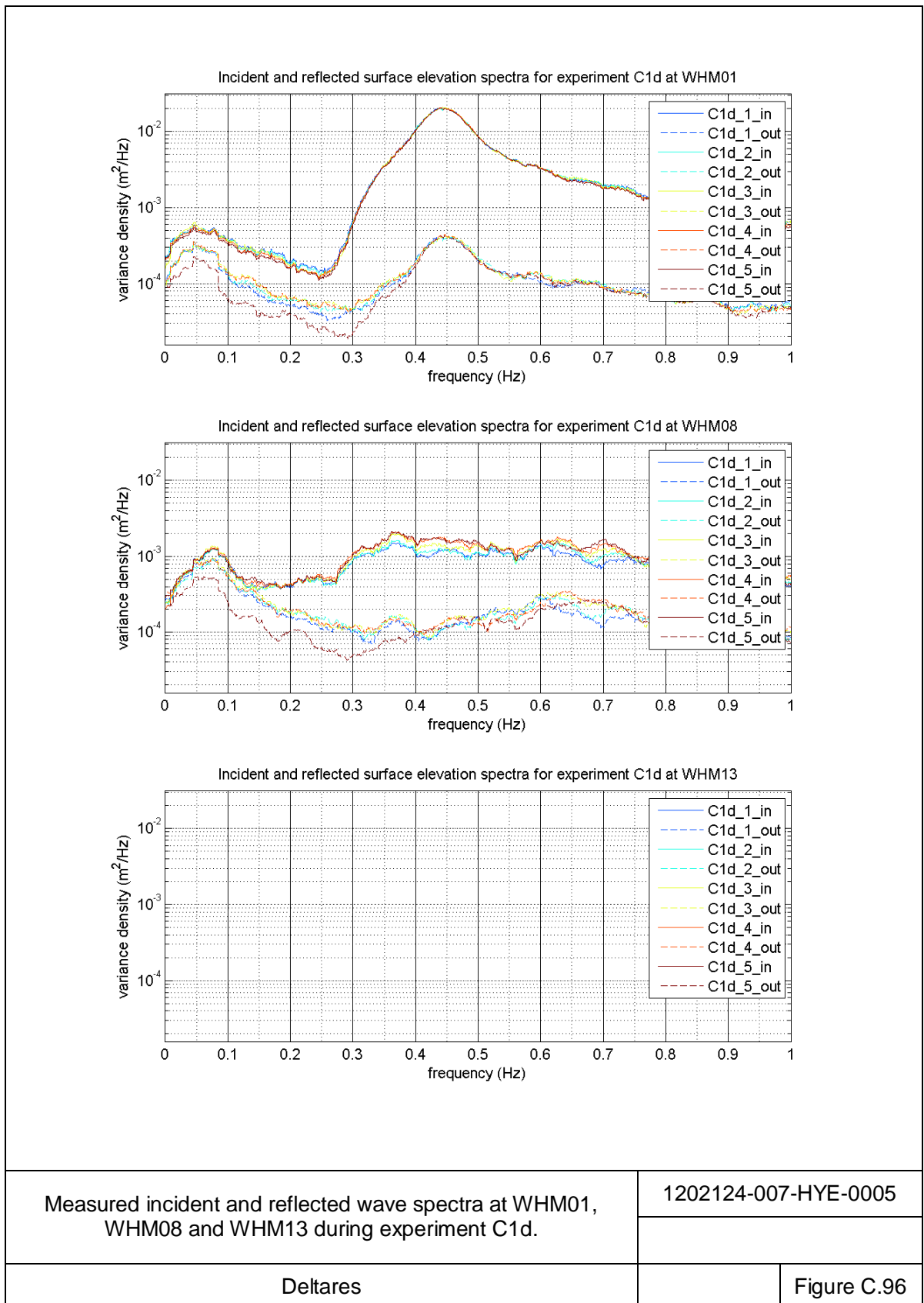
Figure C.93

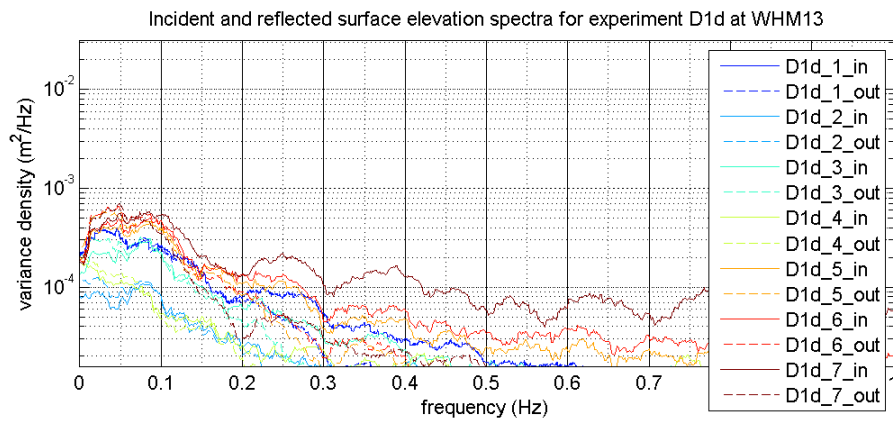
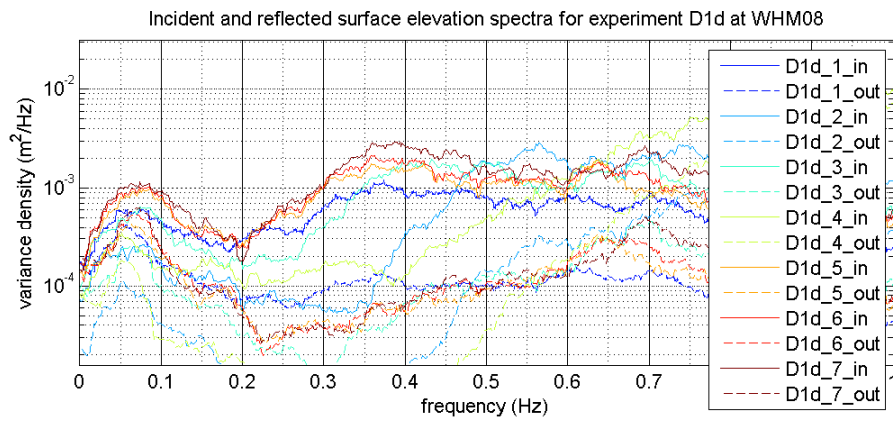
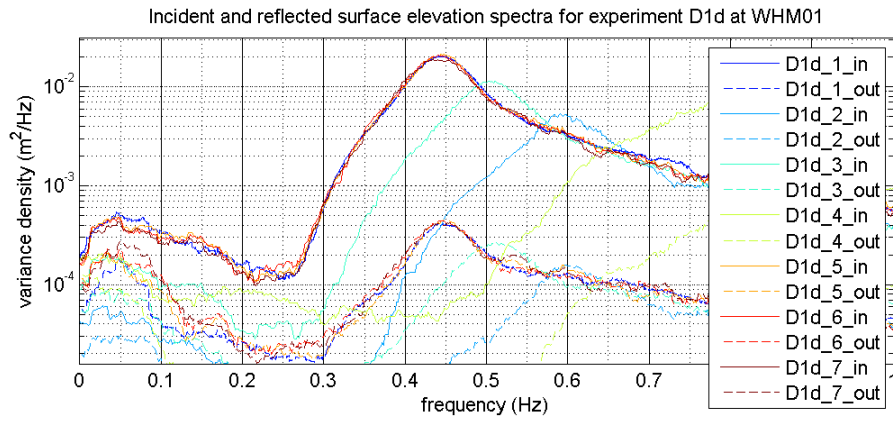




Measured incident and reflected wave spectra at WHM01, WHM08 and WHM13 during experiment C1a.

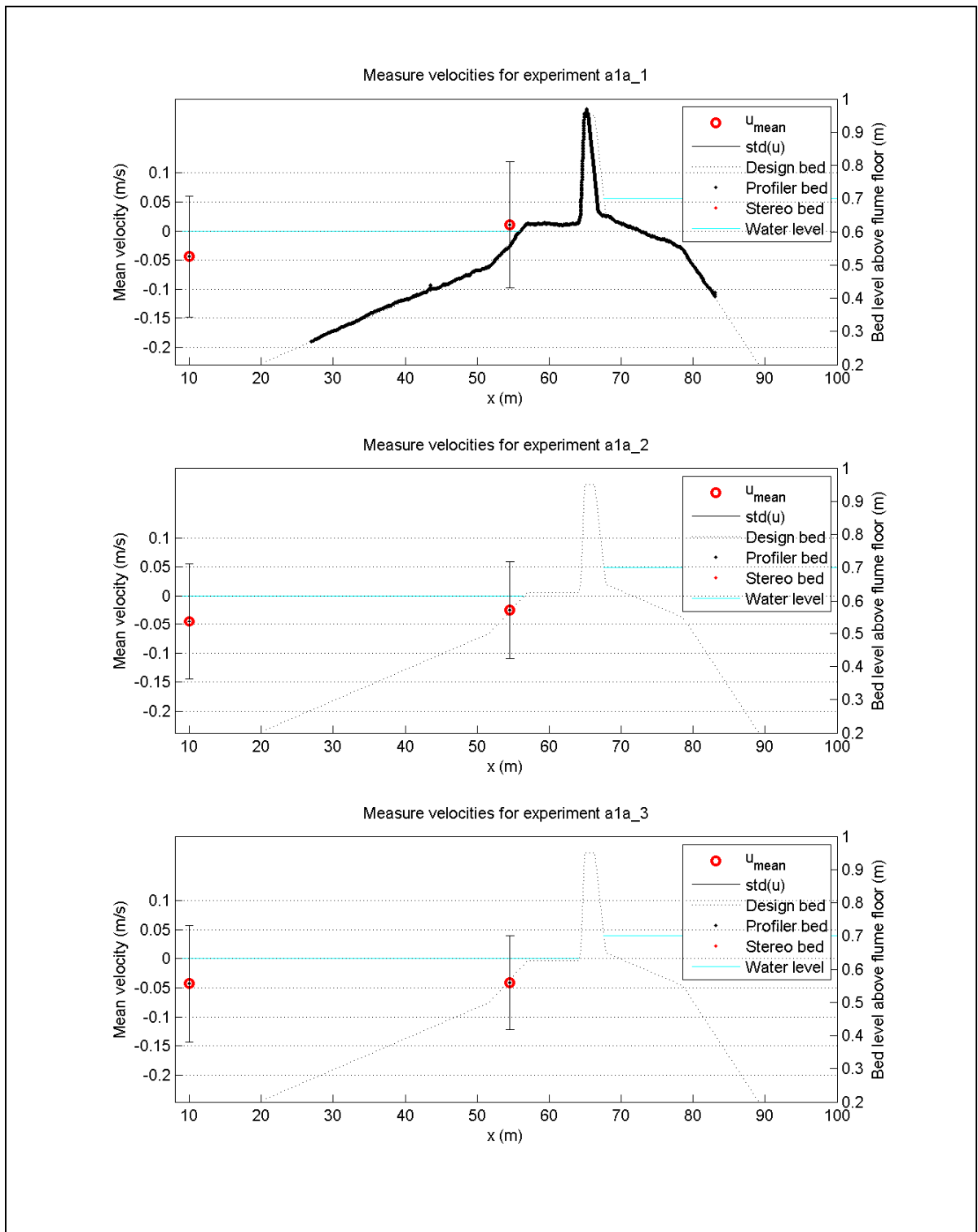
1202124-007-HYE-0005



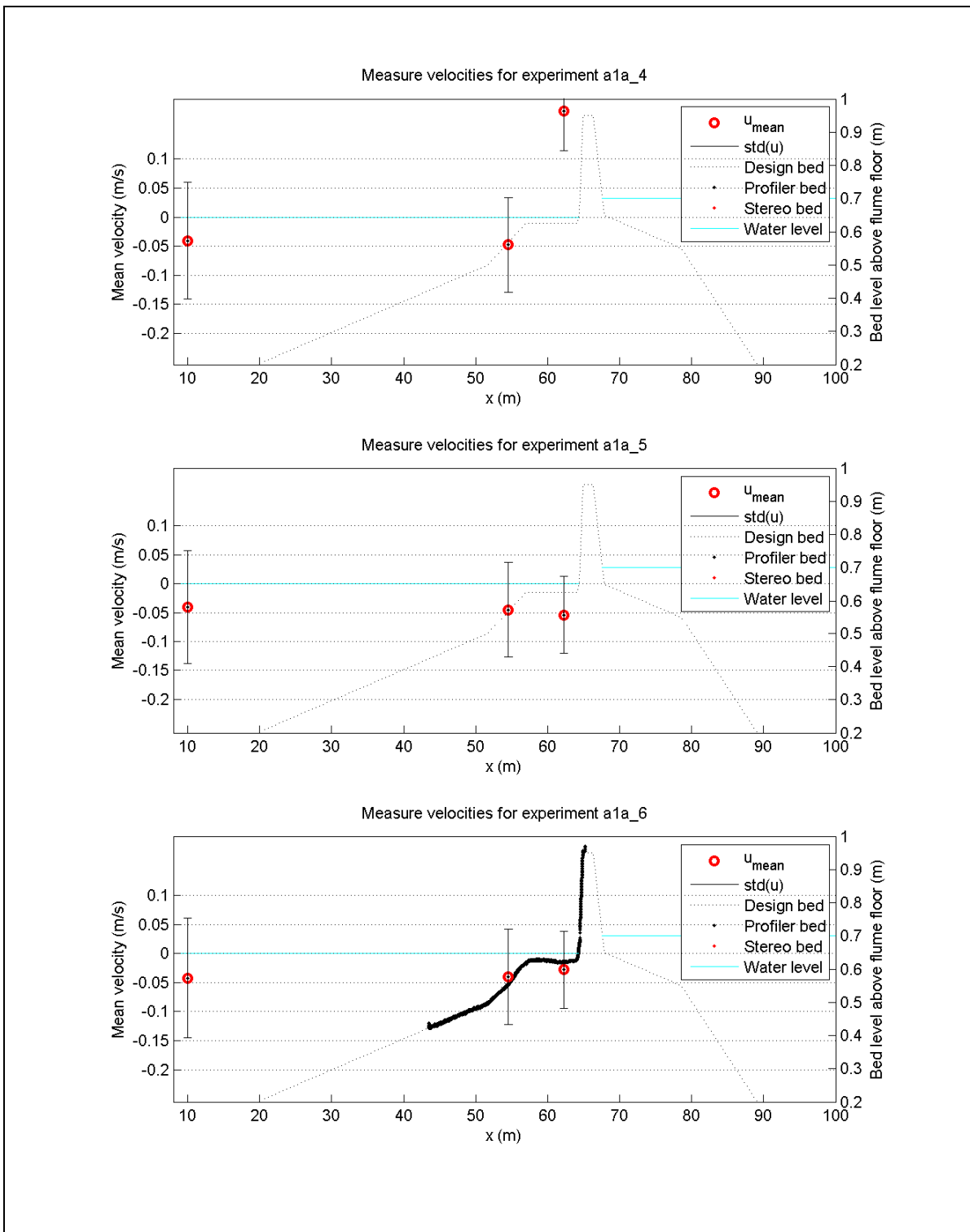


Measured incident and reflected wave spectra at WHM01, WHM08 and WHM13 during experiment D1d.

1202124-007-HYE-0005

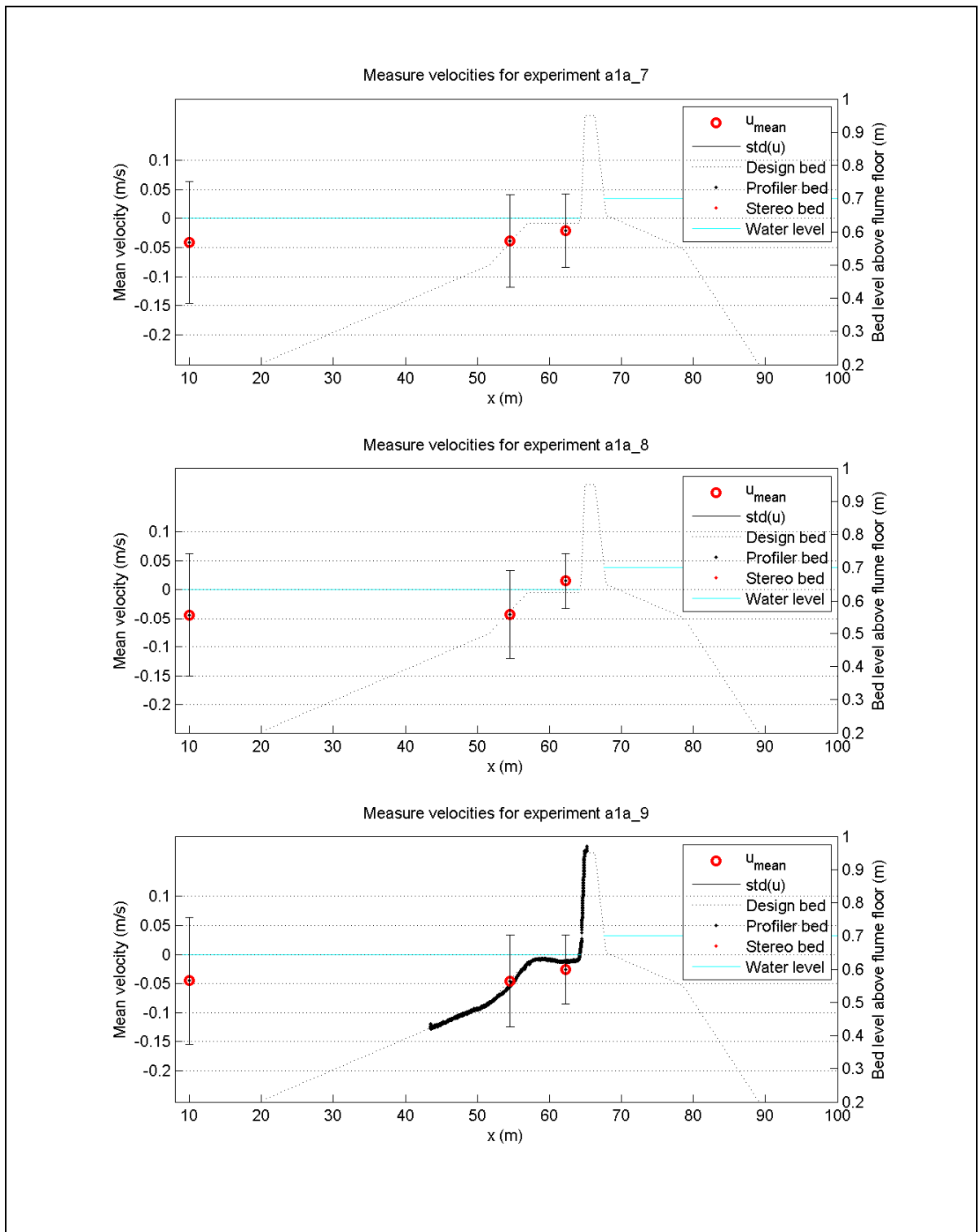


Time-averaged velocity and standard deviation measured at the EMS instruments in experiment A1a.	1202124-007-HYE-0005	
	Deltares	Figure C.98

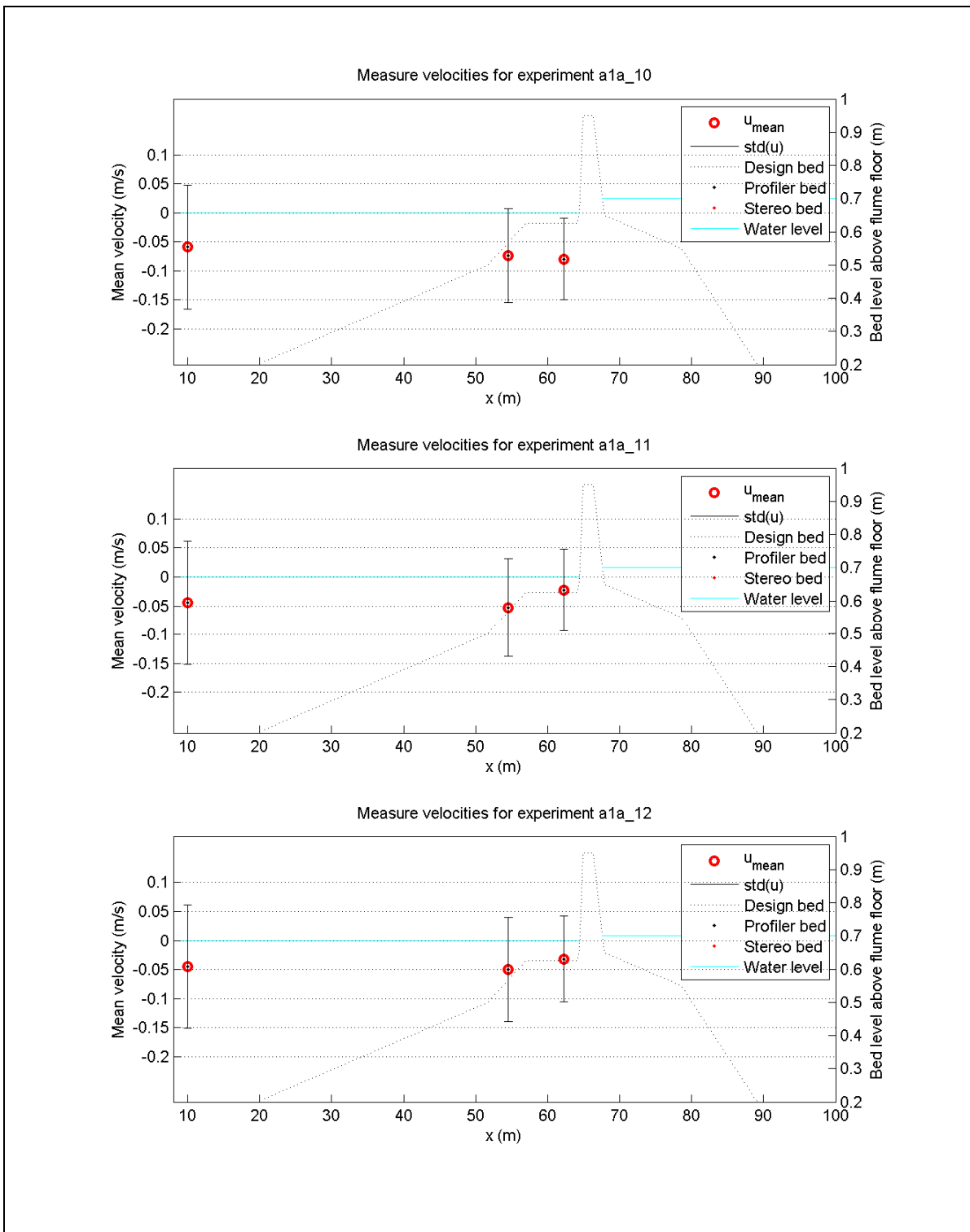


Time-averaged velocity and standard deviation measured at the EMS instruments in experiment A1a.	1202124-007-HYE-0005	
	Deltares	Figure C.99



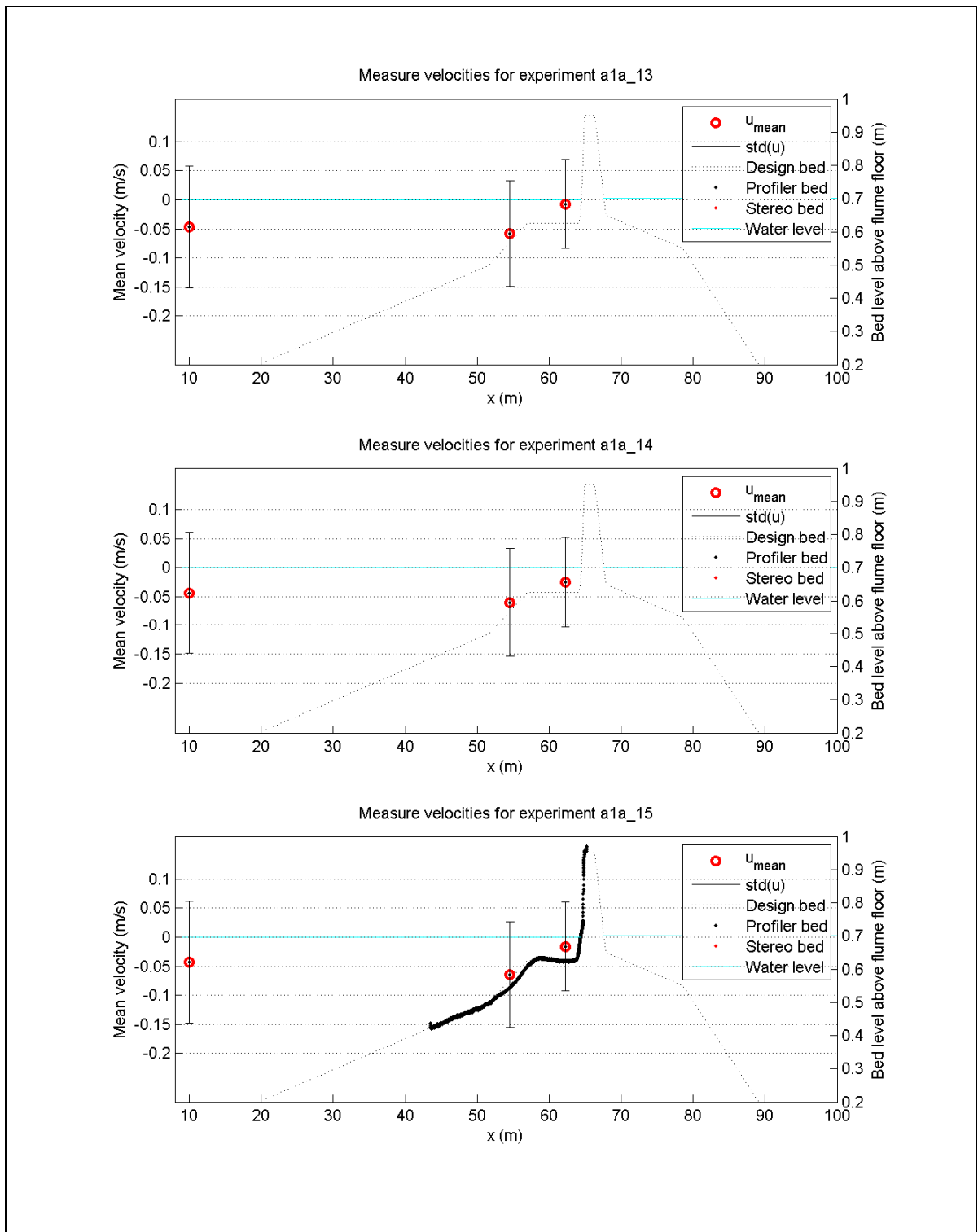


Time-averaged velocity and standard deviation measured at the EMS instruments in experiment A1a.	1202124-007-HYE-0005	
	Deltares	Figure C.100

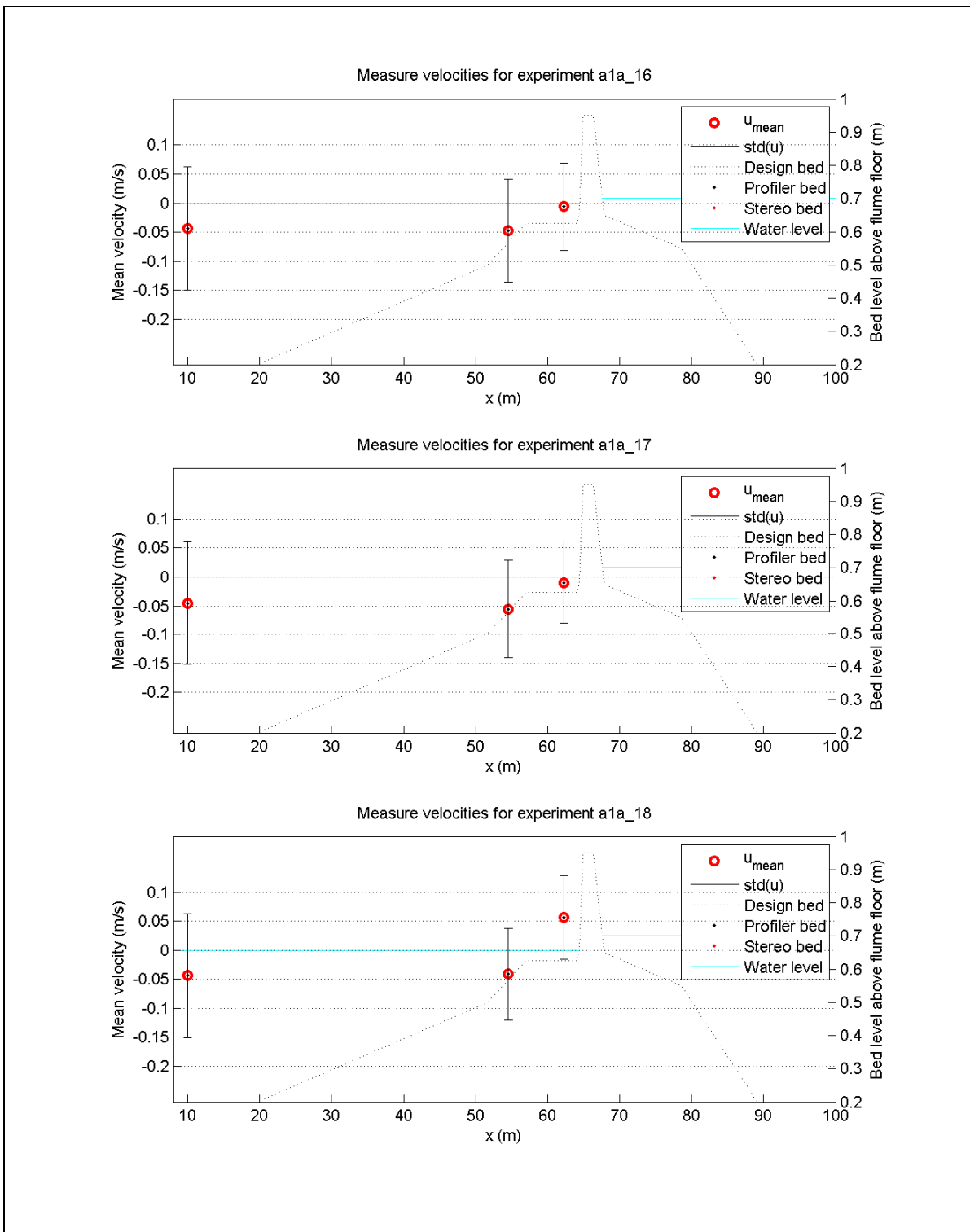


Time-averaged velocity and standard deviation measured at the EMS instruments in experiment A1a.

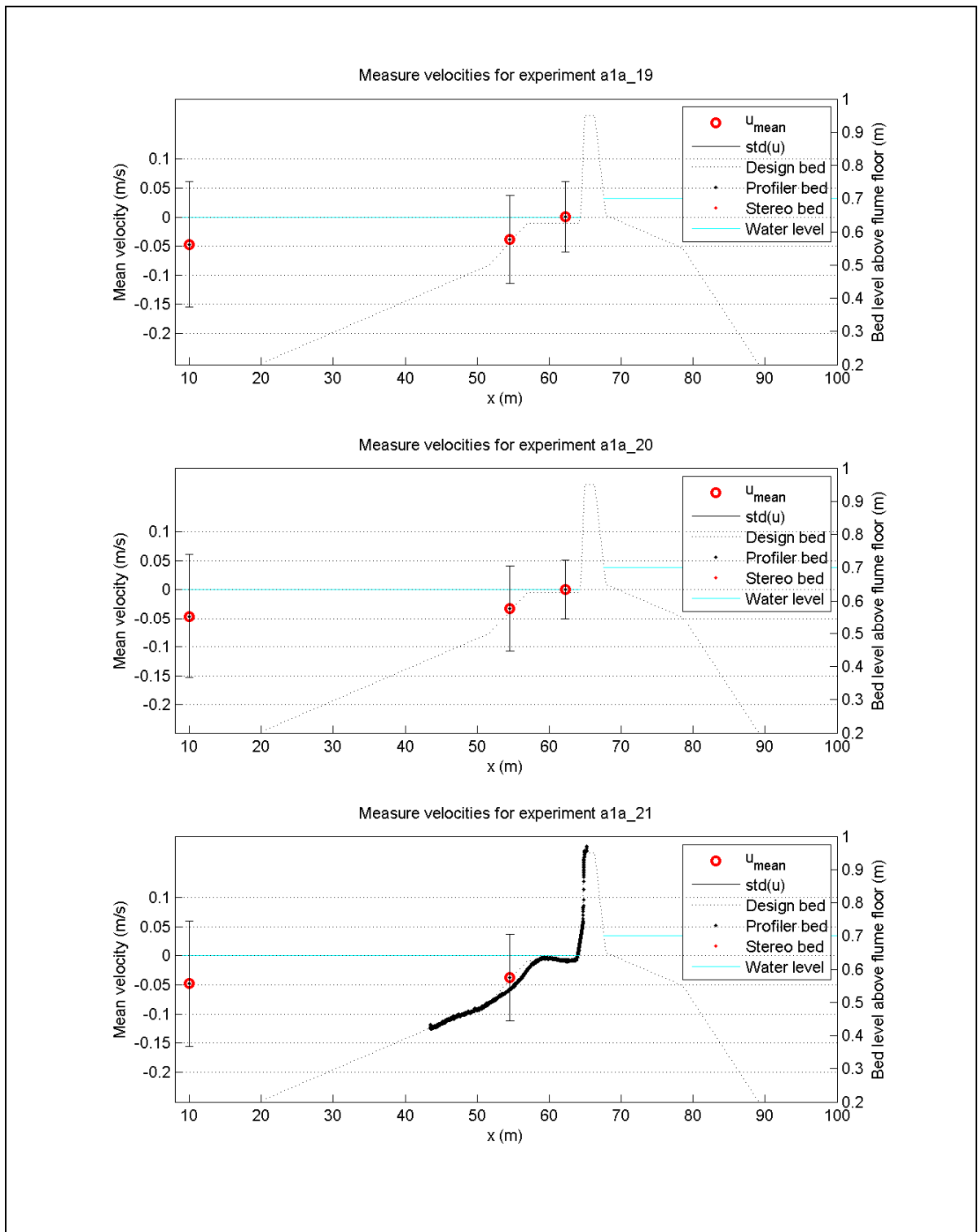
1202124-007-HYE-0005



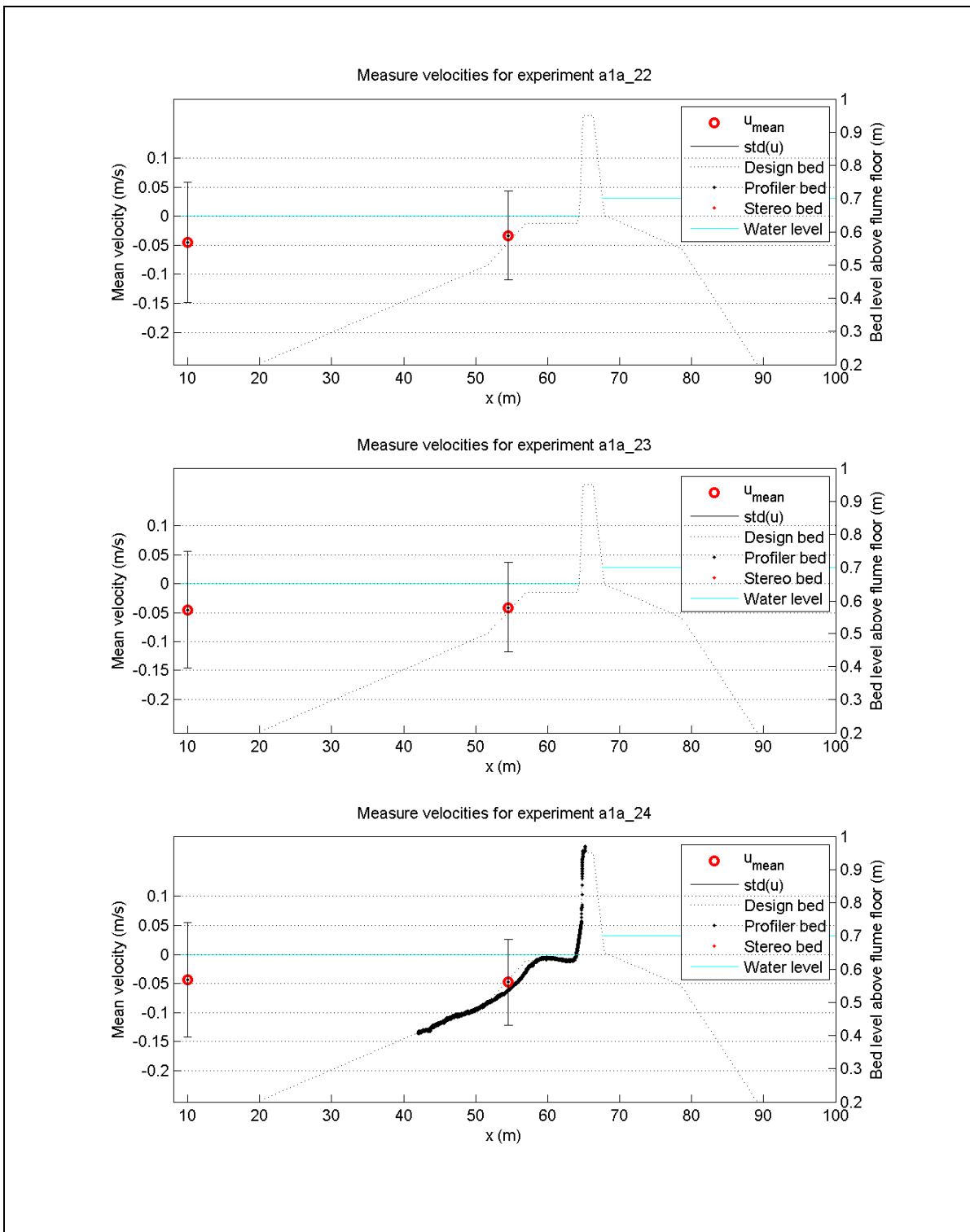
Time-averaged velocity and standard deviation measured at the EMS instruments in experiment A1a.	1202124-007-HYE-0005	
	Deltares	Figure C.102



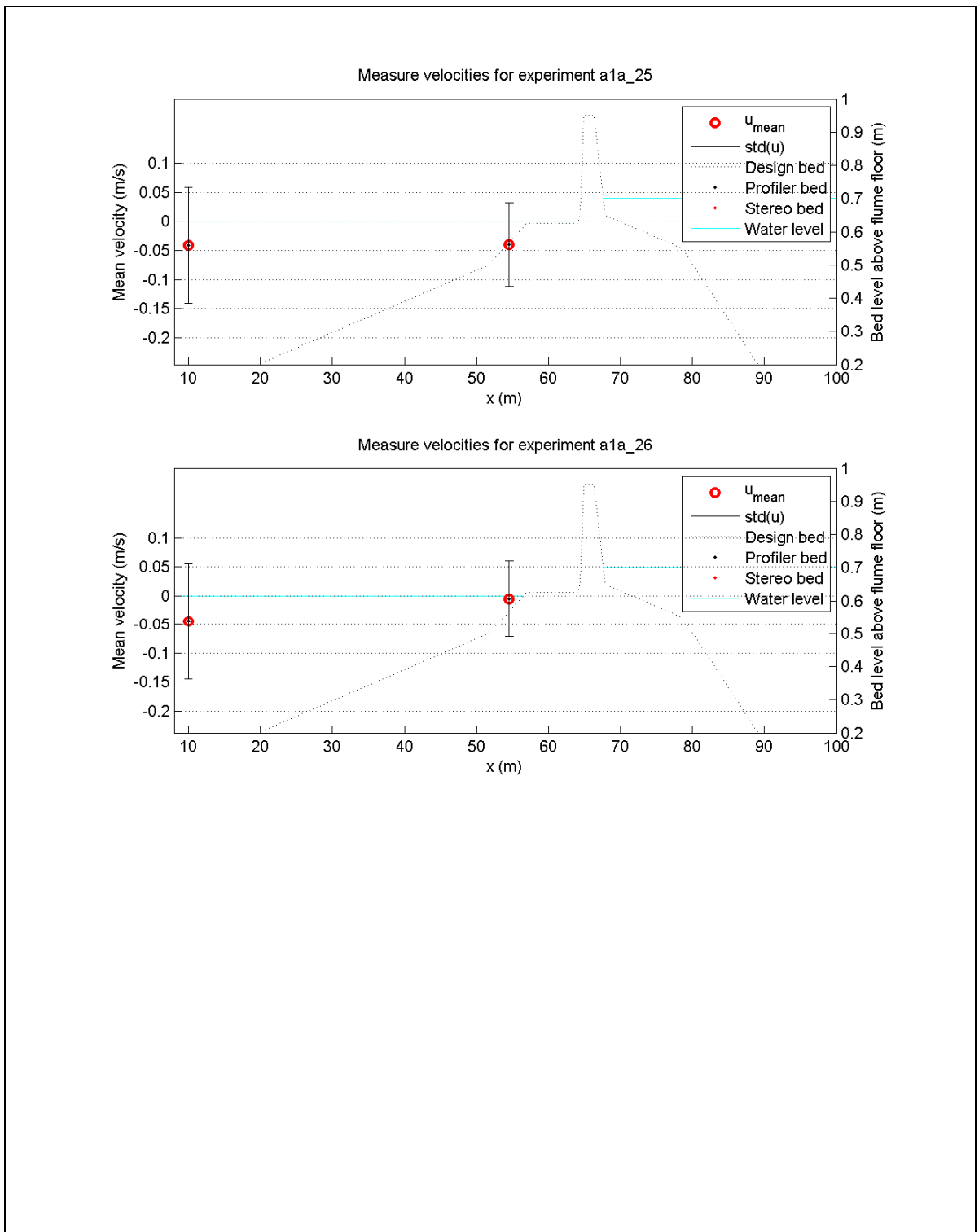
Time-averaged velocity and standard deviation measured at the EMS instruments in experiment A1a.	1202124-007-HYE-0005	
	Deltares	Figure C.103



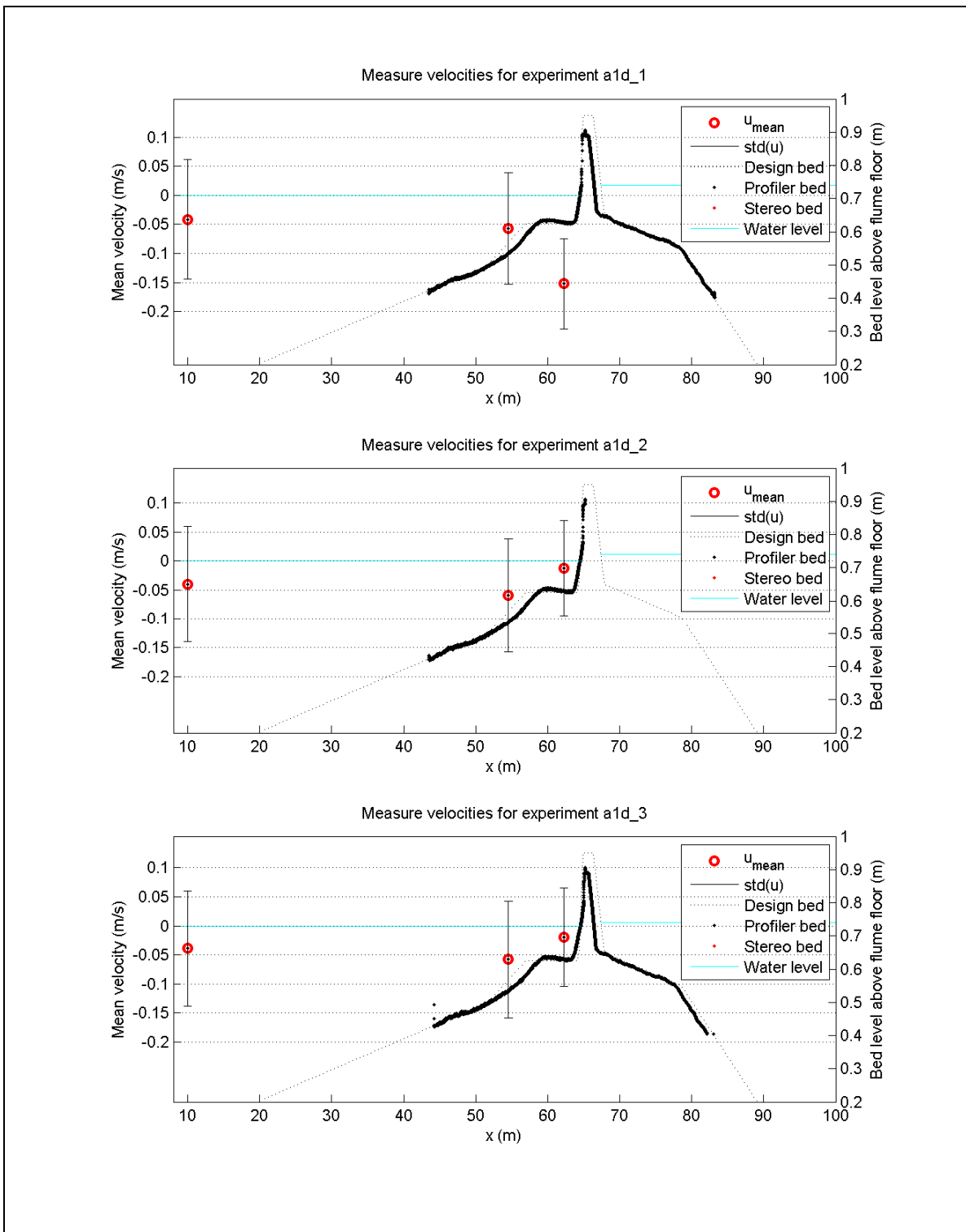
Time-averaged velocity and standard deviation measured at the EMS instruments in experiment A1a.	1202124-007-HYE-0005	
	Deltares	Figure C.104



Time-averaged velocity and standard deviation measured at the EMS instruments in experiment A1a.	1202124-007-HYE-0005	
	Deltares	Figure C.105

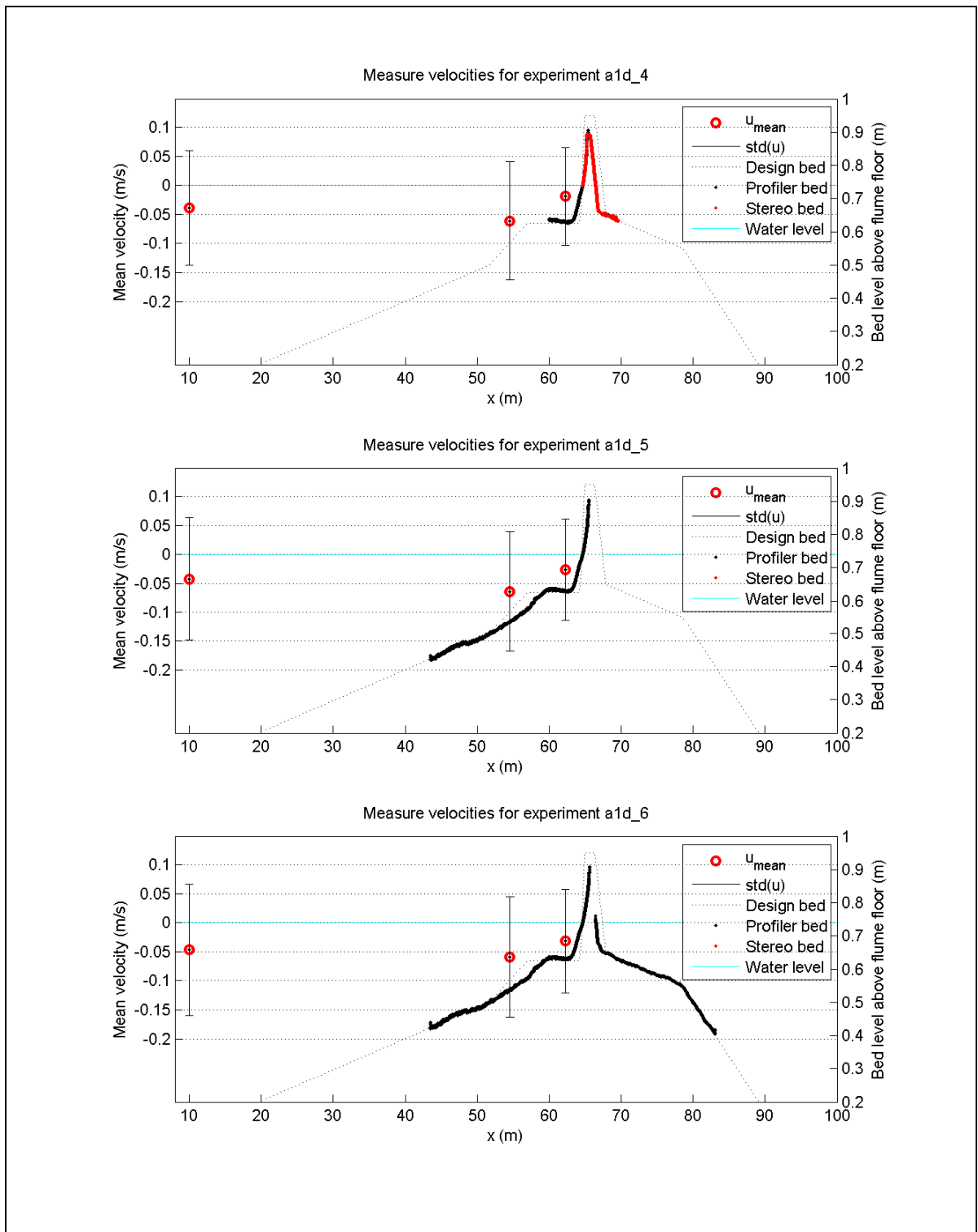


Time-averaged velocity and standard deviation measured at the EMS instruments in experiment A1a.	1202124-007-HYE-0005	
	Deltares	Figure C.106

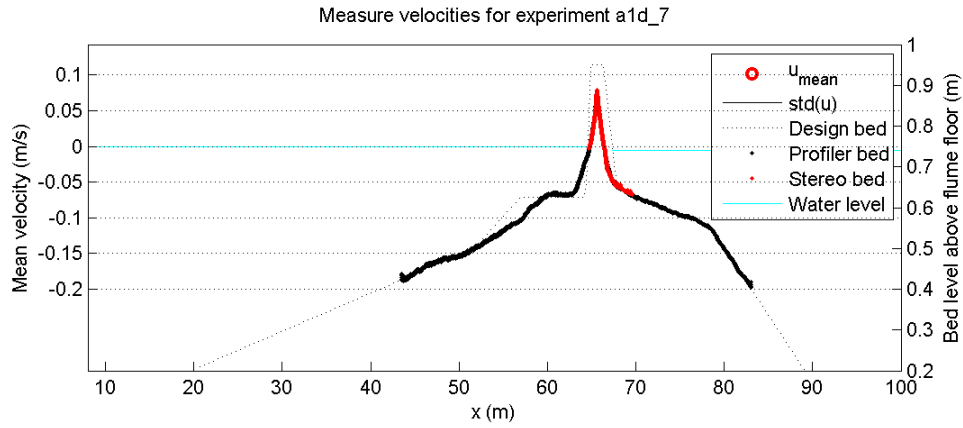


Time-averaged velocity and standard deviation measured at the EMS instruments in experiment A1d.	1202124-007-HYE-0005	
	Deltares	Figure C.107





Time-averaged velocity and standard deviation measured at the EMS instruments in experiment A1d.	1202124-007-HYE-0005	
	Deltares	Figure C.108

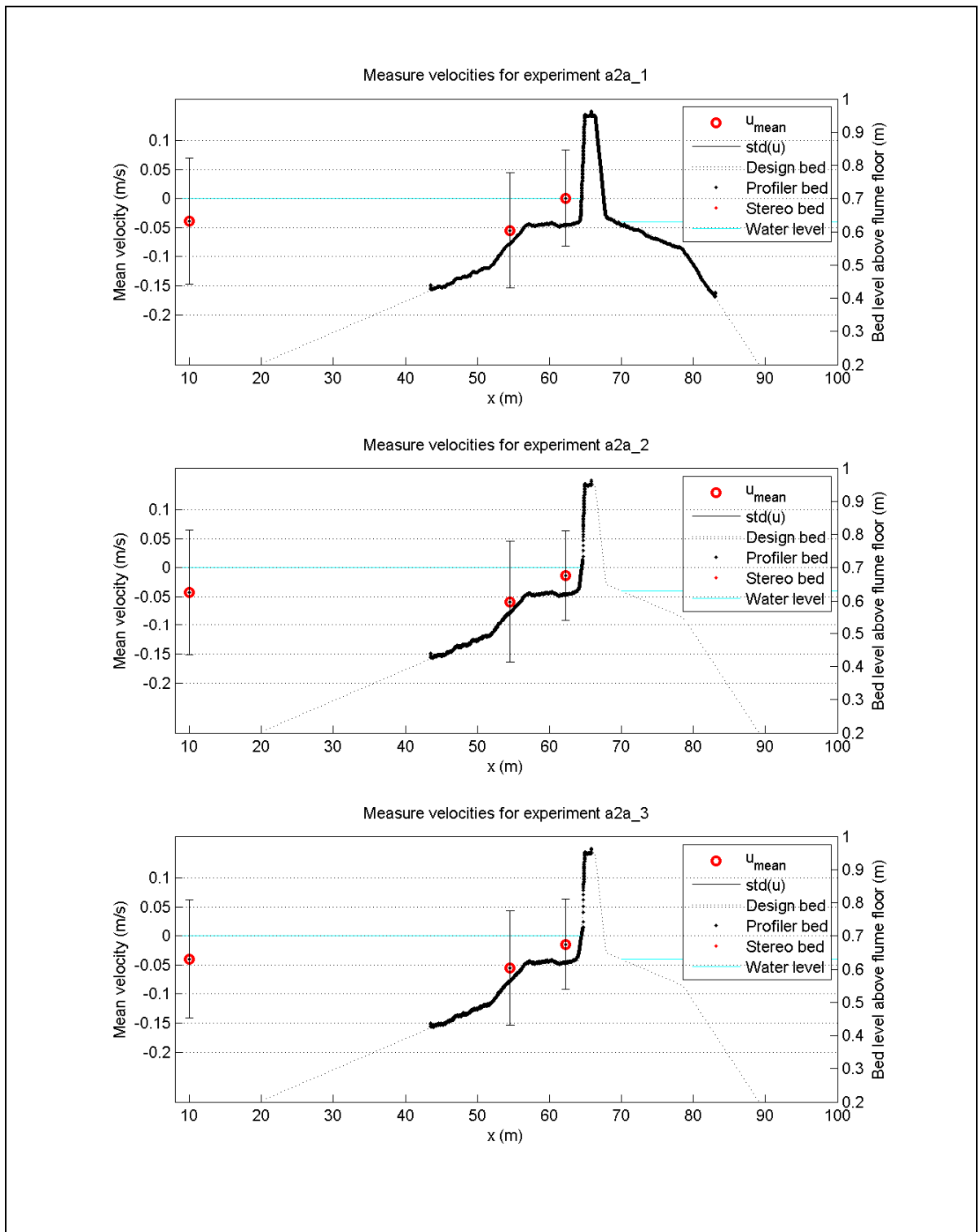


Time-averaged velocity and standard deviation measured at the EMS instruments in experiment A1d.

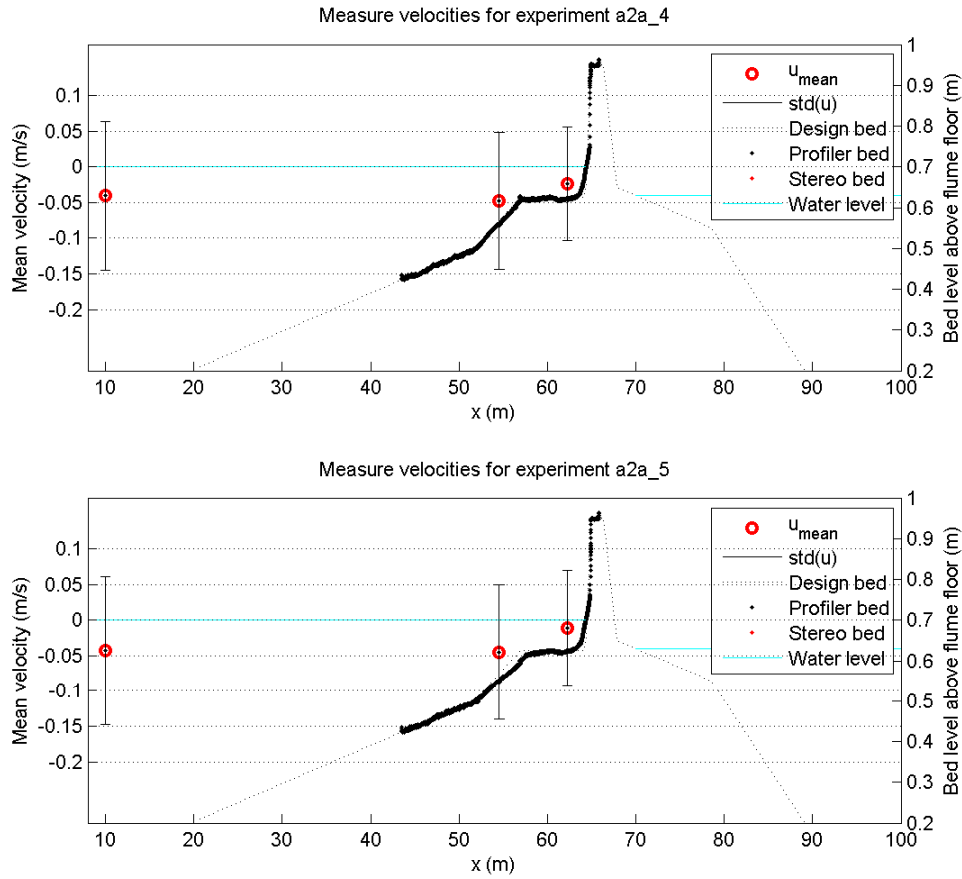
1202124-007-HYE-0005

Deltares

Figure C.109



Time-averaged velocity and standard deviation measured at the EMS instruments in experiment A2a.	1202124-007-HYE-0005	
	Deltares	Figure C.110

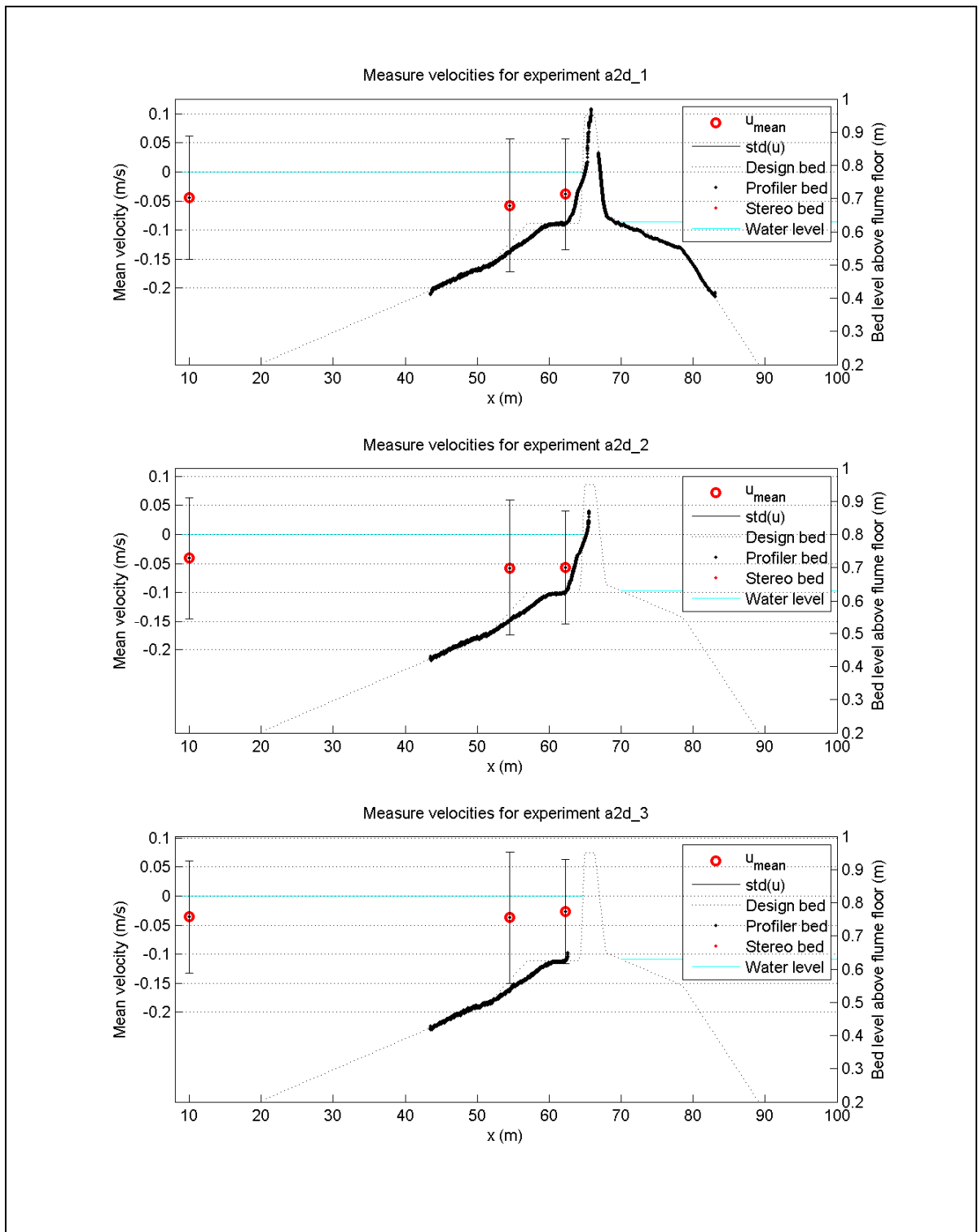


Time-averaged velocity and standard deviation measured at the EMS instruments in experiment A2a.

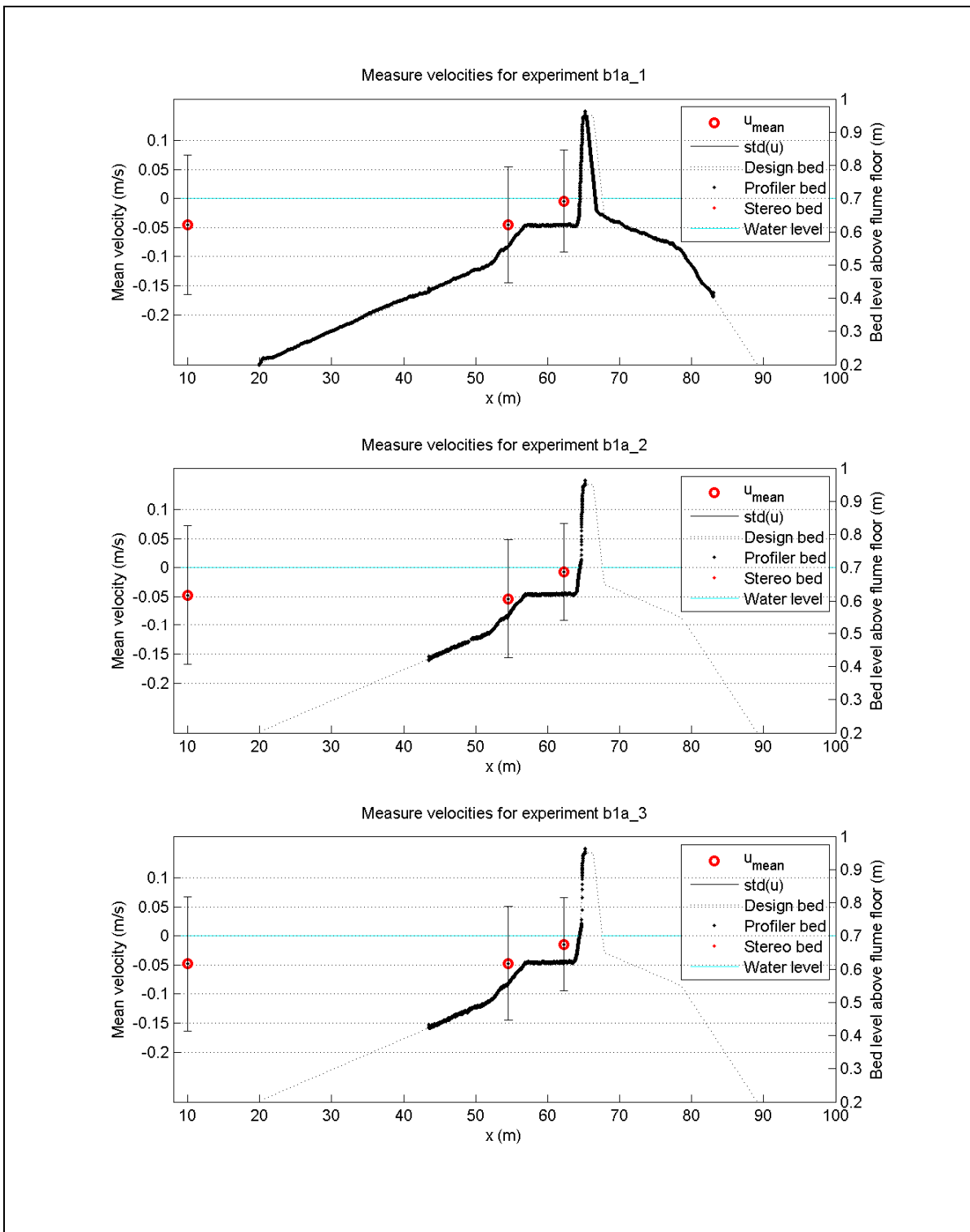
1202124-007-HYE-0005

Deltares

Figure C.111



Time-averaged velocity and standard deviation measured at the EMS instruments in experiment A2d.	1202124-007-HYE-0005	
	Figure C.112	
Deltares		

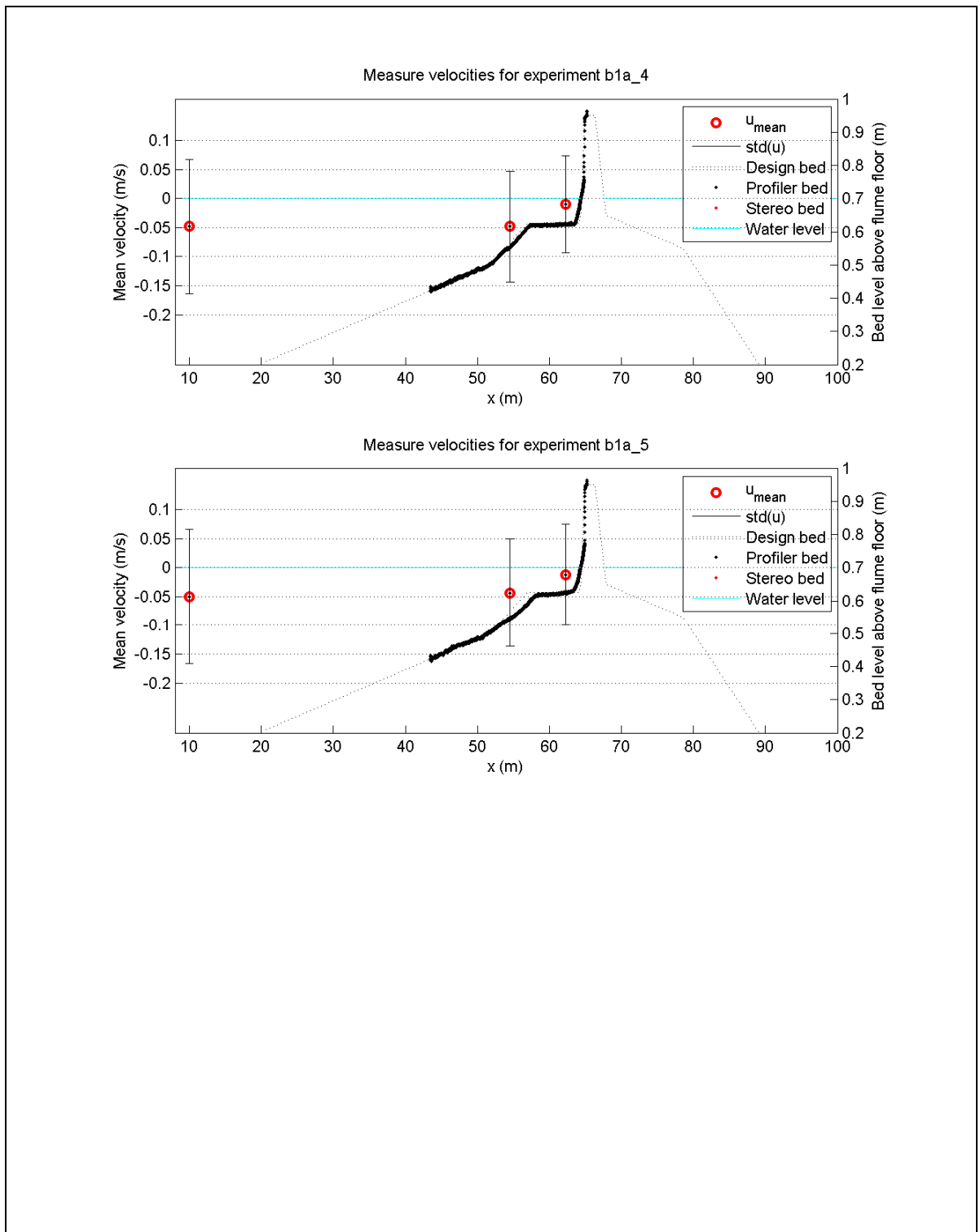


Time-averaged velocity and standard deviation measured at the EMS instruments in experiment B1a.

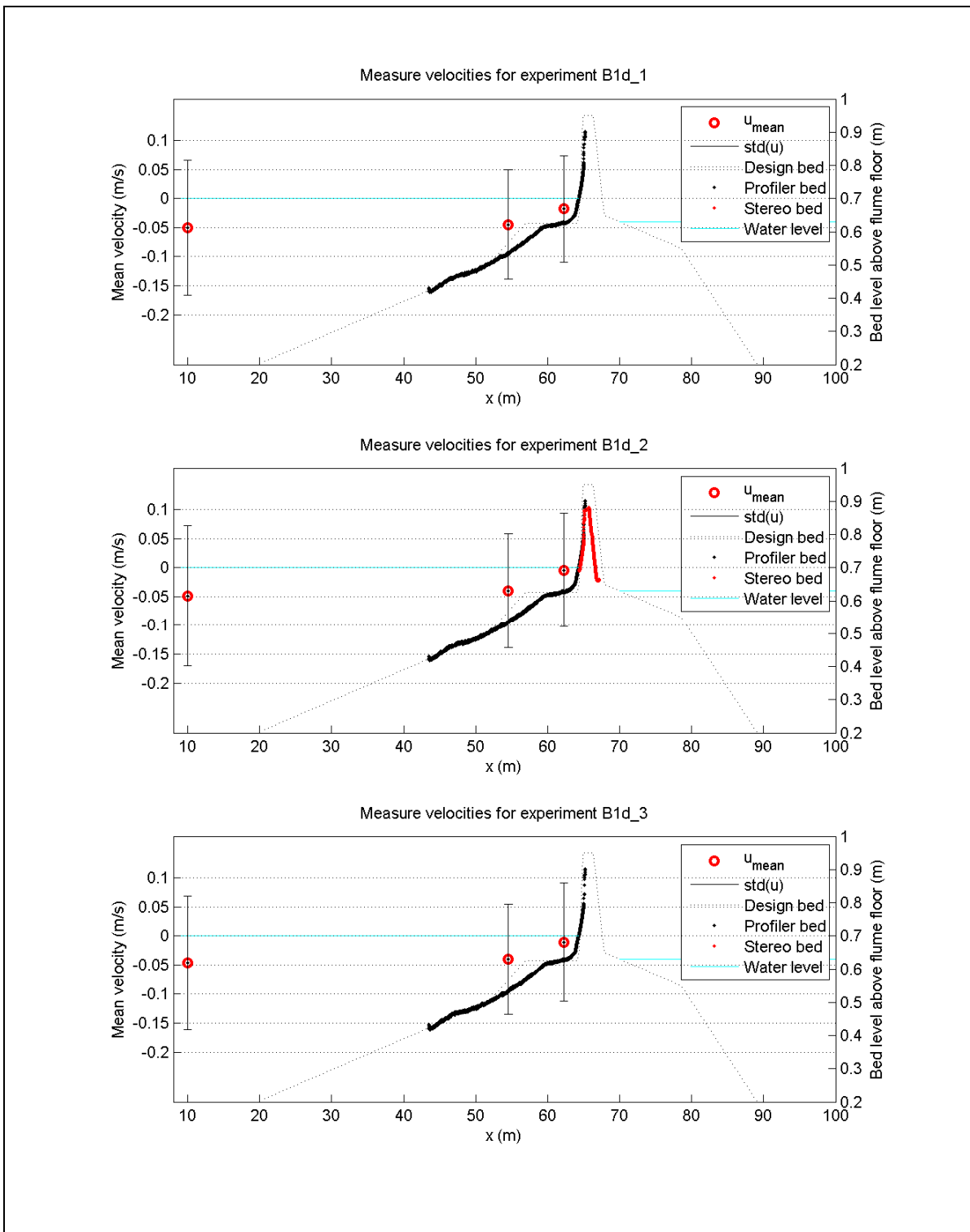
1202124-007-HYE-0005

Deltares

Figure C.113



Time-averaged velocity and standard deviation measured at the EMS instruments in experiment B1a.	1202124-007-HYE-0005	
	Deltares	Figure C.114



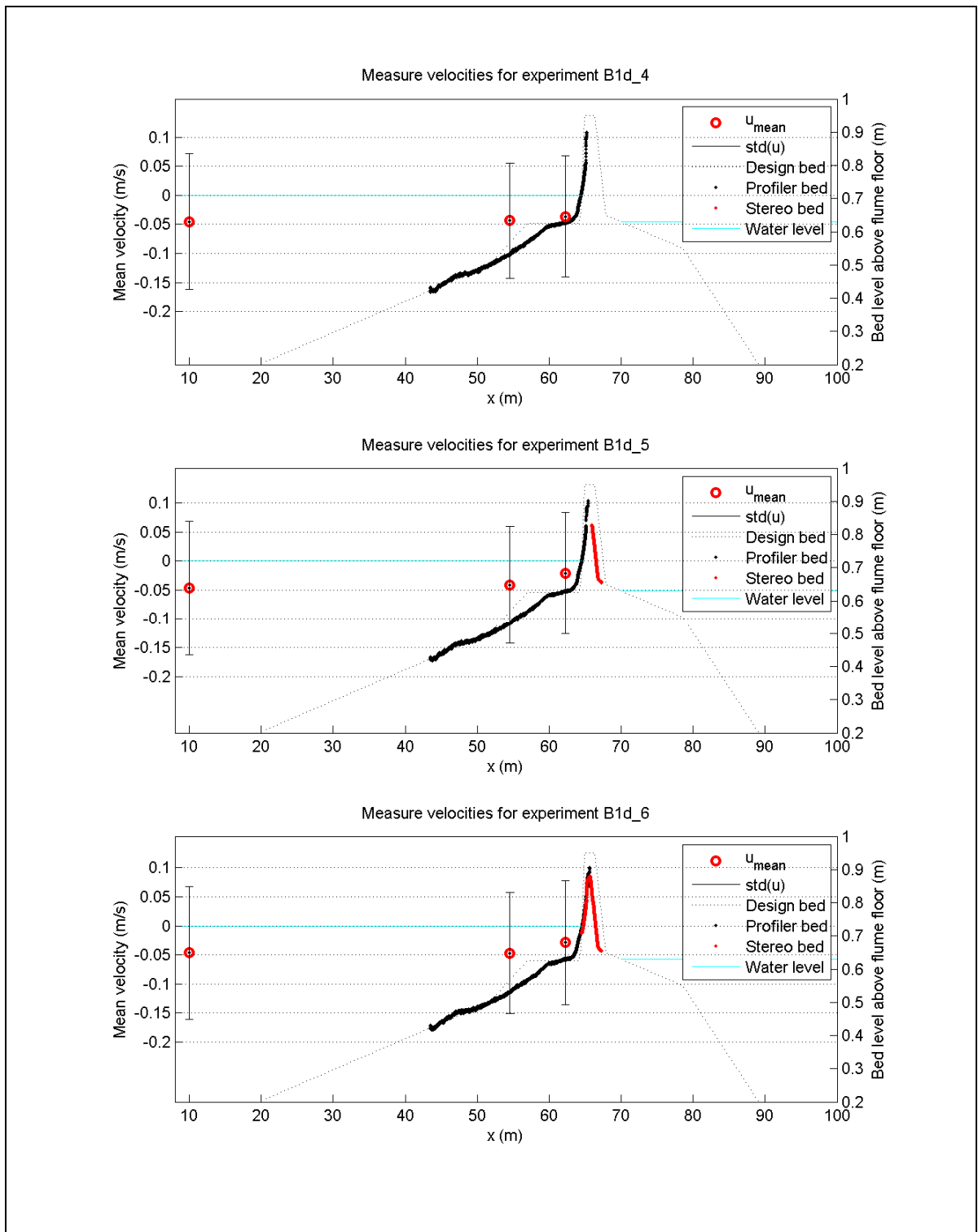
Time-averaged velocity and standard deviation measured at the EMS instruments in experiment B1d.

1202124-007-HYE-0005

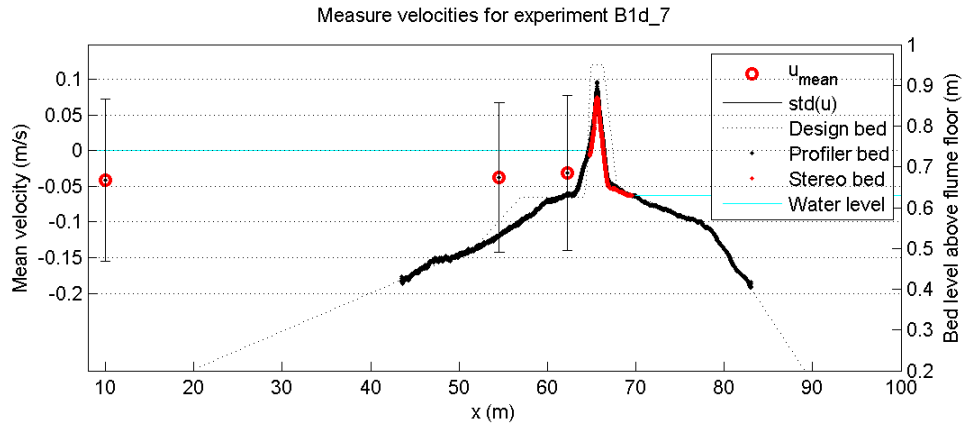
Deltares

Figure C.115





Time-averaged velocity and standard deviation measured at the EMS instruments in experiment B1d.	1202124-007-HYE-0005	
	Deltares	Figure C.116

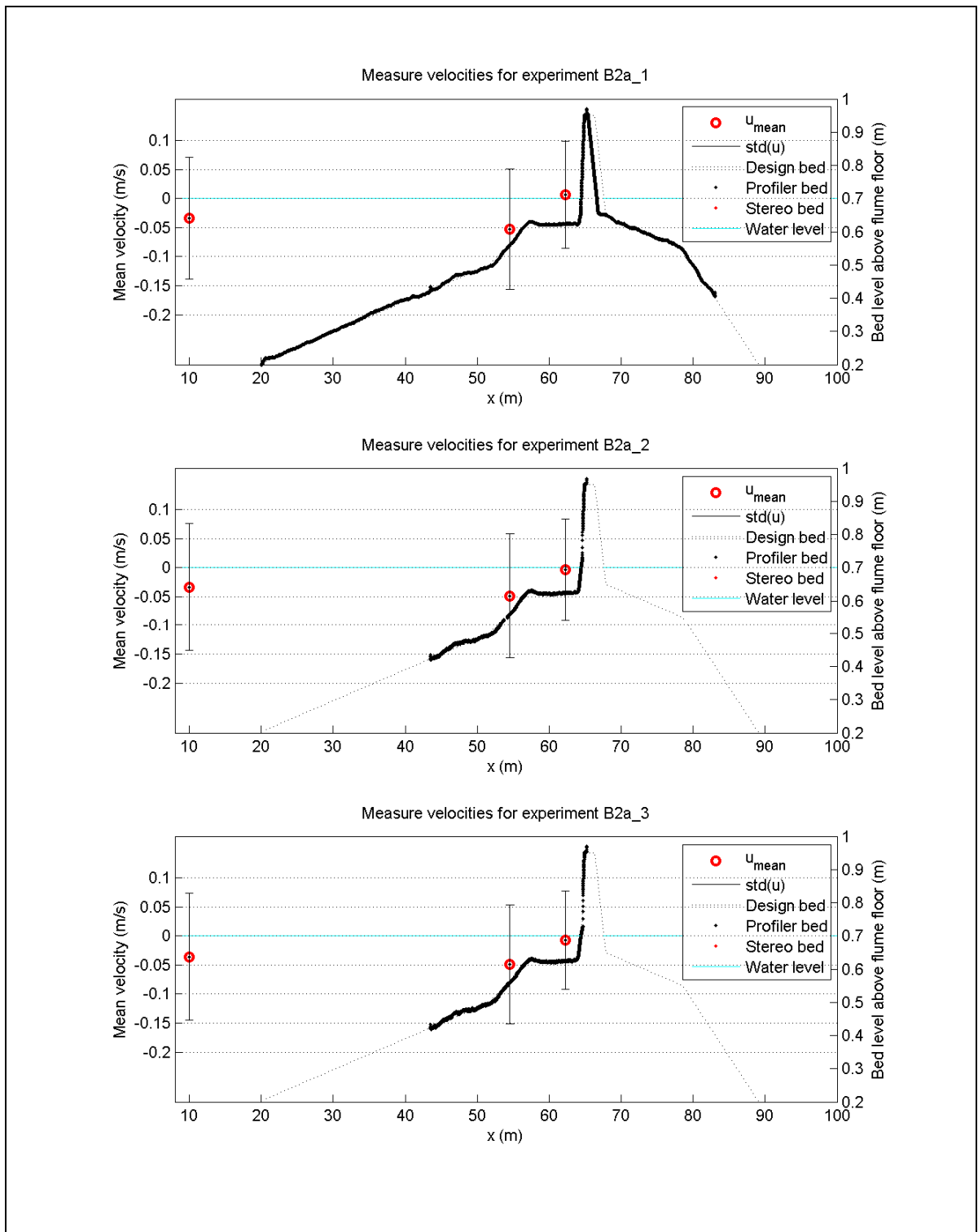


Time-averaged velocity and standard deviation measured at the EMS instruments in experiment B1d.

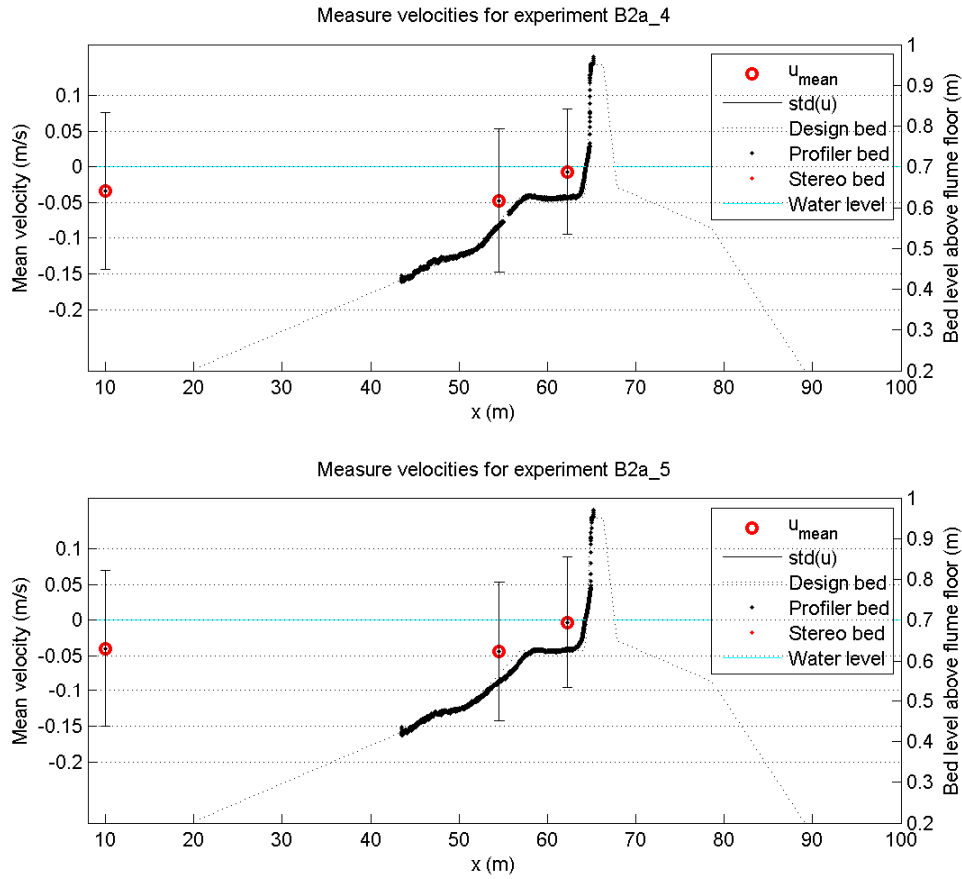
1202124-007-HYE-0005

Deltares

Figure C.117



Time-averaged velocity and standard deviation measured at the EMS instruments in experiment B2a.	1202124-007-HYE-0005	
	Deltares	Figure C.118

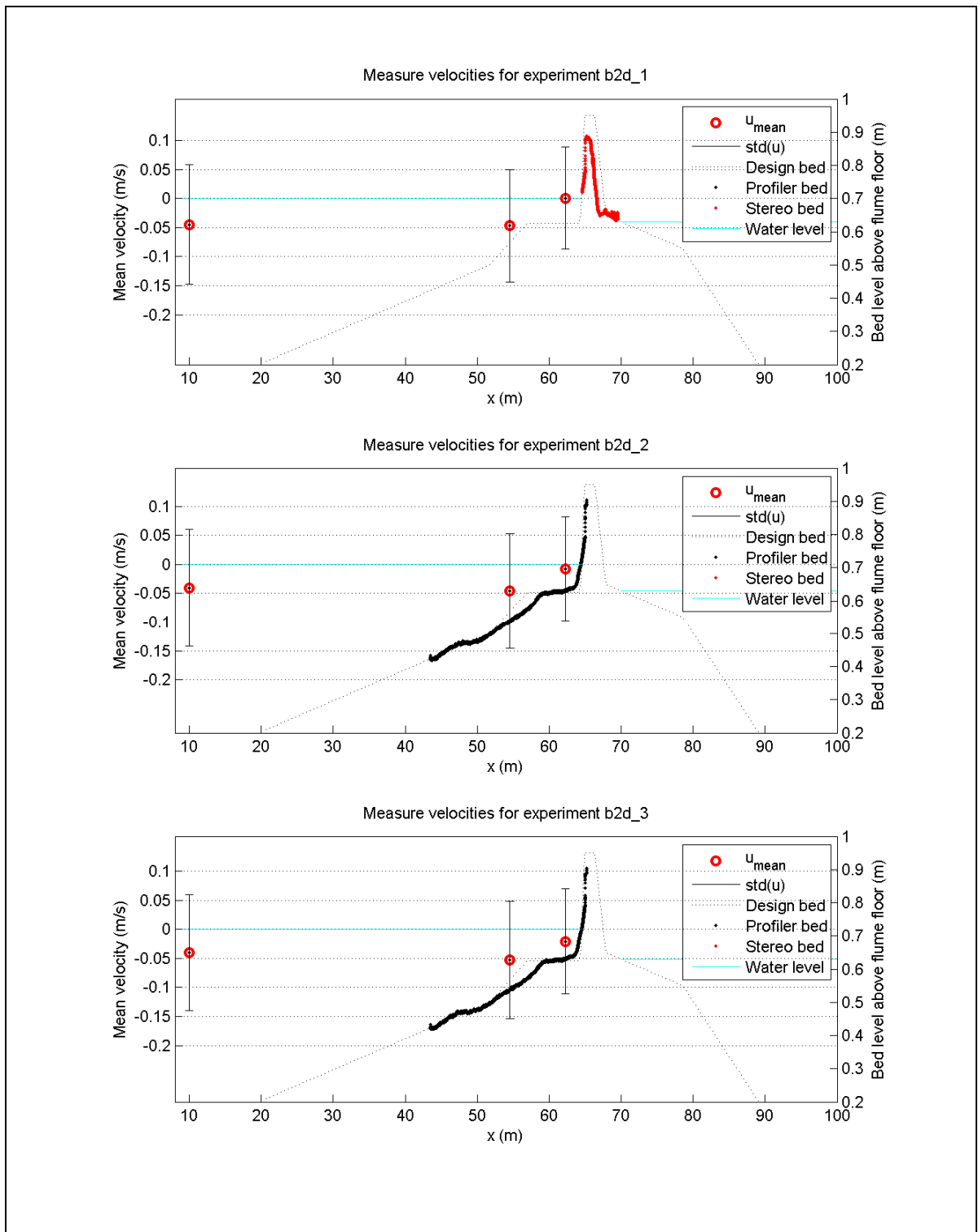


Time-averaged velocity and standard deviation measured at the EMS instruments in experiment B2a.

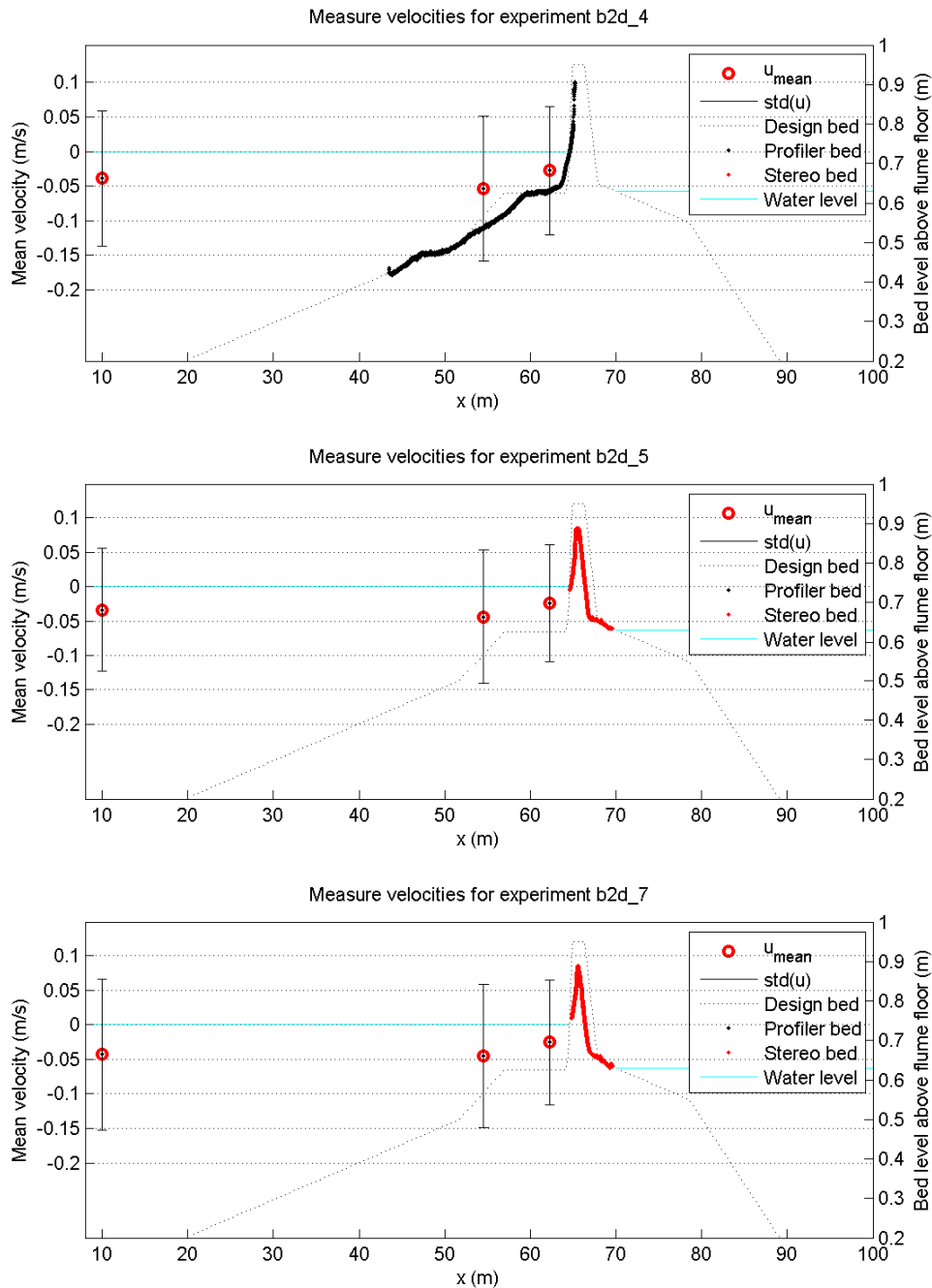
1202124-007-HYE-0005

Deltares

Figure C.119



Time-averaged velocity and standard deviation measured at the EMS instruments in experiment B2d.	1202124-007-HYE-0005	
	Deltares	Figure C.120

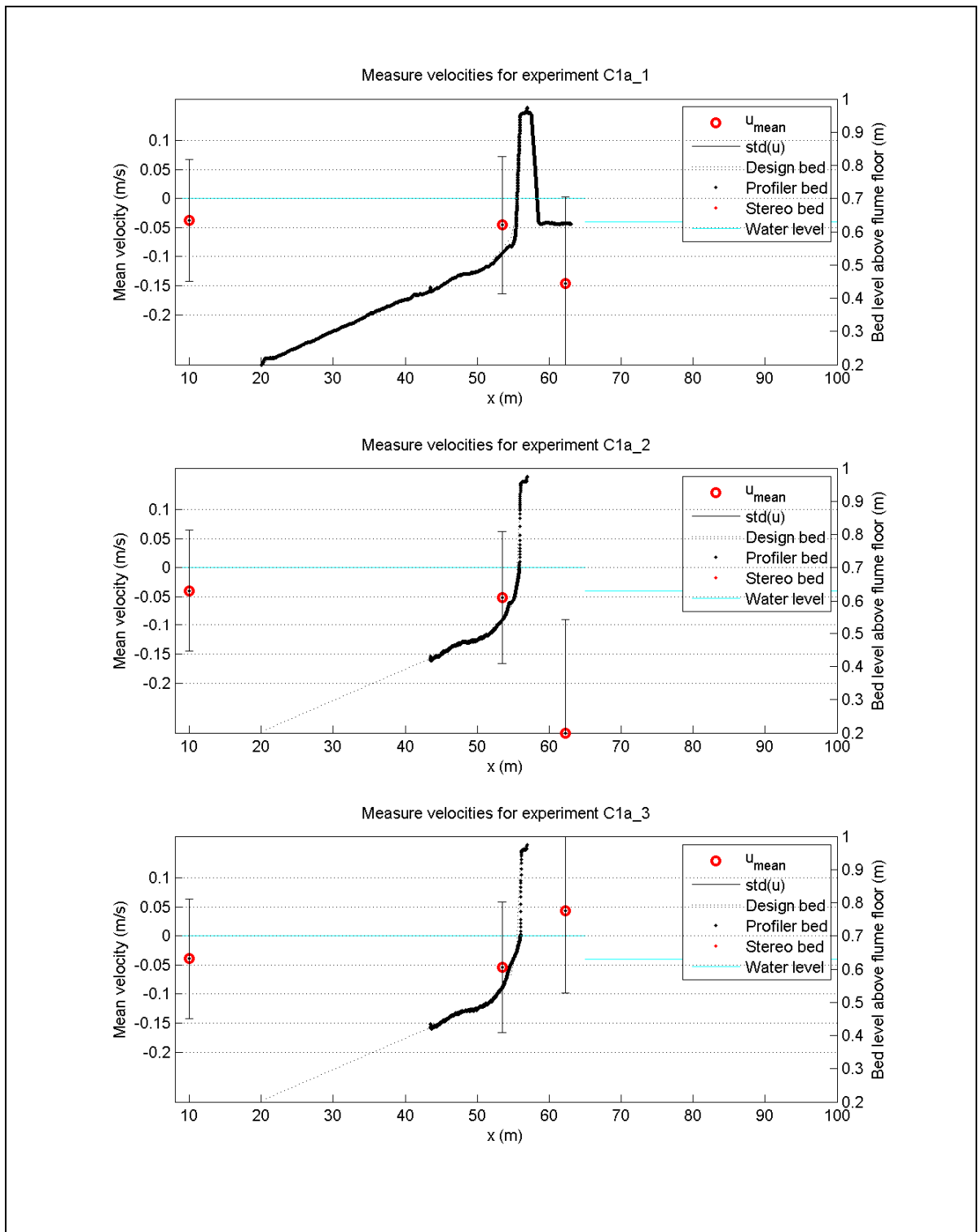


Time-averaged velocity and standard deviation measured at the EMS instruments in experiment B2d.

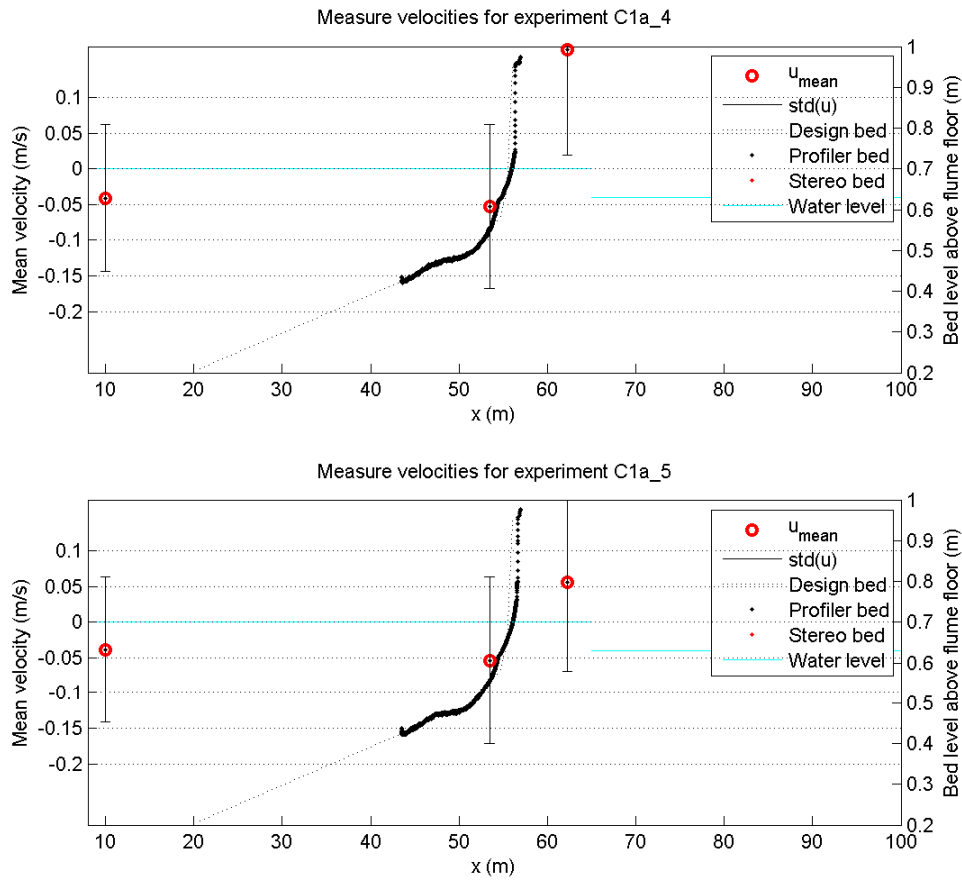
1202124-007-HYE-0005

Deltares

Figure C.121



Time-averaged velocity and standard deviation measured at the EMS instruments in experiment C1a.	1202124-007-HYE-0005	
	Deltares	Figure C.122



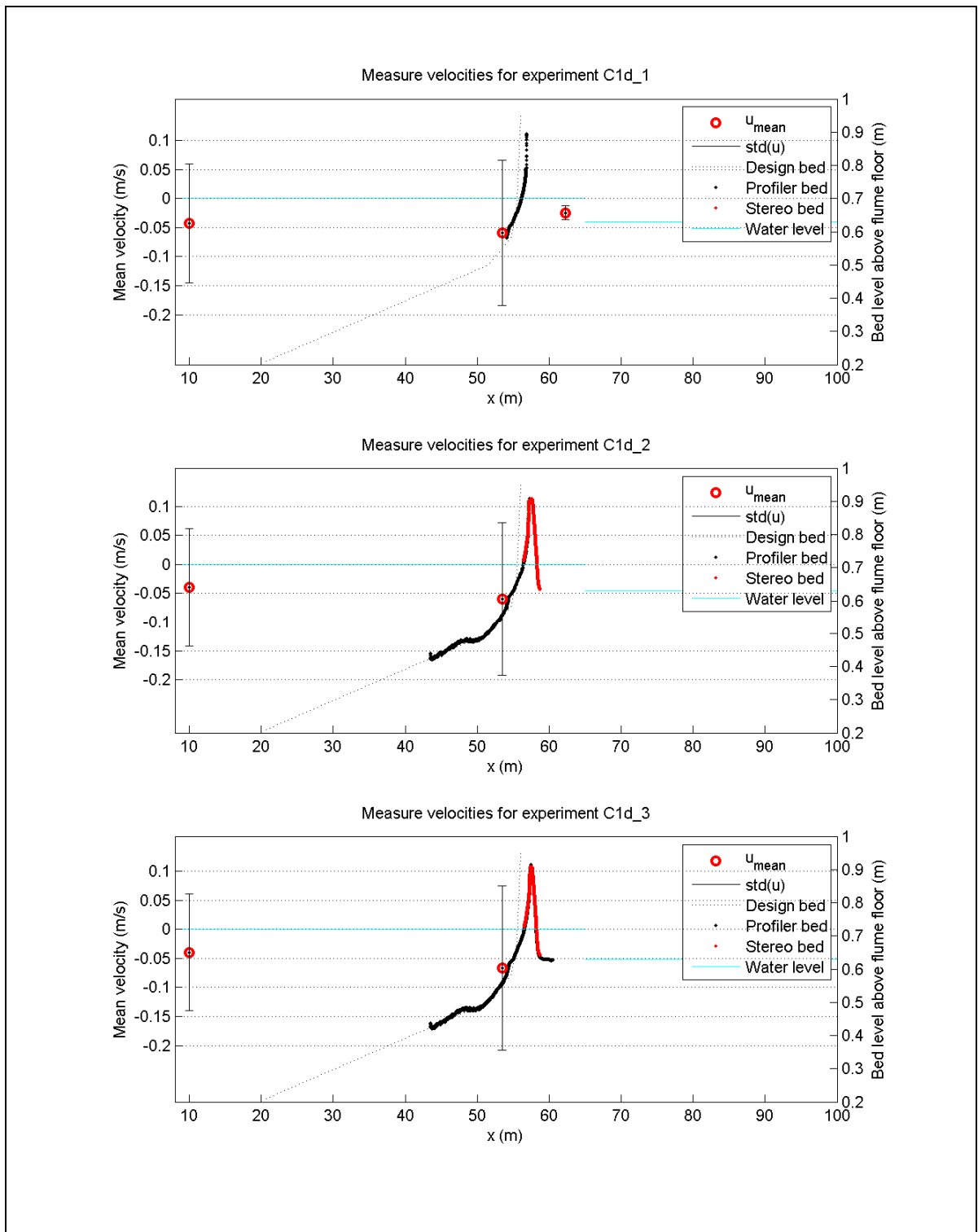
Time-averaged velocity and standard deviation measured at the EMS instruments in experiment C1a.

1202124-007-HYE-0005

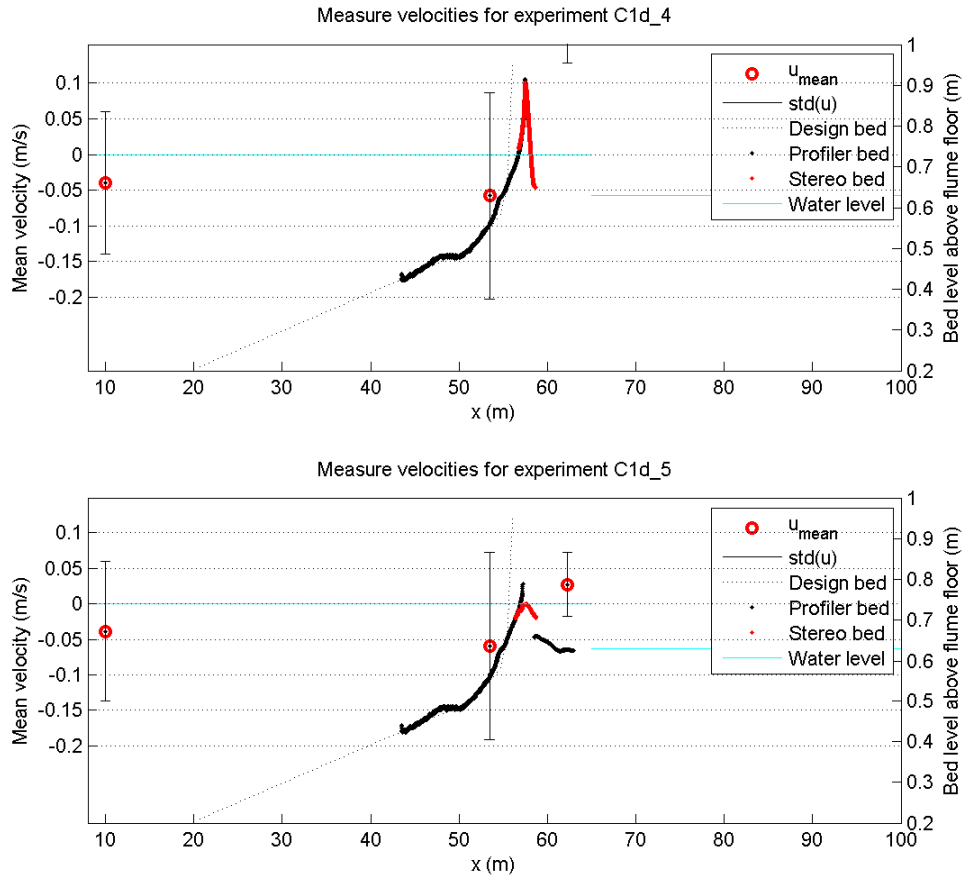
Deltares

Figure C.123





Time-averaged velocity and standard deviation measured at the EMS instruments in experiment C1d.	1202124-007-HYE-0005	
	Deltares	Figure C.124

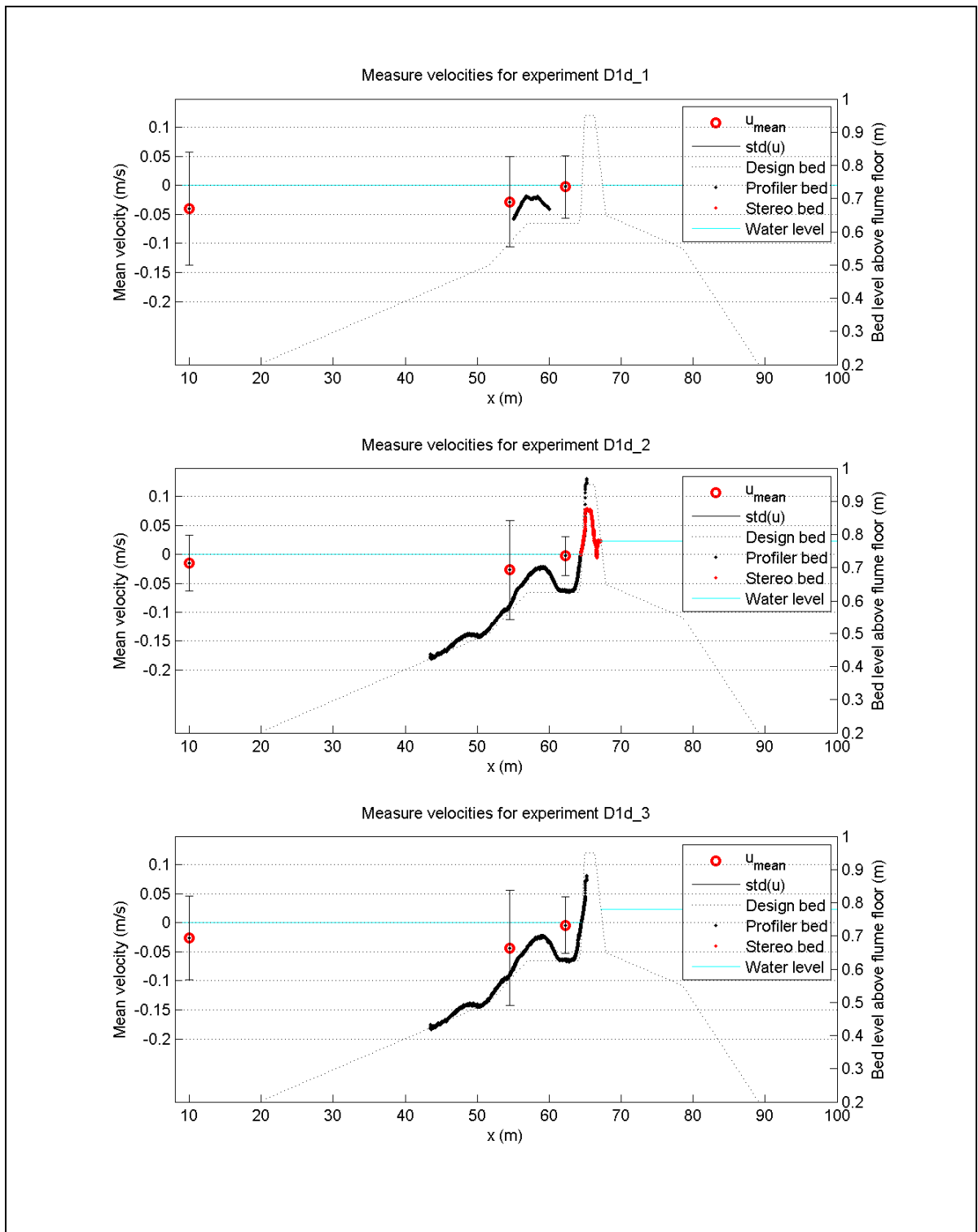


Time-averaged velocity and standard deviation measured at the EMS instruments in experiment C1d.

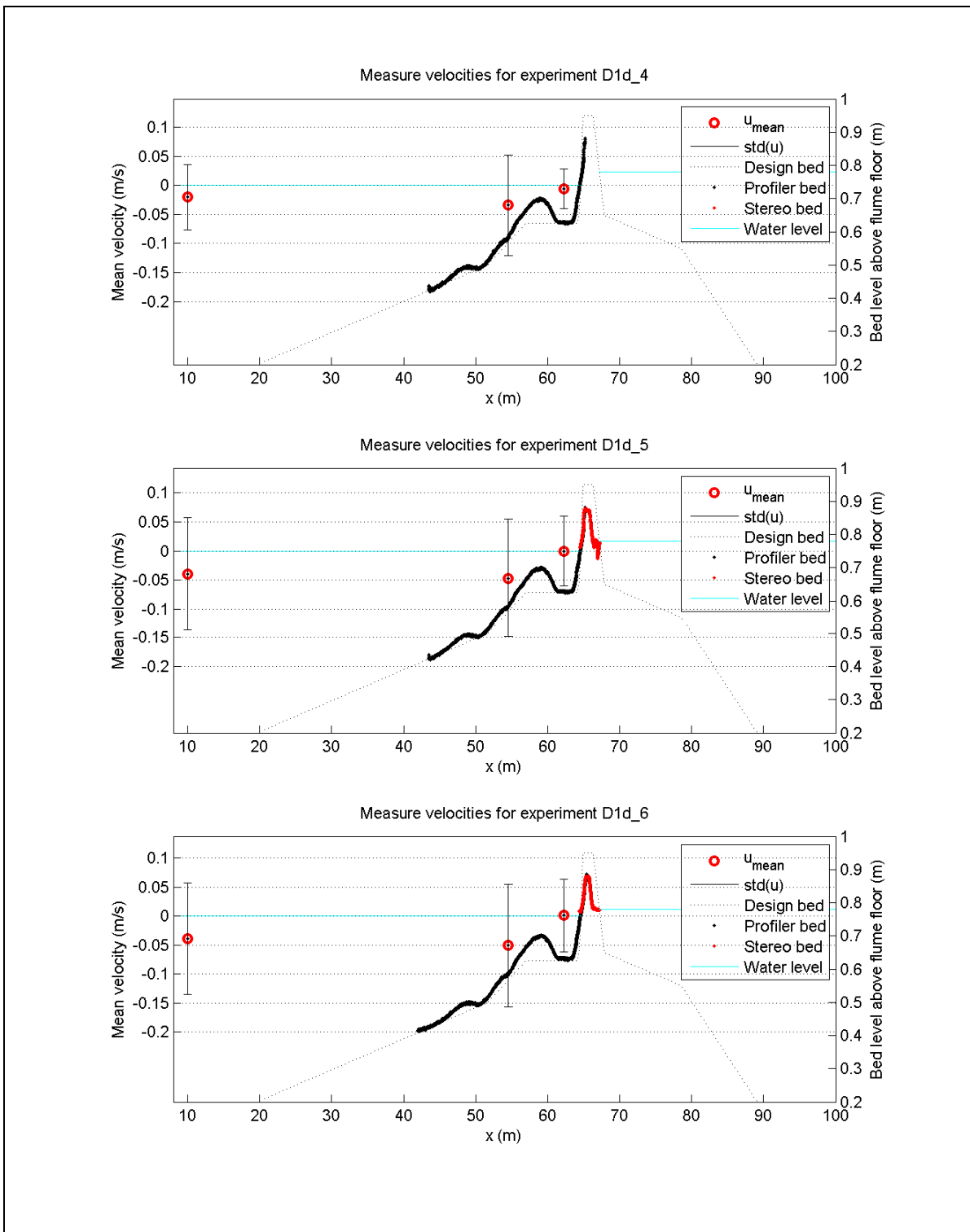
1202124-007-HYE-0005

Deltares

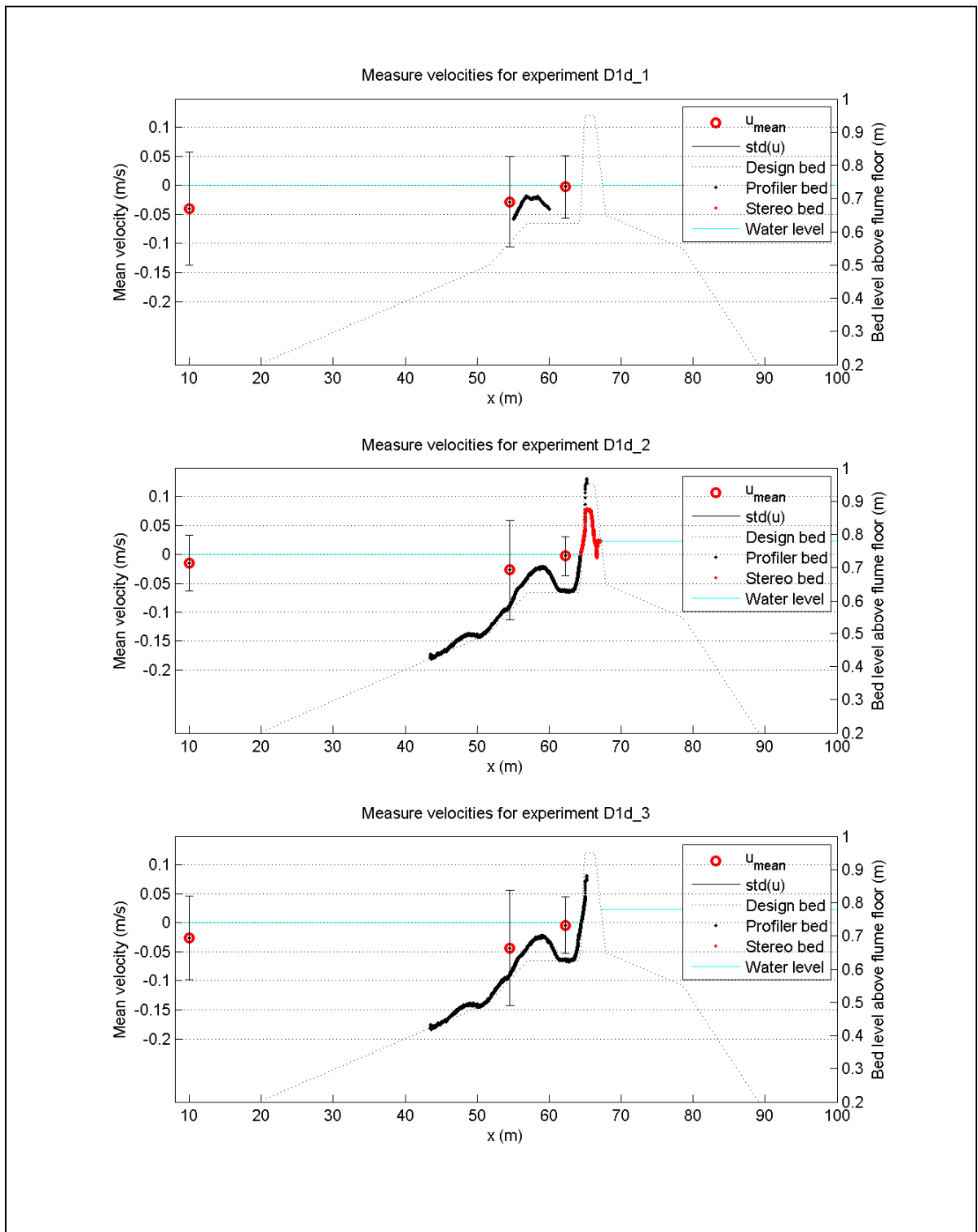
Figure C.125



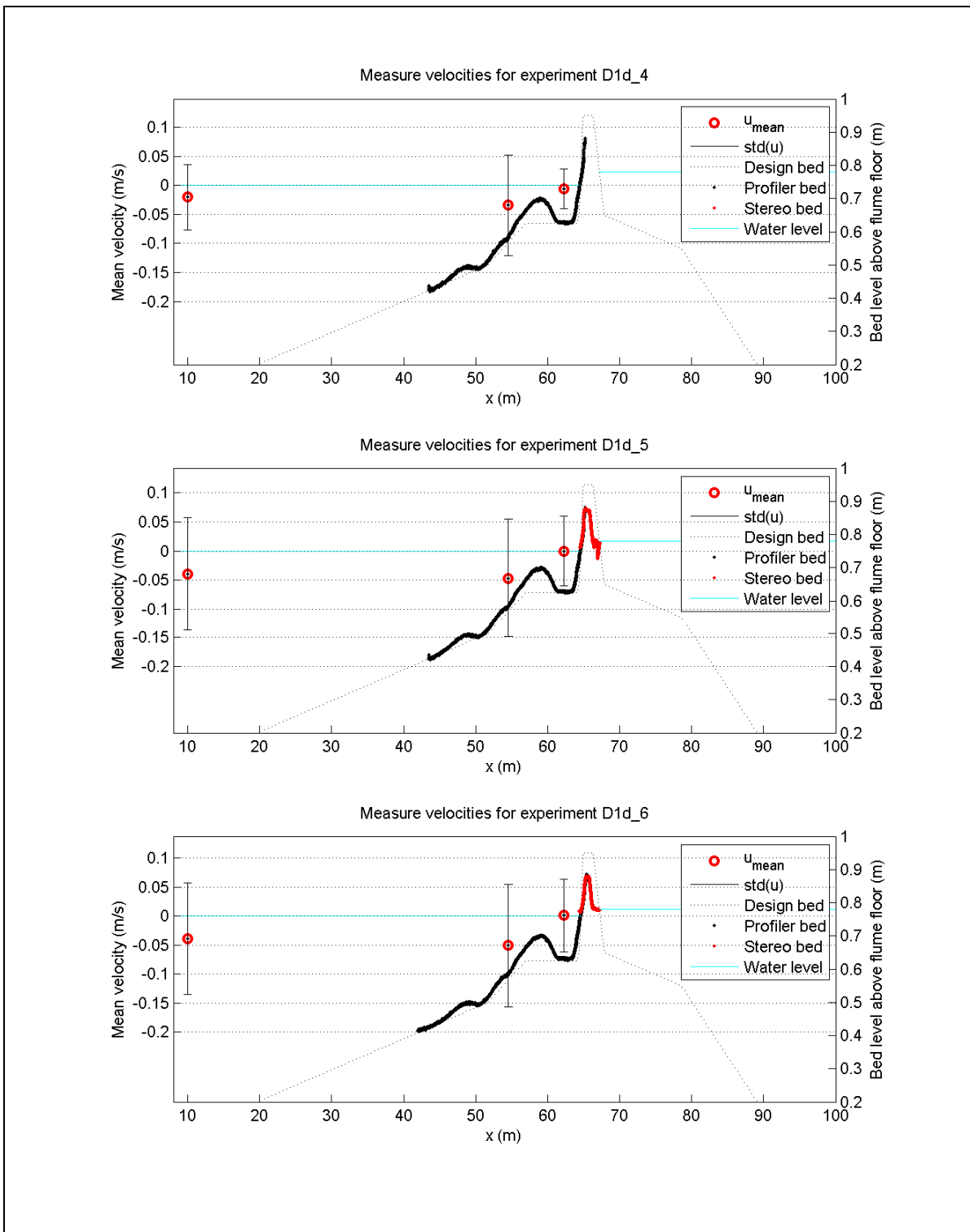
Time-averaged velocity and standard deviation measured at the EMS instruments in experiment D1d.	1202124-007-HYE-0005	
Deltares		Figure C.126



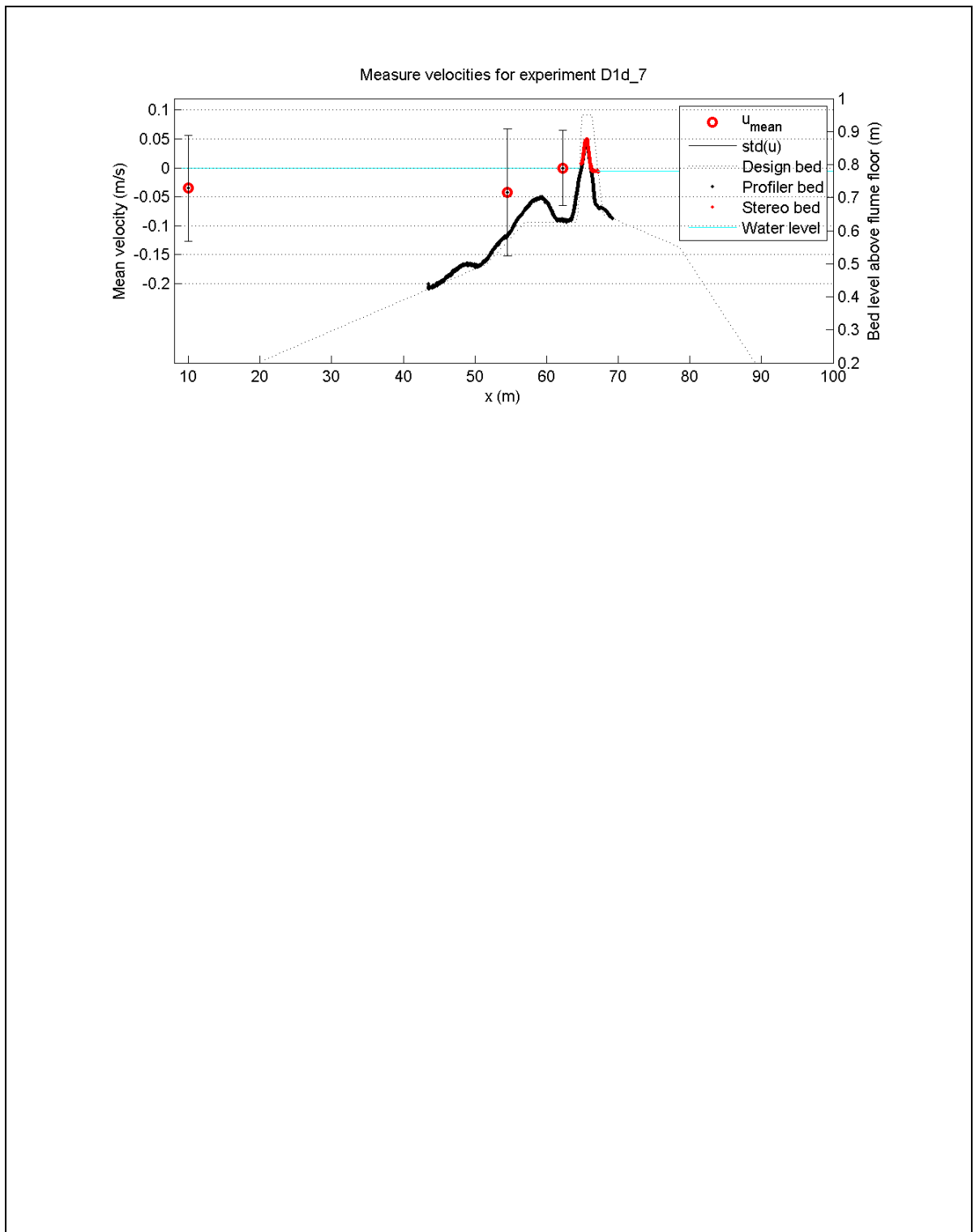
Time-averaged velocity and standard deviation measured at the EMS instruments in experiment D1d.	1202124-007-HYE-0005	
	Deltares	Figure C.127



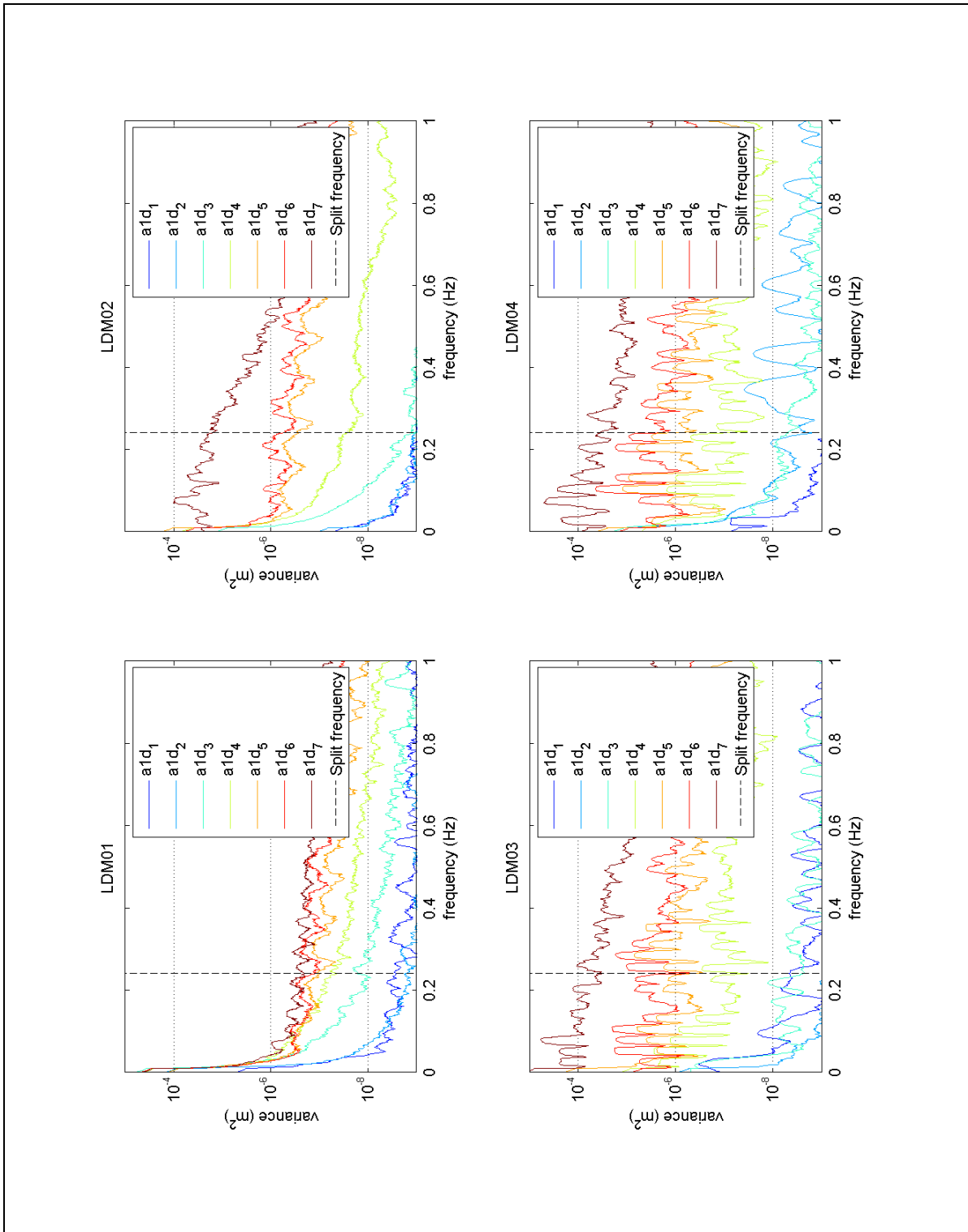
Time-averaged velocity and standard deviation measured at the EMS instruments in experiment D1d.	1202124-007-HYE-0005	
	Deltares	Figure C.128



Time-averaged velocity and standard deviation measured at the EMS instruments in experiment D1d.	1202124-007-HYE-0005	
	Deltares	Figure C.129

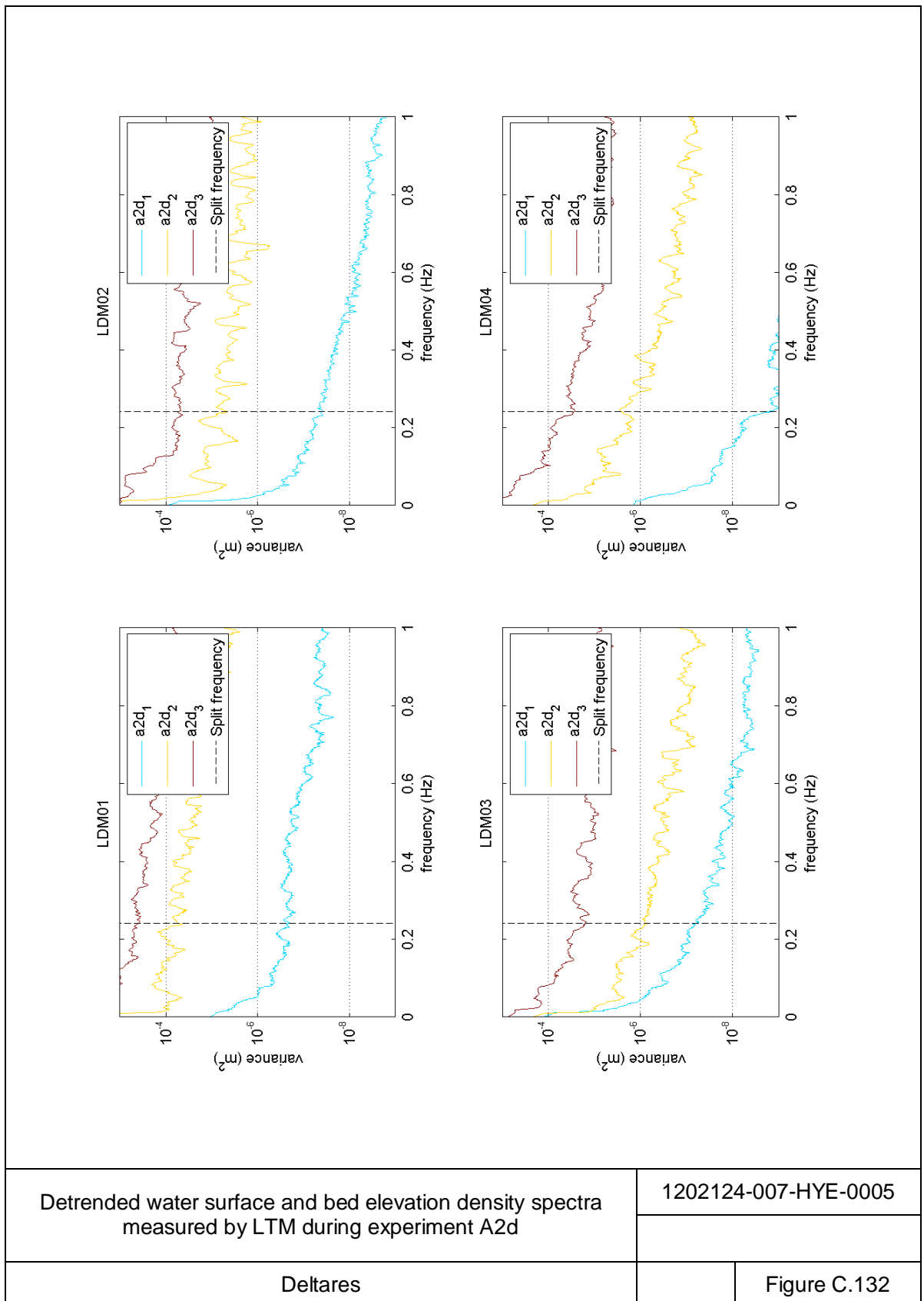


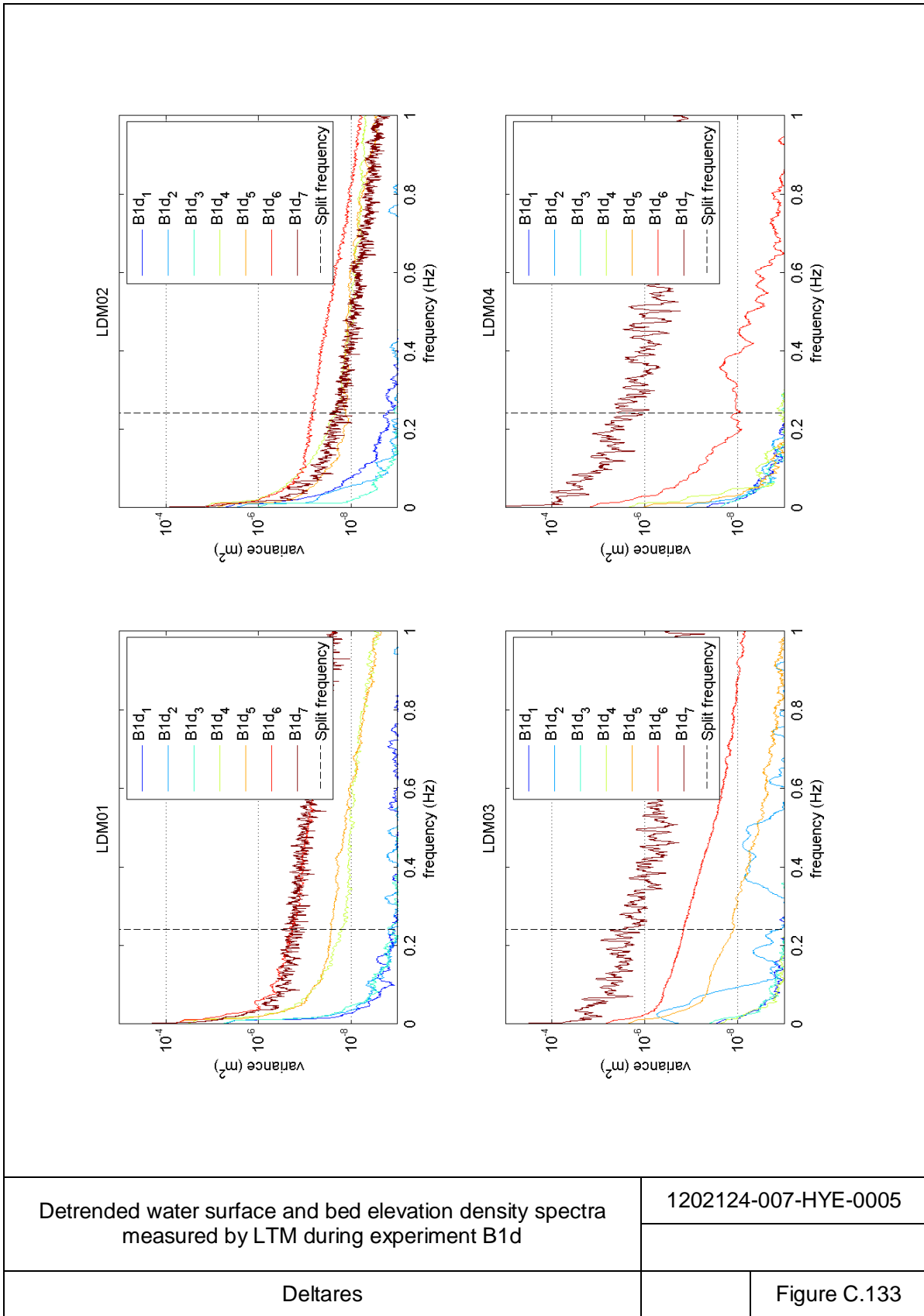
Time-averaged velocity and standard deviation measured at the EMS instruments in experiment D1d.	1202124-007-HYE-0005	
Deltares		Figure C.130

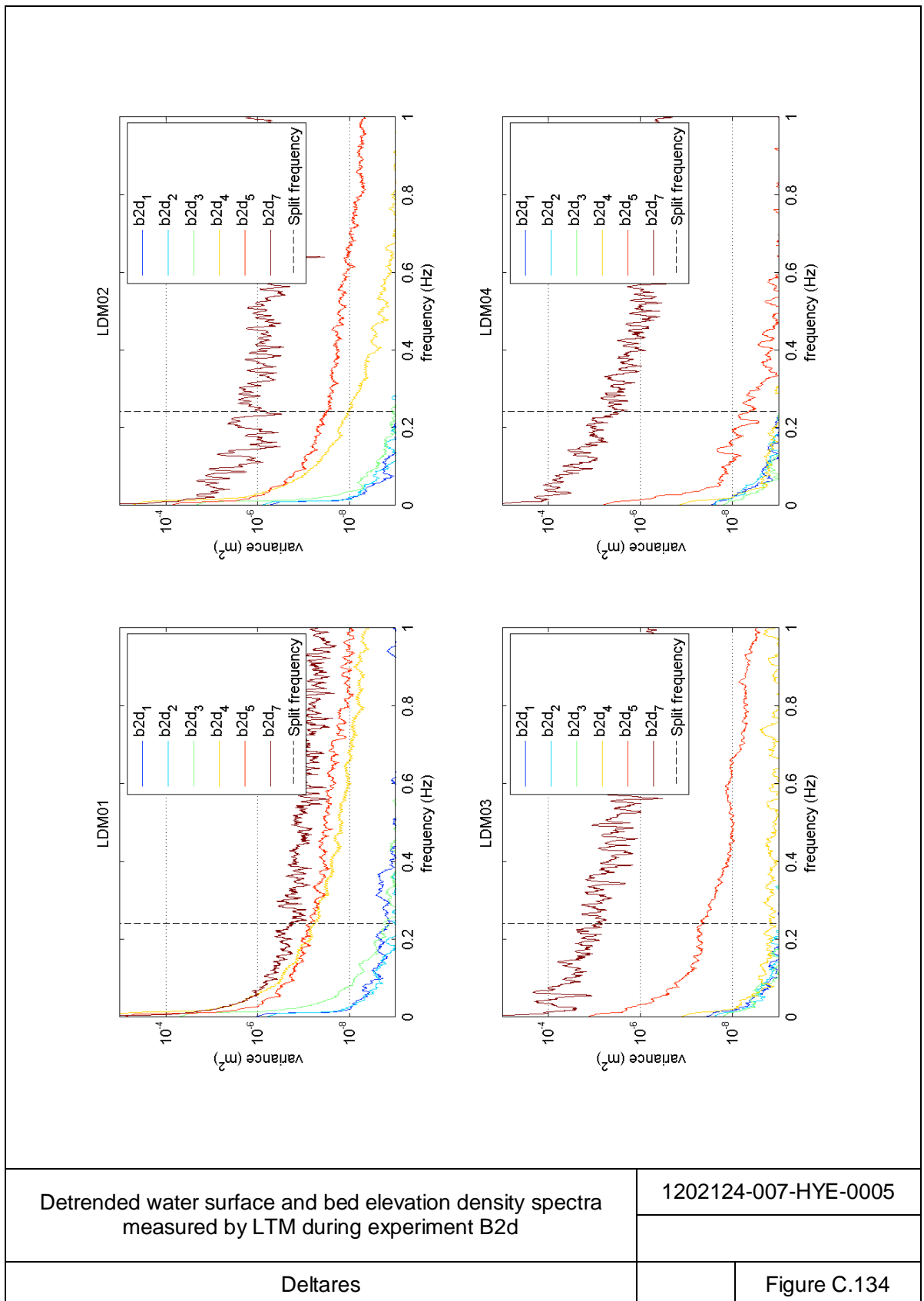


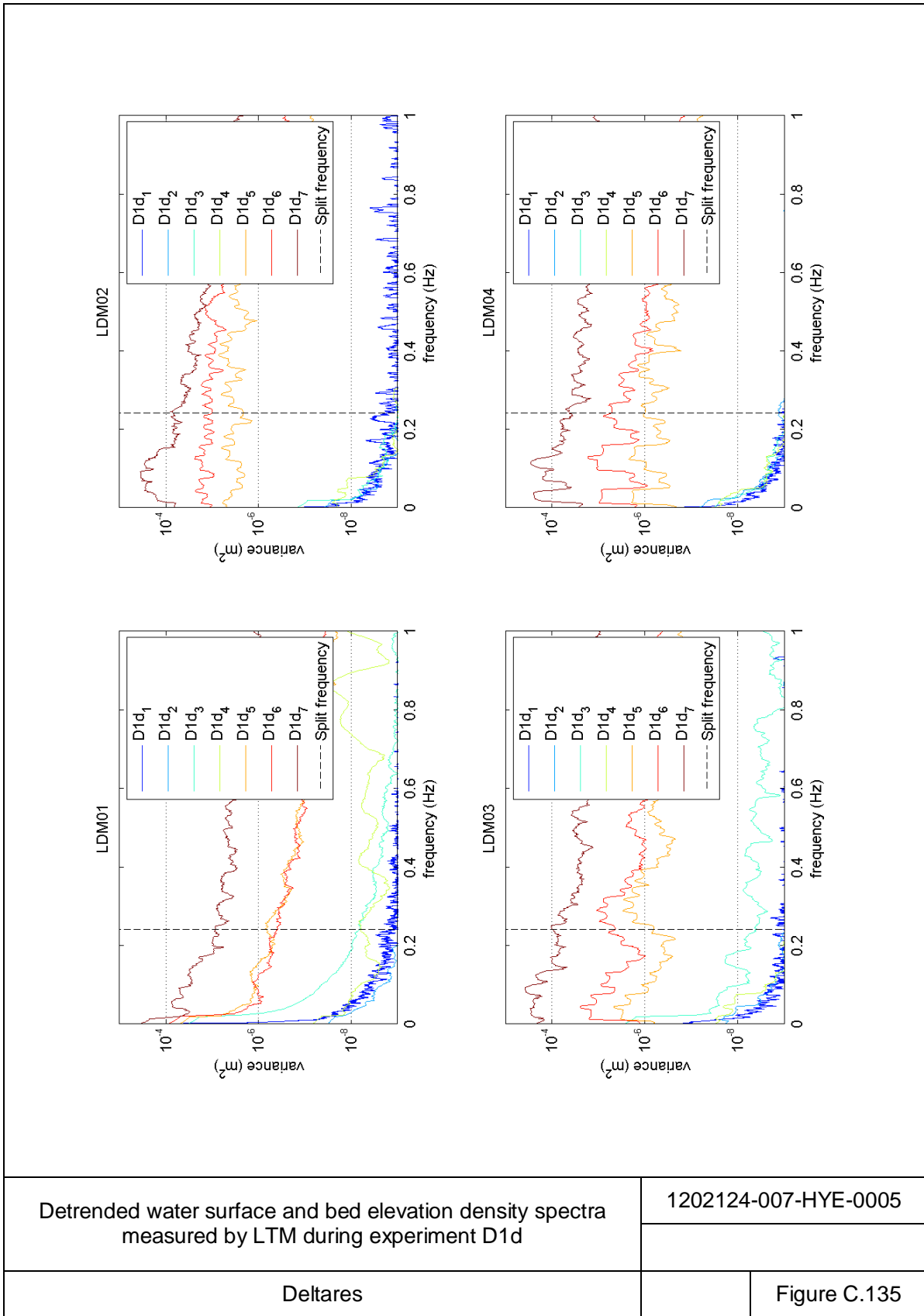
Detrended water surface and bed elevation density spectra measured by LTM during experiment A1d	1202124-007-HYE-0005	
	Deltares	Figure C.131











## D Naming conventions and datasources

### D.1 Naming conventions

During the experiments, naming conventions are used to distinguish different measurements. A test identifier consists of a letter (A – D) indicating the series (see paragraph 2.4 Measurement Programme), a number indicating the test order within the series starting from 1, a letter indicating the type of test (a = dune erosion, d = dune overwash) and another number prefixed by an underscore and starting from 1, indicating the number of the subtest. A subtest is a period between two breaks during an experiment, either to measure a cross-shore profile or to adjust the hydraulic conditions (experiment A1a).

Measurements obtained during an experiment, like hydrodynamic measurements or video images are tagged with the experiment identifier of the experiment at the time of the measurement. For example, WHM, EMS, LTM and cameras #1 to #3. Measurements obtained during a break between two subtests are tagged with the experiment identifier of the experiment following the break. For example, wheel-profiler measurements, stereophotos, etcetera. The final profile of an experiment therefore has an identifier that is not present in the hydrodynamic measurements.

### D.2 Datasources

The raw data obtained from the experiments exceeded the amount of 5TB. Therefore, it was not feasible to provide the data on portable media. Profiles and hydrodynamic measurements are converted to netCDF format and published on the Deltares OpenDAP server. The data can be found via the following URL:

[http://opendap.deltares.nl/thredds/catalog/opendap/deltares/scheldt\\_flume/1202124.007\\_sbw\\_dune\\_erosion\\_2010/](http://opendap.deltares.nl/thredds/catalog/opendap/deltares/scheldt_flume/1202124.007_sbw_dune_erosion_2010/)

For other datasources, like the photographs taken with cameras #1 to #3 and the stereocamera, please contact Deltares.